THE UNIVERSITY OF ADELAIDE

Department of Mechanical Engineering

PROPAGATION AND REACTIVE ATTENUATION OF LOW FREQUENCY SOUND IN HARD-WALLED DUCTS WITH AND WITHOUT FLOW

by

C.R. Fuller, B.E.

Thesis for the Degree of Doctor of Philosophy

July, 1978

Elected Silence, sing to me

And beat upon my whorlèd ear,

Pipe me to pastures still and be

The music that I care to hear.

from "The Habit of Perfection"
by G.M. Hopkins.

SUMMARY

Propagation and reflection of low frequency sound in single and coupled pairs of straight and curved ducts is investigated with and without flow of the propagating medium. The work is divided into three sections.

The first section deals with general propagation theory in straight and curved radial ducts of rectangular cross section with and without uniform flow. The effects of flow on the propagation of energy and the cut-off frequencies of higher modes are investigated experimentally and theoretically. A theoretical explanation in terms of wave number of why the cut-off frequency is independent of direction of propagation of sound relative to the flow is presented. The behaviour of phase velocity and group velocity near cut-on is also considered.

Sound propagation in radial bends of rectangular cross section is investigated using two methods, the first of which utilizes the traditional solution of the wave equation in cylindrical co-ordinates. An iterative method of solution of the characteristic equation is discussed and used to predict the acoustic pressure and particle velocity distributions of two propagating modes. Comparison is made with experimental results and the results of other workers. Good agreement is obtained. The theoretical investigation using cylindrical co-ordinates is limited to the case without flow.

An approximate method of analysis of low frequency sound in

radial bends is developed using conformal mapping techniques. As well as overcoming the need to evaluate complicated expressions of Bessel and Neumann functions, this approach allows theoretical consideration of the effects of flow. Simple equations are developed which predict the angular wave numbers of the (0,0) mode and higher evanescent modes as well as the cut-off frequencies of higher modes with and without flow. The results of the analysis agree with results obtained by other workers using cylindrical co-ordinates solution. The effects of flow on the pressure distribution and cut-off frequencies of higher modes are considered.

The second part of the thesis is concerned with sound generation and propagation in duct systems. Sound generated in a rectangular straight duct with rigid walls by a dipole piston source is theoretically investigated. The pistons are of equal area and fill the cross section of the duct. The characteristic impedance and radiation efficiency of the source is investigated for varying phase angle between pistons. The source is shown to be an extremely good radiator of sound when the pistons are in phase and to radiate no sound power at all below the cut-off frequency of the first cross mode of the duct when the pistons are π radians out of phase.

The effects of a curved axial partition on the impedance of a curved bend are investigated theoretically and experimentally. Whereas previous investigations have established that a curved bend provides negligible discontinuity to acoustic propagation, the presence of a central partition is found to drastically modify the propagational characteristics of the bend resulting in high reflection of sound at a number of discrete frequencies. By contrast, presence of a central partition in a straight duct would have no effect at all below the

cut-off frequency for the first cross mode of the duct.

The third part of the work deals with the development and testing of two reactive attenuators, based upon a principle mentioned by Rayleigh (Theory of Sound, Vol. II, p.63) and attributed to Herschel. Sound propagation in a single duct is caused to split into two parts which travel along separate parallel ducts and when recombined produce non-propagating modes. The sound is thus reflected and the device becomes an effective attenuator in prescribed frequencies. Such attenuators might be used for rigid walled ducts.

The first attenuator is designed to fit into a 90 degree bend in a rectangular duct system and relies on a center body to create an impedance mismatch at the attenuator exit. The center body is shaped to provide a low pressure drop across the device. The performance of the attenuator is theoretically analysed with and without flow. The analysis allows the redesign of the configuration of the attenuator to optimize its performance. An optimum attenuator is developed which provides a transmission loss of at least 10 dB over three quarters of an octave and losses of 30 to 50 dB at a number of discrete frequencies in the three quarters octave frequency range.

Flow is found to substantially reduce the high attenuation obtained at the discrete frequencies but a transmission loss of 10 dB is still obtained over three quarters of an octave for a flow rate of $M = 0.08$ in the upstream straight duct. The effects of flow on the design frequency and the pressure reflection coefficient are quantified.

The second attenuator is designed for use in straight ducts of circular cross section and relies on an acoustic delay line to generate a series of evanescent modes and a resultant impedance mismatch at the device exit. The attenuator is investigated

experimentally with and without flow for speeds up to M = 0.37. The device is shown to provide higher levels of attenuation and a 10 dB rejection band over an octave for the case without flow. The disturbance to the fluid flow in the main duct is negligible. A theoretical analysis of the delay line attenuator over its operating frequency range is not attempted. However, it may be theoretically described for the very low frequency portion of its range using a lumped circuit analysis. The theory predicts reasonably well the positions of the amplification of sound, measured in the very low frequency range.

TABLE OF CONTENTS

STATEMENT OF ORIGINALITY

This thesis contains no material which has been accepted for the award of any other degree or diploma in any University. To the best of the author's knowledge and belief, this thesis contains no material previously published or written by another person, except where due reference is made in the text.

C.R. FULLER

July, 1978.

ACKNOWLEDGEMENTS

The author wishes to express his sincere thanks and appreciation to his supervisor, Dr D.A. Bies for the stimulating help, the constant encouragement and the support he has given throughout the duration of the research, and for the criticism of this thesis. His ideas have provided the inspiration of a major part of this work and it has been a pleasure working under him.

Similarly, the author acknowledges the keen interest taken by Dr C. Abell in part of this work and the helpful suggestions he has provided.

The author is also indebted to Professor S.E. Luxton who provided the opportunity to conduct this research and also gave much time and encouragement.

There are many members of both the mechanical and electronic workshop staff who are acknowledged for their assistance in the construction of the experimental apparatus. In particular, the author would like to thank Mr M. Bethune and Mr C. Price for their part in the construction of duct work and Mr G. Osborne for the construction and advice on the electronic support equipment.

The author gratefully acknowledges Ms J. Prince for the support she provided in the form of constant encouragement during difficult parts of the research work.

Finally, acknowledgement is made of the financial assistance provided by the Commonwealth Postgraduate Research Award, the University Research Grant and the Australian Research Grants Committee.

FIGURES

PLATES

TABLES

SYMBOLS

a	Aspect ratio = R_1/R_2
A	Amplitude constant
A_b	Curved duct constant = $-J'_{\nu_s}(k_r R_1)/Y'_{\nu_s}(k_r R_1)$
A_o	Cross sectional area of orifice
A_s	Area of slit
$A_{d\ell}$	Cross section area of delay line
A_m	Complex matrix
A_{md}	Cross sectional area of main duct
A^*	Area of source
B	Amplitude constant
B_m	Complex matrix
c_g	Group velocity
c_p	Phase velocity
c_p^*	Equivalent curved duct linear phase velocity
c_o	Speed of sound in undisturbed medium
$c^c(r)$	Curved duct acoustic velocity distribution
C	Amplitude constant
C_{eq}	Equivalent capacitance
D	Amplitude constant
D_i	Internal diameter of duct
e, $\exp$	Exponential operator
E	Amplitude constant
f	Frequency
f_c	Modal cut-off frequency
$f(y)$	Superposition function

F	Complex function
$g(y)$	Superposition function
G	Total number of equations
h	Transverse duct dimension
i	$\sqrt{-1}$
$\underset{\sim}{i}$	Unit vector in the x direction
I	Acoustic intensity
$\underset{\sim}{j}$	Unit vector in the y direction
$J_{\nu_n}(k_o r)$	Bessel function
k	Wave number
$k^c(r)$	Curved duct wavenumber distribution
$\ddot{k}_1$	$=(k_m^2 + k_n^2)^{\frac{1}{2}}$
$\ddot{k}_2$	$= (1-M^2)\ddot{k}_1^2$
K	Function domain
ℓ	Integer 0, 1, 2 ...
$\ln$	Natural logarithm
$\log_{10}$	Logarithm to the base 10
ℓ_e	Effective length of orifice
L	Number of modes considered in Sections 1 and 6
L_{eq}	Equivalent inductance
m	Integer 0, 1, 2...
M	Mach number = V/c_o
M^c	Curved duct Mach number distribution
n	Integer 0, 1, 2...
n_s	Standing wave ratio
N	Number of modes considered in Sections 5 and 3
p	Acoustic pressure

P	Amplitude constant
Q	Number of modes considered in Sections 2 and 4
r	Radial coordinate
r_m	Position of pressure maximum
R	Pressure reflection coefficient
$R(r)$	Radial separable variable
R_i	Resistive impedance
R_m	Mean radius
R_1	Inside radius
R_2	Outside radius
s	Integer 0, 1, 2 ...
t	Time
t_o	Orifice thickness
T	Period
T_o	Temperature of undisturbed air
T_s	Static temperature of air
$T(t)$	Time separable variable
u	Acoustic particle velocity
u_o	Velocity amplitude
U	Number of unknown coefficients
v	Acoustic particle velocity
v_o	Velocity amplitude
V	Velocity magnitude
V_{nm}	Nodal voltage drop
$\underset{\sim}{V}$	Velocity vector
w	Complex function
W	Acoustic power
x	Axial duct coordinate

X	Distance
X_m	Complex matrix
X_s	Circumferential length of slit
$X(x)$	Separable axial variable
$X_{d\ell}$	Distance between delay line orifice plates
y	Transverse duct coordinate
y_1, y_2	Dimensions of straight duct in mapping analysis
y'	$= y - y_2$
$Y(y)$	Separable transverse variable
$Y_{\nu_n}(k_o r)$	Neumann function
z	Transverse duct coordinate
$\underset{\sim}{z}$	Unit vector in the z direction
Z	Acoustic impedance.
$Z(z)$	Separable transverse variable
α_r	Power reflection coefficient
α_t	Power transmission coefficient
α^*	End correction factor
β	Function of x and y
γ	Angle of propagation (ray theory)
γ_s	Ratio of specific heats
Δ	Difference
ε	$= [1 - (\ddot{k}_1/k_o)^2(1 - M^2)]^{\frac{1}{2}}$
ζ	Coordinate of χ complex plane
η	Complex plane of the mapping analysis
θ	Polar coordinate or angle of propagation
θ_p	Experimental phase angle

$\theta(\Theta)$	Separable angular variable
κ	Coordinate of χ complex plane
λ	Wavelength
ν	Angular wavenumber
ξ	$= k_o(\epsilon - M)/(1 - \epsilon M)$
π	$= 3.1415927...$
ρ_o	Density of undisturbed medium
Σ	Summation of terms
σ	Radiation efficiency
ϕ	Velocity potential function
χ	Complex plane of the mapping analysis
χ_i	Reactive impedance
χ_m	Bulk modulus
ψ	Theoretical phase angle
ψ_{mn}	Characteristic function
Ψ	Stream function
ω	Angular frequency
∞	Infinity
∂	Differential operator
$\left.\begin{matrix}-\\ \vert\vert\end{matrix}\right\}$	Absolute value
∇	Gradient operator
∇^2	Laplacian operator
$\backsim$	Maps to
$\rightarrow$	Approaches
$\approx$	Approximately

Superscripts

c	Curved
d	Downstream
i	Incident
r	Reflected
s	Straight
t	Transmitted
u	Upstream

Subscripts

i	Incident
ℓ, n	Axial mode number
m	Transverse mode number
m, n	Axial mode number
n	Transverse mode number
0	m, n = 0
r	In the radial direction
s, n	Axial mode number
t	Transmitted
x	In the axial direction
y	In the transverse y direction
z	In the transverse z direction
θ	In the tangential direction

GENERAL INTRODUCTION

As the demand for faster flow in duct systems increases so does the noise generated by the fan and fluid-duct interaction. Part of the noise generated by the fan and flow is of long wavelength relative to the dimensions of the duct, and the level of this low frequency noise is often unacceptable in such application as libraries or sound studios. In the usual method of low frequency noise control a system of resonators or lined expansion chambers may be employed, but these devices have the disadvantage of excessive size or large pressure drop and usually operate over a narrow frequency range. Alternatively lining the duct with absorbent material is relatively ineffective at low frequencies and unsuitable for low frequency noise control.

The principal aim of this research work is thus to develop an alternative attenuator suitable for control of low frequency sound in rigid walled ducts. It is hoped to eliminate the stated problems of excessive size and pressure drop as well as narrow operating band. The operation of the attenuator is based on a principle described by Rayleigh and attributed to Hershel. It depends upon the generation of impedance mismatches at planes across the duct surface which then cause reflection of sound. The degree of impedance mismatch is controlled by the degree to which series of evanescent modes are generated at these surfaces. The performance of the attenuator is independent of the downstream terminating impedance, a characteristic which distinguishes it from the usual reactive devices such as an expansion chamber.

Two configurations of the attenuator are investigated; one suitable for use in bends in ducts of rectangular cross section and the other designed for use in straight ducts of circular cross section. Investigation of the effects of flow on the performance of these devices is included in the study.

Necessary to the theoretical understanding of the performance of the reactive attenuator is a detailed understanding of propagation theory in hard-walled ducts with and without flow. Such factors as the effect of flow on the cut-off frequencies of higher modes, sound propagation in curved bends with and without flow and the impedance of a surface whose pressure distribution is approximated by a Fourier sum of evanescent modes are closely related to the performance of the attenuator and are carefully considered in the investigation. A large part of the thesis is therefore dedicated to a theoretical and experimental study of propagation of low frequency sound in hard-walled ducts with and without flow. The remainder is concerned with investigation of the proposed attenuator.

PART 1: PROPAGATION THEORY

CHAPTER 1

SOUND PROPAGATION IN STRAIGHT DUCTS OF RECTANGULAR CROSS SECTION

1.1 INTRODUCTION

The basic analysis of sound propagation in straight ducts of rectangular cross section with no mean flow has been investigated thoroughly and is well documented in several texts such as Rschevkin (1963) and Morse and Ingard (1968). Perhaps the first to work on the problem of sound propagation in straight ducts was Rayleigh (1877). His work outlined the essential harmonic nature of sound propagation and showed how the wave equation can be solved in terms of a velocity potential consisting of an infinite Fourier sum of waves. The first major work to outline acoustic distributions and propagation parameters of sound in ducts was due to Morse (1939). Morse considered the case of one absorbing wall in a rectangular duct and laid down the standard boundary conditions used to match general solutions to a particular case. The basic ground work of duct theory has lately been extended to include the more subtle points of propagation with no mean flow. Two papers by Doak (1973) summarize well the more complex cases of modal propagation. He considers the generalized relationships for acoustic power and pressure distributions as well as the effect of different types of sources on spatial distribution of acoustic parameters. Doak also considered the effect of different duct terminations on modal coupling within the duct.

In recent years most work concerning sound propagation in rectangular ducts has been centered on the effect of convection of the propagation medium (particularly on the attenuation obtained due

to lined duct walls). Although the basic derivation of the wave equation and simple solution have been well discussed such as by Morse and Ingard (1968) there are still particular problems that need more investigation. Two of these, the effect of flow on modal cut-off and energy propagation, will be discussed in this thesis.

The first significant work on sound propagation in ducts with shear flow was published by Pridmore-Brown (1958). In a comprehensive analysis Pridmore-Brown developed equations for the variation in sound pressure across the duct which is brought about by the presence of a flow gradient. He also considered the effect of flow on the attenuation obtained from lined walls for both upstream and downstream cases. His work was followed by a spout of others of which most have been concerned with attenuation in lined ducts with flow. The advent of the computer allowed a numerical approach to the solution of the eigen equation, which previously was prohibitively time consuming. Since the following analysis is limited to rigid walled ducts only those relevant works will be discussed.

Ingard (1959) considered the reflection of waves from a boundary between two fluids moving at different relative velocities and showed that the normal impedance was increased by $(1+M\sin\theta)$ where θ is the angle of incidence of the acoustic wave. More importantly his work illustrated the necessity to use continuity of particle displacement as a boundary condition in this case rather than continuity of particle velocity (as used in the no flow case). Morfey (1971) has published a series of important papers concerned with wave propagation in flow. He developed relationships for the impedance and intensity of travelling waves in rigid ducts for higher modes above or below cut-off as well as the plane wave. In particular he found that uniform flow has the effect (for modes well above cut-off) of increasing the

sound power transmitted by a single mode by the factor $(1+M)^2$ in the direction of flow and of decreasing the power transmitted by the factor $(1-M)^2$ in the direction opposite to the flow.

Mason (1969) has experimentally and theoretically investigated the effect of flow on the modal cut-off frequencies in circular ducts. He defined cut-off as the frequency above which propagation occurs without attenuation and found that the cut-off frequency decreased by a factor of $(1-M^2)^{\frac{1}{2}}$ independent of the direction of propagation relative to flow. However his physical explanation for why the cut-off frequency is independent of direction of propagation of sound relative to flow is hard to follow so that the physical explanation will be considered in detail in this thesis.

From the experimental point of view Alfredson (1970) in work on exhaust mufflers, has developed equations for correctly using the impedance tube method for determining reflection coefficients with flow. He shows from an energy transport view that the reflection coefficient can have a maximum of $R_{max} = (1+M)/(1-M)$ before flux reversal occurs for downstream propagation of sound. Thus Alfredson modified the usual standing wave theory to allow determination of reflection coefficients greater than unity.

In this chapter the equations for sound propagation in straight ducts with and without flow are developed. The case of no flow, although well known, will serve to illustrate the method of solution for the less familiar cases of sound propagation in straight ducts with flow and in curved ducts with and without flow. The equations will also be used in analyses in later chapters. For the case of flow the basic equations are developed and discussed. Consideration is given both theoretically and experimentally to the effect of flow on modal cut-off frequencies. A physical explanation of why

cut-off frequencies are independent of direction of propagation relative to flow is proposed. Relationships for the pressure and power reflection coefficients as well as power transmission coefficients for the (0,0) mode of propagation are developed and the effects of flow on these parameters are discussed.

1.2 STRAIGHT RECTANGULAR DUCTS WITHOUT FLOW

In a straight infinite duct with rigid walls the propagating acoustic wave has two major forms. When the wavelength of sound transmitted is much larger than the transverse duct dimensions, the fluctuations travel as a plane wave with a constant pressure and velocity amplitude across the duct. However when the wavelength is small relative to the transverse duct dimensions, an increasing set of non-uniform waves appear, as well as the plane wave. The propagational characteristics of the non-uniform waves are determined by the boundary conditions of the duct. Equations describing this type of behaviour are obtained from a solution of the wave equation in rectangular co-ordinates. The assumptions involved in the derivation of the different forms of the wave equation used are discussed in Appendix 1.

Assuming sinusoidal oscillation, the wave equation takes the well known form of the Helmholtz equation

$$\nabla^2 p - k_o^2 p = 0 \qquad (1.1)$$

where the wave number $k_o = \omega/c_o$. (The constant k_o will be shown to have important physical significance). The derivation of the equations relating pressure and particle velocity in the acoustic field as dictated by equation (1.1) is well known but will be reviewed here as it will serve as a convenient basis for consideration of other less well known properties. The wave is assumed to propagate in a semi-infinite

rigid walled duct. The x axis of the co-ordinate system is chosen parallel to the direction of propagation and the plane normal to the x axis is bounded by the walls of the duct. The origin of the rectangular co-ordinate system is chosen to be the lower corner of one of the duct walls as shown in Figure 1.1.

A general solution of equation (1.1) in separable rectangular co-ordinates is

$$p(x,y,z,t) = X(x)\,Y(y)\,Z(z)\exp[i\omega t] \tag{1.2}$$

After substituting into the wave equation we obtain using separation of variables

$$\frac{X''}{X} = -k_{mn}^2\,,\quad \frac{Y''}{Y} = -k_m^2 \text{ and } \frac{Z''}{Z} = -k_n^2 \tag{1.3}$$

where the prime (') indicates differentiation with respect to the relative co-ordinate.

Solutions to the equations (1.3) are

$$X(x) = \exp[-i\,k_{mn}x] \tag{1.4}$$

$$Y(y) = \cos(k_m y) \tag{1.5}$$

$$Z(z) = \cos(k_n z) \tag{1.6}$$

Thus substituting into equation (1.2) we obtain the general form of the solution of the wave equation

$$p(x,y,z,t) = \sum_{m=o}^{\infty}\sum_{n=o}^{\infty} A_{mn}\,\psi_{mn}(y,z)\,\exp[i(\omega t - k_{mn}x)] \tag{1.7}$$

where

$$\psi_{mn}(y,z) = \cos(k_m y)\cos(k_m z) \tag{1.8}$$

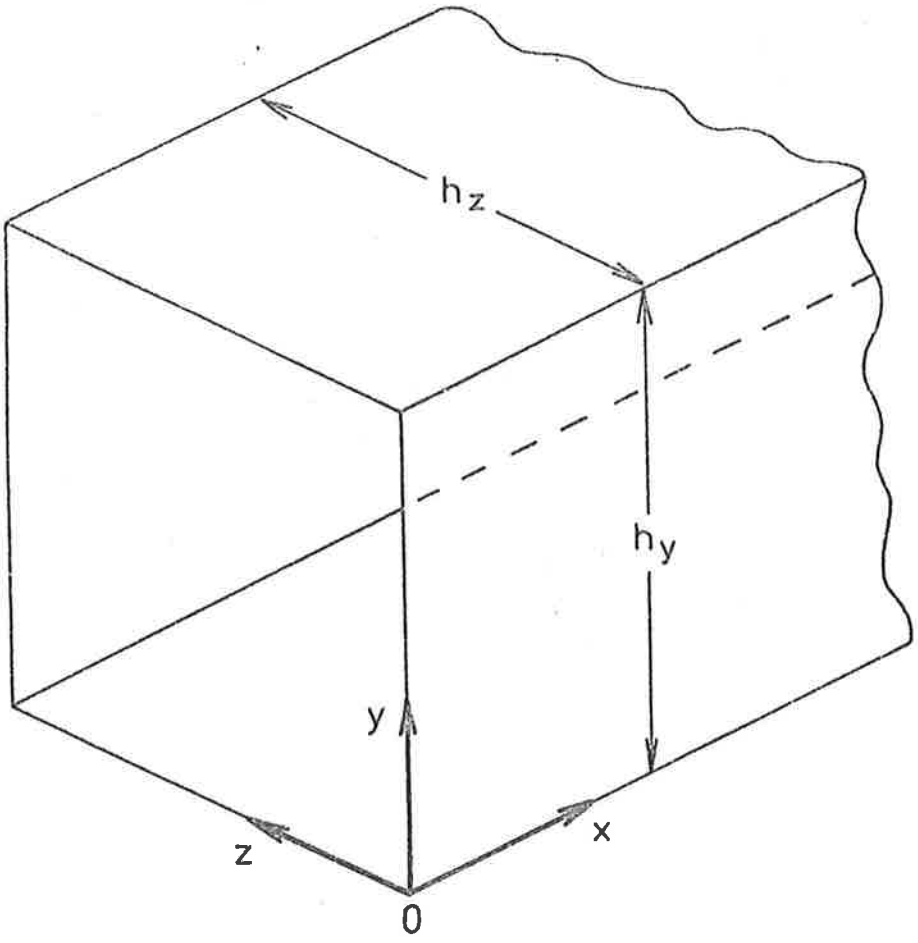

FIGURE 1.1. The rectangular co-ordinate system.

$\psi_{mn}(y,z)$ is called the characteristic function. It has special significance in that it describes the variation in pressure and velocity amplitude over a plane normal to the direction of propagation (the x axis) bounded by the duct walls.

Substitution of equation (1.7) back into the wave equation (1.1) provides an equation relating the wave numbers in the direction of each axis of the co-ordinates system as

$$k_{mn}^2 = k_o^2 - k_m^2 - k_n^2 \tag{1.9}$$

Values of k_m and k_n are obtained by applying the relevant boundary conditions at the duct walls. In this analysis the duct walls are assumed perfectly rigid, therefore the normal acoustic particle velocity at the wall surface is zero. Hence,

$$v_y\Big|_{y = h_y} = 0 \qquad , \qquad v_z\Big|_{z = h_z} = 0 \tag{1.10}$$

From these boundary conditions it follows that

$$k_m = m\pi/h_y \qquad \text{and} \qquad k_n = n\pi/h_z \tag{1.11}$$

where h_y and h_z are the transverse duct dimensions in the y and z directions respectively. Equations (1.11) provide eigen values for the particular problem which govern the natural oscillations in the y-z plane and determine how the wave will propagate.

The modal wave number k_{mn} which determines sound propagation in the x direction is obtained from solutions of the characteristic equation (1.9). Thus

$$k_{mn} = \pm \left[k_o^2 - (m\pi/h_y)^2 - (n\pi/h_z)^2 \right]^{\frac{1}{2}} \tag{1.12}$$

for m, n = 0,1,2 ...

The ± signs of the square root imply propagation in the ± x direction respectively. Each particular combination of integers m and n represent different modes of the corresponding acoustic wave. The characteristics of the corresponding acoustic wave are thus determined by the modal wave number k_{mn}. We note the possibility for a given m and n, not both zero, that for low values of k_o, the value of k_{mn} may be imaginary. In this case the corresponding mode is cut-off and no wave propagates.

If k_{mn} is real or for frequencies such that

$$k_o^2 \geq k_m^2 + k_n^2 \tag{1.13}$$

propagation of the (m,n) mode as described by equation (1.7) will occur in the x direction without attenuation. If m and n are both zero it can be seen that the characteristic function ψ_{mn} will have a value of unity independent of y and z and the corresponding wave will have uniform amplitude across the duct. Similarly from equation (1.12) $k_{oo} = \pm k_o$ and thus this wave number will always be real for all frequencies. The (0,0) mode is the well known plane wave which propagates without attenuation and has uniform phase velocity at all frequencies. A wave such as this is called non-dispersive, that is, its phase velocity is independent of frequency.

If m and n are both not zero then the (m,n) mode will have amplitude variation in the y-z plane as described by equation (1.8). Waves of this type are amplitude modulated over the wave-front. It can be seen that symmetrical distributions about the duct centerline will occur for even values of m and n while odd values of m and n will give rise to asymmetric distributions. The pressure amplitude distributions for the (0,0), (1,0) and (2,0) modes are shown in Figure 1.2.

Phase velocity, the velocity at which the phase angle of a simple harmonic wave of frequency $\omega/2\pi$ progresses along the duct

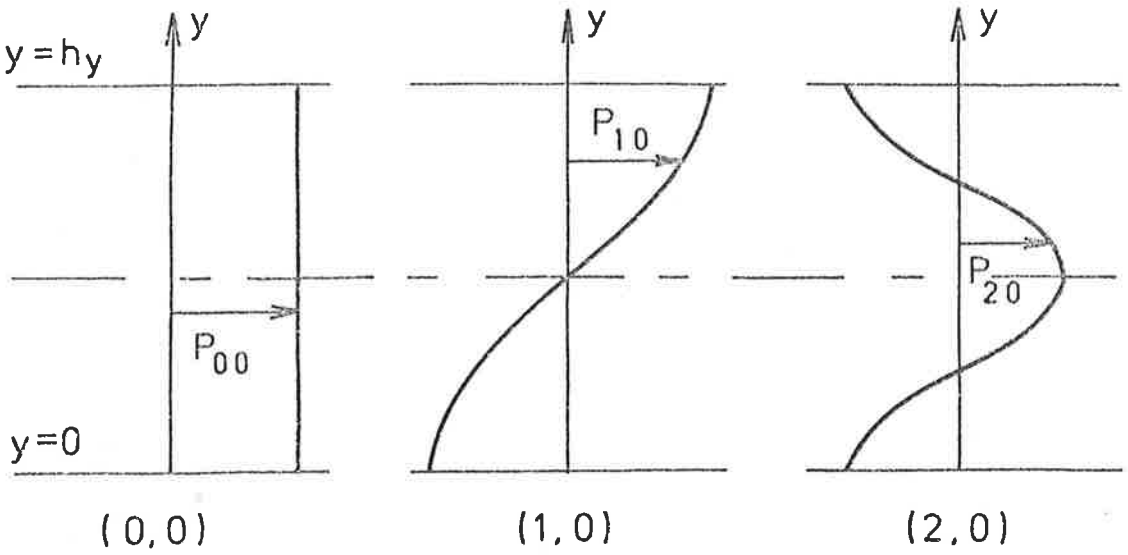

FIGURE 1.2. Pressure amplitude distribution for three modes in a rectangular hard walled duct.

(more generally the wave velocity) follows from equation (1.9) as

$$c_p = \omega/k_{mn} = \frac{\omega}{[k_o^2 - k_m^2 + k_n^2]^{\frac{1}{2}}} \quad . \tag{1.14}$$

When m and n are both zero equation (1.14) shows that the phase speed c_p of the corresponding plane wave is the same as that of a plane wave in free space. Thus when m and n are not both zero the phase velocity of the (m,n) mode is higher than the speed of sound in free space. The plane wave whose phase velocity is independent of frequency is said to be non-dispersive. By contrast equation (1.14) shows that the phase velocities of the higher modes are all frequency dependent and are thus dispersive.

The group velocity is defined as the velocity of progress of a center of waves containing a narrow range of frequencies. Morse and Ingard (1968) give the following expression for the group velocity

$$c_g = \partial\omega/\partial k_{mn} \quad . \tag{1.15}$$

From equation (1.12) it follows that

$$c_g = c_o[1 - (k_m^2 + k_n^2)/k_o^2]^{\frac{1}{2}} \tag{1.16}$$

The group velocity provides an approximate indication of the rate of propagation of energy. Figure 1.3 shows a theoretical plot of the group and phase velocities for three modes plotted as functions of the non-dimensional frequency parameter $k_o h$.

Considering equation (1.12) again, if either m and n are not zero there will always be a frequency below which k_{mn} is imaginary and the corresponding (m,n) mode will not propagate. At this frequency commonly called the "cut-off" frequency defined by equation (1.17)

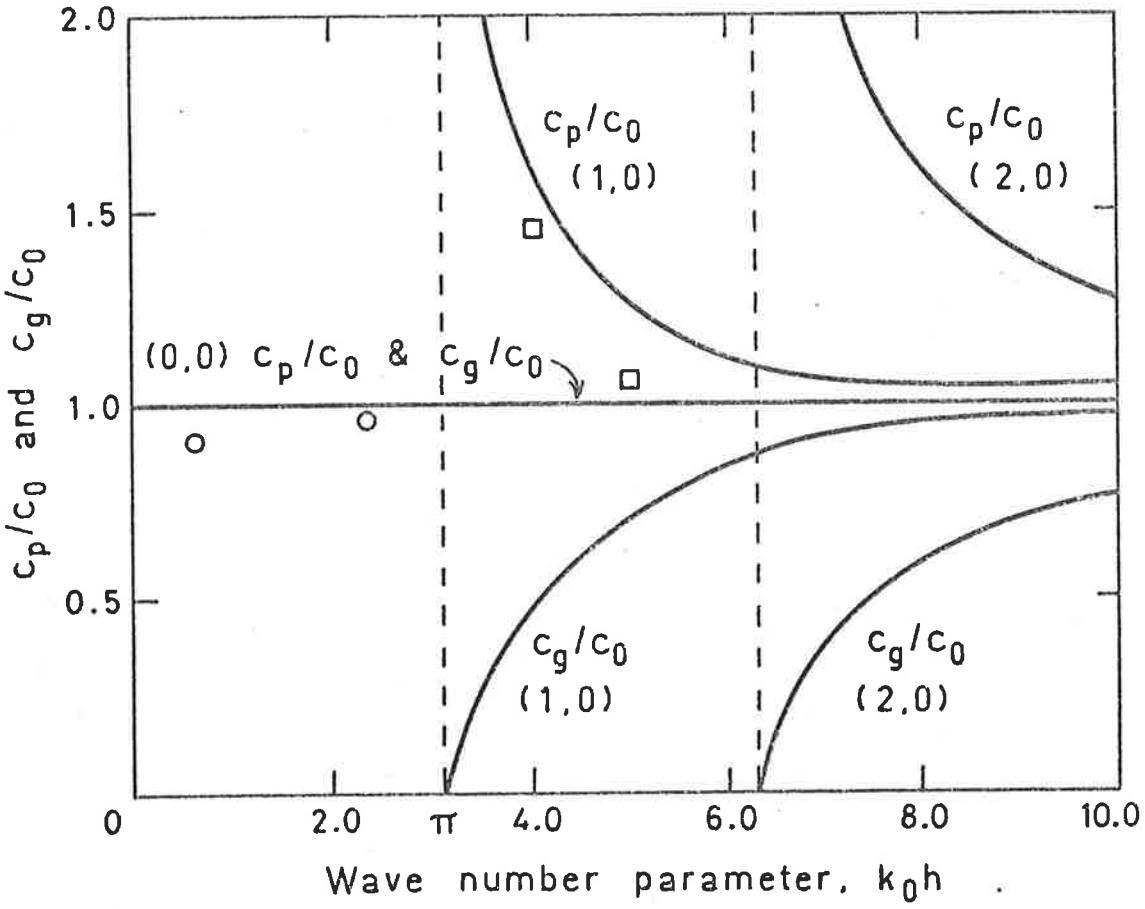

FIGURE 1.3. Phase and group velocity of the (0,0) and (1,0) mode in a rectangular duct. ——— , theoretical; O , experimental c_p/c_o for (0,0) mode; □, experimental c_p/c_o for (1,0) mode.

$$f_c = (c_o/2\pi)[k_m^2 + k_n^2]^{\frac{1}{2}} \qquad (1.17)$$

the corresponding modal wave number k_{mn} has the value zero. At these discrete frequencies the wave consists of standing waves in the y-z plane and the wave as such does not propagate. Furthermore at the cut-off frequency the mode under consideration can be seen from equation (1.14) to have an infinite phase velocity; all oscillations are in phase along the x axis. As such the vibrations are induced down the duct rather than propagated. Equation (1.16) predicts that the group velocity will be zero at cut-off and this implies that all energy flow away from the generating surface ceases.

For frequencies below the cut-off frequency of a particular mode, k_{mn} is imaginary. Thus from equation (1.7) the mode does not propagate; the disturbance decays exponentially with increasing distance x away from the generating surface by the factor e^{-1} in a distance $1 / k_{mn}$. Thus as the driving frequency of an evanescent mode approaches cut-off the rate of decay with distance decreases. Furthermore the axial acoustic particle velocity of the non-propagating evanescent mode is in quadrature with the acoustic pressure so that an evanescent mode carries no nett energy away form the generating surface. Such a mode might be thought of as a standing wave in the y-z plane whose amplitude decays with distance x.

From the above considerations we conclude that acoustic waves in straight ducts may consist of a plane wave and the sum of a large number of propagating or non-propagating modes as well. The Fourier amplitude coefficients A_{mn} of these waves are determined by applying boundary conditions at the generating surface in the y-z plane which may be taken at the origin of the x axis ($x = 0$) for convenience. Higher modes are usually generated in ducts by discontinuities such as a step

change in area of the duct or by non-uniformities in the driving surface. Higher modes, below cut-off, generated at such a discontinuity will decay rapidly away from their origin leaving the lower modes to transmit energy along the duct.

It is useful here to introduce the concept of "ray" propagation. Higher propagating modes in straight ducts with rigid walls can be imagined in terms of plane acoustic waves called "rays" which travel in straight lines at an angle γ to the x axis with propagational speed c_o as shown in Figure 1.4 for the two-dimensional case ($z = 0$).

The direction of propagation of the waves is given by

$$\cos\gamma = \pm \frac{k_{mo}}{k_o} \tag{1.18}$$

Here advantage has been taken of the vectorial properties of the wave numbers. The wave field at any point is obtained by vectorial superposition of these waves. At the cut-off frequency for each mode the rays travel in a transverse direction to the x axis and there is no propagation. At frequencies below cut-off this representation is not possible however, as all quantities including the resulting angles of propagation are imaginary. Figure 1.4 can also be described in terms of vectorial wave numbers. For the two-dimensional case for which $k_n = 0$, equation (1.9) can be seen to satisfy the arrangement of Figure 1.4 where k_{mn} is the wave number vector parallel to the x axis, k_m is the wave number in the transverse direction and k_o the vector of the plane wave front.

The acoustic intensity of propagating waves without flow is defined as

$$I_x = \langle p\, v_x \rangle \tag{1.19}$$

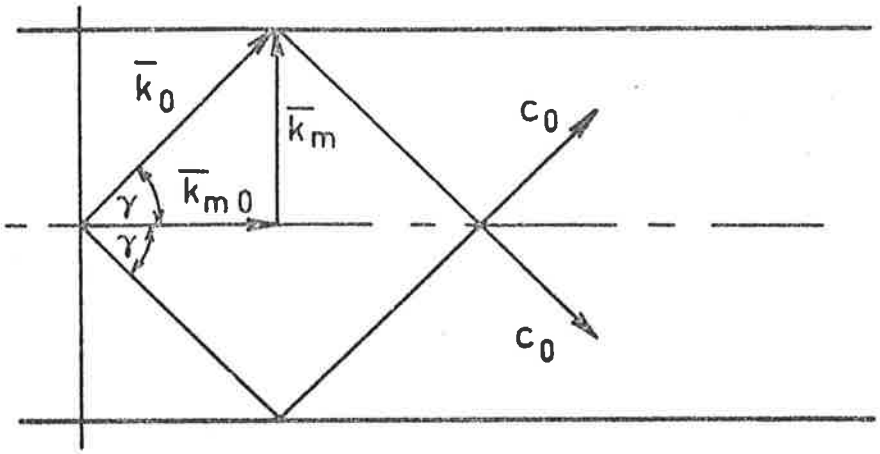

FIGURE 1.4. Ray theory of propagation.

On the other hand the particle velocity of a plane wave is given by $p/\rho_o c_o$ thus reference to Figure 1.4 and equation (1.18) gives the following for the component of particle velocity v_x

$$v_x = \frac{k_{mn}}{\rho_o c_o k_o} p \tag{1.20}$$

Therefore the intensity in the x direction is

$$I_x = \frac{\pm|p|^2 (k_{mn}/k_o)}{2\rho_o c_o} \tag{1.21}$$

where the ± signs refer to intensity in the positive and negative x directions respectively. Below cut-off the intensity is imaginary and thus no nett energy is propagated.

For two plane waves P^i_{oo} and P^r_{oo} travelling in opposite directions in a rigid wall duct of constant cross section the pressure reflection coefficient is defined as

$$R = |P^r_{oo}/P^i_{oo}| \tag{1.22}$$

where P^r_{oo} and P^i_{oo} are complex amplitudes of incident and reflected waves respectively.

The ratio of reflected power to incident power is called the power reflection coefficient and is defined as

$$\alpha_r = |P^r_{oo}/P^i_{oo}|^2 \tag{1.23}$$

On the other hand the ratio of transmitted energy to incident energy is called the transmission coefficient and is defined as

$$\alpha_t = |P^t_{oo}/P^i_{oo}|^2 \tag{1.24}$$

P^t_{oo} is the resultant pressure amplitude of the propagating wave. From conservation of acoustic energy the plane reflection and transmission coefficients are related by

$$\alpha_t + \alpha_r = 1 \tag{1.25}$$

1.3 STRAIGHT RECTANGULAR DUCTS WITH UNIFORM FLOW

The propagation of sound in straight ducts with uniform flow of the propagating medium is characterized, as for straight ducts with no flow, by modes which decay with distance at low frequencies and propagate at high frequencies. However the frequency at which these modes "cut on or off" is not as clearly defined as in the case without flow.

The wave equation for sound propagation with uniform flow of the propagating medium is according to Morse and Ingard (1968)

$$c_o^2 \nabla^2 p - (\partial/\partial t + \underset{\sim}{V}\cdot\nabla)^2 p = 0 \tag{1.26}$$

where $\underset{\sim}{V} = V_x \underset{\sim}{i} + V_y \underset{\sim}{j} + V_z \underset{\sim}{z}$ is the vector describing the magnitude and direction of the fluid flow. In the following analysis the fluid flow is assumed uniform, irrotational, inviscid and parallel to the x axis but independent of x.

For flow in the x direction, parallel to the direction of propagation, equation (1.26) reduces to

$$c_o^2 \nabla^2 p - (\partial^2/\partial t^2 + 2V_x \partial^2/\partial x \partial t + V_x^2 \partial^2/\partial x^2)\, p = 0 \tag{1.27}$$

The solution of the wave equation (1.27) is obtained using a similar process to the case without flow and can be written in separable rectangular co-ordinates as

$$p(x,y,z,t) = X(x)\,Y(y)\,Z(z)\exp[i\omega t] \tag{1.28}$$

As previously after substitution of equation (1.28) into the wave equation (1.27) and separation of variables we arrive at the general form of the pressure solution for sound propagation in straight ducts with superimposed flow,

$$p(x,y,z,t) = \sum_{m=o}^{\infty}\sum_{n=o}^{\infty} P_{mn}\cos(k_m y)\cos(k_n z)\exp[i(\omega t \pm k_{mn} x)] \tag{1.29}$$

Substitution of equation (1.29) into the original wave equation provides the following relation between the wave numbers

$$k_{mn}^2(1-M^2) + 2Mk_o k_{mn} + (k_m^2+k_n^2) - k_o^2 = 0 \tag{1.30}$$

Equation (1.30) describes downstream sound propagation. In contrast to the case without flow (see equation 1.12) the relation is now dependent upon the Mach number of the flow $M = V_x/c_o$.

Rather than use one form of the exponential in equation (1.29) and let the ± signs determine the direction of propagation it is clearer in this case to assume that sound propagates in the positive x direction and consider upstream and downstream sound propagation by appropriate choice of the sign of the Mach number. Thus for upstream propagation

$$k_{mn}^2(1-M^2) - 2Mk_o k_{mn} + (k_m^2+k_n^2) - k_o^2 = 0 \tag{1.31}$$

Equations (1.30) and (1.31) are the characteristic equations determining modal propagation characteristics with flow. Solutions of the quadratic equations provide values of modal wave numbers for the downstream and upstream cases, for varying Mach numbers, as follows,

$$k_{mn}^d = [-Mk_o + (k_o^2 - (1-M^2)(k_m^2+k_n^2))^{\frac{1}{2}}]/[1-M^2] \tag{1.32}$$

and $$k^{u}_{mn} = [M k_o + (k_o^2 - (1-M^2)(k_m^2 + k_n^2))^{\frac{1}{2}}] / [1-M^2] \quad (1.33)$$

In equations (1.32) and (1.33) superscripts d and u denote downstream and upstream propagation of sound respectively.

Eigen values of k_m and k_n are derived by applying the boundary condition for rigid walls. As the particle velocity is normal to the walls it is sufficient to use continuity of normal particle velocity. The result is the same as the case without flow for perfectly rigid walls.

$$k_m = m\pi/h_y \quad , \quad k_n = n\pi/h_z \quad (1.34)$$

For $m = n = o$ equations (1.32) and (1.33) reduce to

$$k^{d}_{oo} = k_o/(1+M) \quad (1.35)$$

$$k^{u}_{oo} = k_o/(1-M) \quad (1.36)$$

The characteristic function $\psi(y,z)$ is identical to the case without flow and is equal to unity. Thus the (0,0) mode with superimposed flow also has uniform pressure and velocity amplitude across the duct. Equations (1.35) and (1.36) imply that flow has the effect of increasing the wavelength for the (0,0) mode for downstream propagation and decreasing the wavelength for upstream propagation. Similarly, as the acoustic waves will travel at c_o relative to the flow, the speed of propagation of the (0,0) mode relative to the duct is

$$c^{d}_{o} = c_o(1+M) \quad (1.37)$$

and $$c^{u}_{o} = c_o(1-M) \quad (1.38)$$

Thus for an observer at rest the frequency measured is the same irrespective of the direction of propagation and is unchanged by superimposed

flow of the propagating medium.

The phase velocity relative to the duct co-ordinate system is more generally

$$c_p^d = \omega/k_{mn}^d \tag{1.39}$$

and

$$c_p^u = \omega/k_{mn}^u \tag{1.40}$$

Substitution of $m = n = o$ in equations (1.39) and (1.40) gives the same value of phase speed or wave velocity as given by equations (1.37) and (1.38) derived on the basis of relativistic considerations.

The group velocity c_g as defined by equation (1.15), remains unchanged. Thus for the case of downstream flow, using equations (1.15) and (1.32)

$$c_g^{-1} = \partial k_{mn}/\partial\omega = \frac{-M}{c_o[1-M^2]} + \frac{1}{[1-M^2]}\,(k_o^2 - (1-M^2)\ddot{k}_1^2)^{-\frac{1}{2}}\,\frac{\omega}{c_o^2} \tag{1.41}$$

where $\ddot{k}_1^2 = k_m^2 + k_n^2$.

Hence $c_g^{-1} = \dfrac{1}{c_o[1-M^2]}\,[-M + (k_o^2 - (1-M^2)\ddot{k}_1^2)^{-\frac{1}{2}} k_o]$

$$= \frac{1}{c_o[1-M^2]}\,[-M + \frac{k_o}{(k_o^2 - (1-M^2)\ddot{k}_1^2)}\,]$$

$$= \frac{1}{c_o[1-M^2]}\,[\,\frac{-M(k_o^2 - (1-M^2)\ddot{k}_1^2)^{\frac{1}{2}} + k_o}{(k_o^2 - (1-M^2)\ddot{k}_1^2)^{\frac{1}{2}}}\,]$$

$$= \frac{1}{c_o[1-M^2]}\,[\,\frac{-M(1 - (1-M^2)(\ddot{k}_1/k_o)^2)^{\frac{1}{2}} + 1}{(1 - (1-M^2)(\ddot{k}_1/k_o)^2)^{\frac{1}{2}}}\,]$$

$$\text{Thus } c_g^d = \frac{c_o[1-M^2][1-(1-M^2)(\ddot{k}_1/k_o)^2]^{\frac{1}{2}}}{1-M[1-(1-M^2)(\ddot{k}_1/k_o)^2]^{\frac{1}{2}}} \tag{1.42}$$

The case for upstream flow is obtained by changing the sign of the Mach number. Hence

$$c_g^u = \frac{c_o[1-M^2][1-(1-M^2)(\ddot{k}_1/k_o)^2]^{\frac{1}{2}}}{1+M[1-(1-M^2)(\ddot{k}_1/k_o)^2]^{\frac{1}{2}}} \tag{1.43}$$

For $M = 0$ equations (1.42) and (1.43) reduce to

$$c_g = c_o[1-(\ddot{k}_1/k_o)^2]^{\frac{1}{2}}$$

which is identical to the case without flow given by equation (1.16). Figure 1.5 shows a plot of theoretical phase and group velocities for a flow of $M = 0.1$. Inspection of equation (1.29) and use of equations (1.34) provides the characteristic function $\psi(y,z)$ with flow

$$\psi(y,z) = \cos[(m\pi/h_y)y]\cos[(n\pi/h_z)z] \tag{1.44}$$

This is exactly of the form given by equation (1.8) for the case without flow. Thus the amplitude distribution of modes in the plane transverse to the direction of propagation is identical to the case without flow and thus the mode shapes will be identical to those given in Figure 1.2.

1.3.1 Cut-off Frequencies with Flow

As for the case of propagation of sound in a stationary medium, modal propagation in a medium that is convecting relative to the duct walls is characterized by frequencies at which the propagational behaviour of the mode, other than the plane wave, will drastically change. In the case without flow, this frequency is defined clearly as when the modal wave number k_{mn} is zero. At this frequency the phase

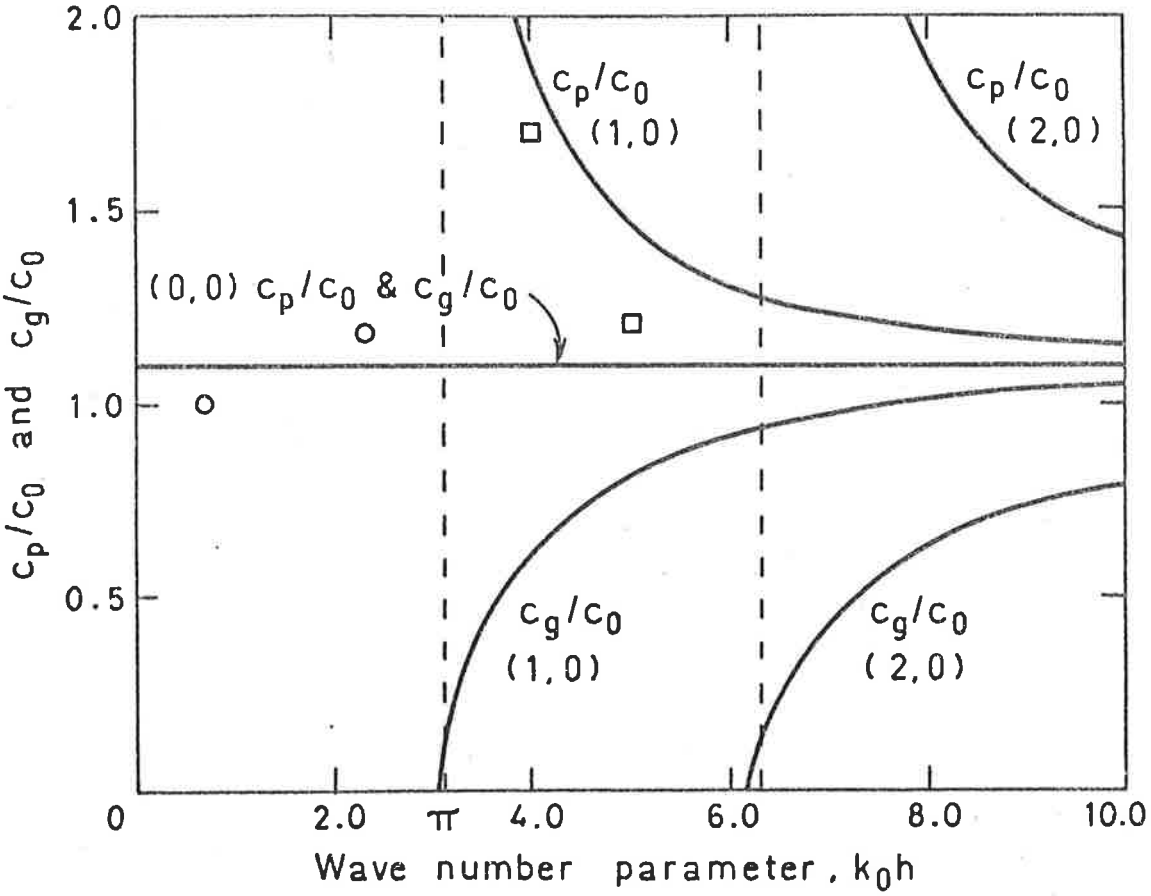

FIGURE 1.5. Phase and group velocity of the (0,0) and (1,0) mode with downstream propagation of sound at M = 0.1. ——, theoretical; ○, experimental c_p/c_o for (0,0) mode; □, experimental c_p/c_o for (1,0) mode.

velocity of the mode is infinite as previously discussed and for all frequencies less than the cut-off the wave number is imaginary and no wave propagates: the disturbance decays exponentially with distance x along the duct. Similarly the group velocity is zero at the cut-off frequency in the case without flow. All of these marked changes in the propagational characteristics of a particular mode occur at one discrete frequency, thus there is no difficulty in defining the cut-off frequency. However in the case of convection of the propagating medium, the definition of cut-off is not quite so clear, as some of the previous mentioned characteristics occur at different frequencies.

To discuss this matter we define two important wave numbers

$$\ddot{k}_1^2 = k_m^2 + k_n^2 \tag{1.45}$$

$$\ddot{k}_2^2 = (1 - M^2)(k_m^2 + k_n^2) < \ddot{k}_1^2 \ , \ M < 1 \tag{1.46}$$

The explanation of mode behaviour with frequency will be based upon the parameters of group velocity, phase velocity and vectorial wave number. For discussion of the latter parameter equations (1.30) and (1.31) can be rewritten as

$$k_{mn}^2 + (k_m^2 + k_n^2) = (k_o - M\, k_{mn})^2 \tag{1.47}$$

and

$$k_{mn}^2 + (k_m^2 + k_n^2) = (k_o + M\, k_{mn})^2 \tag{1.48}$$

for the downstream and upstream cases respectively. On inspection of equations (1.47) and (1.48) it can be seen that each term represents vectorial components, the sum of which can be represented graphically. The components, assumed travelling in their correct directions (i.e., k_{mn} in the x direction) and the

resultant angles of propagation of the wave front discussed previously in the ray theory are shown in Figure 1.6 for different frequency ranges to be discussed next. We shall consider the case of downstream propagation of sound first. In this case equation (1.32) can be rearranged as

$$k_{mn}^{d} = k_o[-M + (1-(1-M^2)(\ddot{k}_1^2/k_o^2))^{\frac{1}{2}}]/[1-M^2] \tag{1.49}$$

Thus when $k_o > \ddot{k}_1$ the modal wave number k_{mn} is a positive real number and the wave propagates downstream as assumed. This situation is shown vectorially in Figure 1.6.

When $k_o = \ddot{k}_1$ equation (1.49) reduces to

$$k_{mn}^{d} = k_o[-M+M]/[1-M^2] = 0 \tag{1.50}$$

Thus when $k_o = \ddot{k}_1$ the modal wave number is zero and as given by equation (1.39) the phase velocity is infinite. Thus at this frequency, identical to the no-flow cut-off frequency, the acoustic oscillations along the duct are in phase independent of x. In the case without flow, this condition gave a group velocity of zero implying no energy propagation. In the case of superimposed flow the group velocity is not zero and is

$$c_g = \frac{c_o[1-M^2][1-(1-M^2)]^{\frac{1}{2}}}{1-M[1-(1-M^2)]^{\frac{1}{2}}}$$

$$= \frac{c_o[1-M^2]M}{[1-M^2]}$$

$$= c_o M$$

$$= V_x \tag{1.51}$$

Equation (1.51) implies that for $k_o = \ddot{k}_1$ (downstream propagation)

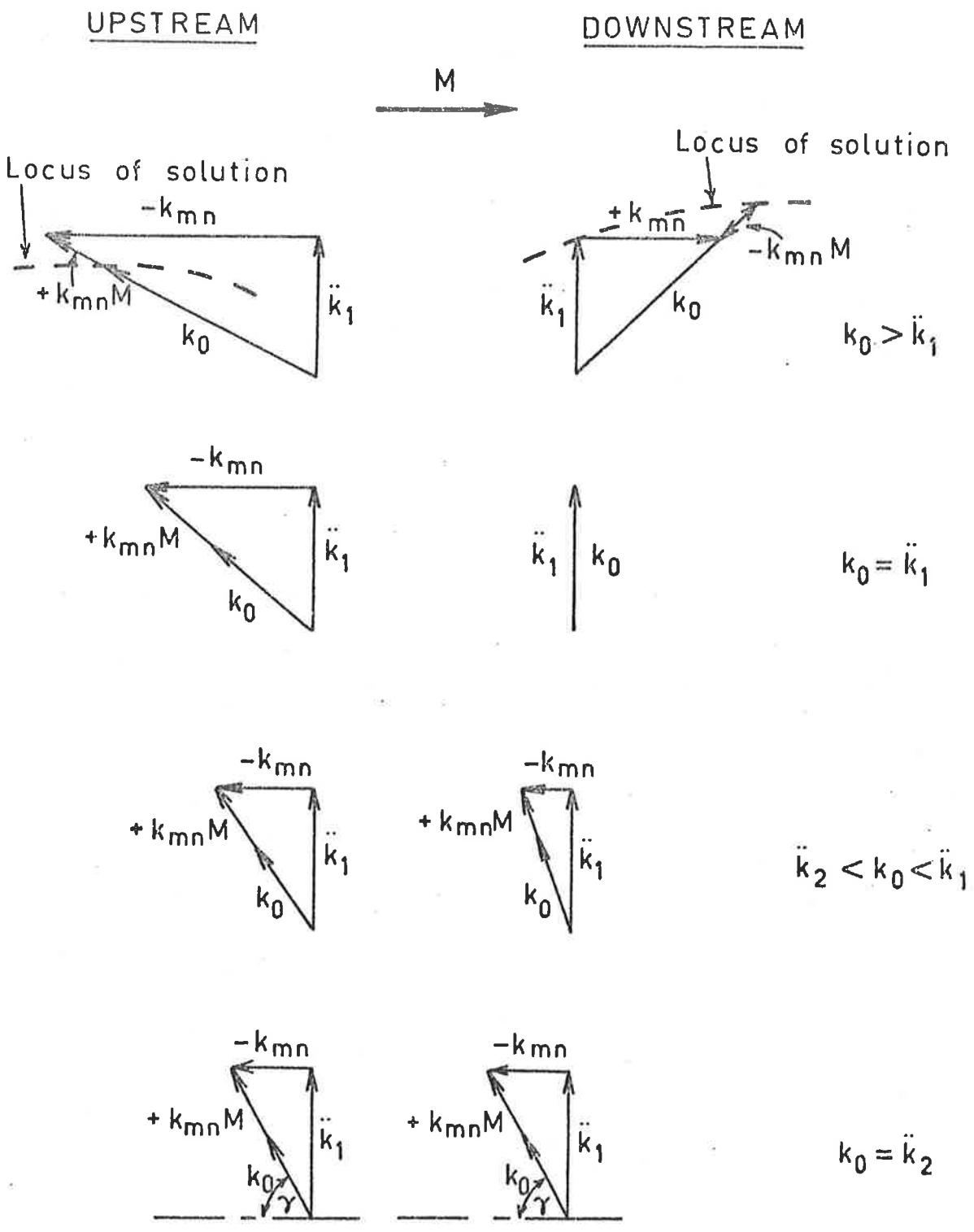

FIGURE 1.6. Vectorial representation of wave numbers with uniform flow.

the wave motion consists of a series of convected standing waves, transverse to the x axis, with no real acoustic propagation. As all acoustic vibrations are in phase, independent of x (in the positive x direction) no energy is propagated due to acoustic motion (as implied by an infinite phase velocity), the resultant energy flux being due entirely to convection of the fluid (as implied by a group velocity equal to the velocity of the flow). Thus convection of the propagating medium gives rise to a "psuedo wave" at $k_o = \ddot{k}_1$ for downstream propagation.

This characteristic is also demonstrated vectorially in Figure 1.6. As k_o decreases in magnitude until $k_o = \ddot{k}_1$, the locus of the solution, moves as shown in Figure 1.6 for the downstream case until when $k_o = \ddot{k}_1$ there is no resultant acoustic propagation (since $\ddot{k}_1$ and k_o are parallel). However to obtain the actual flow induced propagation the effect of flow velocity has to be considered. This will be discussed in more detail at the cut-off condition.

When $\ddot{k}_1 > k_o > \ddot{k}_2$ for downstream propagation of sound the modal wave-number will be

$$k_{mn} = k_o[-M + (1 - \ddot{k}_2^2/k_o^2)^{\frac{1}{2}}] / [1 - M^2] \qquad (1.52)$$

which is a negative real number as shown vectorially in Figure 1.6. The negative value of the wave number does not imply that the acoustic wave is now propagating in the opposite direction (i.e. upstream) to what was initially assumed, as convection of the particle velocities relative to phase speed and wave number has to be considered. This will be discussed in more detail in the next frequency range. Similarly the group velocity from equation (1.42) can be seen to have a positive value in the frequency range $\ddot{k}_1 > k_o > \ddot{k}_2$ implying downstream propagation of energy as assumed initially. Thus the direction of vectorial wave numbers derived from equation (1.52) are relative to k_m convecting with

the flow. This situation is shown vectorially in Figure 1.6. It must be remembered for $\ddot{k}_1 > k_o \gtrless \ddot{k}_2$ that since k_{mn} changes sign so does $k_{mn}M$ and this component changes direction vectorially.

When $k_o = \ddot{k}_2$ equation (1.43) predicts that the group velocity will be zero and there will be no propagation of energy due to either wave motion or convection. At this frequency the modal wave number is

$$k_{mn} = -Mk_o / [1 - M^2] \tag{1.53}$$

and equation (1.47) becomes (in a magnitude sense) for $k_o = \ddot{k}_2$

$$\bar{k}_m^2 + \bar{\ddot{k}}_1^2 = (\bar{k}_o + M\bar{k}_{mn})^2 \tag{1.54}$$

as demonstrated vectorially in Figure 1.6. If one imagines a co-ordinate system convecting with the flow (i.e. the plane wave has a phase speed equal to c_o rather than $c_o(1+M)$) and considers the propagation in terms of the vectorial "ray model" discussed in the case without flow then the angle γ at which the plane wave front will propagate is derived from the vector diagram of Figure 1.6 as

$$\cos\gamma = \frac{\bar{k}_{mn}}{\bar{k}_o + M\bar{k}_{mn}} \quad , \ddot{k}_2 \leqslant k_o < \ddot{k}_1 \tag{1.55}$$

To obtain the actual direction of the wave, however, one has to vectorially add the flow velocity to restore the situation to the state we were initially considering. In terms of velocities (since this is the physically measureable parameter of the flow) a flow velocity of V_x must be subtracted vectorially from the wave travelling at c_o at an angle γ to the transverse axis to obtain the direction of propagation of the "ray" relative to the stationary duct walls. It must be remembered that the moving co-ordinate system is only used to determine angles of

propagation of the "rays" to visualize the directions of wave fronts. Actual magnitudes of wave numbers and phase speeds are still determined from equations (1.32) and (1.33) and equations (1.39) and (1.40) respectively. At cut-off the particles will vibrate in normal direction to the stationary duct walls. This situation is shown in Figure 1.7. From this figure the angle γ necessary to produce a natural standing wave with flow (and no nett propagation of the wave) can be seen to be

$$\cos\gamma = \frac{V}{c_o}$$

$$= M \qquad (1.56)$$

Thus equating the condition for cut-off as defined by equation (1.56) to the vectorial representation of wave numbers for $\ddot{k}_1 > k_o \geq \ddot{k}_2$ we see that

$$M = \frac{\bar{k}_{mn}}{\bar{k}_o + M\bar{k}_{mn}}$$

Hence $$M\bar{k}_o + M^2\bar{k}_{mn} = k_{mn}$$

and at cut-off $$\bar{k}_{mn} = \frac{M\bar{k}_o}{(1-M^2)} \qquad (1.57)$$

As demonstrated previously the frequency at which k_{mn} assumes the value given by equation (1.57) is that given by $\ddot{k}_2$. Thus when $k_o = \ddot{k}_2 = (1-M^2)\ddot{k}_1^2$ the particles will vibrate normal to the walls and there will be no resultant propagation. This is identical to the physical condition, in terms of direction of particle velocity, of the no flow case. Below this frequency the wave does not propagate.

It can also be seen from Figure 1.7 that although the phase speed is negative for $\ddot{k}_1 > k_o > \ddot{k}_2$ the resultant propagation after consideration of convection is downstream as assumed.

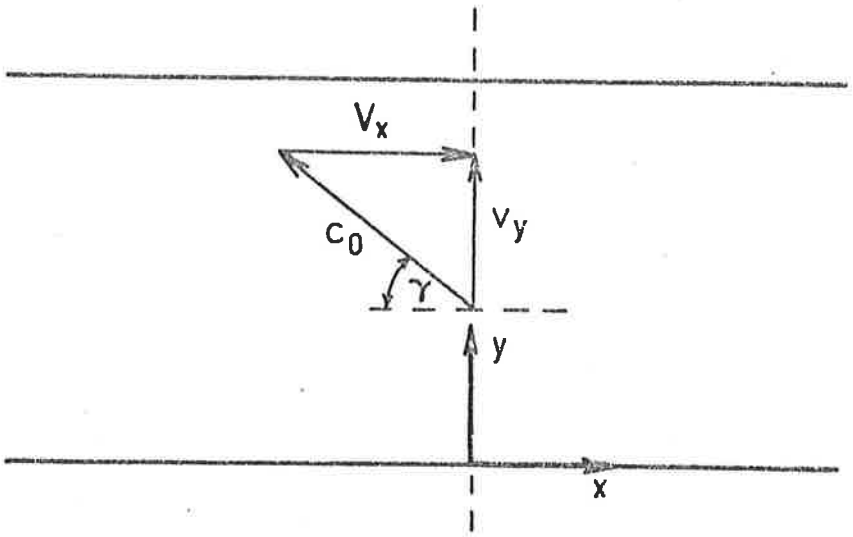

FIGURE 1.7. The vector condition at cut-off.

For $k_o < \ddot{k}_1$ the modal wave number is the following complex number

$$k_{mn} = -(Mk_o/[1-M^2]) - i(\ddot{k}_2^2 - k_o^2)^{\frac{1}{2}}/[1-M^2] \qquad (1.58)$$

In this case the wave process consists of a series of standing waves whose amplitudes decay with increasing distance downstream. The real part of the expression is identical to k_{mn} when $k_o = \ddot{k}_2$ and thus as discussed previously ensures that the particles are vibrating normal to the duct walls after superposition of convection. As such no wave propagation or energy propagation occurs. In this frequency range the group velocity is imaginary implying no propagation of energy.

For upstream propagation of sound the modal wave number is derived from equation (1.33).

When $k_o > \ddot{k}_1$ the wave number is a positive real number and propagation will occur in the upstream direction as assumed (note corresponding form of the exponential in the upstream case). The vectorial representation of the wave numbers for the upstream case given by equation (1.48) is shown in Figure 1.6.

When $k_o = \ddot{k}_1$ the modal wave number is

$$k_{mn} = 2Mk_o/[1-M^2] \neq 0 \qquad (1.59)$$

Hence at this frequency for the upstream case the phase velocity is not infinite as for the downstream case and propagation will continue upstream purely due to acoustic motion. The corresponding group velocity at this frequency is negative and hence there is a nett energy flux upstream. As k_o decreases towards $\ddot{k}_1$ the locus of the vector k_o moves as implied in Figure 1.6.

For $\ddot{k}_1 > k_o > \ddot{k}_2$ the modal wave number for the upstream case is a positive real number given by

$$k_{mn} = k_o[M + (1 - \ddot{k}_2^2/k_o^2)^{\frac{1}{2}}] / [1 - M^2] \qquad (1.60)$$

From the vector diagram of Figure 1.6, the angle at which this ray propagates relative to a wave travelling at speed c_o upstream is less than the angle γ discussed previously, necessary for cut-off. Thus even though the flow convects the particles downstream there is still a nett propagation of the wave upstream. This also is expressed by the value of group velocity in this frequency range which is still negative indicating upstream propagation of energy.

When $k_o = \ddot{k}_2$ for the upstream case

$$k_{mn} = M k_o /[1 - M^2] \qquad (1.61)$$

The vectorial arrangement of the wave numbers for $k_o = \ddot{k}_2$ and upstream propagation of sound is shown in Figure 1.6. As can be seen from the figure and deduced from equation (1.48) the vectorial arrangement of wave numbers for the upstream case is identical to the downstream case, due to reversal of the sign of k_{mn} in the frequency range $\ddot{k}_1 > k_o \geq \ddot{k}_2$ for the downstream case. Hence the resultant angle of propagation relative to a moving co-ordinate system is identical to the downstream case. Thus at this frequency the upstream wave motion will also consist of a transverse standing wave with a resultant particle velocity normal to the duct wall. At this frequency the group velocity is also zero and hence there is no nett energy of propagation upstream.

When $k_o < \ddot{k}_2$ the wave number k_{mn} is complex and the wave process will consist of a series of attenuated standing waves. In this frequency range there is no energy or wave propagation.

Thus if one chooses energy propagation as the determination of a cut-off frequency as it is identical for both the upstream and downstream cases, then the frequencies at which modes cut-off are given by,

$$f_c = (c_o/2\pi)[k_m^2 + k_n^2]^{\frac{1}{2}} [1 - M^2]^{\frac{1}{2}} \qquad (1.62)$$

The preceding analysis also shows why the cut-off frequency is identical independent of the direction of propagation of sound relative to the flow. This phenomena, which appears confusing if one tries to determine the cut-off frequency in terms of wavelength considerations, is due to the negative value of phase speed and wave number which occurs when $\ddot{k}_2 \leq k_o < \ddot{k}_1$ for the downstream case.

The above equations show that the axial wave numbers for higher modes are real for $k_o \geq \ddot{k}_2$ and complex for $k_o < \ddot{k}_2$. For $k_o \geq \ddot{k}_2$ the corresponding wave number k_{mn} may be either positive or negative for downstream propagation of sound. As Morfey states "it is worth noting that the + and - signs (of the exponential) do not necessarily correspond to positive and negative phase velocities in x direction. What they do correspond to is direction of energy transmission along the duct". Morfey came to this conclusion by developing equations for the intensity of sound in ducts with flow. These equations will be discussed in a later section.

Equation (1.62) predicts that the cut-off frequency will decrease with increasing Mach number of the convecting flow. This effect has been experimentally observed by Mason (1969). Mason also proposed a vectorial arrangement identical to Figure 1.7 to predict the frequency at which the particle velocity is normal to the wall. However Mason explains the fact that the cut-off is identical for both upstream and downstream propagation by stating that in a figure identical to Figure 1.7 "no assumption has been made concerning the basic direction in which the sound is propagating".

The analysis presented here clearly demonstrates that the independence of cut-off frequency from direction of propagation of

sound is due to the identical sign and magnitude of phase velocity for the upstream and downstream cases when $k_o = \ddot{k}_2$. Mason's derivation of the cut-off frequency depends upon the assumption that the ratio of the duct radius to the acoustic wavelength is invariant with flow speeds, and the result only holds for low Mach numbers. However the analysis here in terms of convected wave numbers exactly predicts the cut-off frequency for all Mach numbers less than unity.

It is useful to expand Figure 1.5 for the small frequency region near $\ddot{k}_1$ and $\ddot{k}_2$ to demonstrate the difference in phase velocity for the downstream and upstream cases near cut-off. Figure 1.8 shows that the phase velocity of the downstream propagating higher mode approaches positive infinity for k_o approaching $\ddot{k}_1$. When $k_o < \ddot{k}_1$ however the phase velocity changes sign to negative and reduces to a fixed value of $c_p/c_o = -(1-M^2)/M$ when $k_o = \ddot{k}_2$. The phase velocity of the upstream propagating mode never approaches infinity but steadily increases as k_o approaches $\ddot{k}_1$ to a constant value of $-(1-M^2)/M$ when $k_o = \ddot{k}_2$, a value equal in sign and magnitude to the upstream case.

1.3.2 Energy Transmission

The equations describing sound power transmission along a duct with mean flow have been derived by Morfey (1971). Assuming a pressure form of the wave equation with flow the axial particle velocities for the forward and reflected waves are derived from the linearized momentum equation and are,

$$v_x^d = \left(\frac{p}{\rho_o c_o}\right)(\varepsilon - M)/(1 - \varepsilon M) \tag{1.63}$$

$$v_x^u = -\left(\frac{p}{\rho_o c_o}\right)(\varepsilon + M)/(1 + \varepsilon M) \tag{1.64}$$

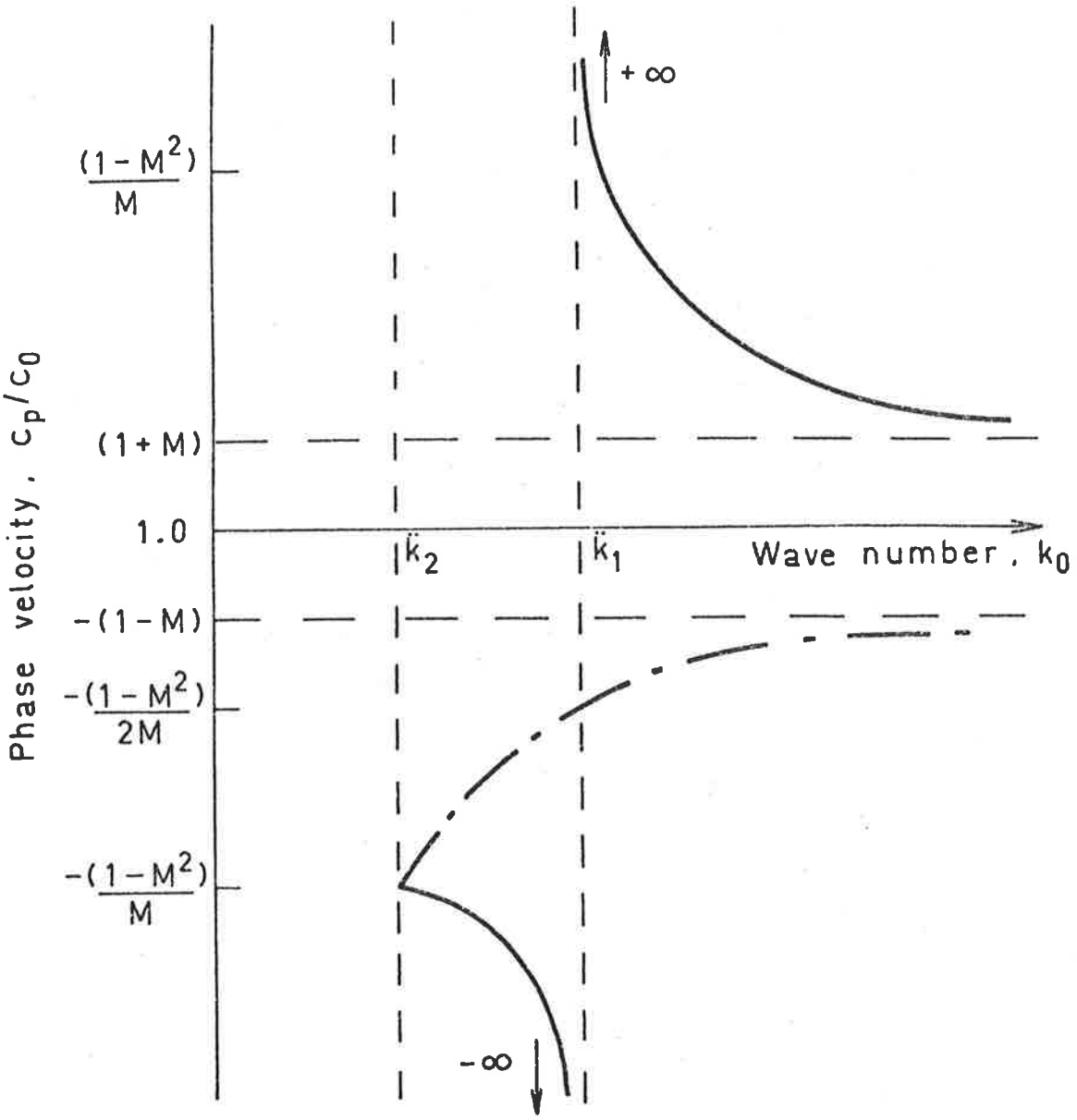

FIGURE 1.8. Phase velocity of a higher mode near cut-off with convection. ——— , downstream propagation; — - — , upstream propagation.

where $$\varepsilon = [1 - (\ddot{k}_1/k_o)^2(1-M^2)]^{\frac{1}{2}} \tag{1.65}$$

From equations (1.63) and (1.64) it can be seen that the particle velocities of the (0,0) mode will reduce to

$$v_x^d = \frac{p}{\rho_o c_o} \tag{1.66}$$

$$v_x^u = -\frac{p}{\rho_o c_o} \tag{1.67}$$

Thus flow does not effect the acoustic impedance of the plane wave. However for higher modes the acoustic impedance will be modified due to convection terms retained in the linearized momentum equation.

The forward and backward wave intensities are obtained from the generalized definition of acoustic intensity in an isentropic irrotational flow

$$I_x = \langle p v_x \rangle + \frac{V_x}{\rho_o c_o^2} \langle p^2 \rangle + \frac{V_x^2}{c_o^2} \langle p v_x \rangle + \rho_o V_x \langle v_x^2 \rangle \tag{1.68}$$

and as derived by Morfey are

$$I_x^d = \left(\frac{|p|^2}{2\rho_o c_o}\right) \varepsilon (1-M^2)^2/(1-\varepsilon M)^2 \tag{1.69}$$

$$I_x^u = -\left(\frac{|p|^2}{2\rho_o c_o}\right) \varepsilon (1-M^2)^2/(1+\varepsilon M)^2 \tag{1.70}$$

Equations (1.69) and (1.70) hold for waves above cut-off. For waves below cut-off, ε is imaginary, and $I_x = 0$. Hence below cut-off there is no energy propagation along the duct for either the upstream or downstream case. This result should be compared to the value of group

velocity obtained at and below cut-off.

In the case of the plane wave, for which $\varepsilon = 1$, equations (1.69) and (1.70) predict that flow will have the effect of increasing downstream intensity by a factor of $(1+M)^2$ and decreasing upstream intensity by $(1-M)^2$. Flow can thus be expected to modify power reflection and transmission coefficients due to convection of energy.

For a duct of constant cross section, in which two plane waves are propagating in opposite directions at the same frequency, the ratio of reflected energy to incident energy with flow can be written as

$$\alpha_r^d = \left| \frac{P_{oo}^r}{P_{oo}^i} \right|^2 \left(\frac{1-M}{1+M} \right)^2 \tag{1.71}$$

and

$$\alpha_r^u = \left| \frac{P_{oo}^r}{P_{oo}^i} \right|^2 \left(\frac{1+M}{1-M} \right)^2 \tag{1.72}$$

where P_{oo}^i and P_{oo}^r are the pressure amplitudes of the incident and reflected waves respectively.

The power transmission coefficient defined as the ratio of transmitted energy (or actual energy propagation) to incident energy propagation is

$$\alpha_t = \left| \frac{P_{oo}^t}{P_{oo}^i} \right|^2 \tag{1.73}$$

for both upstream and downstream propagation of sound, P_{oo}^t is the transmitted pressure amplitude of P_{oo}^i and P_{oo}^r.

Equation (1.73) predicts that α_t will be the same irrespective of direction and magnitude of the flow. Any changes in power transmission coefficient will be due to changes in impedance of the reflecting surface and not due to convection of energy.

From conservation of acoustic energy, as for the no flow case

$$\alpha_t = 1 - \alpha_r \tag{1.74}$$

Hence as α_t is identical for both upstream and downstream cases then α_r, from equation (1.74) must also be identical for both cases. By examining equations (1.71) and (1.72) it is logically deduced that the identical nature of α_r for upstream and downstream propagation occurs due to flow induced changes in the pressure reflection coefficient R, defined to be the ratio of reflected wave pressure amplitude to incident wave pressure amplitude. Thus convection of the propagating medium must have the effect of increasing the no flow reflection coefficient by a factor of $(1+M)/(1-M)$ for downstream propagation and decreasing the no flow pressure reflection coefficient by a factor of $(1-M)/(1+M)$ for upstream propagation.

This agrees with predictions determined by Alfredson (1970) who showed that the pressure reflection coefficient can exceed unity without reversal of flux of energy in a duct with mean downstream flow. In particular, the maximum value of pressure reflection coefficient for downstream propagation before reversal of flux is

$$R'_{max} = (1+M)/(1-M) \tag{1.75}$$

In the no flow case, the maximum value R_{max} can take is unity when total reflection of sound occurs, thus equation (1.75) agrees with the predictions of this analysis. It can be seen from the identical nature of α_r^u and α_r^d that R will be increased by a factor of $(1+M)/(1-M)$ for all values of R and not only when $R = R_{max}$.

Thus flow can be seen to alter the pressure reflection coefficients due to differences in rates of convection of energy for the upstream and downstream cases. In fact this is necessary for the

system to maintain conservation of energy.

The major effects of flow on wave amplitudes and energy flux of waves propagating in a single mode can be summarized as:

(1) an increase and a decrease in the pressure reflection coefficient for downstream and upstream propagation respectively,

(2) an increase and decrease in the wave intensity for downstream and upstream propagation respectively,

(3) no alteration in the specific acoustic impedance of the (0,0) mode,

(4) an alteration in the specific acoustic impedance of higher modes,

(5) no alteration, due to convected energy, in the power reflection and transmission coefficients of the (0,0) mode.

Most of these factors are well illustrated in the analysis of a reactive acoustic attenuator to follow in Chapters 5 and 6.

1.4 EXPERIMENTAL INVESTIGATION - EQUIPMENT, PROCEDURE AND RESULTS

In this section the effect of flow on phase velocity and cut-off frequency is to be investigated. It is hoped to isolate the two discrete frequencies $\ddot{k}_1$ and $\ddot{k}_2$ of the preceding analysis and show that the phase velocity is infinite at $\ddot{k}_1 = 0$ for the downstream case proving that propagation of energy at this frequency is due purely to convection and not acoustic motion.

The arrangement of the experimental apparatus used is shown in Figure 1.9. The duct system has a 0.0635 x 0.127 meters internal cross section and was constructed in removable sections from 0.0254 meter thick wood lined with laminex on the inside to fulfil the rigid wall boundary condition. A centrifugal fan driven by a variable speed D.C. motor provides air flow through the duct system at different Mach numbers.

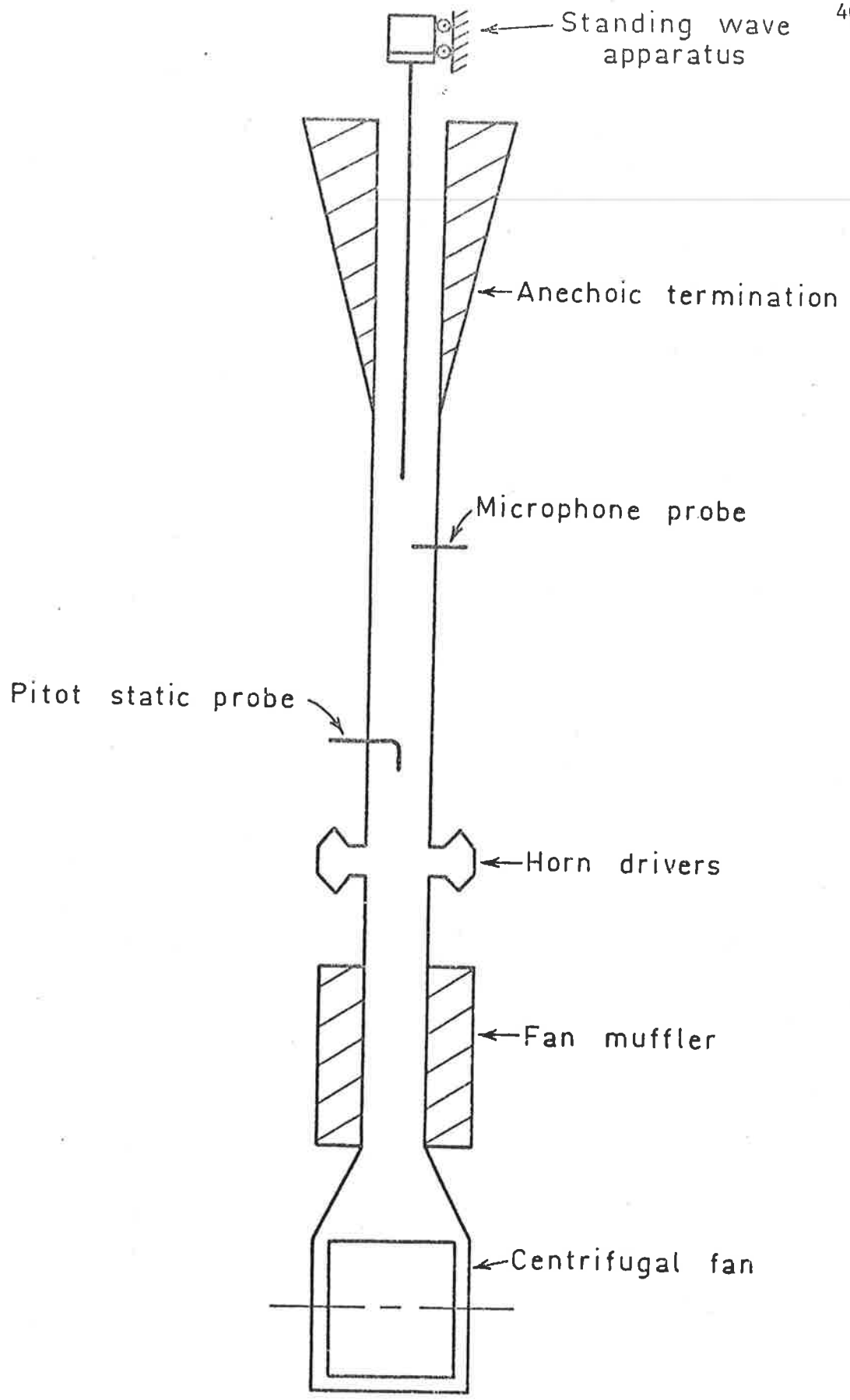

FIGURE 1.9. Arrangement of the experimental apparatus for detection of modal cut-off frequencies and phase speeds with flow.

Flow velocity profiles were measured by traversing a pitot static tube across the duct and an equivalent uniform velocity was calculated from the flow distribution. At the maximum rating of the motor a flow rate of $M = 0.1$ was measured in the incident duct. A fan muffler was positioned downstream of the fan to reduce fan generated noise and to attenuate negative travelling waves.

For measurements of sound propagating with the flow the sound source was positioned 1.5 meters from the test section at which distance any locally generated unwanted cross modes have sufficiently decayed to be negligible. To eliminate reflections from the exit of the duct, and resultant modal coupling, the downstream duct was anechoically terminated. For measurements of the sound propagating with the flow the anechoic termination was removed and the sound source positioned well downstream of the test section. In this case the fan muffler acts as an anechoic termination to waves travelling upstream.

The mode to be investigated is the (1,0) cross mode. This was achieved by mounting two Toa 35 watt horn drivers on opposite walls of the larger dimension of the duct and driving the horns 180° out of phase with a pure tone. This arrangement resulted in a strong generation and propagation of the (1,0) mode above the cut-off frequency. Below the cut-off frequency of the (1,0) mode, the (0,0) mode was propagated very weakly due to phase interference of the horn drivers. At the cut-on of the (1,0) mode, sound pressure levels recorded at the wall in the test section consistently rose sharply to 30 dB above that recorded for the (0,0) mode alone (i.e. just below cut-off).

The main piece of experimental equipment used was a Brüel & Kjaer Heterodyne Analyser (HA). This instrument has the capability to be used as a narrow band filter and also as a Beat Frequency Oscillator (BFO) simultaneously. The center frequency of the band being filtered

corresponds exactly to the frequency of the BFO output signal. Thus when the output of the BFO is amplified and used to drive the horn drivers and the same instrument is used to filter the measured sound levels, the operator is ensured that the center frequency of the band is exactly on the signal being measured. This characteristic of a tracking filter is particularly desirable if one is using a very narrow filter band and is traversing the acoustic signal over a range of frequencies. However a disadvantage of the Heterodyne Analyser is that its output signal is at a constant frequency and thus cannot be used for phase measurements. For phase measurements a Brüel and Kjaer Constant Percentage Bandwidth Filter was used (set to a 10% bandwidth) in conjunction with a Brüel and Kjaer Digital Phase Meter.

At the maximum flow rate of the fan, with the (1,0) mode above cut-off, the HA when set to a 3.16 Hz bandwidth provided a signal to noise ratio of greater than 50 dB , while the Constant Percentage Filter provided a signal to noise ratio of greater than 30 dB at maximum flow.

Three parameters were investigated experimentally. The transverse pressure distribution of the (1,0) mode propagating downstream was measured in the test section by traversing a microphone probe across the duct and recording the sound pressure levels at known distances. The sound pressure level was then normalized to the value recorded at $y = 0$. Experimental values of relative pressure amplitude, defined by equation (1.76) are shown in Figure 1.10 with the theoretical distribution derived from equation (1.44) for $M = 0.1$

$$\text{Relative pressure amplitude} = 10^{\Delta dB/20} \qquad (1.76)$$

where ΔdB is obtained from the sound pressure level data as

$$\Delta dB = S.P.L_y - S.P.L_{y=0}$$

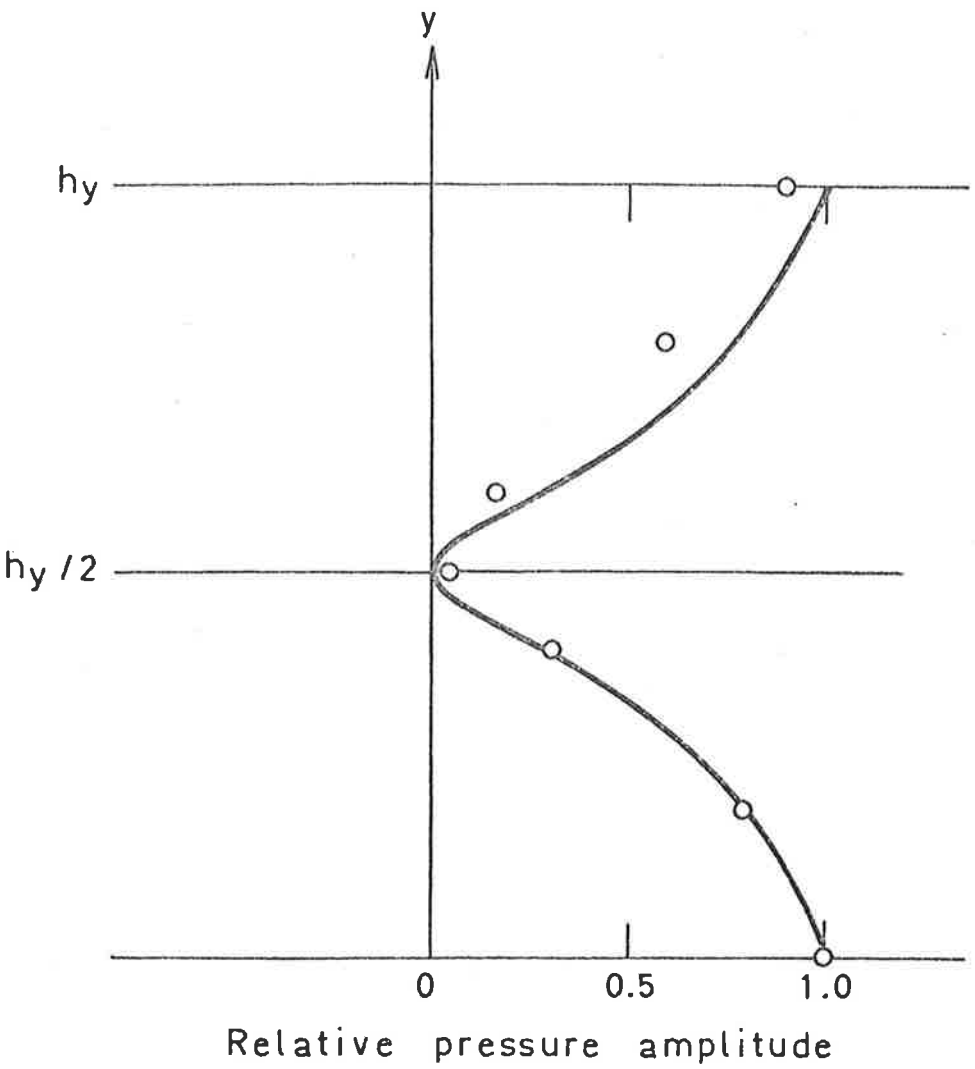

FIGURE 1.10. Transverse pressure distribution of the (1,0) mode. ——— , theoretical; O , experimental.

The phase velocities of the (0,0) mode and the (1,0) mode were measured by traversing a microphone probe down the duct a known distance X. The change in phase $\Delta\theta_p$ over this distance was measured using a Brüel and Kjaer Phase Meter. Particular care was taken to ensure the probe tip moved parallel to the duct wall, as in the case of the (1,0) mode there is phase variation across the duct wall as well as along its length. The phase velocity is then

$$c_p = \omega X/\Delta\theta_p \tag{1.77}$$

Phase velocities of the (0,0) mode and the (1,0) mode measured for the zero flow case are plotted in Figure 1.3. Values of the phase velocity of the (0,0) mode and (1,0) mode for a flow rate of M = 0.1 and downstream propagation are plotted in Figure 1.5.

The phase velocity of the (1,0) mode was measured for small frequency increments near cut-off with and without flow. For the consideration of flow both the upstream and downstream cases were measured, with a flow rate of M = 0.1. The frequency of interest was gradually lowered and the phase difference measured, until the mode had "cut-off". Values of measured phase velocity for the (1,0) mode without flow are given in Table 1.1. Values of measured phase velocity for the (1,0) mode propagating in the downstream and upstream cases are given in Tables 1.2 and 1.3 respectively. In each case the distance X over which the phase difference was measured was standardized to .17 meters. The values of phase velocity measured for the case of flow should be compared to the theoretical phase velocity plot of Figure 1.8.

The "cut-off" frequency of the (1,0) mode was investigated at flow rates of M = 0, M = 0.05 and M = 0.1 for both downstream and upstream

Table 1.1 : Phase Velocities of the (1,0) Mode Near Cut-Off, M = 0

Frequency (Hz)	Measured Phase Difference (radians)	c_p/c_o
1400	-2.68	1.63
1380	- .39	10.93
1356	- .17	24.84
1355	- .16	26.37
1354	- .15	28.11
1353	- .16	26.33
1352	- .18	23.39
1351	- .18	23.37
1350	- .20	21.02

Table 1.2 : Phase Velocities of the (1,0) Mode Near Cut-Off, M = 0.1, Downstream Propagation of Sound

Frequency (Hz)	Measured Phase Difference (radians)	c_p/c_o
1400	-1.38	+ 3.159
1380	- .36	+ 11.94
1370	- .10	+ 42.66
1368	- .07	+ 60.86
1367	- .04	+106.42
1366	- .01	+425.39
1365	+ .05	- 85.01
1364	+ .05	- 84.95
1360	+ .13	- 32.58
1355	+ .13	- 32.46
1350	+ .01	-420.40
1349	- .04	+105.02
1348	- .03	+ 24.69

Table 1.3 : Phase Velocities of the (1,0) Mode Near Cut-Off, M = 0.1, Upstream Propagation of Sound

Frequency (Hz)	Measured Phase Difference (radians)	c_p/c_o
1400	+1.05	- 4.152
1370	+1.00	- 4.27
1360	+ .42	-10.08
1355	+ .46	- 9.17
1353	+ .5	- 8.43
1352	+ .3	-14.03
1351	+ .5	- 8.41
1350	+ .48	- 8.76

propagation of sound. Detection of the frequency at which cut-on of the mode occurred was by means of an observed rise in sound pressure level in the duct. To detect this a microphone probe was mounted flush with the duct inside wall in the test section. The Heterodyne Analyser was connected to a Brüel and Kjaer Level Recorder by a mechanical drive. Thus the frequency of the acoustic signal was slowly and uniformly increased and the resulting sound pressure levels at the duct wall were recorded graphically on frequency scaled paper by the Level Recorder. As discussed previously the filter, set to 3.16 Hz bandwidth, tracks the acoustic signal.

Figure 1.11 shows a typical frequency response of the sound pressure level in the test duct section for the no flow case. Figure 1.12 shows a similar frequency response for a flow rate of $M = 0.1$ and downstream propagation. From these figures it can be clearly seen that the "cut-on" of the (1,0) mode is characterized by a rapid increase in sound pressure level at the duct wall as the BFO sweeps through frequencies near cut-on. To accurately find this frequency, the BFO frequency was slowly increased manually until the recorded sound pressure level first started to rise rapidly. The frequency at which this occurred was taken as the "cut-off" frequency of the (1,0) mode and was read from the BFO Nixie display of frequency of generation. The accuracy of this measured frequency for cut-off of the (1,0) mode was considered to be ± 1 Hz.

Values of cut-off frequency found experimentally using this method for $M = 0$, $M = 0.05$ and $M = 0.1$ are shown in Table 1.4 for both downstream and upstream propagation of sound. These values are also plotted in Figure 1.13 for comparison with a theoretical curve of "cut-off" frequency derived from equation (1.62).

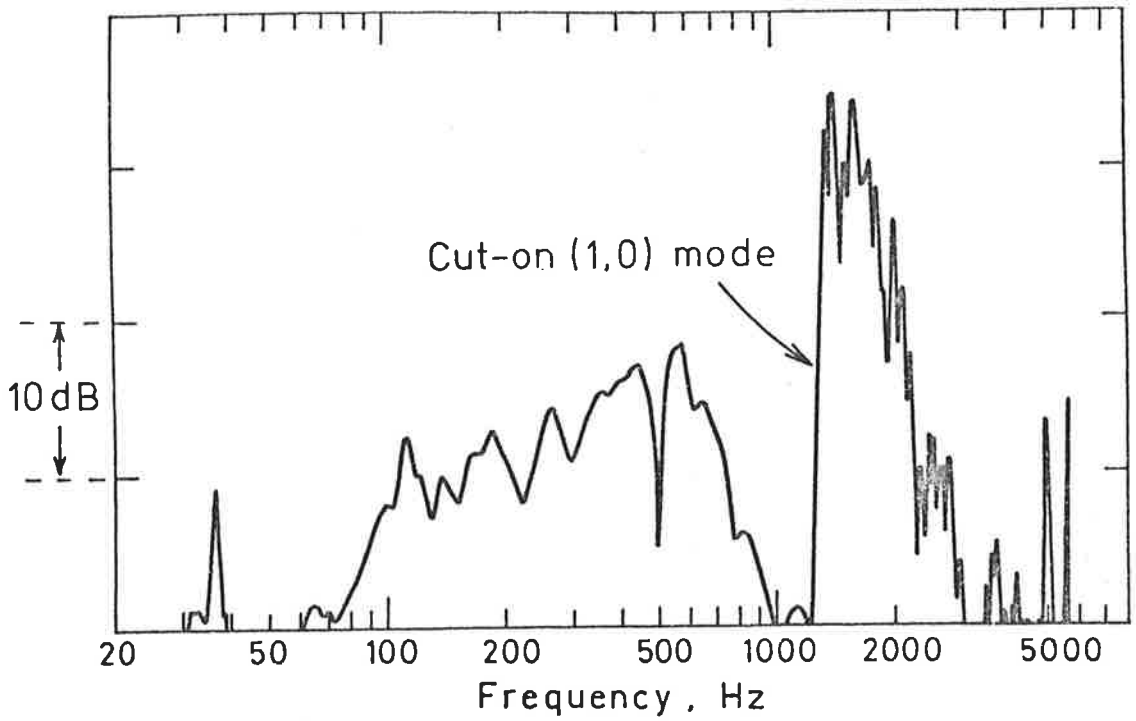

FIGURE 1.11. Frequency response of the sound pressure level in the test duct near cut-on of the (1,0) mode.

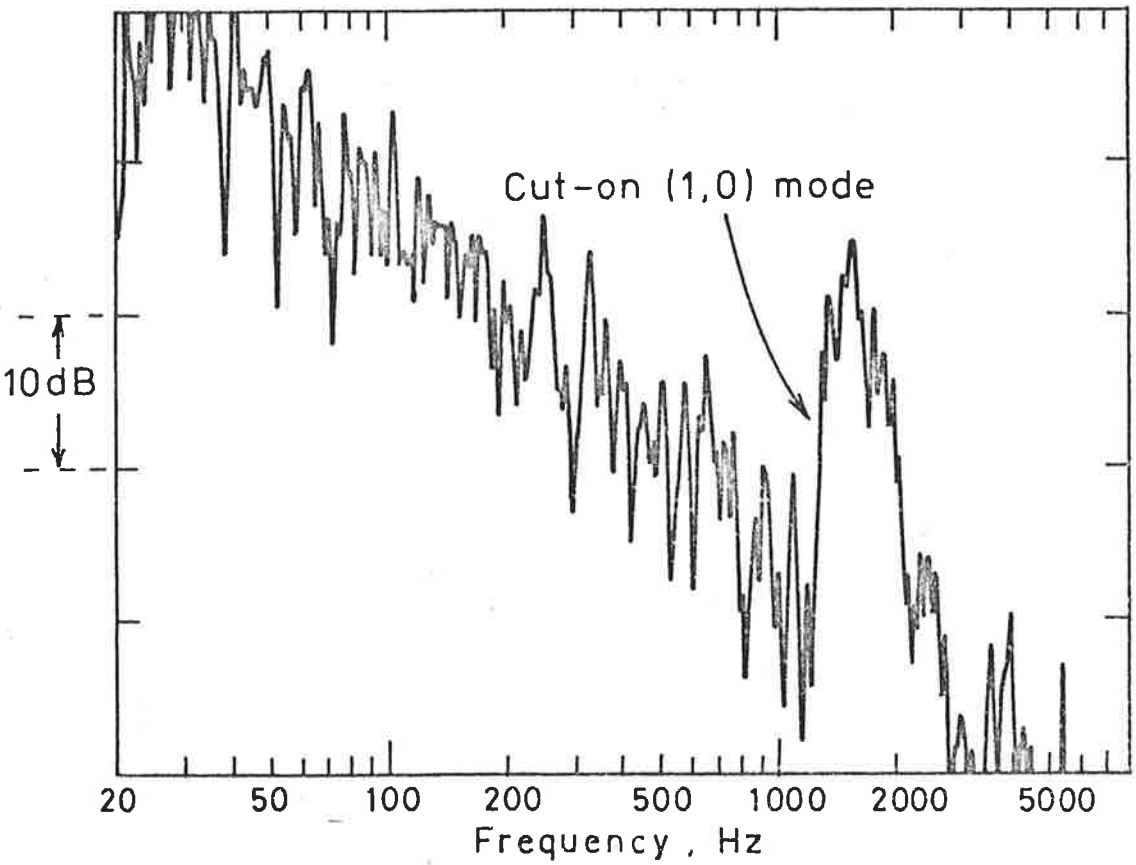

FIGURE 1.12. Frequency response of the sound pressure level in the test duct near cut-on of the (1,0) mode with a flow rate of M = 0.1.

Table 1.4 : Experimentally Measured Cut-off Frequencies of the (1,0) Mode with Flow

Cut-off Freq. (Hz)

Mach Number	0.0	0.05	0.1
Downstream	1353	1350	1346
Upstream	1352	1350	1348

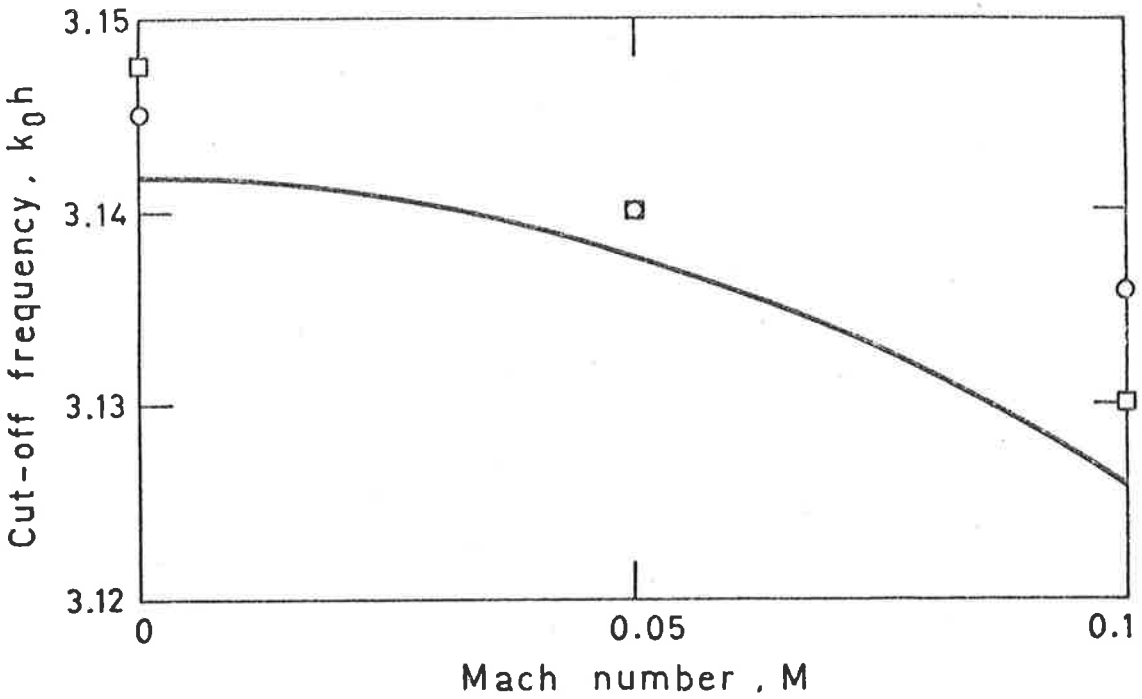

FIGURE 1.13. Variation in cut-off frequency of the (1,0) mode for different flow rates. ——— , theoretical; □ , downstream propagation; O , upstream propagation.

1.5 DISCUSSION OF RESULTS

Before the propagation characteristics of the (1,0) mode could be investigated it was necessary to check that this mode in fact was propagating through the test section. Figure 1.10 shows a comparison between the theoretical and experimentally measured pressure amplitude distribution of the (1,0) mode in the test section. The results of this figure shows that the arrangement of horn drivers employed results in a strong driving of the (1,0) mode for frequencies above cut-off. Below the cut-off frequency of the (1,0) mode a very weak plane wave remains. The experimental values agree very well with the theoretical distribution. The small errors in the minimum at the duct centerline and at the duct wall ($y = h_y$) are attributed to the presence of a weakly propagating (0,0) mode. The amplitude of (0,0) mode was quite weak in comparison to the (1,0) mode above cut-off, the sound pressure level at the duct wall increasing in the order of 20 to 30 dB through the cut-off frequency.

The experimental values of phase velocity for both the (0,0) mode and the (1,0) mode are seen from Figures 1.3 and 1.5 to agree with their corresponding theoretical values for $M = 0$ and $M = 0.1$ respectively. The phase velocity of the (0,0) mode with no flow was measured to be 330 m/sec. For an ambient temperature of 22°C recorded during the experiment, the corresponding theoretical speed of sound (equal to the phase speed of the (0,0) mode) is 343.8 m/sec. For a flow rate of $M = 0.1$ and downstream propagation of sound the phase speed of the (0,0) mode was measured to be 418 m/sec. This compares with the theoretical phase speed of

$$c_o^d = c_o(1+M) \tag{1.78}$$

$$= 378 \text{ m/sec} \quad \text{for } M = 0.1$$

The above phase measurements were made at 1 kHz .

Thus as theory predicts, flow has the effect of increasing the phase speed of the (0,0) mode by a factor of (1+M) for downstream propagation of sound.

As expected from the analysis the phase velocity of the (1,0) mode without flow is very large near cut-off. Table 1.1 shows that the largest phase velocity measured was $c_p/c_o = 28.11$ at 1354 Hz . It was hoped to measure an infinite phase velocity (i.e. zero phase variation along the duct) for the (1,0) mode exactly at the cut-off freqeuncy, but this proved difficult. At cut-off, the (0,0) mode which is propagating weakly appears to interfere with the phase characteristics of the (1,0) mode. As well as this, dimensional variations in the cross section along the length of the duct lead to a slight variation in cut-off frequency at different positions in the duct. Hence in the no flow case the cut-off frequency was taken as the frequency at which the highest value of phase velocity was measured. The measured cut-off frequency of the (1,0) mode for the experimental rig was $f_c = 1354$ Hz (or $\ddot{k}_1 = 24.8$) for zero flow. The corresponding theoretical value of cut-off frequency for the (1,0) mode in a duct of dimensions $h_y = 0.127$ meters, from equation (1.62), is equal to 1350.5 Hz . The slight differences between the theoretical and experimental result was thought to be due to dimensional inaccuracies in the duct size and the presence of the weakly propagating (0,0) mode.

For the case of flow and downstream propagation of sound, Table 1.2 shows that the phase velocity of the (1,0) mode approaches infinity at a frequency of 1366 Hz . This frequency corresponds to $\ddot{k}_1$ of the analysis. However the theory predicts that $\ddot{k}_1$ should be identical to the no flow cut-off frequency. The error between the measured no flow cut-off frequency and the measured value of $\ddot{k}_1$ is thought to be due to

the non-uniform flow in the duct. Refraction of waves at the boundary layer surface may cause an alteration in the angle of particle velocity vibrations. Theory predicts that for the downstream case that the phase velocity should change sign as the frequency is traversed through $\ddot{k}_1$ as shown graphically in Figure 1.8. This prediction is verified in the experimental results of Table 1.2 where the phase velocity changes from a positive value to a negative value as the frequency decreases through 1366 Hz. It is interesting to note that the sign of the phase velocity changes back to positive at 1350 Hz which corresponds more closely to the expected cut-off frequency with flow. Thus it appears that the frequency $\ddot{k}_1$ at which the phase velocity is theoretically infinite for the downstream case is most affected by the non-uniform flow.

This effect is also demonstrated in the phase measurements of the (1,0) mode propagating upstream, the results of which are given in Table 1.3. The phase speed is seen to steadily increase to a maximum at 1352 Hz and then decrease again. This maximum of phase velocity for the upstream case is seen from Figure 1.8 to occur at the cut-off frequency $\ddot{k}_2$. Similarly for the upstream case no change in sign of the phase speed was measured at $\ddot{k}_1$ as opposed to the downstream case and demonstrated theoretically in Figure 1.8. The phase speed of the upstream propagating mode does not approach infinity at $\ddot{k}_2$ but approaches a maximum value of $c_p/c_o = -(1-M^2)/M$. For a flow rate of $M = 0.1$ the theoretical maximum phase speed is $c_p/c_o = -9.9$. At the experimentally measured value of $\ddot{k}_2$ (1352 Hz) the phase speed was measured to be $c_p/c_o = -14.03$. The experimental result is seen to be of the same order as the theoretical prediction. The discrepancy between experiment and prediction is most likely due to duct cross dimension variation and perhaps due to the presence of the flow boundary layer as previously discussed.

The result of Tables 1.2 and 1.3 for the (1,0) mode supports

the prediction of the analysis that for the downstream case there is a discrete frequency $\ddot{k}_1$ at which the phase velocity is infinite even though the mode still propagates downstream, while cut-off of propagation of energy occurs at the lower frequency $\ddot{k}_2$. Since the phase velocity of the mode is infinite at $\ddot{k}_1$ as suggested by experimental results here, energy propagation at this frequency is due to convection of the propagating medium and not due to acoustic wave motion. This result is also supported by theoretical group velocity considerations as discussed previously. The results also show that the phase velocity of the (1,0) mode propagating upstream never approaches infinity but reaches a maximum at $\ddot{k}_2$, the cut-off frequency.

The frequency response of the wall pressure spectrum in the test section shows that the use of a rise in sound pressure level is quite successful in detecting the cut-off frequency of the (1,0) mode with and without flow. The experimental values of cut-off frequency found using this method agree well with those predicted by theory as given in Figure 1.13. The small error was thought to be due to dimensional inaccuracies and non-uniform flow in the duct. It should also be noted that some reduction in cut-off frequency is due to the cooling of the ambient air as it is drawn into the flow rig. The static temperature of air flow at Mach number M in this case will be

$$T_s = \frac{T_o}{1 + \frac{\gamma_s - 1}{2} M^2} \tag{1.79}$$

Thus the speed of propagation of sound in the flow duct will be for air

$$c_o' = \frac{c_o}{\sqrt{1 + 0.2\,M^2}} \tag{1.80}$$

and equation (1.62) will be modified to (M.K. Bull, personal communication),

$$f_c' = f_c/[1+0.2M^2]^{\frac{1}{2}} \tag{1.81}$$

where f_c' is the "cut-off" frequency with flow and reduction of temperature taken into consideration. This variation may account for some of the resultant error. The no flow cut-off frequency was determined to be 1352 Hz using the pressure method. This agrees well with the cut-off frequency determined by the phase velocity method.

Figure 1.13 demonstrates that the cut-off frequency decreases by a factor of $[1-M^2]^{\frac{1}{2}}$ for increasing flow rates independent of the direction of propagation of sound relative to the flow. Hence the experimental results here compare well with those obtained previously by Mason (1969).

1.6 SUMMARY

Propagation of the (0,0) and (1,0) mode in a rectangular hard walled straight duct has been examined theoretically and experimentally. It is found that the amplitude distribution of the (0,0) mode and the (1,0) mode are identical to those in a rectangular duct with no mean flow.

Flow is found to lower the cut-off frequency by a factor of $[1-M^2]^{\frac{1}{2}}$ irrespective of direction of propagation with respect to flow. The reason for the identical nature is determined to be the negative value of k_{mn} occuring for downstream propagation in the frequency range $\ddot{k}_1 > k_o \geq \ddot{k}_2$.

The "cut-off" condition is demonstrated vectorially using wave numbers and the frequency at which the particle velocity is normal to the duct walls (i.e. cut-off) is derived exactly.

Although cut-off occurs in an energy sense at $\ddot{k}_2$ there remains a discrete frequency $\ddot{k}_1$, equal to the no flow cut-off frequency, at which the phase velocity of the mode is infinite for the downstream case. At this frequency propagation is in the form of a "psuedo wave" purely due to convection and not acoustic motion.

Expressions are derived for the group and phase velocity of modes with flow and these are found to indicate well the important frequencies that establish the propagational characteristics of acoustic waves in rectangular ducts with uniform flow. The phase velocity of the (0,0) mode is found to be increased by a factor of (1+M) for downstream propagation as indicated by theory.

The theoretical effect of flow on the pressure and power reflection coefficients of the (0,0) mode are examined. Flow is found to increase the no flow reflection coefficient for all values by a factor of (1+M)/(1- M) for downstream propagation and decrease the coefficient by (1- M)/(1+M) for upstream propagation. The power reflection coefficient is found to be unaffected by changes in energy flux due to convection of the propagating medium.

CHAPTER 2

SOUND PROPAGATION IN RADIAL BENDS OF RECTANGULAR CROSS SECTION

2.1 INTRODUCTION

The complex case of sound propagation in curved bends has until recently defied satisfactory solution, although sound propagation in straight ducts has been well covered. None-the-less in most practical cases, such as air conditioning or jet engine ducts, bends are a necessary part of the system and in such cases they play an integral part in any resultant sound propagation. It is therefore necessary to understand the acoustical behaviour of bends with and without flow.

The earliest consideration of the problem of propagation of sound in curved bends was probably by Rayleigh (1877). Rayleigh showed that motion of waves of long wavelength in narrow ducts of large radius of curvature behaved exactly as in straight ducts of similar length. This conclusion provides the limit to which all equations developed to describe sound propagation in curved ducts must tend.

Work on curved bends was initially concentrated on the propagation of electromagnetic waves. Bucholz (1939) introduced the use of separation of variables to solve the wave equation in cylindrical co-ordinates and was the first to consider the problem of travelling waves.

Krasnushkin (1945) also used separation of variables to solve the wave equation and separated the wave propagation constant that determines the propagational characteristics of each mode and subsequently called this the "angular wave number". However Krasnushkin only considered the case of slightly bent tubes. Grigoryan (1963) developed equations which correctly predicted the sound field in the

curved duct but again his results for the angular wave number are only applicable to a very narrow pipe.

Until recently all the analyses were characterized by a simplification in the boundary conditions in order to solve the problem and in most cases, although the basic analytic procedure of use of separation of variables was clearly laid out, the results obtained were of limited direct usefulness. Recent advances, however, have led to a more complete understanding of the mechanism of sound propagation in curved bends.

Rostafinski has attacked the problem from various stages. Firstly Rostafinski (1972) limited his analysis to long wavelengths and thus used simplified expressions for the power series expansions of the Bessel Functions which appear in the characteristic equation of the problem. He considered two cases of an infinite bend (with a piston source) and the junction between a straight duct and a semi-infinite curved bend of rectangular cross section. He derived expressions for the particle velocity (tangential and radial) distribution of both the (0,0) propagating mode and non-propagating higher modes generated at the discontinuity. Although his analysis is limited to low frequencies it does highlight the nature of the sound field in a curved duct section.

Rostafinski (1974) next extended his analysis to higher propagating modes by using a closed form of the Bessel Function of order $(n + \frac{1}{2})$ to interpolate curves of angular wave number for any non-dimensional frequency. In this analysis, he also compared the curved duct velocity distributions of higher modes to the equivalent mode in a straight duct section. He found theoretically that at low frequencies $(k_o R_1 < 1)$, the radial distribution of tangential velocities was that of a potential vortex, inversely proportional to radius, while for

higher frequencies ($k_o R_1 \simeq 3.0$), the distribution was closer to a forced vortex, proportional to radius. Whereas in a straight duct the (0,0) mode wave speed is independent of frequency (i.e. it is non-dispersive) in a curved duct the angular wave speed is strongly dependent on frequency for all modes including the (0,0) mode (i.e. the plane wave mode is dispersive).

Finally Rostafinski (1976) considered non-propagating modes at high frequencies by solving the curved duct characteristic equation with Bessel Functions of purely imaginary order using relationships for such Bessel Functions developed by Buckens. Values of angular wave number for evanescent modes were found and used to predict the velocity distribution of evanescent modes at increasing angles into the curved duct. The analysis showed that as for straight ducts non-propagating modes decay rapidly with increasing distance from the generating surface.

Cummings (1974) has investigated the problem more generally with particular consideration given to the practical application of the derived equations. As well as investigating the discontinuity caused by a 180° bend, Cummings investigated theoretically and experimentally the radial variation in pressure amplitude in the bend and the impedance of a bend terminated with a rigid wall. From these investigations he proposed a model by which curved ducts could be considered as straight ducts of adjusted length. The adjustment arises from the consideration that the wave number across the curved duct equals k_o at values other than the mean radius. Cummings also gave brief consideration to the effect of mean flow, propagation in "soft" walled ducts and curved ducts of circular cross section.

Other work on curved ducts has been carried out separately by Osborne (1974), (1976) and Ko and Ho (1977). Osborne (1974) concentrated on solving the characteristic equation of the curved duct. He proposed

a numerical method, suitable for use on a computer, by which the angular wave numbers could be obtained without any limitation in frequency or boundary condition. He (1976) also investigated higher mode propagation in short curved bends and he gives theoretical and experimental values of pressure distribution in a practical curved duct-straight duct system. His results show that sound propagation of higher modes through curved bends is also characterized by a lack of discontinuity.

Work on sound propagation in curved ducts with attenuating walls has recently been completed by Ko and Ho (1977). They found that the (0,0) mode was the least attenuated. They considered the effect of aspect ratio, bend angle and acoustic impedance on the sound attenuation obtained and found that the total attenuation obtained increased with an increase in bend angle.

All of the above work have used a cylindrical co-ordinates solution of the wave equation and except for a brief consideration by Cummings (1974) all of the analysis have been without flow of the propagating medium. Presumably flow has been neglected and analyses thus far have been restricted to a section of a cylinder because of the complexity of the characteristic equations. Its use for the determination of appropriate angular wave numbers has been the principle concern of the analyses thus far.

Recently Fuller and Abell (1978) have proposed a method of solution of the curved duct problem using conformal mapping. They have developed simple equations for the angular wave numbers of the (0,0) mode as well as evanescent modes at low frequencies ($k_o h^c \lesssim 2.0$) with and without flow. They also derived simple expressions for values of the cut-off frequencies for higher modes with and without flow.

In this chapter the solution of sound propagation in radial bends of rectangular cross section is investigated using two procedures.

Firstly the classical procedure of solution of the wave equation in cylindrical co-ordinates is used. A numerical solution, is developed to find values of angular wave number for different frequencies and geometries of ducts. The numerical solution is used to predict the pressure distribution of the (0,0) mode and higher modes in curved ducts at various frequencies. The effects of varying frequency and radii on the radial pressure distributions are discussed.

Secondly the problem is solved using the non-classical approach of conformal mapping. Conformal mapping has been used previously by Morse and Feshbach (1953) to provide equations for the impedance of right angled bends in duct systems and by Morse and Ingard (1968) to similarly describe the equivalent resistance and inductance of an orifice of a thin width in a two dimensional duct. Cummings (1975) has also used the mapping technique or "potential flow" model to predict the transmission coefficient of a 180° bend in a straight duct system. He compared the results obtained to that of a modal solution of the same problem and showed that the "potential" model gave good agreement at low frequencies.

The basic assumption used is that for low frequencies, for which the wavelength of sound is much longer than the transverse duct dimension, the velocity potential solution of the acoustic wave equation will approximate a solution of Laplace's equation. Hence the name "potential flow" model. The solutions will thus obey the Cauchy-Riemann equations and can be transferred from various complex planes using mapping procedures. Whereas in the previous mapping analyses of Morse and Ingard (1968) and Cummings (1975) the Schwartz-Christofell transformation was used to reduce the physical shape of an orifice or a right angled duct to an arrangement affording simpler solutions of the boundary conditions, in the following analysis a similar but far simpler

approach is used and the derived mapping equations are less complicated.

Equations are developed which predict the angular wave number for the (0,0) mode of propagation and higher evanescent modes in the frequency range $k_o h^c \lesssim 2.0$ with and without mean flow. Simple equations are derived which predict the cut-off frequencies of higher modes with and without flow. Values of these parameters for the no flow case are compared to values obtained from a cylindrical co-ordinate solution of the problem. Discrepancies between the two methods are discussed and the range of applicability of the conformal mapping method in terms of frequency and aspect ratio is discussed.

The conformal mapping also provides approximate predictions of the pressure and velocity distributions of the (0,0) mode and evanescent modes. These are compared to values derived from the cylindrical solution and to experimental values of the pressure distribution with and without flow. The analysis also predicts the impedance of the bend relative to a straight duct with and without flow and this is investigated experimentally for both cases.

2.2 CYLINDRICAL CO-ORDINATES SOLUTION WITHOUT FLOW

The equations for sound propagation in radial bends with rectangular cross section are obtained from solutions of the wave equation in separable cylindrical co-ordinates as illustrated in Figure 2.1. The wave equation has the form

$$\nabla^2 p = (1/c_o)\partial^2 p/\partial t^2 \qquad (2.1)$$

where from Appendix 1 for cylindrical co-ordinates

$$\nabla^2 p = (\partial^2/\partial r^2 + (1/r)(\partial/\partial r) + (1/r^2)(\partial^2/\partial\theta^2) + \partial^2/\partial z^2)\, p \qquad (2.2)$$

Following Grigoryan (1963) we assume a solution of equation

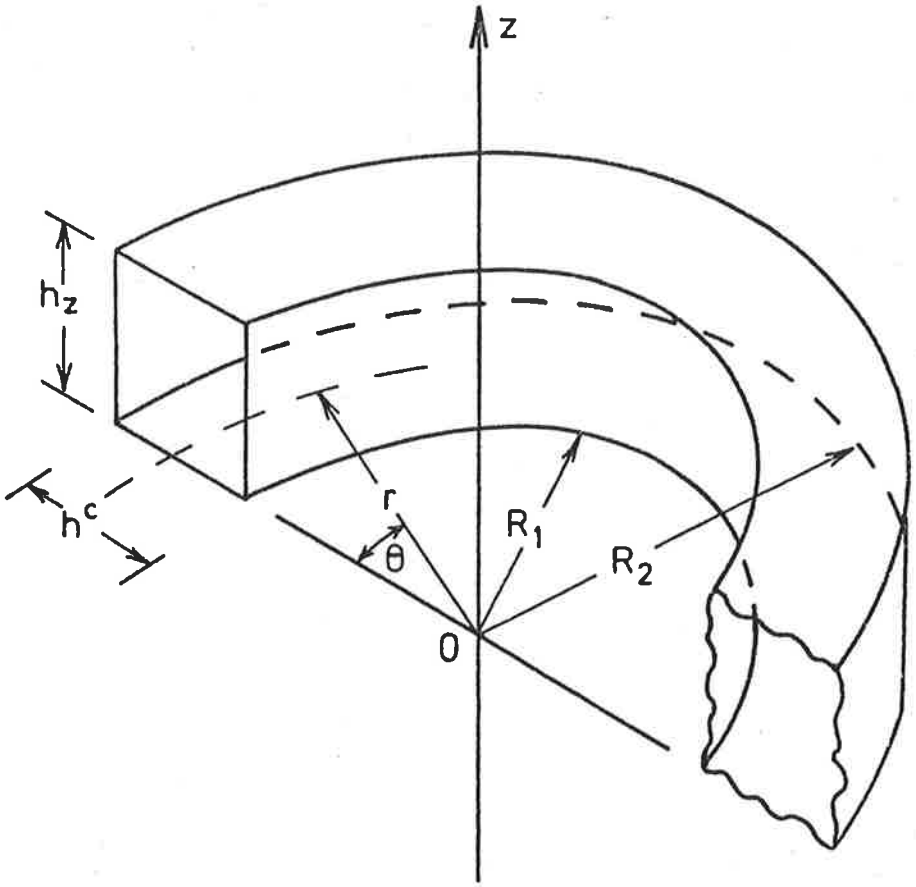

FIGURE 2.1. The cylindrical co-ordinate system.

(2.1) in separable cylindrical co-ordinates for the pressure distribution as

$$p(r,\theta,z,t) = R(r)\theta(\theta)Z(z)T(t) \tag{2.3}$$

We assume a harmonic solution so that this may be reduced to

$$p(r,\theta,z,t) = R(r)\theta(\theta)Z(z)\exp[i\omega t] \tag{2.4}$$

By substitution of equation (2.4) into equation (2.1) and separation of variables we obtain

$$\theta''/\theta = -\nu^2 \ , \tag{2.5}$$

$$R'' + (1/r)R' + (k_o^2 - \nu^2/r^2)R = 0 \tag{2.6}$$

and

$$Z''/Z = -k_n^2 \tag{2.7}$$

General solutions of equations (2.5), (2.6) and (2.7) are

$$\theta(\theta) = \exp[-i\nu\theta] \tag{2.8}$$

$$R(r) = J_\nu(k_r r) + A_b Y_\nu(k_r r) \tag{2.9}$$

and

$$Z(z) = \cos(k_n z) \tag{2.10}$$

where the radial wave number is related to the wave number in the z direction by

$$k_r^2 = k_o^2 - k_n^2 \tag{2.11}$$

Thus the general solution of equation (2.1) in cylindrical co-ordinates can be written as

$$p(r,\theta,z,t) = \sum_{s=o}^{\infty} \sum_{n=o}^{\infty} C_{sn}^{c}[J_{\nu_s}(k_r r) + A_b Y_{\nu_s}(k_r r)] \cos[k_n z] \exp[i(-\nu_s\theta + \omega t)] \tag{2.12}$$

The constants of equation (2.12) can be determined by the application of the appropriate boundary conditions. The Fourier coefficient C^c_{sn} is determined by matching the acoustic distribution of the driving surface at the bends entrance to the distribution within the bend (this will be discussed in a later section). The variable ν_s is called the angular wave number and determines the mode propagation characteristics of waves in the curved section.

If one assumes that the duct walls are perfectly rigid then the particle velocity normal to the walls is zero i.e.

$$u_r \Big|_{r=R_1}^{r=R_2} = 0 \tag{2.13}$$

$$u_z \Big|_{z=0}^{z=h_z} = 0 \tag{2.14}$$

where R_1 and R_2 are the inside and outside duct radii and h_z is the duct width in the z direction.

Using the cylindrical form for the derivation of velocity from pressure from Appendix 1

$$u_r = -(1/i\rho_o c_o k_o)\partial p/\partial r \tag{2.15}$$

we obtain from equation (2.12) at $r = R_1$

$$J'_{\nu_s}(k_r R_1) + A_b Y'_{\nu_s}(k_r R_1) = 0 \tag{2.16}$$

Thus the constant $A_b = -J'_{\nu_s}(k_r R_1)/Y'_{\nu_s}(k_r R_1)$ (2.17)

where the prime (') denotes differentiation with respect to r.

Application of the boundary condition at $z = h_z$ results in

$$\sin(k_n h_z) = 0 \tag{2.18}$$

Thus as for the straight duct case

$$k_n = n\pi/h_z \quad n = 0,1,2 \ldots. \tag{2.19}$$

The characteristic function $\psi^c_{sn}(r,z)$ describing amplitude variation across an r-z plane in the curved duct is

$$\psi^c_{sn}(r,z) = [J_{\nu_s}(k_r r) - (J'_{\nu_s}(k_r R_1)/Y'_{\nu_s}(k_r R_1))Y_{\nu_s}(k_r r)]\cos[k_n z] \tag{2.20}$$

As one would intuitively expect for a cylindrical co-ordinate solution, acoustic motion in a curved duct obeys a radial dependence in r direction and a rectangular (or similar to straight duct solution) in the z direction with respect to amplitude.

Applying the boundary condition at $r = R_2$ results in

$$J'_{\nu_s}(k_r R_1)Y'_{\nu_s}(k_r R_2) - J'_{\nu_s}(k_r R_2)Y'_{\nu_s}(k_r R_1) = 0 \tag{2.21}$$

Alternatively using expressions for Neumann Functions in terms of Bessel Functions from McLachlan (1934), the characteristic equation can be rewritten as

$$J'_{\nu_s}(k_r R_1)J'_{-\nu_s}(k_r R_2) - J'_{\nu_s}(k_r R_2)J'_{-\nu_s}(k_r R_1) = 0 \tag{2.22}$$

Equation (2.22) is the characteristic equation of the curved duct system. Solutions of equation (2.22) for the angular wave number ν_s determine the propagational characteristics of a particular mode for a given duct geometry.

Inspection of equation (2.22) demonstrates why the theory of sound propagation in curved ducts has not been completed until recently.

Due to the complicated form of equation (2.22) in order to obtain values of angular wave number ν_s some simplifying assumptions have to be made (e.g. low frequency by Rostafinski or slightly curved bends by Krasnushkin). However with the advent of modern computer techniques equation (2.22) can be solved using an iterative numerical process.

In the present analysis equation (2.22) was written in terms of power series expansions of Bessel Functions and values of angular wave number ν_o at which zeros of equation (2.22) occurred were found using an iterating process on a computer. In this process an initial value of ν_o close to zero was assumed at a particular frequency. Using this value of ν_o, equation (2.22) was evaluated at points obtained by adding successive increments to the initial value of ν_o until a change in sign of equation (2.22) occurred. When a change in sign of the characteristic equation occurred the added increment was halved and the process returned to the point before which a change in sign occurred. In this way the process was continued until equation (2.22) was evaluated to a value of less than 10^{-4}. The point at which this occurred was taken as ν_o.

As shown by equation (2.22) the values of angular wave number are dependent upon the inner and outer duct radii R_1 and R_2. The dependence of the angular wave number on these radii may be expressed in terms of the dimensionless parameter $a = R_2/R_1$ which will be called the aspect ratio. The value of the aspect ratio may range between one and infinity.

Figure 2.2 shows a typical solution of the angular wave number of the (0,0) mode of propagation in curved ducts of various aspect ratios plotted against a non-dimensional frequency $k_o h^c$. As application of the curved duct theory of propagation in later chapters is limited to low frequencies less than cut-off of the (1,0) mode equation (2.22) was only solved continuously for this frequency range. However the

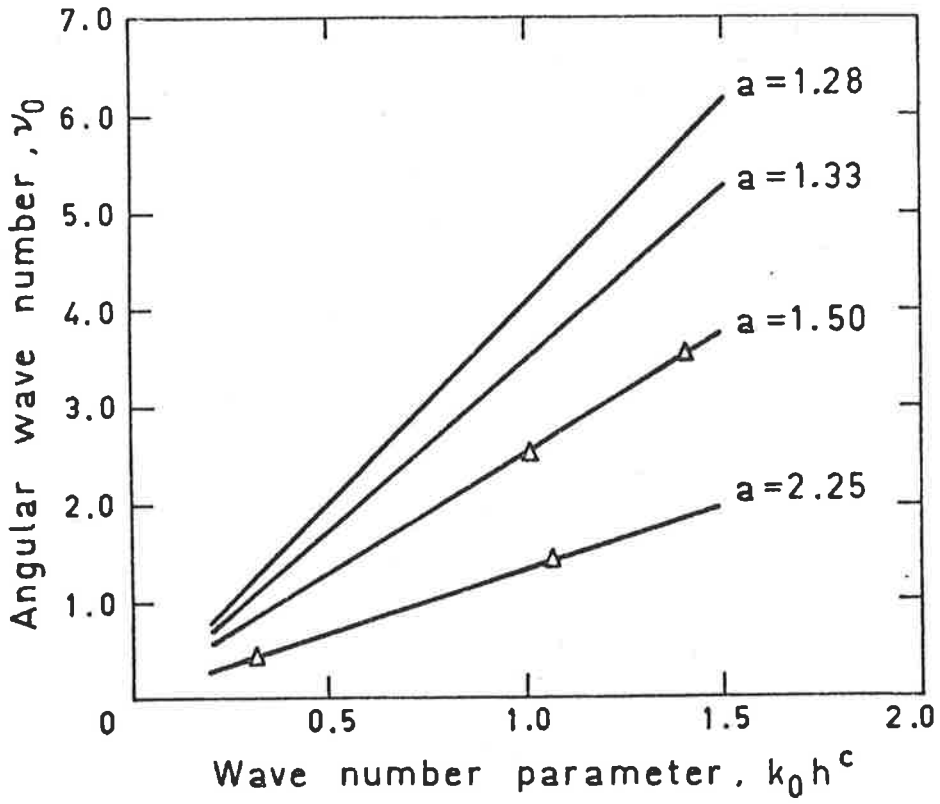

FIGURE 2.2. Angular wave numbers of the (0,0) mode. ——— ,iterative solution; Δ , values due to Rostafinski, (1974).

technique is applicable with modification, by ordering the zeros of the characteristic equation to find the angular wave number of higher propagating modes. In this case the first zero found corresponds to the wave number of the highest propagating mode. The progress is then continued on with increasing angular wave number until successive zeros are found corresponding to successive lower modes (above cut-off). Two discrete points were found by this method and used to determine the pressure distribution of higher modes for later discussion.

Values of angular wave number derived by Rostafinski who used a closed form solution of the Bessel Function of order $(n+\frac{1}{2})$ are also shown in Figure 2.2 for comparison. It can be seen from Figure 2.2 that the angular wave number of the (0,0) mode is strongly dependent on duct geometry and frequency as compared to the wave number of the (0,0) mode in a straight duct. The agreement is considered good.

Values of angular wave number for the evanescent modes (1,0), (2,0) and (3,0) for frequencies less than cut-off were obtained by solving equation (2.22) using the iterative process outlined but using Bessel Functions of purely imaginary order. As for straight ducts the angular wave number of non-propagating modes (in rigid walled ducts) was assumed to be purely imaginary. Cummings (1974) has shown from an energy flow point of view that this assumption is likely to be true and the assumption is borne out by the results of the analysis. Thus values of angular wave number of three evanescent modes derived using the method outlined are shown in Figure 2.3.

As for straight ducts with rigid walls, waves in curved radial bends will either propagate without attenuation when ν_s is real or decay with distance when ν_s is imaginary. As Rostafinski (1972) has shown, the angular wave number of the (0,0) mode is always real, thus this mode will always propagate. However as discussed later the

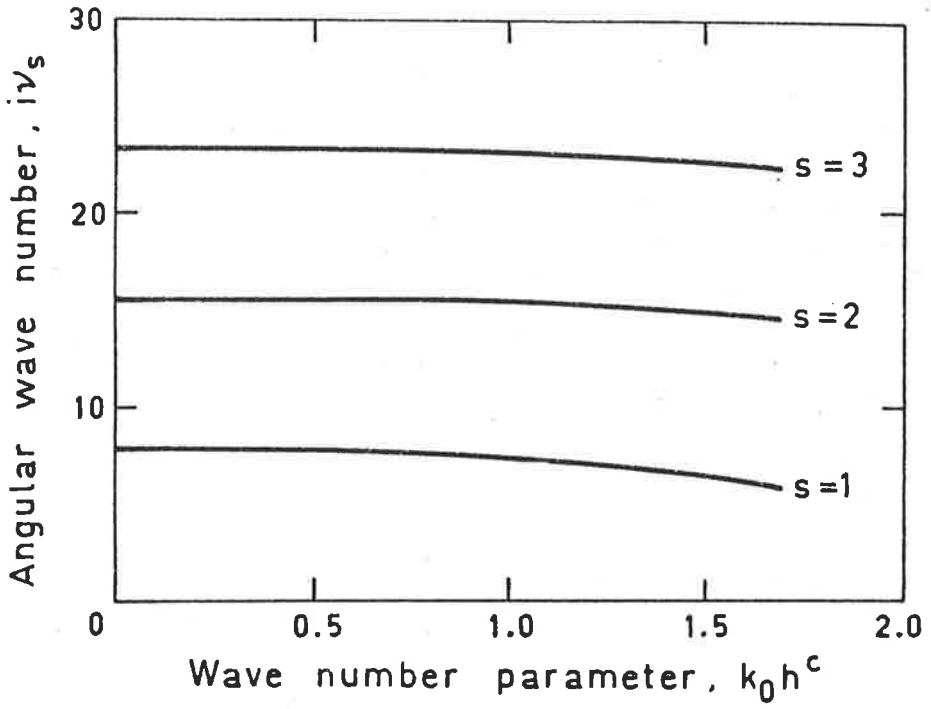

FIGURE 2.3. Angular wave numbers of three evanescent modes for a curved duct of aspect ratio, a = 1.5.

amplitudes of the (0,0) mode are not uniform across the duct cross section as opposed to straight ducts.

The cut-off frequency at which a mode changes from non-propagating to propagating is given by the zero order roots of

$$J'_o(k_r R_1)Y'_o(k_r R_2) - J'_o(k_r R_2)Y'_o(k_r R_1) = 0 \qquad (2.23)$$

Values of non-dimensional cut-off frequency $k_o R_1$ for ducts of different aspect ratio, derived by Osborne (1976) using an iterative solution of equation (2.23) are given in Table 2.1.

The variation in radial amplitude of waves in a curved duct may be obtained using the curved duct characteristic equation. For convenience the radial variation in absolute pressure amplitude may be defined as the ratio of pressure amplitude at r to the pressure amplitude at R_1 thus

$$\text{relative pressure amplitude} = \left| \frac{(\psi^c_{so})_r}{(\psi_{so})^c_{r=R_1}} \right| \qquad (2.24)$$

Relative pressure amplitude was investigated for two modes, the (0,0) mode and the (1,0) mode. Figures 2.4 and 2.5 show radial variation in pressure amplitude of the (0,0) mode for curved ducts of different aspect ratios at two different frequencies.

Figure 2.6 shows the radial variation in pressure amplitude of the (1,0) mode for a curved duct of aspect ratio a = 2 and two non-dimensional frequencies. The tangential particle velocity is given by

$$v_\theta = -(1/r)(1/i\rho_o c_o k_o)\partial p/\partial\theta \qquad (2.25)$$

Hence the variation in absolute tangential velocity amplitude across

Table 2.1 : Cut-off Frequencies of Higher Modes for Two Dimensional Ducts of Different Aspect Ratio, Derived by Osborne (1976).

Roots of Equation (2.23), $k_o R_1$

R_2/R_1	S=1	2	3	4	5	6
1.2	15.728	31.426	47.131	62.837	78.544	94.251
1.5	6.322	12.586	18.863	24.143	31.424	37.706
2.0	3.197	6.312	9.445	12.581	15.720	18.860
2.5	2.157	4.223	6.307	8.395	10.486	12.576
3.0	1.636	3.179	4.738	6.303	7.870	9.441
4.0	1.112	2.134	3.170	4.210	5.253	6.298
∞	3.832	7.016	10.174	13.324	16.471	19.616

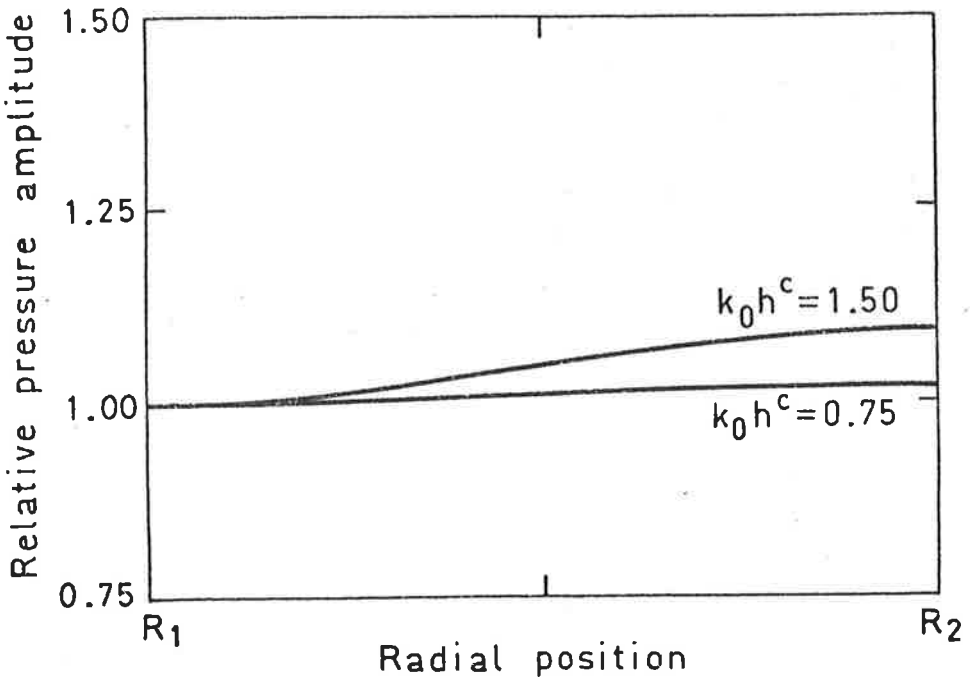

FIGURE 2.4. Radial variation in pressure amplitude of the (0,0) mode in a curved duct of aspect ratio, a = 1.28.

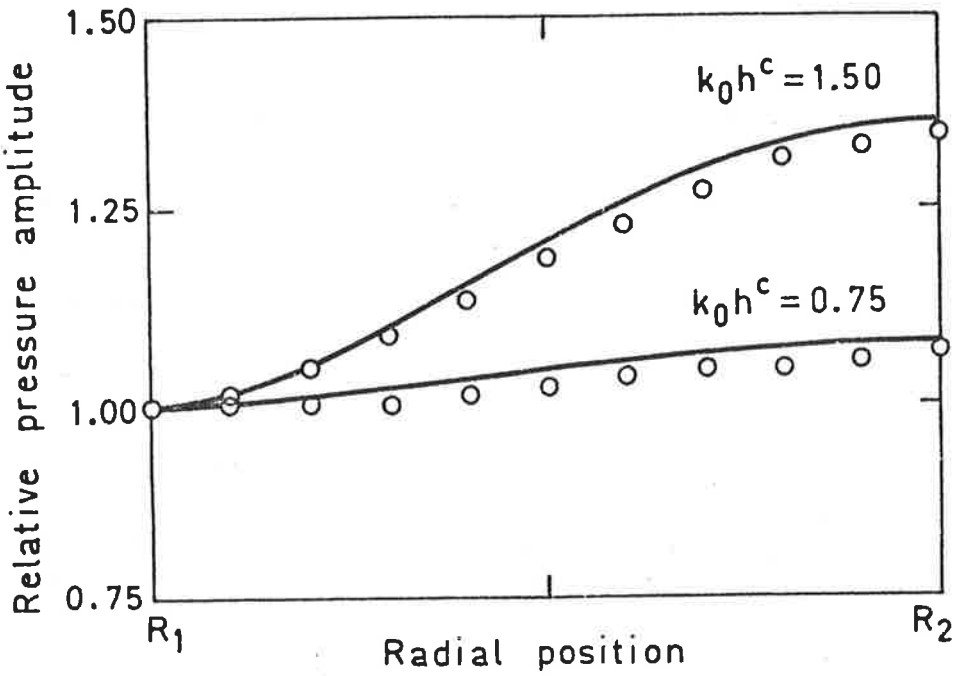

FIGURE 2.5. Radial variation in pressure amplitude of the (0,0) mode in a curved duct of aspect ratio, a = 2.25.
——— , theoretical; O , experimental.

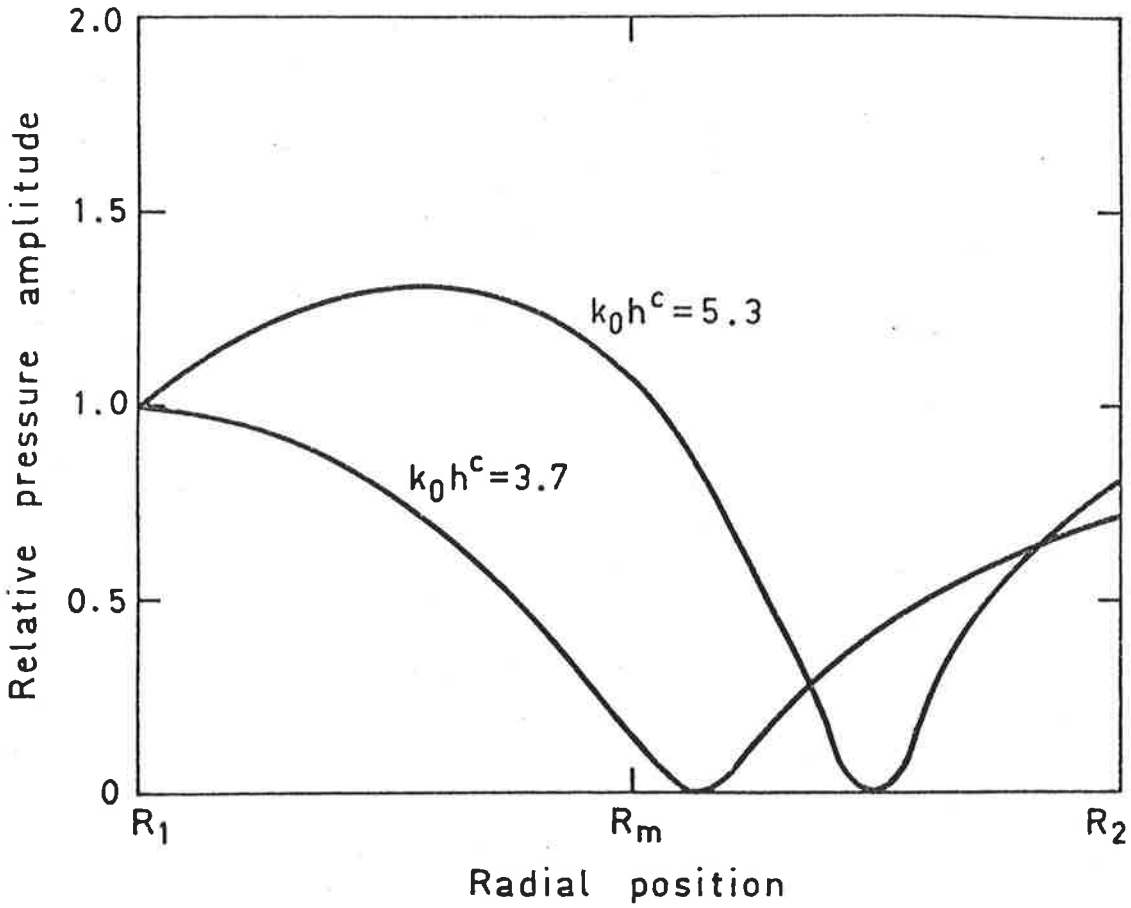

FIGURE 2.6. Radial variation in pressure amplitude of the (1,0) mode for a curved duct of aspect ratio, a = 2.

the curved duct is given by

$$v_\theta = (R_1/r)\left|(\psi^c_{so})_r \,/\, (\psi^c_{so})_{R_1}\right| \tag{2.26}$$

where the distribution is normalized to the amplitude at R_1.

The theoretical variation in tangential velocity amplitude for the (0,0) mode is shown in Figures 2.7 and 2.8 for the same curved ducts and frequencies as those used in the pressure amplitude distribution (Figures 2.3 and 2.4 respectively). The tangential velocity distribution for the (1,0) mode for a curved duct of aspect ratio a = 2 is shown in Figure 2.9.

2.3 ANALYSIS OF SOUND PROPAGATION IN RADIAL BENDS BY CONFORMAL MAPPING

Conformal mapping as described by Korn and Korn (1968) is a method by which an analytic complex function in a given region may be mapped onto a region with simpler geometry affording an easier solution for the complex potential at the boundaries. The resulting solution when transformed back to the original (physical) plane by the developed equations will provide the solution to the problem. The practical importance of conformal mapping results from the fact that harmonic functions of two real variables remain harmonic under a change of variables arising from a conformal transformation. However before a particular complex function may be mapped it must obey the Cauchy-Riemann equations in the domain being considered. These are defined as

$$\partial\eta/\partial x = \partial\beta/\partial y \tag{2.27}$$

and

$$\partial\eta/\partial y = -\partial\beta/\partial y \tag{2.28}$$

where the complex function $w = \eta(x,y) + i\beta(x,y)$. If these equations are satisfied for a complex function in a domain K then that function

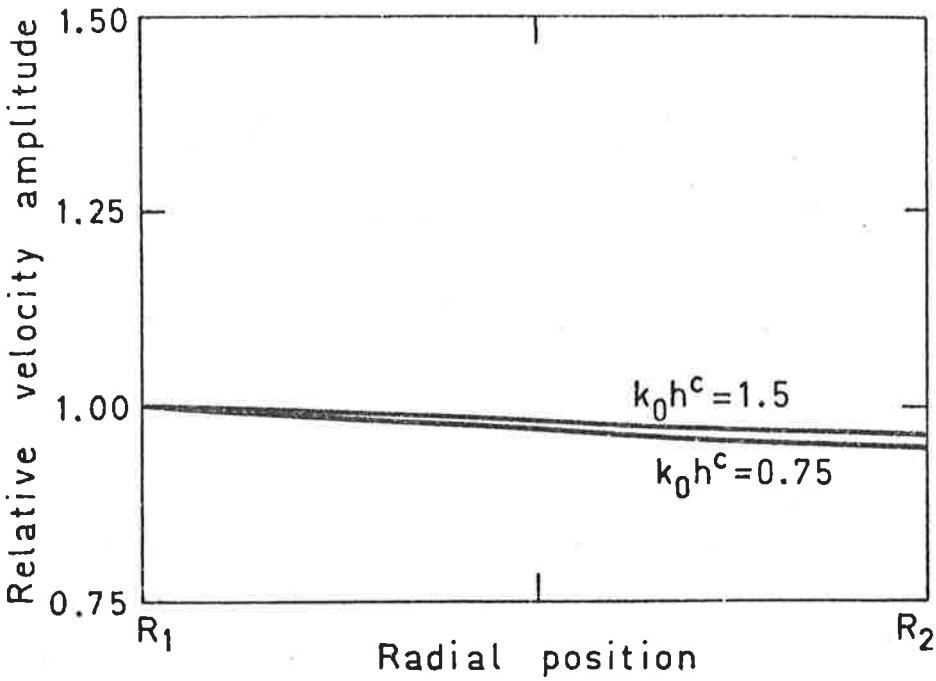

FIGURE 2.7. Tangential velocity amplitude distribution of the (0,0) mode in a curved duct of aspect ratio, a = 1.28.

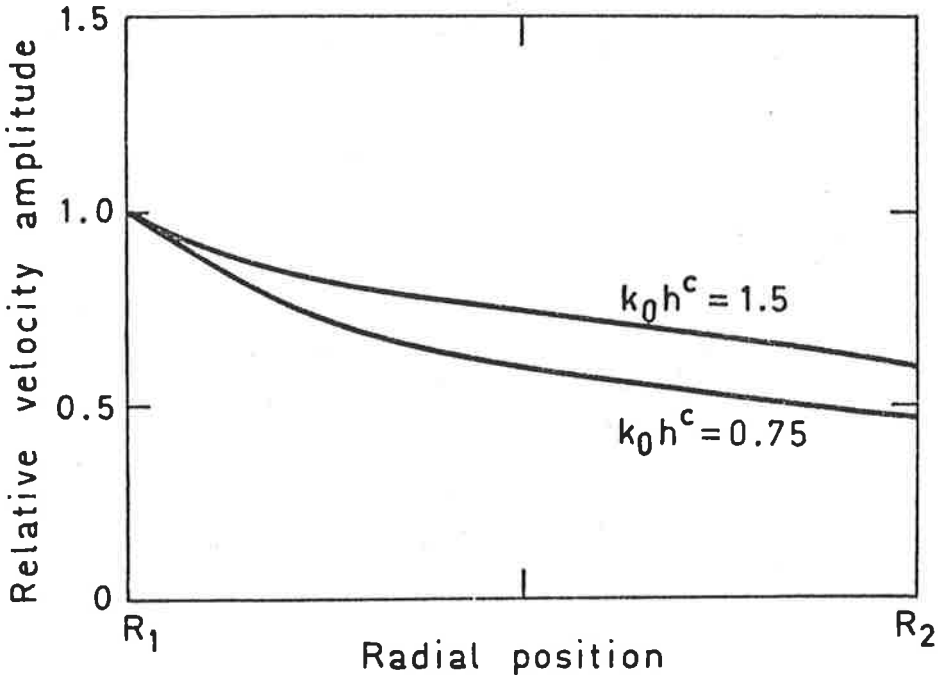

FIGURE 2.8. Tangential velocity amplitude distribution of the (0,0) mode in a curved duct of aspect ratio, a = 2.25.

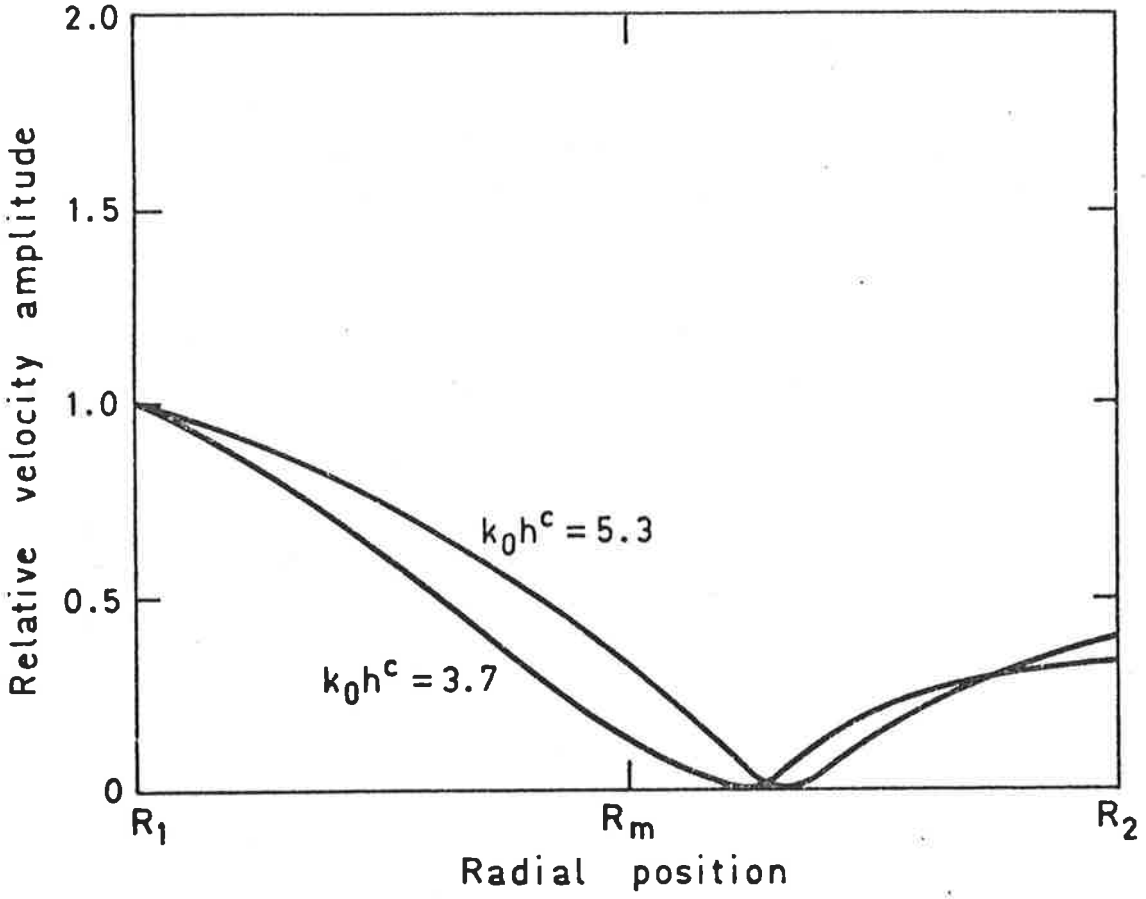

FIGURE 2.9. Tangential velocity amplitude distribution of the (1,0) mode in a curved duct of aspect ratio, a = 2.

is said to be analytic in K. This can be physically interpreted as when two intersecting curves of an analytic function are mapped, then the included angle of these curves is preserved in magnitude and sense.

Thus to solve the problem of sound propagation in a radial bend it is proposed to map the curved boundary conditions of the χ plane shown in Figure 2.10 onto the straight duct boundary conditions of the η plane shown in the same Figure. The problem is necessarily limited to a two-dimensional one and vibration in the z direction (i.e. out of the plane of the paper) is ignored. The frequency range is necessarily kept low such that the wavelength of sound is long compared to the duct width. As most practical acoustic problems in ducts are associated with low frequencies this is not thought to severely limit the application of the technique.

Simple equations relating the angular wave number of the (0,0) mode and higher non-propagating modes to the driving frequency are developed. An equation which predicts the cut-off frequencies of higher modes is given. Values obtained for the case without flow are compared to results of other workers using cylindrical co-ordinates.

The analysis is extended to include mean flow of the propagating medium. In the practical case the flow profile is far from uniform and an approximate method is proposed. Equations for the angular wave number of the (0,0) mode and higher evanescent modes with mean flow are developed and the effect of flow on the cut-off frequencies of higher modes is quantified.

A limited experimental investigation into the pressure distribution and impedance of a curved bend is undertaken with and without flow. The results are compared to the approximate prediction of the mapping analysis.

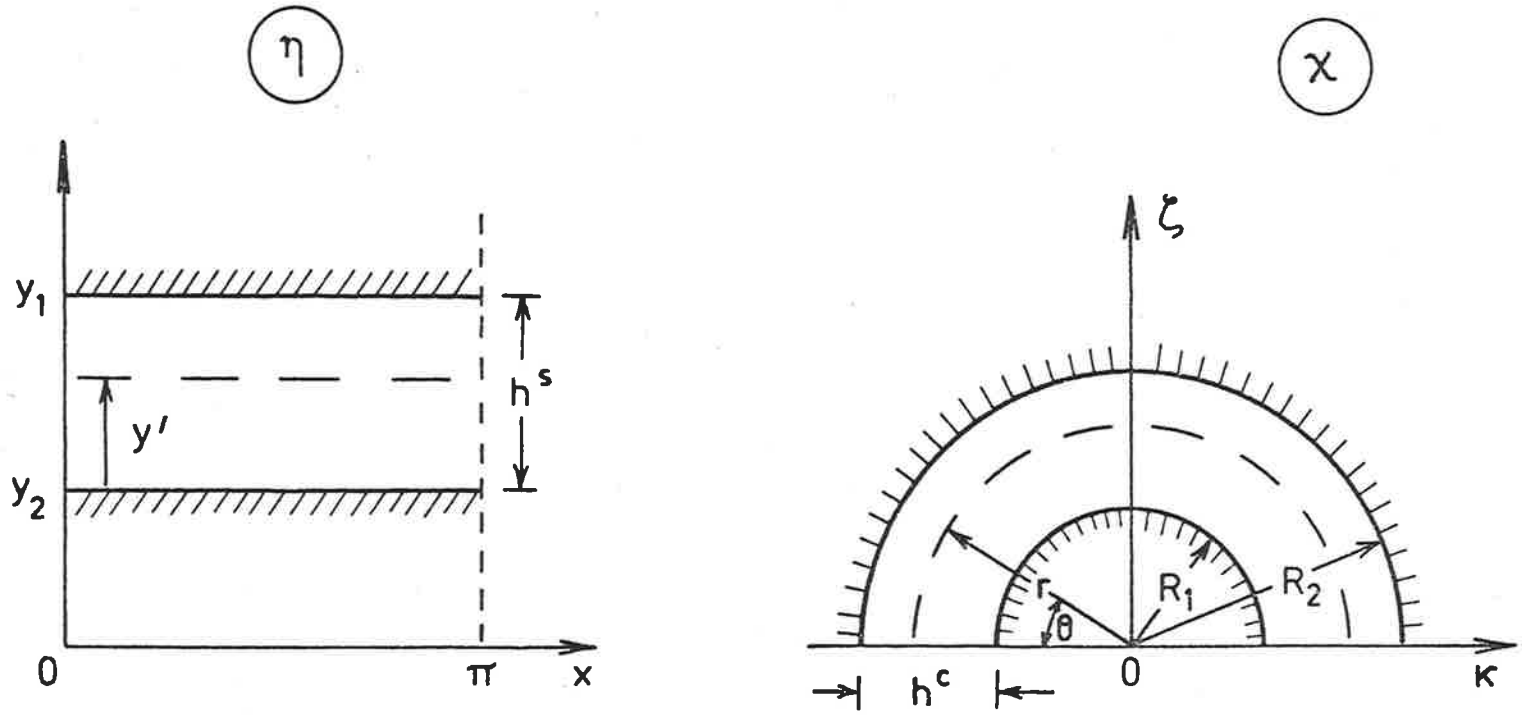

FIGURE 2.10. The η and χ complex planes used in the mapping analysis.

2.3.1 Derivation of Mapping Equations

Consider the χ and η planes as defined in Figure 2.10. The complex function mapped in the η plane is given by $\eta = x + iy$ and the function mapped in the χ plane is given by $\chi = \kappa + i\zeta$. Using the transformation $\chi = e^{i\eta}$ we see that

$$r\,e^{i\theta} = e^{ix-y} \quad ; \quad 0 < \theta < \pi \tag{2.29}$$

where the left hand side of equation (2.29) is the polar co-ordinate equivalent in the χ plane.

Thus $r\,e^{i\theta} = e^{-y}e^{ix}$ from which,

$$x = \theta \tag{2.30}$$

and

$$y = -\ln r \; ; \quad r < 1 \tag{2.31}$$

Equations (2.30) and (2.31) define the correspondence of points in the η and χ planes of Figure 2.10 under the mapping $\chi = e^{i\eta}$.

2.3.2 Sound Propagation in Radial Bends Without Mean Flow

The wave equation in velocity potential form is

$$\nabla^2\phi + (\omega/c_o)^2\phi = 0 \tag{2.32}$$

where $\phi(x,y)$ is the velocity potential.

A general solution of equation (2.32) in separable rectangular two-dimensional co-ordinates is

$$\phi(x,y,t) = \sum_{m=o}^{\infty} A_{mo}\cos(k_m y)\exp[+i(-k_{mo}x+\omega t)] \tag{2.33}$$

where the x axis is parallel to the direction of propagation. The wave number k_{mo} which describes sound propagation in the x direction is

$$k_{mo} = \pm [k_o^2 - k_m^2]^{\frac{1}{2}} \tag{2.34}$$

where for a rigid walled duct $k_m = m\pi/h^s$, while $k_o = \omega/c_o$.

Following Morse and Ingard (1968), at low frequencies ($\omega \to 0$), for which the wavelength of sound is much larger than the transverse duct dimension, $\phi(x,y)$ will approximate a solution of Laplace's equation $\nabla^2\phi = 0$. In this case $\phi(x,y)$ will be the real part of a function of the complex variable $\eta = x + iy$ defined as

$$F(\eta) = \phi(x,y) + i\psi(x,y) \tag{2.35}$$

and the velocity potential $\phi(x,y)$ and the stream function $\psi(x,y)$ will be related by the Cauchy-Riemann equations to the requirements of the method. Hence the x and y components of the acoustic particle velocity and pressure are

$$u_x = \text{Real } \partial F/\partial\eta = +\partial\phi/\partial x \tag{2.36}$$

$$u_y = -\text{Imag } \partial F/\partial\eta = +\partial\phi/\partial y \tag{2.37}$$

$$p = i\rho_o\omega \text{ Real } F = -i\rho_o\omega\phi \tag{2.38}$$

Since the analysis is limited to low frequencies for which the (0,0) mode will be the only mode propagating it is only necessary to consider the m = o part of equation (2.33). The acoustic particle velocities and pressure for the (0,0) mode in the straight duct (η plane) are from equations (2.36), (2.37) and (2.38)

$$u_x = -ik_o\phi \tag{2.39}$$

$$u_y = 0 \tag{2.40}$$

$$p = -i\rho_o\omega\phi \tag{2.41}$$

The phase speed of the (0,0) mode in the straight duct (η plane) is determined simply by

$$c_o = x/t \tag{2.42}$$

Applying mapping equation (2.30), the straight duct (0,0) mode phase speed transforms back to the χ (physical) plane as †

$$c_o \sim \theta/t \tag{2.43}$$

where time t is invariant under transformation. Equation (2.43) determines the basic non-dimensional requirement of the solution in the χ plane and can be rewritten as

$$c_o \sim (1/r)c^c(r) \tag{2.44}$$

where $c^c(r)$ is a linear phase speed which varies inversely with radius across the curved section.

Thus the straight duct wave number k_o is seen to map to the curved (physical) plane as

$$k_o \sim r\,k^c(r) \tag{2.45}$$

Equation (2.45) agrees with theoretical predictions obtained from a cylindrical co-ordinate solution of the problem. Rostafinski (1972) has theoretically demonstrated that the wavelength of low frequency sound in radial bends for the (0,0) mode varies linearly across the duct, being larger at the outer than the inner radius. This most basic nature of low frequency sound propagation in curved ducts is thus determined simply by the mapping procedure without any prior assumptions.

As k^c is a function of r, to establish a usable value and relate it to the driving frequency k_o, it is averaged across the duct and denoted equal to k_o at the average position. Two different averages

---

† the symbol $\sim$ is used to mean "maps to".

are investigated. A simple arithmetic average would lead to

$$k_o \sim k_o R_1 (a+1)/2 \tag{2.46}$$

while a geometric average of wave number across the curved section would provide

$$k_o \sim k_o R_1 a^{\frac{1}{2}} \tag{2.47}$$

Equations (2.46) and (2.47) define correspondences between the respective wave numbers of the straight duct η plane and the curved (physical) plane. The curved duct wave number has been previously called the angular wave number ν_o due to its non-dimensional nature.

Thus
$$\nu_o \simeq k_o R_1 (a+1)/2 \tag{2.48}$$

or
$$\nu_o \simeq k_o R_1 a^{\frac{1}{2}} \tag{2.49}$$

depending upon the form of averaging assumed.

Rayleigh has shown that waves in curved ducts of large radius should propagate as if the duct were straight. In equations (2.48) and (2.49) as $a \to 1$ it can be seen that $\nu_o \to k_o R_1$. Thus equations (2.48) and (2.49) fulfil the limiting Rayleigh condition.

Values of angular wave number were derived using both equations (2.48) and (2.49) for ducts of different aspect ratio. Equation (2.48) was found to most accurately predict the angular wave numbers of the (0,0) mode over the widest frequency range and values derived from this equation for different aspect ratios are plotted in Figure 2.11 as a function of wave number non-dimensionalized against the curved duct width. Figure 2.11 also shows for comparison values of angular wave number derived by Rostafinski who used a closed form solution of the cylindrical characteristic equation. As Rostafinski's analysis is limited to ducts of aspect

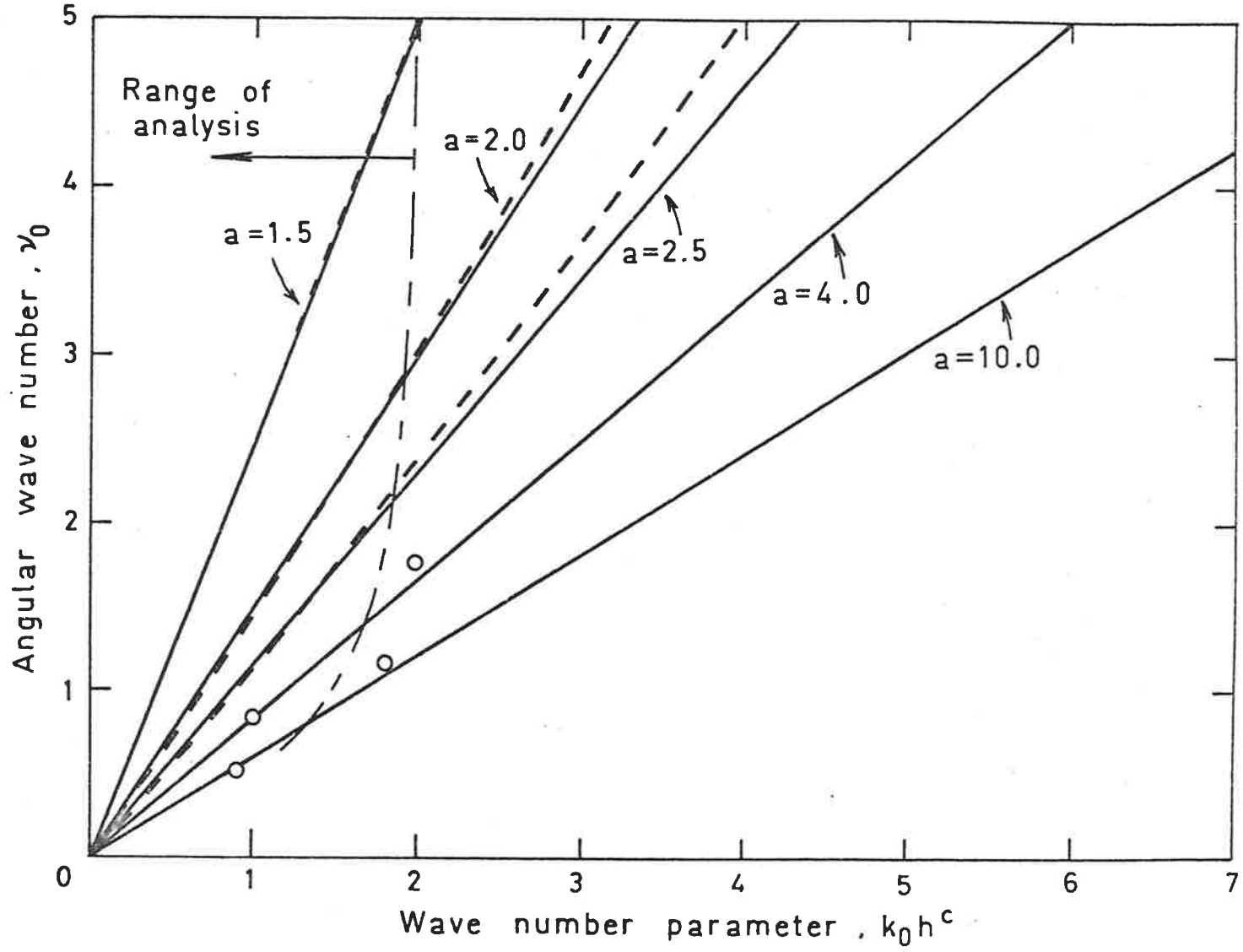

FIGURE 2.11. Angular wave numbers of the (0,0) mode. ——— , mapping analysis; — — — , cylindrical co-ordinates solution due to Rostafinski (1974); O , cylindrical co-ordinates solution due to Fuller and Bies (1978).

ratio $a \lesssim 2.5$, values of ν_o for two bends of aspect ratio $a = 4$ and $a = 10$ determined by the iterative solution of the cylindrical characteristic equation as discussed previously are given. In practice the curved duct wave number equals k_o at some other position than the arithmetic mean radius, as discussed by Cummings (1974), but for the low frequency range considered, this is found to cause only marginal error in the analytic results particularly in curved ducts of aspect ratio $a \lesssim 4$. This will be discussed in a later section.

It should be noted at this stage, that although equation (2.48) could have been arrived at largely by physical reasoning, this would involve an initial assumption of the wave number distribution in the curved duct or a prior knowledge of curved duct wave behaviour, whereas in this analysis the relationship is a simple result of the non-dimensional nature of the mapping process without any prior assumptions or knowledge of curved duct behaviour.

The angular wave number of higher non-propagating modes in curved ducts can be derived from the straight duct characteristic equation (2.34) written in complex form as

$$k_{mo} = \pm i[(m\pi/h^s)^2 - k_o^2]^{\frac{1}{2}} \qquad (2.50)$$

Using the mapping equations (2.30) and (2.31) the angular wave numbers for evanescent modes in the curved duct (physical) plane are given by the mapped solution of equation (2.50). Thus since

$$h^s = y_2 - y_1$$

$$h^s \sim -\ln R_1 + \ln R_2$$

$$h^s \sim \ln a \qquad (2.51)$$

the angular wave numbers of evanescent modes are

$$\nu_m \simeq i[(m\pi/\ln a)^2 - \nu_o^2]^{\frac{1}{2}} \tag{2.52}$$

It was found for the case of evanescent modes that the geometric averaged form of ν_o used in equation (2.52) provided the closest agreement with values derived from a cylindrical analysis. Values of ν_m for three decaying modes, m = 1,2,3 derived from equation (2.52) for a curved duct of aspect ratio a = 2 are plotted in Figure 2.12 with curves obtained by Rostafinski for comparison. It should be noted that at low frequencies ($k_o R_1 \to 0$) equation (2.52) reduces to

$$\nu_m \to im\pi/\ln a \tag{2.53}$$

which is identical to the result of the extensive cylindrical analysis of Rostafinski for $k_o R_1 << 1$.

The agreement shown by Figure 2.12 for ν_m approaching zero (i.e. near cut-on) encourages the development of an equation for the cut-off frequencies of higher modes in the curved section. At cut-off from equation (2.52)

$$\nu_o = m\pi/\ln a \tag{2.54}$$

Thus using equation (2.49) we see that cut-off frequencies in terms of the non-dimensional driving frequency are given by

$$k_o R_1 \simeq m\pi/(a^{\frac{1}{2}}\ln a) \tag{2.55}$$

Cut-off frequencies derived from equation (2.55) for ducts of different aspect ratio and three modes are shown in Table 2.2. These values should be compared to those of Table 2.1 which are cut-off frequencies derived by Osborne using an iterative solution of the cylindrical characteristic equation.

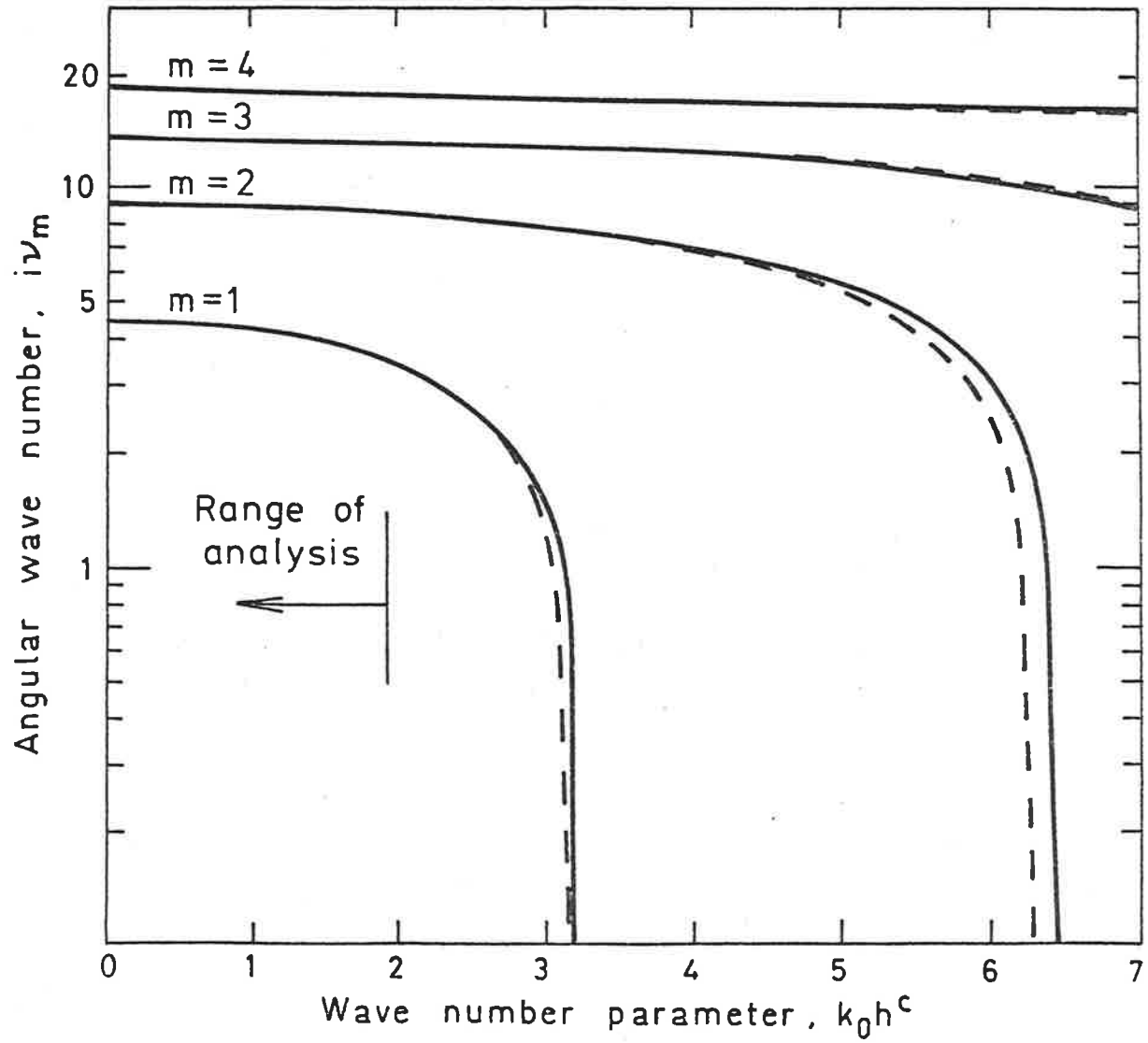

FIGURE 2.12. Angular wave numbers of higher order evanescent modes. ——, mapping analysis; – – –, cylindrical co-ordinates solution due to Rostafinski (1976).

Table 2.2 : Cut-off Frequencies for Higher Modes for Curved Ducts of Different Aspect Ratio Derived Using Conformal Mapping

Cut-off Frequency, $k_o R_1$

$a = R_2/R_1$	m = 1	m = 2	m = 3
1.2	15.72	31.46	47.19
1.5	6.33	12.65	18.98
2.0	3.20	6.41	9.61
2.5	2.17	4.34	6.51
3.0	1.65	3.3	4.95
4.0	1.13	2.27	3.40

The particle velocities and pressure of the (0,0) mode in the curved duct plane are obtained from the mapped solution of the straight duct equations. Before this mapping procedure can be undertaken, we must discuss the mapping of ρ_o. As for the analysis leading to equation (2.48) from both the dimensional form of the mapping and a consideration of relative areas of the χ and η planes it can be seen that the constant density of the η plane will map to a density that varies linearly with radial distance in the χ plane.

$$\text{i.e.} \qquad \rho_o \sim r\rho^c(r) \tag{2.56}$$

This result follows from the stretching of the line elements involved in the mapping from the η plane to the χ plane. Thus as with phase velocity, if we arithmetically average the mapped density in the χ plane and denote this approximately equal to ρ_o, we see that

$$\rho_o \sim \rho_o R_1(a+1)/2 \qquad \text{approximately} \tag{2.57}$$

To derive the pressure and velocity distributions for the (0,0) mode within the curved duct we apply the derived mapping equations (2.30) and (2.31) to the solution of the velocity potential in the η plane, equations (2.39), (2.40) and (2.41), and thus transform them back to the (physical) χ plane. In this case the curved duct solutions are

$$u_\theta \simeq -i\nu_o A_{oo} \exp[i(-\nu_o\theta + \omega t)] \tag{2.58}$$

$$u_r \simeq 0 \tag{2.59}$$

$$p \simeq -i\omega\rho_o R_m A_{oo} \exp[i(-\nu_o\theta + \omega t)] \tag{2.60}$$

where R_m is the mean radius of the curved section. Using equation (2.48) for the mean value of ν_o, the impedance of the curved section, defined

as the ratio of pressure to particle velocity is thus

$$Z^c \simeq \rho_o c_o \tag{2.61}$$

These equations will be discussed in a later section.

The pressure and velocity distributions of evanescent modes close to the generating surface can be determined by mapping the corresponding distribution for evanescent modes in the straight duct plane. The solution of the velocity potential in the η plane for higher modes is

$$\phi_{m\neq 0} = \sum_{m=1}^{\infty} A_{mo} \cos(k_m y) \exp[i(-k_{mo} x + \omega t)] \tag{2.62}$$

and the corresponding solutions for particle velocity and pressure distribution within the straight duct are

$$u_x = -i k_{mo} \sum_{m=1}^{\infty} A_{mo} \exp[i(-k_{mo} x + \omega t)] \cos(k_m y') \tag{2.63}$$

$$u_y = +i k_m \sum_{m=1}^{\infty} A_{mo} \exp[i(-k_{mo} x + \omega t)] \sin(k_m y') \tag{2.64}$$

and

$$p = -\omega i \rho_o \sum_{m=1}^{\infty} A_{mo} \exp[i(-k_{mo} x + \omega t)] \cos(k_m y') \tag{2.65}$$

Applying mapping equations (2.30) and (2.31) to transform these solutions back to the χ (physical) curved plane the corresponding curved duct acoustic distributions for evanescent modes are

$$u_\theta \simeq -i\nu_m \sum_{m=1}^{\infty} A_{mo} \exp[i(-\nu_m \theta + \omega t)] \cos[(m\pi/\ln a) \ln(r/R_1)] \tag{2.66}$$

$$u_r \simeq i(m\pi/\ln a) \sum_{m=1}^{\infty} A_{mo} \exp[i(-\nu_m \theta + \omega t)] \sin[(m\pi/\ln a) \ln(r/R_1)] \tag{2.67}$$

$$p \simeq -\omega i \rho_o R_m \sum_{m=1}^{\infty} A_{mo} \exp[i(-\nu_m \theta + \omega t)] \cos[(m\pi/\ln a) \ln(r/R_1)] \qquad (2.68)$$

where from Figure 2.10 it can be seen using equation (2.31) that

$$y' = y - y_2$$

$$y' \sim -\ln r + \ln R_1$$

$$\sim -\ln(r/R_1) \qquad (2.69)$$

From these equations the characteristic function describing amplitude variation radially across the curved duct for evanescent modes is determined to be;

for tangential particle velocity and pressure:

$$\psi^c_{mo} \simeq \cos[(m\pi/\ln a) \ln(r/R_1)] \qquad (2.70)$$

for radial particle velocity:

$$\psi^c_{mo} \simeq \sin[(m\pi/\ln a) \ln(r/R_1)] \qquad (2.71)$$

Figure 2.13 shows a theoretical tangential velocity distribution derived from equation (2.70) for ducts of different aspect ratio. Figure 2.14 shows a similar radial velocity distribution derived from equation (2.71). Values of velocity distribution derived by Rostafinski (1976) using an approximate solution in cylindrical co-ordinates are shown for comparison.

The characteristic function for evanescent modes indicates that the amplitude distribution will be either a distorted cosine or sine. The position at which a minimum in amplitude occurs for pressure and tangential velocity and a maximum for radial velocity amplitude is given approximately by setting the argument of equations (2.66), (2.67) and (2.68) equal to $\pi/2$. Thus

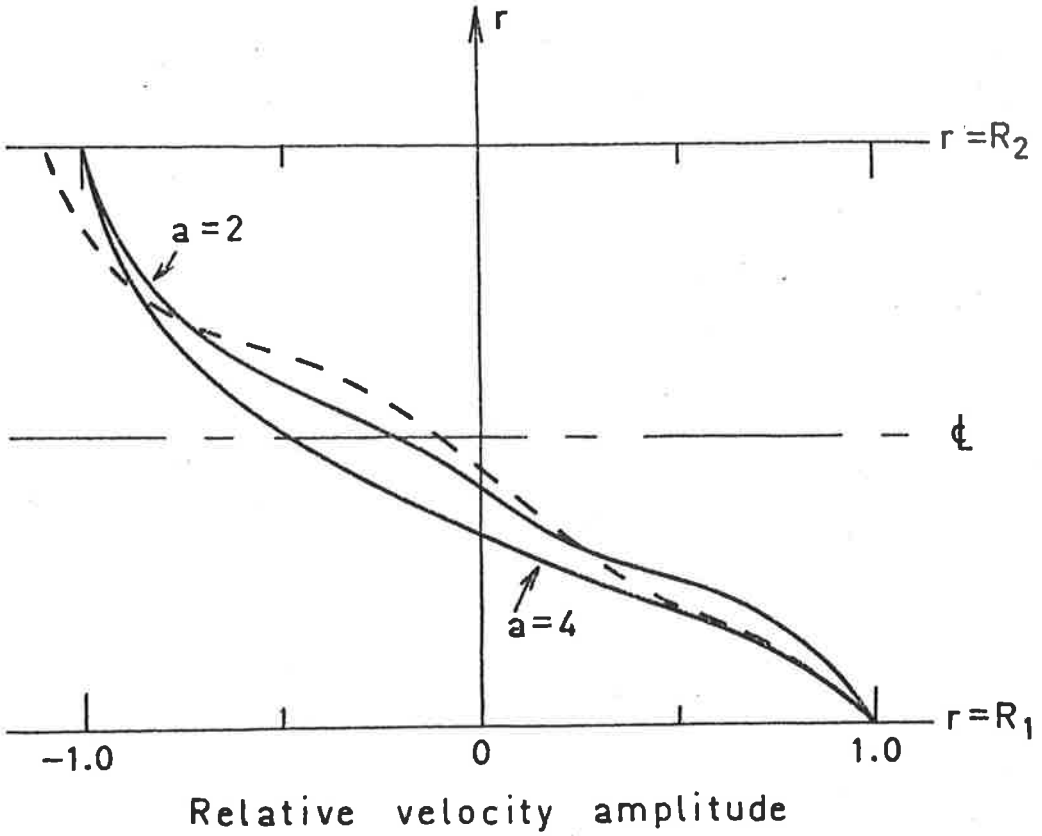

FIGURE 2.13. Tangential velocity amplitude distribution of the (1,0) evanescent mode. ——— , mapping analysis; – – – , cylindrical co-ordinates solution, a = 2, $k_o h^c$ = 1.01, due to Rostafinski (1976).

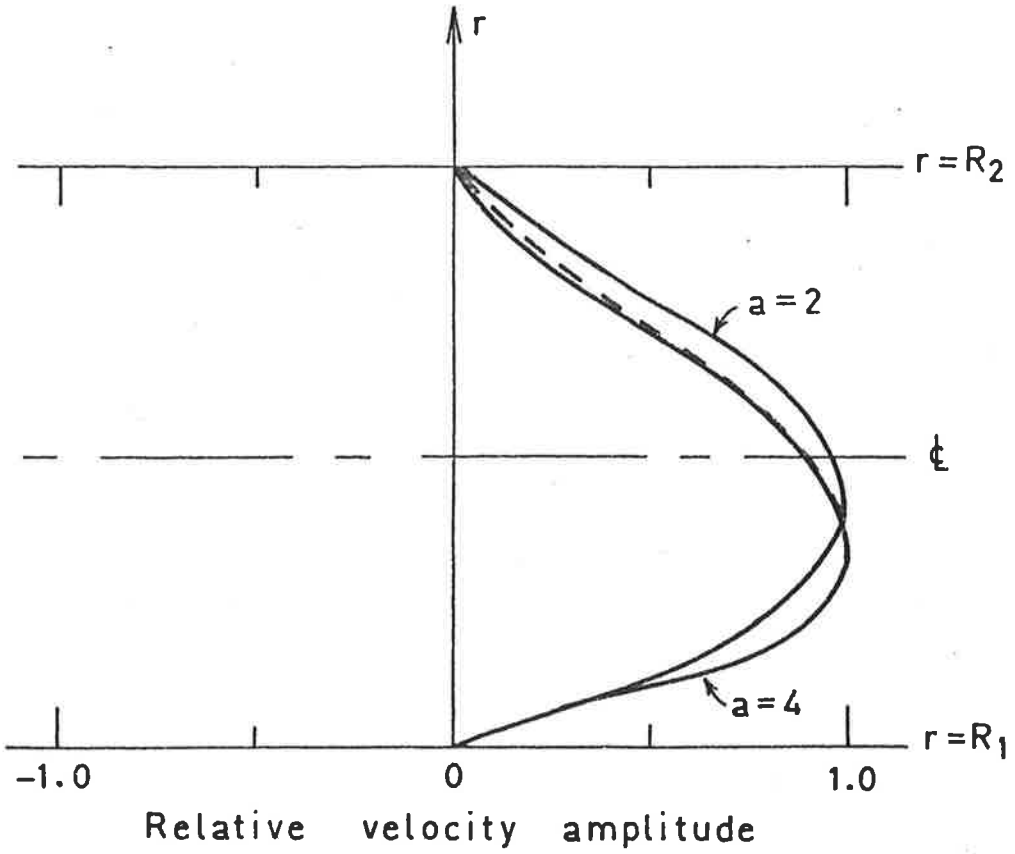

FIGURE 2.14. Radial velocity amplitude distribution of the (1,0) evanescent mode. ——, mapping analysis; — — —, cylindrical co-ordinates solution, a = 2, $k_o h^c$ = 1.01, due to Rostafinski (1976).

$$r_m/R_1 = a^{\frac{1}{2m}} \tag{2.72}$$

The acoustic distribution functions, equations (2.66) and (2.67) also provide us with information about the dominance of an evanescent mode. From the harmonic term of these equations, since ν_m is imaginary, the waves attenuate by a factor of e^{-1} in an angle of propagation (in radians) of $\theta \simeq 1/\nu_m$. Angles for which the amplitude of the (1,0) mode has decayed by a factor of e^{-1} for two different aspect ratios are shown in Figure 2.15.

2.3.3 Sound Propagation in Radial Bends with Mean Flow

The derivation of the curved duct equations with mean flow follows exactly the same procedure as the cased without flow except that convection of the propagating medium must be taken into account.

The wave equation with convection is

$$\nabla^2\phi + (\omega/c_o)^2(1 + i(1/\omega)\,\underset{\sim}{V}\cdot\nabla)^2\phi = 0 \tag{2.73}$$

where $\underset{\sim}{V} = V_x\underset{\sim}{i} + V_y\underset{\sim}{j} + V_z\underset{\sim}{z}$ is the velocity vector describing magnitude and direction of flow. For flow parallel to the x axis a general two-dimensional solution of equation (2.73) is

$$\phi = \sum_{m=o}^{\infty} A_{mo}\cos(k_m y)\exp[i(-k_{mo}x + \omega t)] \tag{2.74}$$

where the modal wave number, as derived in Chapter 1 is given by

$$k_{mo}^{d} = [-Mk_o \pm [k_o^2 - (1-M^2)(k_m^2)]^{\frac{1}{2}}] \,/\, [1-M^2] \tag{2.75}$$

For the (0,0) mode, equation (2.75) predicts that flow will have the effect of decreasing the downstream wave number by a factor of $1/(1+M)$

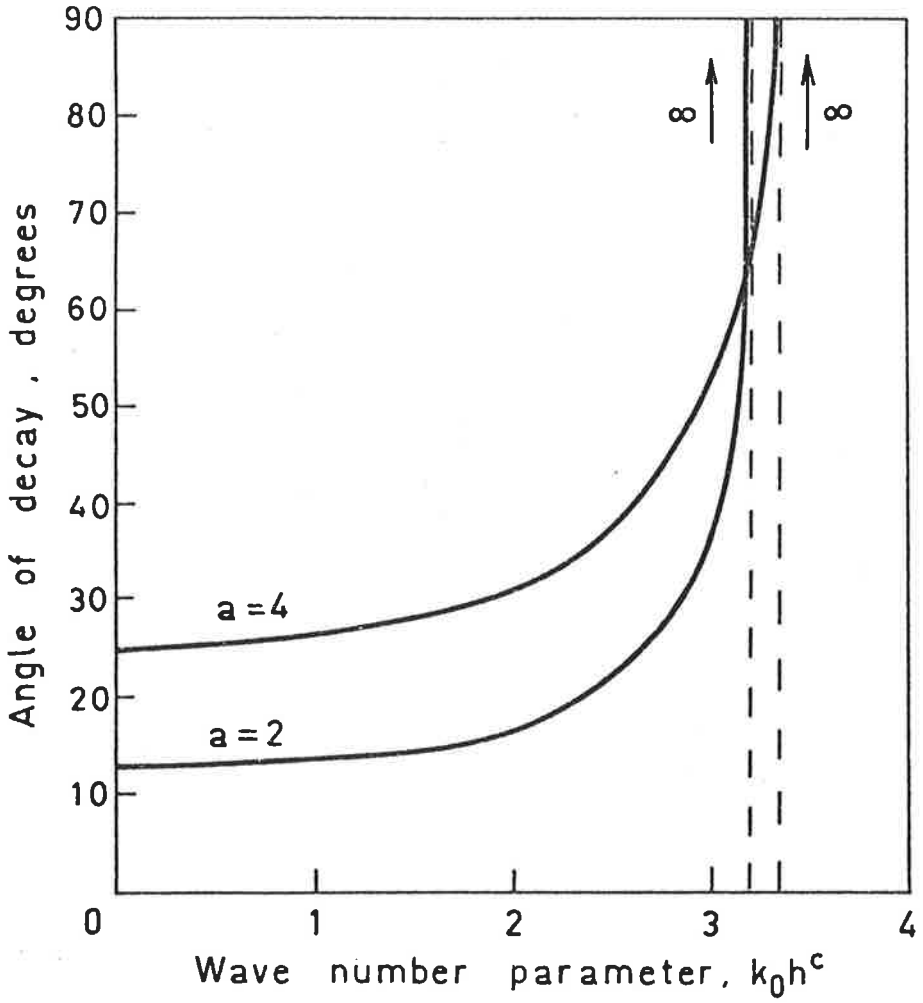

FIGURE 2.15. Decay rates of the evanescent (1,0) mode derived from the mapping analysis.

and increasing the upstream wave number by $1/(1-M)$.

For low frequencies ($k_o \to 0$) solutions of equation (2.73) are approximate solutions of Laplace's equation $\nabla^2\phi = 0$. Thus using the complex form derived in the case without flow the acoustic particle velocity components and pressure are for the (0,0) mode

$$u_x = -ik^d_{oo}\phi \tag{2.76}$$

$$u_y = 0 \tag{2.77}$$

$$p = \rho_o c_o u_x \tag{2.78}$$

The acoustic pressure is written in simplified form applicable to the (0,0) mode to eliminate the convection term (see section 1.3.2).

It is assumed that the flow has a uniform velocity profile in the straight duct η plane. Thus when this profile is mapped to the curved χ plane, the resultant flow distribution is found to vary linearly as for the phase speed i.e.

$$V_x \sim (1/r)V^c(r) \tag{2.79}$$

Hence at each radial position r across the curved duct the flow will have the effect of increasing the phase speed by $V^c(r)$ for downstream propagation, thus equation (2.54) of the no flow analysis is modified to

$$c_o + V_x \sim (1/r)c^c(r) + (1/r)V^c(r) \tag{2.80}$$

hence

$$c_o(1+M) \sim c^c(r)(1/r)(1+M^c) \tag{2.81}$$

since $c^c(r)$ is the speed of propagation of sound at radial position r. Arithmetically averaging equation (2.81) and setting the result equal

to c_o at the mean radius thus provides the angular wave numbers with flow

$$\nu_o^d \simeq \frac{k_o R_1 (a+1)}{2(1+M^c)} \tag{2.82}$$

for downstream propagation of sound. For upstream propagation of sound the sign of the Mach number is reversed, thus the angular wave numbers for upstream propagation is

$$\nu_o^u \simeq \frac{k_o R_1 (a+1)}{2(1-M^c)} \tag{2.83}$$

In practice the curved duct velocity profile would be far different from the potential form used here. However an approximate value M^c can be defined as the average of M across the curved duct which may then be used. This, in fact, is what the mapping process of averaging implies.

The wave numbers of evanescent modes with flow are obtained from equation (2.75) transformed back to the (physical) χ plane and are

$$\nu_m \simeq [-M^c \nu_o \pm i[(1 - (M^c)^2)(m\pi/\ln a)^2 - \nu_o^2]^{\frac{1}{2}} / [1 - (M^c)^2] \tag{2.84}$$

where ν_o is the angular wave number in a stationary medium given by equation (2.49).

The cut-off frequencies of higher modes with flow are thus

$$k_o R_1 \simeq \left(\frac{m\pi}{a^{\frac{1}{2}} \ln a}\right) (1 - (M^c)^2)^{\frac{1}{2}} \tag{2.85}$$

for both upstream and downstream propagation of sound.

The acoustic particle velocities and pressures for the (0,0) mode are obtained approximately from equation (2.76), (2.77) and (2.78)

transformed back to the (physical) χ plane and are,

$$u_\theta^d \simeq -i\nu_o^d \exp[i(-\nu_o^d \theta + \omega t)] \tag{2.86}$$

$$u_\theta^u \simeq -i\nu_o^u \exp[i(-\nu_o^u \theta + \omega t)] \tag{2.87}$$

for downstream and upstream propagation respectively. The radial particle velocity is

$$u_r \simeq 0 \tag{2.88}$$

for both upstream and downstream propagation and the acoustic pressure is approximately

$$p \simeq \rho_o c_o u_\theta \tag{2.89}$$

for both downstream and upstream propagation.

Thus the impedance of the curved section with flow for the (0,0) mode is approximately

$$Z^c \simeq \rho_o c_o \tag{2.90}$$

2.3.4 Range of Applicability of the Conformal Mapping Method

For the solution of the acoustic wave equation to be an approximate solution of Laplace's equation, the frequency is limited such that the wavelength of sound is much greater than the transverse duct dimensions in the straight duct in the plane. Obviously this is an arbitrary definition and some choice of the applicable range of frequency has to be made. The upper limiting frequency is chosen to be such that $k_o h^s = 2$ in the straight duct plane. At this frequency the wavelength is approximately three times the major duct width. To obtain a frequency limit in the curved plane, the straight duct limit

must be transformed back to the χ plane, thus

$$k_o h^s \sim \nu_o \ln a \tag{2.91}$$

Substituting equation (2.48) and using the relation

$$k_o h^c = k_o R_1 (a - 1) \tag{2.92}$$

we see that the limit on the driving frequency in the curved duct is thus

$$k_o h^c \simeq \frac{4(a-1)}{\ln a(a+1)} \tag{2.93}$$

where the wave number is non-dimensionalized against curved duct width. This frequency limit is plotted in Figures 2.11 and 2.12 for different aspect ratios to indicate the expected range of the equation.

In the case of mean flow, equation (2.93) is modified for downstream and upstream propagation respectively as follows

$$k_o h^c = \frac{4(a-1)(1+M^c)}{\ln a\,(a+1)} \tag{2.94}$$

and

$$k_o h^c = \frac{4(a-1)(1-M^c)}{\ln a\,(a-1)} \tag{2.95}$$

2.4 EXPERIMENTAL INVESTIGATION - EQUIPMENT AND PROCEDURE

The experimental equipment and layout used to investigate curved duct wave behaviour with and without flow is shown in Figure 2.16. The duct system has a 0.127 x 0.635 meter rectangular cross section and is constructed in removable sections from 0.0254 meter thick wood lined with laminex to fulfil the rigid wall boundary conditions. The basic

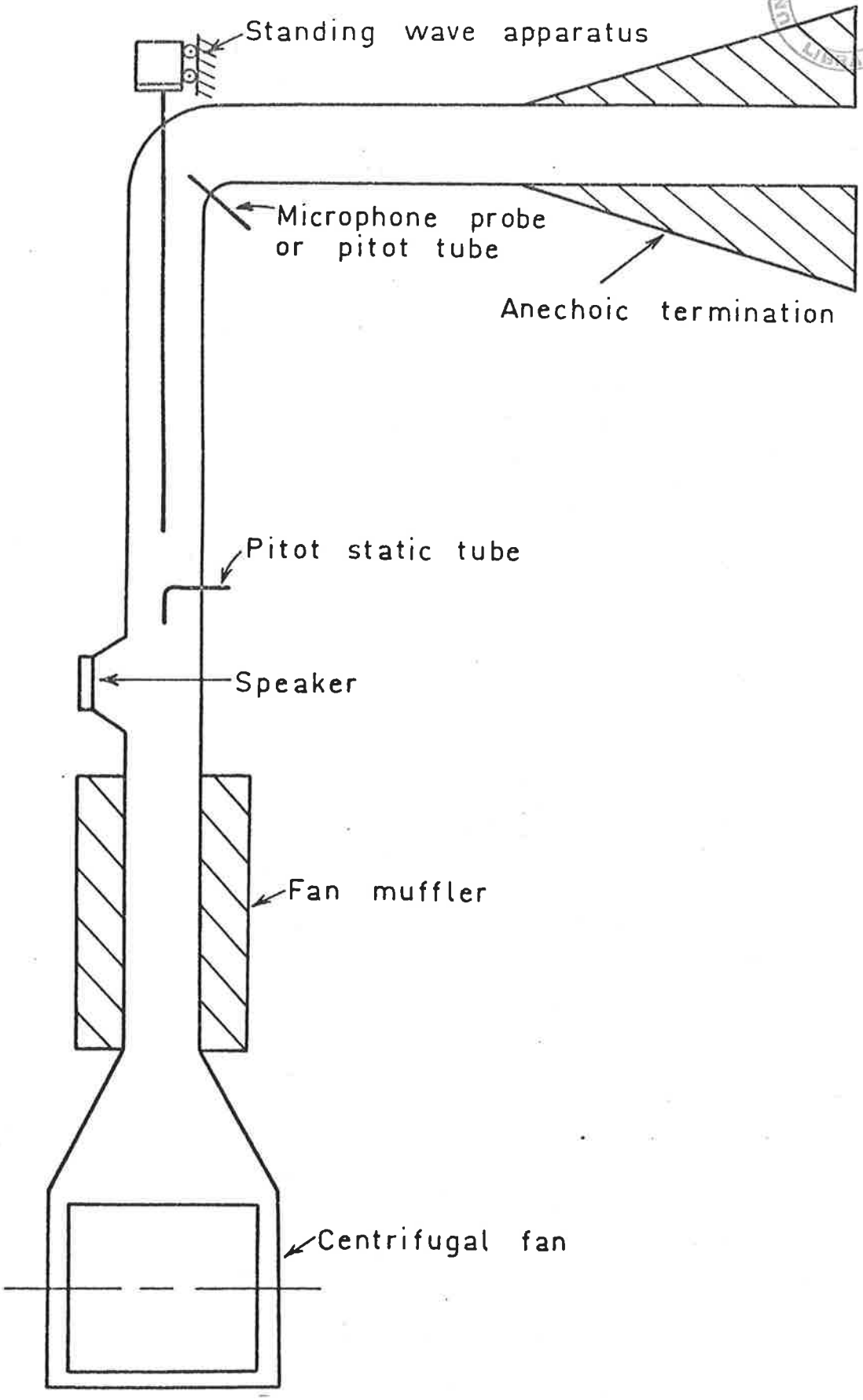

FIGURE 2.16. Arrangement of the experimental apparatus.

parts of the apparatus were as used in the experimental investigation of straight duct behaviour with flow. Two bends were investigated experimentally. Both had a total angle of 90° but differing aspect ratios of a = 3.5 and a = 2.25. These bends were constructed from machined hardwood.

The sound source was a single cone 15 watt loudspeaker and was positioned 1.7 meters upstream of the bend at which distance any locally generated cross modes will have decayed sufficiently to be negligible. To eliminate reflections from the exit plane of the bend the downstream duct was anechoically terminated. For upstream propagation of sound, the anechoic termination was removed and replaced by the sound source. In this case the impedance of the bend is investigated on the source side of the bend.

Fluid flow was achieved by a centrifugal fan as discussed in section 1.4. A Heterodyne Analyser was used for all pressure measurements and as a signal generator. In the case of the experimental apparatus of Figure 2.16 the analyser provided a signal to noise ratio of greater than 50 dB at M = 0.1 in the upstream duct.

The radial pressure distribution in the curved bend was measured by traversing a microphone probe radially across the duct at an angle of 45° from the bend inlet. At this angle any evanescent modes generated at the straight duct - curved duct interface would have decayed to be negligible. The case without flow was considered first. Experimental values of relative pressure amplitude for the (0,0) mode in the bend of aspect ratio a = 2.25, defined by equation (2.96) are shown in Figure 2.5 for comparison with the theoretical results. The following equation was used to define the experimental points in the figure.

$$\text{Relative Pressure Amp} = 10^{\Delta dB/20} \qquad (2.96)$$

where ΔdB is obtained from the sound pressure level data as:

$$\Delta dB = SPL(r) - SPL(R_1) \qquad (2.97)$$

For the case of the conformal mapping analysis the bend of aspect ratio a = 3.5 was investigated experimentally. This was chosen to represent a "sharp" bend and thus provide a relatively severe test for the theory. For a bend of aspect ratio a = 3.5 the proposed upper limit to the theory given by equation (2.93) is $k_o h^c \lesssim 1.76$. Hence the bend was investigated for the case without flow for three non-dimensional frequencies, $k_o h^c$ = 0.5, 1.0 and 1.5. The no flow distributions for these frequencies are shown in Figure 2.17. For the case of flow one frequency $k_o h^c$ = 1.0 at different flow rates of M = 0.04 and M = 0.08 was considered for downstream and upstream propagation respectively. These distributions are plotted in Figures 2.18 and 2.19 respectively.

The impedance of the bend with and without flow was investigated with the standing wave apparatus shown in Figure 2.16. The impedance was determined by analysing the acoustic pressure standing wave in the incident duct to the bend.

To aid with later discussions the flow profiles in the bend (at M = 0.04 and M = 0.08 in the upstream duct) were measured by traversing a stagnation tube radially across the curved section at an angle of 45° from the bend inlet. The mouth of the stagnation tube was flattened to a opening of 2 mm to enable accurate readings. Due to the non-uniform flow in the curved section the static pressure was measured at the incident straight duct wall and the value recorded was taken as the average static pressure in the bend. This approximation was thought to be sufficiently accurate for the low flow velocities investigated. Curved duct flow profiles for M = 0.04 and M = 0.08 in the upstream straight duct are shown in Figure 2.20. The average

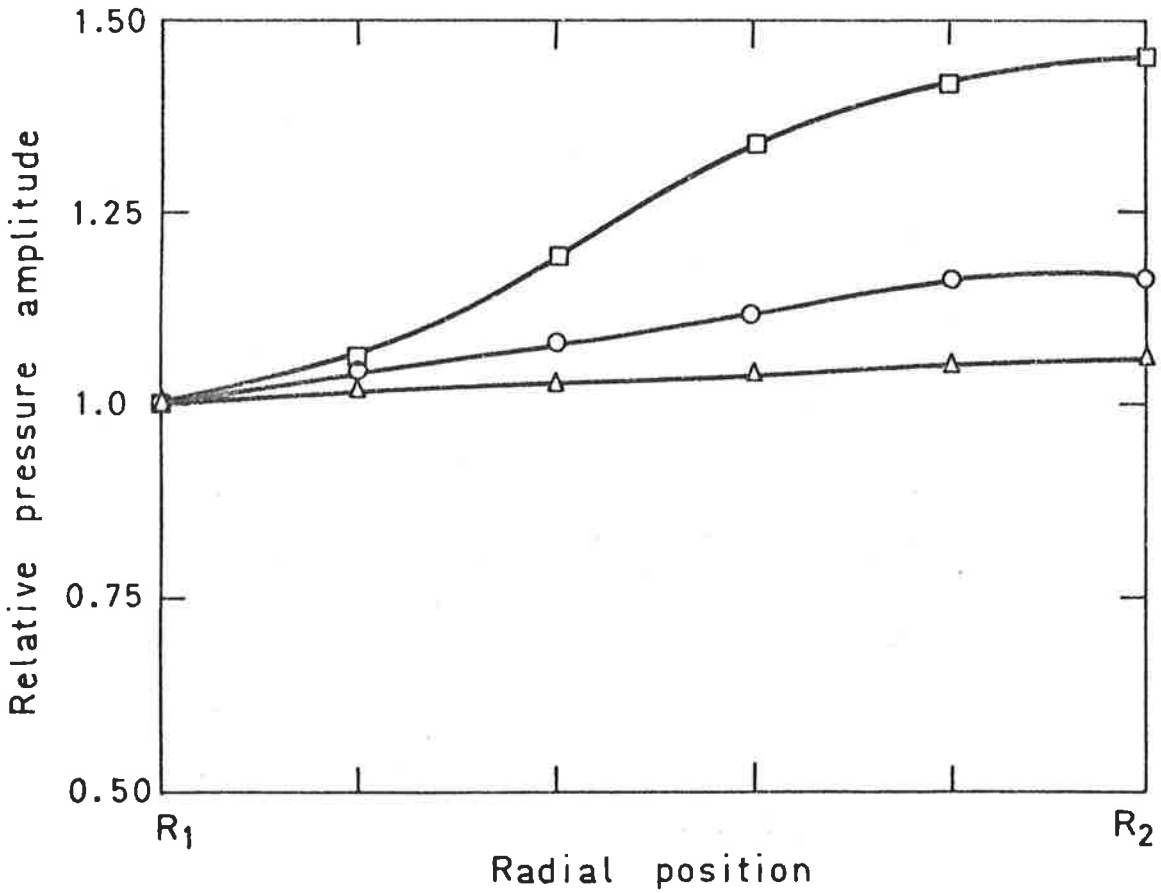

FIGURE 2.17. Experimental variation in relative pressure amplitude in a curved duct of aspect ratio, a = 3.5, Δ , $k_o h^c$ = 0.5; O , $k_o h^c$ = 1.0; □ , $k_o h^c$ = 1.5.

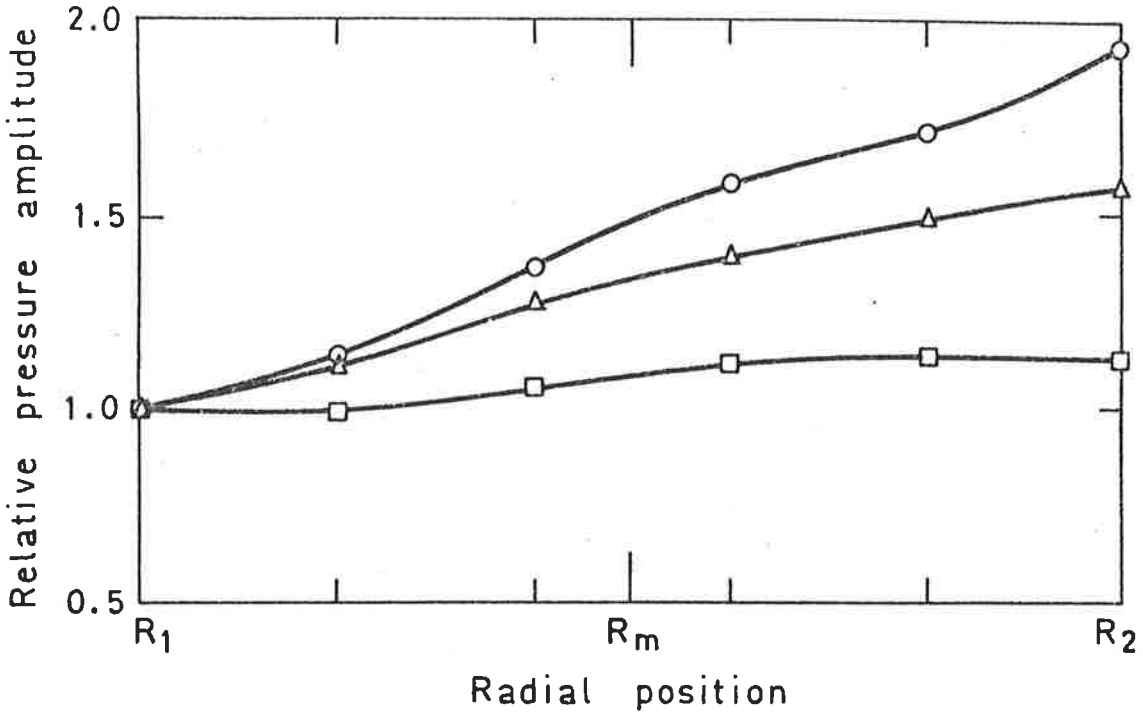

FIGURE 2.18. Experimental variation in relative pressure amplitude in a curved duct of aspect ratio, a = 3.5, $k_o h^c = 1.0$ and downstream propagation of sound. □ , $M^c = 0$; Δ , $M^c = .038$; O , $M^c = .078$.

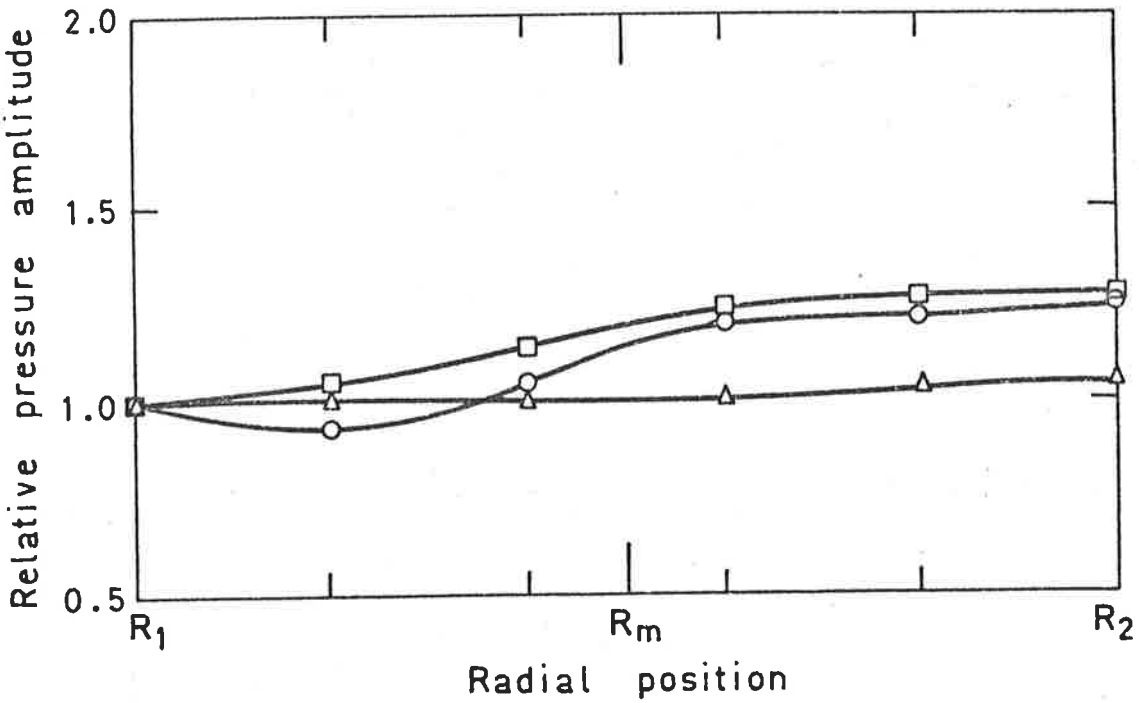

FIGURE 2.19. Experimental variation in relative pressure amplitude in a curved duct of aspect ratio, a = 3.5, $k_o h^c$ = 1.0 and upstream propagation of sound. □ M^c = 0; Δ, M^c = .038; O , M^c = .078.

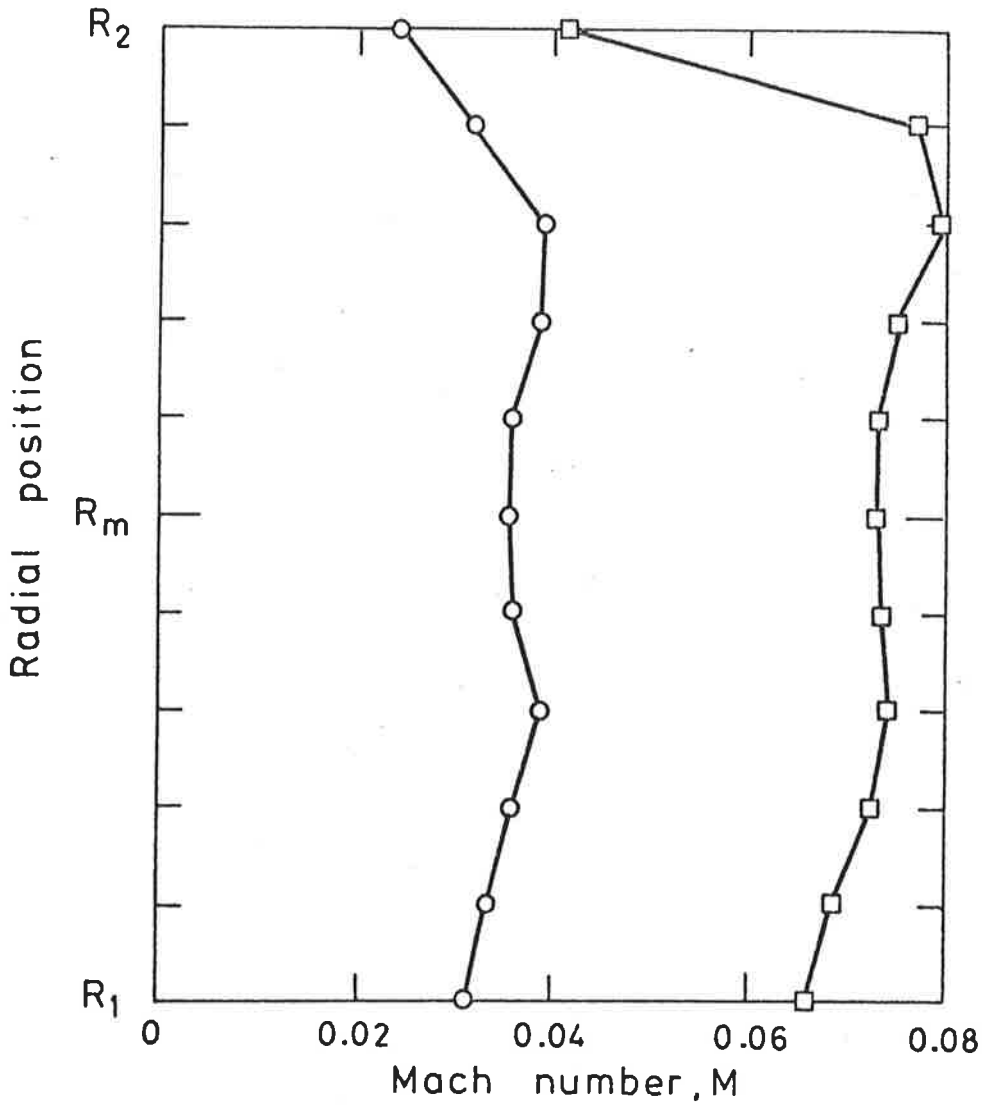

FIGURE 2.20. Flow velocity profiles at θ = 45° in a bend of aspect ratio, a = 3.5. ○ , M^c = .038; □ , M^c = .078.

velocity of the flow in the curved section was calculated to be $M^c = .038$ and $M^c = .078$ from the distributions for the two flow speeds.

2.5 DISCUSSION OF RESULTS

2.5.1 The Cylindrical Solution of the Wave Equation

As for straight ducts the acoustic motion of waves in curved ducts is characterized by a set of modes each of which is either propagating or evanescent (apart from the (0,0) mode) depending upon whether the mode is above or below cut-off. Differences in propagation between straight and curved ducts are to be expected, however, and the main difference occurs with the (0,0) mode. In a straight duct the phase speed of the (0,0) mode is independent of duct geometry being equal to c_o at all frequencies but in a curved duct the phase speed of the (0,0) mode is strongly dependent on duct geometry and frequency. This is borne out in Figure 2.2 which shows angular wave numbers of the (0,0) mode. The angular wave number can be seen from this diagram to be vastly different for ducts of different aspect ratios. Thus while the (0,0) mode in a straight duct is non-dispersive, the (0,0) mode in a curved duct is dispersive. This essential difference between straight and curved bends will be shown in a later chapter to have far reaching consequences on the propagational characteristics of the bend. Figure 2.2 also shows good agreement between the iterative solution of the characteristic equation used here and a closed form solution used by Rostafinski (1974).

Figure 2.2 shows that as the aspect ratio of the curved duct approaches unity, the corresponding angular wave number approaches infinity and when $a = 1$, the plot will be represented by the vertical axis. It can also be shown that if in Figure 2.2, angular wave number was plotted against $k_o R_1$ rather than $k_o h^c$, then as the aspect ratio approaches unity, the plot will tend towards a straight line at 45°

to each axis (for both axis having equal scaling) thus as $a \to 1$, $\nu_o \to k_o R_1$. Hence the cylindrical co-ordinate solution for angular wave numbers is seen to obey the Rayleigh condition that waves in a curved duct of large radii (i.e. $a \to 1$) will propagate as if the duct were straight.

For the curved duct the angular phase velocity of the (0,0) mode is seen to be

$$c_\theta = \omega/\nu_o \tag{2.98}$$

The angular phase velocity can be converted to an equivalent linear phase velocity c_p^* at the mean radius R_m as,

$$c_p^* = \frac{\omega}{\nu_o} R_m \tag{2.99}$$

The ratio of the straight duct phase velocity, given by equation (1.14) and the averaged curved duct phase velocity is thus

$$c_p^*/c_o = \frac{k_o R_m}{\nu_o}$$

$$= \frac{k_o R_1 (a+1)}{2\nu_o} \tag{2.100}$$

or

$$c_p^*/c_o = \frac{k_o h^c (a+1)}{2\nu_o (a-1)} \tag{2.101}$$

From the results of Figure 2.2 it can thus be seen that the average curved duct phase velocity is always marginally higher than in straight ducts for the frequency range $k_o h^c < 1.5$. However Cummings (1974) has demonstrated that for frequencies, such that $k_o h^c > \pi/2$ the reverse is true.

Figure 2.3 shows the angular wave numbers of three evanescent modes. As for straight ducts the angular wave number of evanescent modes was implicitly assumed to be imaginary. This assumption is borne out by energy considerations and will be discussed in more detail in the section dealing with the results of the conformal mapping analysis. Rostafinski (1972) has shown that at low frequencies ($kR_1 << 1.0$) values of angular wave number of evanescent modes are given by

$$\nu_s = is\pi/\ln a\,, \quad s = 0,1,2.....$$

In terms of the duct width the expected applicable range of the above equation is $k_o h^c << (a-1)$. For the duct of Figure 2.3 of aspect ratio $a = 1.5$, the agreement with Rostafinski's equation at low frequencies is seen to be good.

From Table 2.1 of cut-off frequencies of higher modes derived from equation (2.23) by Osborne (1976) it can be seen that increasing the aspect ratio has the effect of lowering the non-dimensional cut-off frequency $k_o R_1$. Thus wider bends tend to admit higher modes more readily. If the values of Table 2.1 are rewritten in terms of $k_o h^c = k_o R_1 (a-1)$ it can be seen that increasing the aspect ratio has the effect of increasing the non-dimensional cut-off frequency $k_o h^c$. Thus for a bend of constant width increasing the sharpness tends to decrease the ability of the bend to admit higher modes. The dependence of modal admittance of curved bends on the aspect ratio is clearly shown by the conformal mapping analysis and will be discussed in this section.

Whereas in a straight duct the (0,0) mode is a plane wave with constant amplitude across the duct, the (0,0) mode in a curved duct is found from Figures 2.4 and 2.5 to be non-plane. However due to the rectangular cross section of the bend the amplitudes will be plane in the z direction. From Figures 2.4 and 2.5 it can be seen that either

increasing the frequency or the aspect ratio independently leads to an increased variation in pressure amplitude across the duct. These figures also show that for bends of low aspect ratio or at very low frequencies the pressure distribution does not vary drastically and is close to that of a plane wave. This agrees with the conclusions of Cummings who showed that the pressure distribution tended towards uniformity for bends of large dimensions (i.e. $a \to 1$). The experimentally measured values of pressure amplitude distribution are seen from Figure 2.5 to agree well with the theoretical predictions. The small error apparent as $r \to R_2$, is most likely due to dimensional inaccuracies in the bend.

Figure 2.6 shows the variation in pressure amplitude distribution of the (1,0) mode in a duct of aspect ratio $a = 2$ at two frequencies. The distribution at the lower frequencies is very close to the distribution of the (1,0) mode in a straight duct, the minima occuring at a value greater than the mean radius. However for the higher frequency the distribution is far more distorted and the minima occurs closer towards the outside bend radius.

The tangential velocity distribution of the (0,0) mode, shown in Figures 2.7 and 2.8, shows an opposite trend to that of the pressure distribution. At low frequencies the distribution is non-uniform. Increasing the aspect ratio and frequency leads the tangential velocity distribution to become more uniform. Thus the increase in variation of pressure amplitude distribution discussed previously is balanced by a simultaneous decrease in variation of tangential velocity amplitude. This is well summarized by Rostafinski (1974) who showed that the tangential velocity distribution of the (0,0) mode follows closely that of a potential vortex for low frequencies ($k_o R_1 < 1$) and is close to a forced vortex at higher frequencies ($k_o R_1 \simeq 3$).

2.5.2 The Conformal Mapping Solution without Mean Flow

From the results of the analysis it can be seen that conformal mapping demonstrates the most basic characteristic of the propagation of the (0,0) mode in a curved bend; the stretching of phase speed radially across the bend. This important result reveals the mechanism of how sound propagates around the bend. Rather than transmitting by a "ray" type process, reflecting from the walls, the waves travel by bending around the curved surfaces maintaining a constant phase radially. A similar occurrence has been observed by both Cummings (1974) and Rostafinski (1972) using the complex cylindrical co-ordinate solution to the problem. This radial variation of magnitude implies that the curved duct parameters of propagation will be non-dimensional as opposed to the inverse units of length in the straight duct case.

From Figure 2.11, the simple relationship for the angular wave number of the (0,0) mode derived by this analysis gives good agreement with values determined using cylindrical co-ordinates in the range of frequencies considered as the limit. As expected, for the wavelength of sound approaching the transverse dimensions of the duct the error is increasingly apparent. However for the range of frequencies considered by this analysis the error between solutions derived by a cylindrical co-ordinates solution and those derived using conformal mapping are greatest at low frequencies ($\omega \to 0$). Increasing the aspect ratio of the bend increases the magnitude of the error. For a duct of aspect ratio $a = 4$ for $k_o \to 0$ the maximum error between the results of this analysis and a cylindrical co-ordinate solution is 6 percent. Hence from the results of Figure 2.11 an aspect ratio of $a \lesssim 4$ is tentatively suggested. In this range equation (2.48) is seen to accurately and simply predict the angular wave number of the (0,0) mode for

$$k_o h^c \lesssim \frac{4(a-1)}{\ln a\,(a+1)} .$$

This result should be compared to the practical guide for rectangular section bends proposed by Cummings (1974). To facilitate analysis of curved bends he developed a design chart for rectangular bends, reproduced in Figure 2.21, which provides k^c/k_o at the mean radius of the bend as a function of driving frequency and aspect ratio. The values of the chart were derived using a cylindrical co-ordinates solution. Cummings compared the reactance of two bends of aspect ratio a = 1.587 and a = 10.309 derived by considering the bend as an equivalent straight duct and using $k^c = k_o$ at the mean radius and k^c adjusted at the mean radius by the design chart of Figure 2.21. Whereas the adjusted circular wave number definitely improved the result at high frequencies ($k_o h^c \to \pi$) at lower frequencies ($0 < k_o h^c < \pi/2$) the discrepancy between the two results is minimal, especially in the less sharp bend. Thus in the range of frequency proposed, the simple equation for the angular wave number of the (0,0) mode, established by deriving the circular wave number distribution by mapping techniques and equating $k^c(r)$ to k_o at the mean radius provides sufficiently accurate values for practical use.

Figure 2.21 also demonstrates why the arithmetic mean provides the most accurate estimate of angular wave number over the widest frequency range. As shown in the Figure when $k_o h^c = \pi/2$, independent of aspect ratio, equation (2.48) will exactly predict the correct value of angular wave number whereas for frequencies lower or higher than this point the equation will respectively underestimate or overestimate the actual value. Thus the straight line plot of equation (2.48) provides an average of the actual plot obtained by a cylindrical co-ordinates solution.

Similarly, the approximate solution for evanescent modes, equation (2.52) is shown in Figure 2.12, to accurately and simply

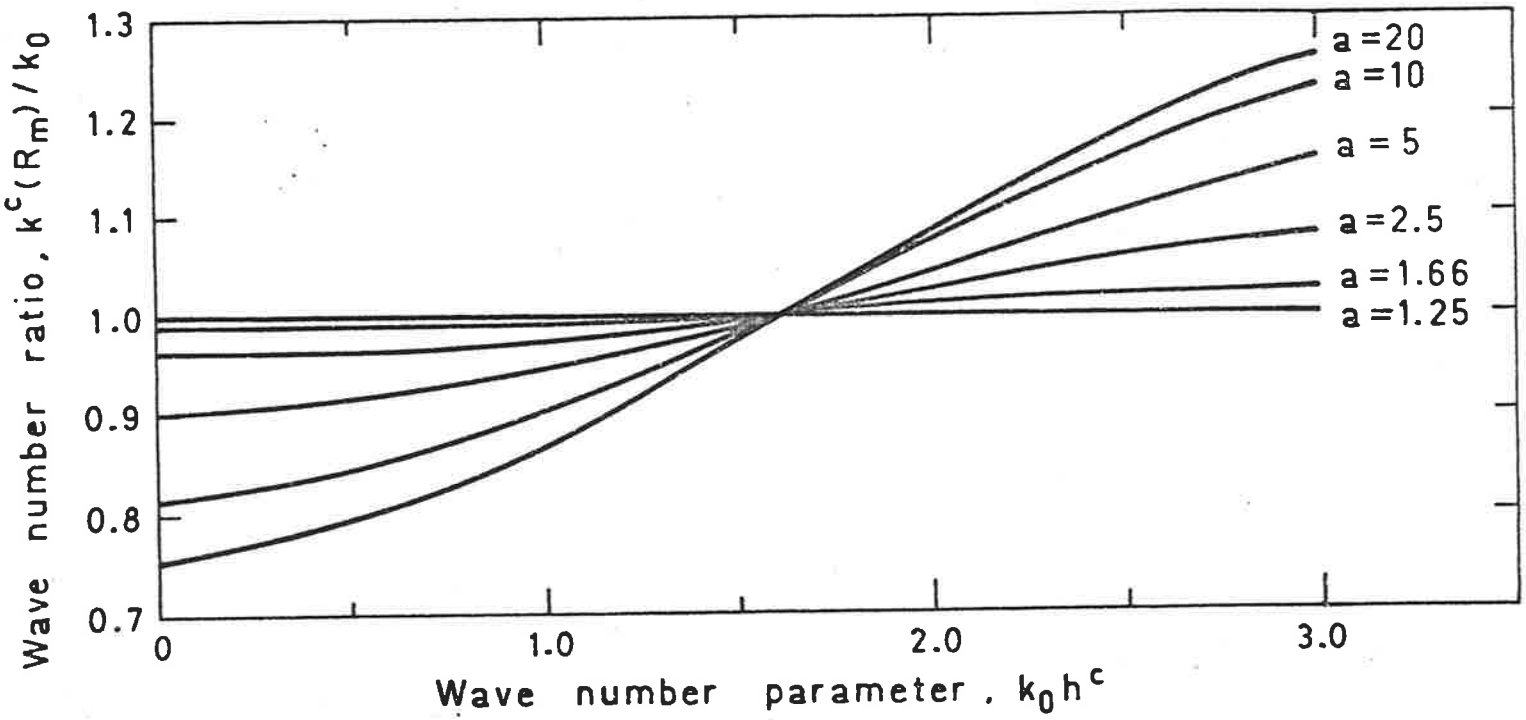

FIGURE 2.21. Variation in k^c/k_o at the mean radius of a curved bend, derived by Cummings (1974).

predict the evanescent angular wave number for low frequencies without the protracted analysis involved in the imaginary roots solution of the characteristic equation written in cylindrical co-ordinates. In fact a direct result of the mapping analysis is that evanescent modes will have a purely imaginary wave number. This fact has been implicitly assumed by previous workers. For very low frequencies ($k_o R_1 \to 0$) the analysis gives an identical result to a relation derived by Rostafinski (1974).

A comparison between the results of Tables 2.1 and 2.2 shows that equation (2.55) provides an accurate estimate of the cut-off frequencies of higher modes up to m (or s) = 3. The agreement is seen to be particularly good for the (1,0) mode but decreases with increasing aspect ratio and modal number. Equation (2.55) predicts that increasing the aspect ratio decreases the non-dimensional cut-off frequency $k_o R_1$. Thus as concluded in the cylindrical result, wider curved ducts admit higher modes more readily while "sharper" bends tend to inhibit higher mode transmission.

Whereas the mapping theory is found to accurately predict the behaviour of the angular wave numbers of the (0,0) mode and evanescent modes, the same agreement is not shown in the predicted pressure amplitude distributions. The mapping theory predicts that the pressure amplitude distribution of the (0,0) mode in the curved duct is approximately plane. This is shown to be true for the experimental results of Figure 2.17 at the two lower frequencies of $k_o h^c = 0.5$ and $k_o h^c = 1.0$, however at the higher frequency of $k_o h^c = 1.5$, which is still within the proposed range of the analysis, the amplitude shows considerable radial variation. Cummings (1974) has shown that the pressure distribution tends towards uniformity for bends in which the aspect ratio approaches unity, thus the agreement is likely to be improved in "less

sharp" bends. Likewise the analysis indicates that the pressure distribution tends towards uniformity with decreasing frequency and this is borne out by experimental results. Equation (2.59) predicts that the radial particle velocity amplitude is extremely small. This agrees with results obtained by Rostafinski (1974), who estimated the radial velocity amplitude of the (0,0) mode to be two orders of a magnitude smaller than the tangential velocity amplitude at low frequencies.

The approximate relationships developed here for the amplitude distributions of evanescent modes at low frequencies compare well with similar values derived by Rostafinski. These distributions are seen to be a distorted sine or cosine shape and an equation which predicts the position of maximum or minimum pressure respectively is given. Figure 2.15 shows the influence of aspect ratio and frequency on the decay rate of evanescent modes. It can be seen that both increasing the frequency (below cut-off) and the aspect ratio leads to a reduced decay rate and the evanescent mode distribution extends further into the curved section. Therefore even though increasing the aspect ratio of a bend of constant width tends to increase the cut-off frequencies of higher modes, evanescent modes will be transmitted further into the curved section away from the surface at which they were generated. Generally speaking, evanescent modes are seen from Figure 2.15 to decay very quickly away from the generating surface except very close to cut-on where the evanescent mode is seen to propagate well into the curved section before decaying substantially. Therefore evanescent modes just below cut-off can be expected to modify the pressure distribution at angles of propagation well into the curved bend. Doak (1973) has shown that evanescent modes right on cut-on can in fact dominate the sound pressure field in a straight duct.

The experimental investigation of the standing wave in the acoustic incident duct to the bend revealed that, as predicted, the bend of aspect ratio a = 3.5 provided negligible discontinuity to acoustic propagation. This was also investigated by Cummings (1974) and his results indicate similar behaviour.

2.5.3 The Conformal Mapping Solution with Mean Flow

As intuitively expected, flow is seen to simply modify the angular wave number of the (0,0) mode by a multiplying factor of $1/(1+M)$ or $1/(1-M)$ for downstream and upstream propagation respectively. Thus as for straight ducts, convection of the propagating medium results in an increased phase speed for downstream propagation, and a decreased phase speed for upstream propagation. Equation (2.84) predicts that the angular wave numbers of evanescent modes will be complex rather than purely imaginary. Furthermore flow is predicted to lower the cut-off frequencies of higher modes by a factor of $(1-M^2)^{\frac{1}{2}}$ independent of the direction of propagation of sound relative to the direction of the flow.

The relationship for the pressure distribution, equation (2.89), predicts that the pressure amplitude distribution for the (0,0) mode is still essentially plane with superimposed flow of the propagating medium. The experimental upstream results of Figure 2.19 agree well with this prediction, however the downstream pressure distribution of Figure 2.18 is far from plane. The situation is obviously complicated by the fact that the flow profile shown in Figure 2.20 is far from what potential theory predicts. It is interesting to note that downstream flow causes an increase in variation in pressure amplitude while upstream flow causes a decrease in amplitude variation.

An investigation of the standing wave in the acoustic incident duct showed that, as predicted, flow did not cause any drastic change in the reflection characteristics of the bend. The bend was still found to provide negligible discontinuity to acoustic propagation with a flow rate of $M = 0.08$, in the incident straight duct.

2.6 SUMMARY

Sound propagation in curved bends has been investigated by the two approaches of a cylindrical co-ordinates solution and a conformal mapping technique. The results of the cylindrical analysis agree well with experimental values and the results of previous workers. The conformal mapping technique likewise gives good agreement with the more exact cylindrical analysis and with experiment but with a very great simplification of the required analysis.

Simple equations have been developed, using a conformal mapping procedure which accurately predict the angular wave numbers of the (0,0) mode and evanescent modes for frequencies such that $k_o h^c \lesssim 4(a-1)/[(a+1)\ln a]$ in curved ducts of aspect ratio $a \lesssim 4$. Being much simpler than those derived using cylindrical co-ordinates, the relationships make analysis of low frequency propagation of sound in curved duct systems an easier task.

The theory in fact is found to agree quite well outside the proposed frequency limit and an equation which accurately predicts the cut-off frequencies of higher modes is given.

The analysis is then extended to develop new equations for sound propagation in curved ducts with mean flow. As expected flow has the effect of decreasing the downstream angular wave number by $(1+M)^{-1}$ and increasing the upstream angular wave number by $(1-M)^{-1}$.

Flow is also predicted to lower the cut-off frequencies of higher modes (in ducts of aspect ratio $a \lesssim 4$) by a factor of $(1 - (M^c)^2)^{\frac{1}{2}}$.

In general the mapping theory does not provide an accurate prediction of the radial pressure amplitude distribution within the bend with and without flow. However the theory did indicate the tendency for the pressure distribution to become more uniform for decreasing frequency. As predicted by the results of the analysis the bend was found to provide negligible discontinuity to acoustic propagation both with and without flow.

PART II: DUCT SOURCES AND SYSTEMS

CHAPTER 3

SOUND RADIATION FROM A DIPOLE PISTON SOURCE IN A SEMI-INFINITE RECTANGULAR DUCT

3.1 INTRODUCTION

The radiation impedance of a vibrating surface is an important theoretical quantity used to describe the mechanical coupling of a vibrating surface to an acoustical field in the surrounding medium. In general it is a complex quantity,the real part of which describes the transmission of power and the complex part of which describes the time rate of change of energy stored in the acoustic near field. The real part may be positive or negative describing respectively either power flow from the vibrating surface to the surrounding medium or power flow from the medium to the surface. Similarly the sign of the reactive part may be given interpretation in terms of the mass or stiffness loading of the medium on the surface.

The radiation impedance is conveniently described in terms of a dimensionless quantity, the radiation ratio or radiation efficiency by comparing the power radiated by a source to that which would be radiated by an equal area of an infinitely plane wave source. Defined in this way the radiation efficiency may be greater than unity contrary to the usual definition of efficiency so that some authors prefer radiation ratio. However the parameter does describe the relative efficiency of radiation of a source and thus other authors prefer radiation efficiency. The latter convention will be adopted here.

Morse and Ingard (1968) have briefly discussed the case of

a non-uniform generating surface and have pointed out that, in this case, the corresponding radiation impedance will contain both a real and reactive part in contrast to a perfectly uniform generating surface which has a purely real or resistive part.

Doak (1973) has considered the effect of source distribution and arrangement on the sound field in a hard walled duct in much detail. He uses superposition of sound fields due to individual sources as a means of representing the radiation of complex vibrating surfaces. His analysis shows that the position of sources in a duct has a significant effect on the duct sound field due to modal coupling and excitation.

Doak has considered the case of a dipole point source in a duct and discussed the energy distribution among the various modes of propagation. Directly relevant to this analysis he has considered the cases of a number of vibrating pistons mounted in the duct walls (as opposed to the duct cross section of this analysis) and has investigated the relationship between size and velocity of the pistons in terms of the excited sound pressure field. An interesting result is that higher modes are inherently better matched to a simple source for transmitting acoustic power than is the plane wave. Doak calculates that each higher order mode may be able to carry up to four times the power of the plane wave mode.

In this chapter the radiation of a dipole piston source mounted at the end of a semi-infinite rectangular duct is investigated. The source is assumed to consist of two pistons of equal area which fill the duct cross section as illustrated in Figure 3.1. The pistons are assumed to vibrate harmonically at the same frequency but with arbitrary relative phase. The analysis is restricted to two dimensions as shown in the figure.

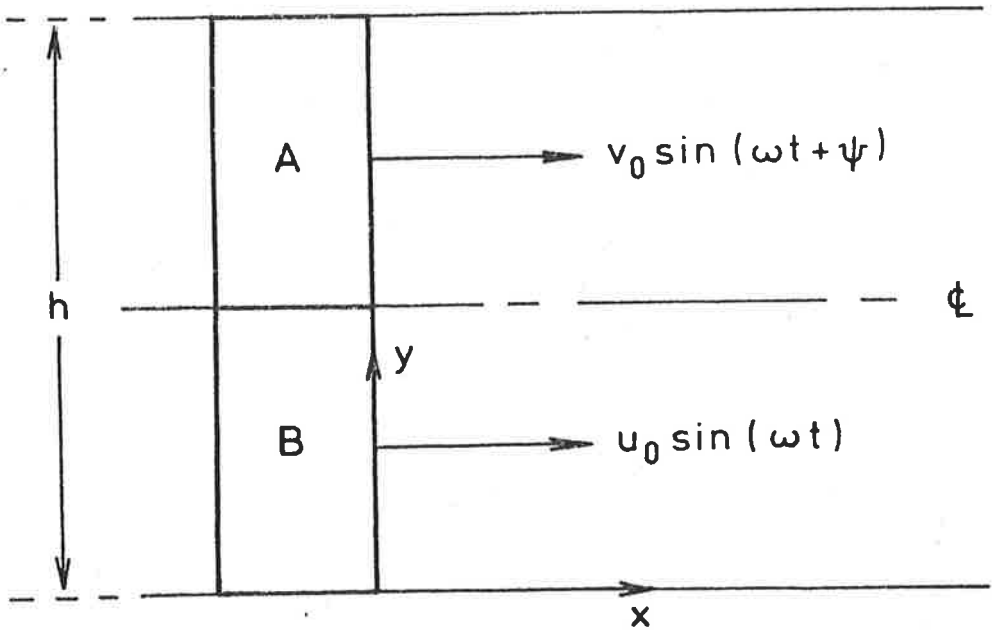

FIGURE 3.1. Arrangement of the dipole piston source.

The sound field excited by the dipole piston source is investigated theoretically by using a method of superposition. The velocity potential due to one piston covering half the duct area is derived and added to the velocity potential due to the other piston with an assumed phase difference. The resulting pressure field is derived from the velocity potential and used in conjunction with the velocity amplitude of the vibrating surface to derive relationships for specific acoustic impedance, radiation efficiency and transmission coefficient.

For the sake of the analysis it will be convenient initially to think of the two pistons as solid surfaces forced to move harmonically at a specified frequency and with a specified relative phase between them. However, the moving surfaces could just as well represent a vibrating air surface and indeed it will be convenient when considering power radiation from two ducts joined to a single duct to think of the vibrating surfaces as conceptual boundaries which are driven by incident plane sound waves.

The duct into which the source radiates is assumed to have perfectly rigid walls and no mean flow. The frequency of the analysis is limited to less than the cut-off frequency of the (1,0) mode in the duct. The effect of phase difference between the two pistons on radiation efficiency and the relationship between higher modes and the resultant sound field is discussed.

3.2 ANALYSIS

In the following analysis a piston is defined as a surface of constant normal velocity. The arrangement of the pistons mounted in the duct and the appropriate two-dimensional rectangular co-ordinate system used are shown in Figure 3.1. The origin of the co-ordinate system is assumed to be the point corresponding to the

bottom most corner of piston B. As there is no discontinuity in the z direction a two-dimensional co-ordinate system is satisfactory. The pistons are assumed of equal area and to move in simple harmonic motion. The normal velocities of the pistons are represented by

$$\text{piston A} \qquad v = v_o \sin(\omega t + \psi) \qquad h \geq y > h/2 \tag{3.1}$$

$$\text{piston B} \qquad u = u_o \sin(\omega t) \qquad h/2 > y \geq 0 \tag{3.2}$$

where u_o and v_o are the velocity amplitudes and ψ is the phase angle by which piston A leads piston B.

The wave equation in velocity potential form for sound propagation with no mean flow is

$$\nabla^2\phi + (\omega/c_o)^2\phi = 0 \tag{3.3}$$

From Chapter 1 a general solution of equation (3.3) in separable rectangular co-ordinates is

$$\phi(x,y,t) = \sum_{m=o}^{\infty} A_{mo} \cos(k_m y)\cos(\omega t - k_{mo} x + \psi) \tag{3.4}$$

This form of the velocity potential is used rather than the exponential form as it highlights the role of the phase angle ψ in the analysis. The relationship between the modal wave number in the x direction k_{mo} and the eigen values of the boundary solutions, k_m, has been derived in Chapter 1 and is

$$k_{mo} = \pm [k_o^2 - k_m^2]^{\frac{1}{2}} \tag{3.5}$$

where for rigid walled ducts $k_m = m\pi/h$. As discussed previously, those modes for which $k_o > k_m$ will have a real wave number and will propagate without attenuation whereas those modes for which $k_o < k_m$ will have an

imaginary wave number and will decay rapidly away from the generating surface. As stated earlier the analysis presented here will be concerned entirely with modes of the latter type and the plane wave mode.

To solve the problem a method of superposition is used. It is well known that the velocity potentials of two separate wave systems in a duct can be superimposed and used to derive the resultant acoustic sound field, (a standing wave is a good example). Thus it is proposed to find the potentials due to piston A and piston B separately and by superimposing the two potentials derive the resultant sound field in the duct. The arrangements of the two separate pistons as employed by the analysis are shown in Figure 3.2. In this case the part of the generating surface not considered as a piston is represented by an area with zero particle velocity.

We shall proceed by deriving the potential ϕ_A due to piston A and follow by deriving the potential ϕ_B due to piston B. The resultant potential due to the dipole source will then be $\phi = \phi_A + \phi_B$. Thus for piston A as shown in Figure 3.2 we require for $h/2 < y \lesssim h$ and at $x = 0$

$$v_x\Big|_{x=0} = v_o \sin(\omega t + \psi) \tag{3.6}$$

and for $0 \lesssim y < h/2$

$$v_x\Big|_{x=0} = 0 \tag{3.7}$$

These are the boundary conditions used to relate the amplitude of the velocity potential in the downstream duct to the velocity distribution of the generating surface. Equation (3.4) can be written in expanded form for piston A as

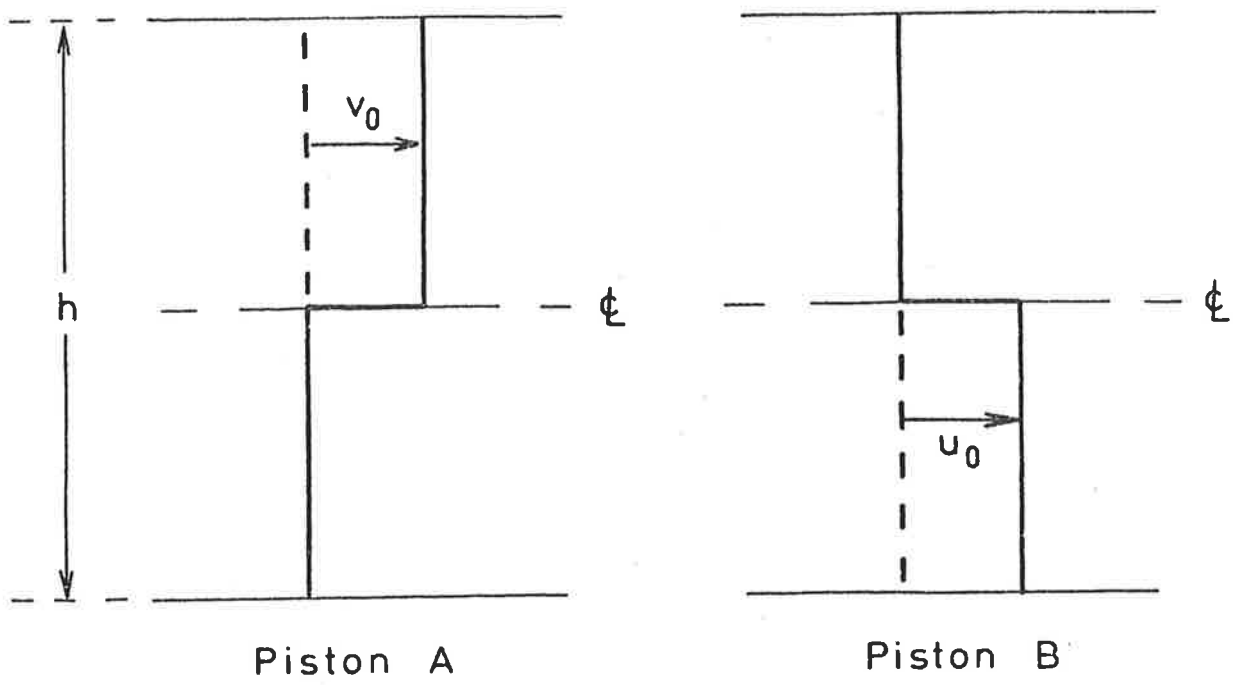

FIGURE 3.2. Velocity distributions of the individual pistons.

$$\phi_A = \sum_{m=o}^{\infty} A_{mo}\cos(k_m y)[\cos(\omega t+\psi)\cos(k_{mo}x) + \sin(\omega t+\psi)\sin(k_{mo}x)] \quad (3.8)$$

The axial particle velocity due to this potential is

$$u_x = \partial\phi/\partial x$$

$$= \sum_{m=o}^{\infty} A_{mo}k_{mo}\cos(k_m y)[\sin(\omega t+\psi)\cos(k_{mo}x) - \cos(\omega t+\psi)\sin(k_{mo}x)] \quad (3.9)$$

Thus at $x = 0$

$$u_x\Big|_{x=0} = \sum_{m=o}^{\infty} A_{mo}k_{mo}\cos(k_m y)\sin(\omega t+\psi) \quad (3.10)$$

We let

$$f(y) = \sum_{m=o}^{\infty} A_{mo}k_{mo}\cos(k_m y) \quad (3.11)$$

then the boundary condition of continuity of axial particle velocity at the generating surface given by equations (3.6) and (3.7) requires that for

$$0 \lesssim y < h/2 \qquad f(y) = 0 \quad (3.12)$$

and

$$h/2 < y \lesssim h \qquad f(y) = v_o \quad (3.13)$$

Equation (3.10) consists of an infinite sum of individual modes with separate Fourier coefficients. To determine these coefficients individually, use is made of the orthogonality property of the $\cos(k_m y)$ function. As is well known

$$\int_o^h \cos(k_m y)\cos(k_n y)\,dy = 0 \qquad \text{if } m \neq n \quad (3.14)$$

$$\neq 0 \qquad \text{if } m = n \quad (3.15)$$

hence $$\int_o^h f(y)\cos(k_m y) = 0 \quad \text{if } m \neq n \tag{3.16}$$

$$= \int_o^h A_{mo} k_{mo} \cos^2(k_m y)\, dy \quad \text{if } m \neq n \tag{3.17}$$

Now $k_m = m\pi/h$ and thus

$$\int_o^h f(y)\cos(m\pi y/h)\, dy$$

$$= (A_{mo}k_{mo})/2 \int_o^h [1 + \cos(2m\pi y/h)]\, dy$$

$$= (A_{mo}k_{mo})/2\, [y + \sin(2m\pi y/h)(2m\pi/h)^{-1}]_o^h$$

Thus if $m = 0$

$$\int_o^h f(y)\, dy = A_{oo}k_{oo}h \tag{3.18}$$

and $$A_{oo} = [1/(k_{oo}h)]\int_o^h f(y)\, dy \tag{3.19}$$

On the other hand if $m \neq 0$ then

$$\int_o^h f(y)\cos(m\pi y/h)\, dy = A_{mo}k_{mo}(h/2) \tag{3.20}$$

and $$A_{mo} = [2/(k_{mo}h)]\int_o^h f(y)\cos(m\pi y/h)\, dy \tag{3.21}$$

The integral can be split into two ranges represented by equations (3.12) and (3.13).

Hence $$\int_o^h f(y)\cos(m\pi y/h)\,dy = 0 + \int_{h/2}^h v_o \cos(m\pi y/h)\,dy$$

$$= v_o h/2 \quad \text{for } m = 0 \tag{3.22}$$

or $$= \left[\frac{v_o h}{m\pi}\sin(m\pi y/h)\right]_{h/2}^{h}$$

$$= -\frac{v_o h}{m\pi}\sin(m\pi/2) \quad \text{for } m \neq 0 \tag{3.23}$$

Thus the Fourier coefficients of equation (3.8) are

$$A_{oo} = [1/(k_{oo}h)][v_o h/2]$$

$$= \frac{v_o}{2k_{oo}} \tag{3.24}$$

and $$A_{mo} = \left(\frac{2}{k_{mo}h}\right)\left(\frac{v_o h}{m\pi}\right)[-\sin(m\pi/2)]$$

$$= -\frac{2v_o}{m\pi k_{mo}}\sin(m\pi/2) \tag{3.25}$$

According to equation (3.25) for even values of m, A_{mo} is zero and the corresponding mode does not exist in the sound field. This will be discussed later. The resulting potential due to piston A alone is thus

$$\phi_A = \sum_{m=o}^{\infty} A_{mo}\cos(k_m y)\cos(\omega t - k_{mo}x + \psi) \tag{3.26}$$

with coefficients given by equations (3.24) and (3.25).

To determine the Fourier coefficients of ϕ_B due to piston B an identical procedure is used except the velocity distribution represented by B of Figure 3.2 is used. Thus we may develop a function

g(y) which will be used to derive the potential ϕ_B due to piston B alone.

For $0 \leq y < h/2$

$$g(y) = u_o \tag{3.27}$$

and for $h/2 < y \leq h$

$$g(y) = 0 \tag{3.28}$$

Using the same procedure as used previously in the derivation of ϕ_A we then have

$$g(y) = \sum_{m=o}^{\infty} B_{mo} k_{mo} \cos(k_m y) \tag{3.29}$$

where B_{mo} are the modal Fourier coefficients of potential ϕ_B.

Thus $$\int_o^h g(y)\cos(k_m y)\, dy = \int_o^{h/2} u_o \cos(k_m y)\, dy + 0$$

$$= u_o h/2 \qquad \text{for } m = 0 \tag{3.30}$$

$$= \frac{u_o h}{m\pi} \sin(m\pi/2) \qquad \text{for } m \neq 0 \tag{3.31}$$

Hence $$B_{oo} = u_o/(2k_o) \tag{3.32}$$

and $$B_{mo} = \frac{2u_o}{m\pi k_{mo}} \sin(m\pi/2) \tag{3.33}$$

and $$\phi_B = \sum_{m=o}^{\infty} B_{mo} \cos(k_m y)\cos(\omega t - k_{mo} x) \tag{3.34}$$

with coefficients given by the above relations. The total potential in the duct due to the pistons vibrating simultaneously is

$$\phi = \phi_A + \phi_B$$

thus using equations (3.26) and (3.34) we may write

$$\phi = \sum_{m=o}^{\infty} A_{mo}\cos(k_m y)\cos(\omega t - k_{mo}x + \psi)$$

$$+ \sum_{m=o}^{\infty} B_{mo}\cos(k_m y)\cos(\omega t - k_{mo}x) \qquad (3.35)$$

$$= \sum_{m=o}^{\infty} \cos(k_m y)[(A_{mo}\cos(\psi) + B_{mo})\cos(\omega t - k_{mo}x)$$

$$- A_{mo}\sin(\psi)\sin(\omega t - k_{mo}x)] \qquad (3.36)$$

For the investigation of specific acoustic impedance it is convenient to rewrite equation (3.35) in exponential form,

thus $$\phi = \sum_{m=o}^{\infty} A_{mo}\cos(k_m y)\exp[i(+\omega t - k_{mo}x + \psi)]$$

$$+ \sum_{m=o}^{\infty} B_{mo}\cos(k_m y)\exp[i(\omega t - k_{mo}x)] \qquad (3.37)$$

The resultant pressure field due to the velocity potential may be derived from

$$p(x,y,t) = -\rho_o \partial\phi/\partial t \qquad (3.38)$$

Therefore the pressure distribution in the duct may be written as

$$p(x,y,t) = -i\rho_o\omega \sum_{m=o}^{\infty} \{A_{mo}\cos(k_m y)\exp[i(\omega t - k_{mo}x + \psi)]$$

$$+ B_{mo}\cos(k_m y)\exp[i(\omega t - k_{mo}x)]\} \qquad (3.39)$$

and the axial particle velocity distribution in the duct is derived from

$$u_x = + \partial\phi/\partial x$$

$$u_x(x,y,t) = -i\sum_{m=o}^{\infty} \{A_{mo}\cos(k_m y)\exp[i(\omega t - k_{mo}x + \psi)]$$

$$+ B_{mo}\cos(k_m y)\exp[i(\omega t - k_{mo}x)]\}k_{mo} \qquad (3.40)$$

The specific acoustic impedance at the dipole piston surface is defined as the ratio of the acoustic pressure to the normal acoustic particle velocity and thus is at x = 0

$$Z = p/u_x\Big|_{x=0} \qquad (3.41)$$

$$\therefore \quad \frac{Z}{\rho_o c} = \frac{k_o \sum_{m=o}^{\infty} [A_{mo}\cos(k_m y)e^{i\psi} + B_{mo}\cos(k_m y)]}{\sum_{m=o}^{\infty} k_{mo}[A_{mo}\cos(k_m y)e^{i\psi} + B_{mo}\cos(k_m y)]} \qquad (3.42)$$

If the two pistons of the dipole source have equal velocity amplitude then $u_o = v_o$ and from equations (3.25) and (3.33) $A_{mo} = -B_{mo}$ for all $m \neq 0$, thus equation (3.42) reduces to,

$$\frac{Z}{\rho_o c} = \frac{k_o A_{oo}(e^{i\psi}+1) + k_o(e^{i\psi}-1)\sum_{1}^{\infty} A_{mo}\cos(k_m y)}{k_o A_{oo}(e^{i\psi}+1) + (e^{i\psi}-1)\sum_{1}^{\infty} k_{mo}A_{mo}\cos(k_m y)} \qquad (3.43)$$

We note that when the pistons are in phase and ψ is 0 or 2π, equation (3.43) reduces to the characteristic impedance of a plane wave,

$$Z = \rho_o c_o \qquad (3.44)$$

Thus as expected when the dipole piston source acts as a single piston the plane wave is the only mode radiated. However if $\psi \neq 0$ or 2π then the radiation impedance will contain an imaginary part representing the reactive loading of the air on the source as below cut-off the k_{mo} are imaginary. In particular if the pistons are exactly opposite in phase and $\psi = \pi$ the specific acoustic impedance will be purely reactive everywhere over the surface of the source plane.

If we limit our attention to the first terms only of the series in the numerator and denominator equation (3.43) reduces to

$$Z/\rho_o c_o = \frac{\pi(e^{i\psi}+1) - 4(k_o/k_{10})\cos(k_1 y)(e^{i\psi}-1)}{\pi(e^{i\psi}+1) - 4\cos(k_1 y)(e^{i\psi}-1)} \qquad (3.45)$$

Values of resistive and reactive impedance derived from equation (3.45) are plotted in Figures 3.3 and 3.4 respectively for different phase angles between pistons.

Our next consideration will be the radiation efficiency of the source. To obtain this we have to determine the power radiated by the source. Reverting back to the original form of the total potential

$$\phi = \sum_{m=o}^{\infty} \cos(k_m y)[(A_{mo}\cos(\psi) + B_{mo})\cos(\omega t - k_{mo}x)$$

$$- A_{mo}\sin(\psi)\sin(\omega t - k_{mo}x)] \qquad (3.46)$$

The resultant pressure field $p = -\rho_o \partial\phi/\partial t$ is

$$p(x,y,t) = \rho_o \omega \sum_{m=o}^{\infty} \cos(k_m y)[(A_{mo}\cos(\psi) + B_{mo})\sin(\omega t - k_{mo}x)$$

$$+ A_{mo}\sin(\psi)\cos(\omega t - k_{mo}x)] \qquad (3.47)$$

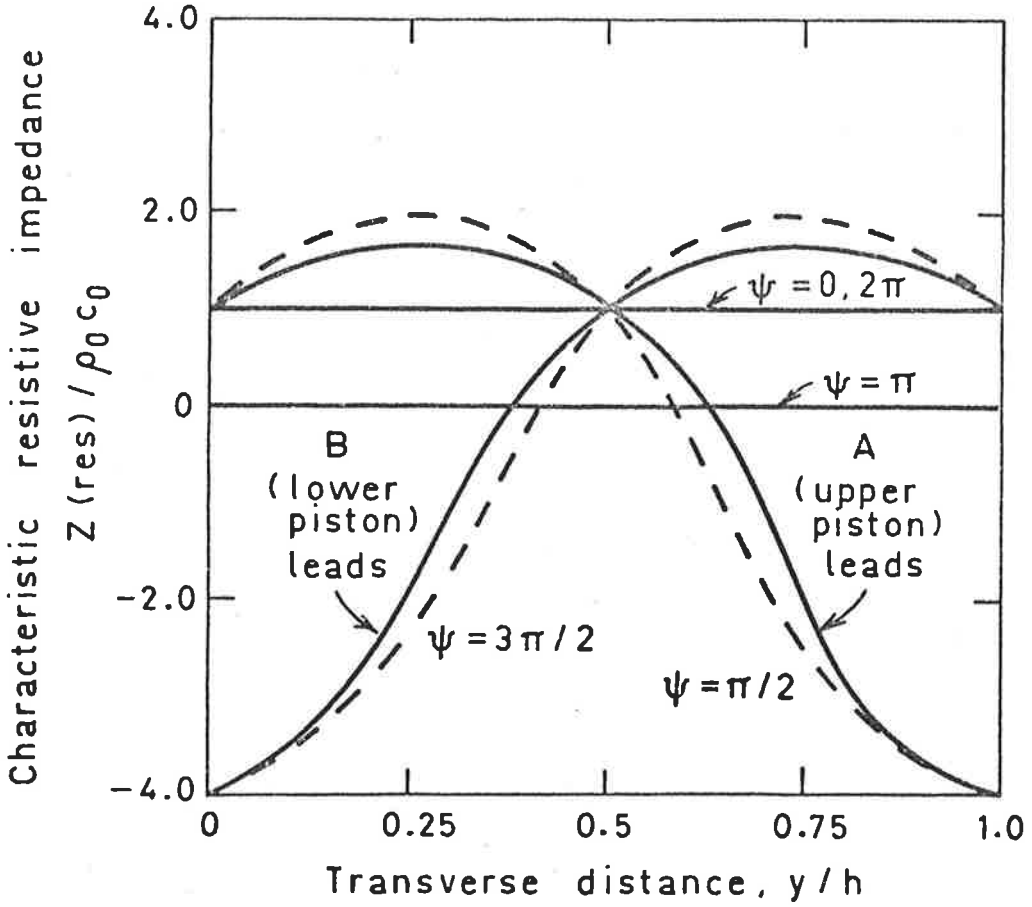

FIGURE 3.3. Characteristic resistive impedance of the dipole piston source. ——, $k_0h = 1.5$; – – –, $k_0h = 3.0$.

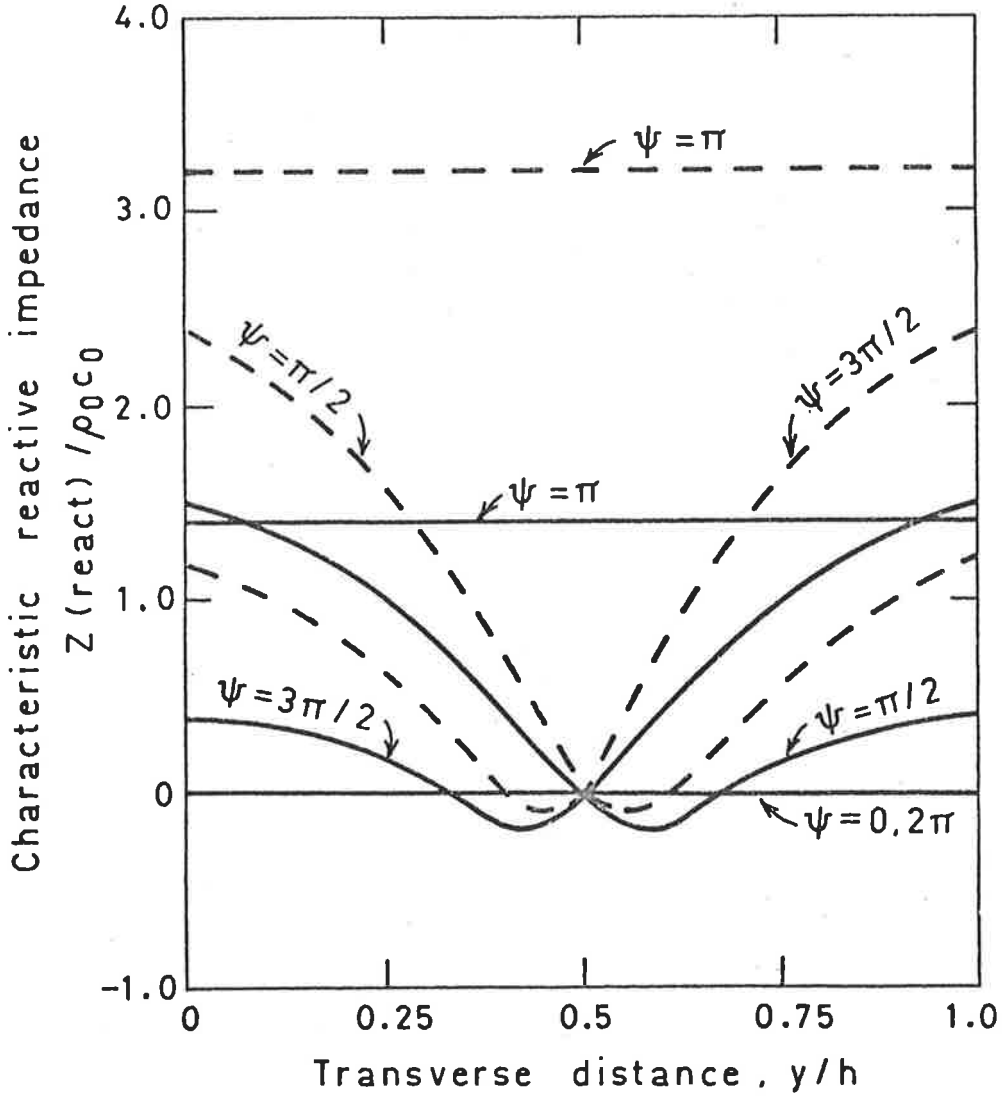

FIGURE 3.4. Characteristic reactive impedance of the dipole piston source. ——— , $k_o h = 1.5$; – – –, $k_o h = 3.0$.

The power radiated and transmitted into the downstream section of the duct is the time averaged and integrated product of pressure multiplied by velocity i.e.

$$W = (1/T)\int_o^T\int_o^h p\, u_x \, dy\, dt \tag{3.48}$$

where T is the period of motion. Therefore in this particular case the power radiated is

$$W = -(1/T)\int_o^T\int_o^{h/2} u_o \sin(\omega t) p\Big|_{x=o} dy\, dt$$

$$- (1/T)\int_o^T\int_{h/2}^h v_o \sin(\omega t + \psi) p\Big|_{x=o} dy\, dt \tag{3.49}$$

Therefore substituting equation (3.47) into (3.49) gives for the power radiated

$$W = -(1/T)\int_o^T [\int_o^{h/2} \rho_o \omega u_o \sin(\omega t) \sum_{m=o}^{\infty} \cos(k_m y)[-(A_{mo}\cos(\psi) + B_{mo})\sin(\omega t)$$

$$- A_{mo}\sin(\psi)\cos(\omega t)]\, dy$$

$$- \int_{h/2}^h \rho_o \omega v_o \sin(\omega t + \psi) \sum_{m=o}^{\infty} \cos(k_m y)[-(A_{mo}\cos(\psi) + B_{mo})\sin(\omega t)$$

$$- A_{mo}\sin(\psi)\cos(\omega t)]\, dy\,]\, dt \tag{3.50}$$

$$\text{Therefore } W = \int_o^{h/2} [\,(1/2)\rho_o \omega u_o \sum_{m=o}^{\infty} \cos(k_m y)[A_{mo}\cos(\psi) + B_{mo}]\,dy$$

$$+ \int_{h/2}^{h} [(1/2)\rho_o \omega v_o \cos(\psi) \sum_{m=o}^{\infty} \cos(k_m y)[A_{mo}\cos(\psi) + B_{mo}]\,dy$$

$$+ \int_{h/2}^{h} [(1/2)\rho_o \omega v_o \sin^2(\psi) \sum_{m=o}^{\infty} A_{mo}\cos(k_m y)]\,dy \qquad (3.51)$$

$$\text{and} \qquad W = \frac{\rho_o \omega}{2} \; [u_o \sum_{m\neq o}^{\infty} A_{mo}\cos(\psi) + B_{mo}(h/m\pi)\sin(m\pi/2)$$

$$- v_o \sin^2(\psi) \sum_{m\neq o}^{\infty} A_{mo}(h/m\pi)\sin(m\pi/2)$$

$$+ u_o(A_{oo}\cos(\psi) + B_{oo})(h/2) + v_o\cos(\psi)(A_{oo}\cos(\psi) + B_{oo})(h/2)$$

$$+ v_o \sin^2(\psi) A_{oo}(h/2)\,] \qquad (3.52)$$

Thus finally

$$W = (\rho_o \omega/2)(h/2)[u_o(A_{oo}\cos(\psi) + B_{oo}) + v_o(A_{oo} + B_{oo}\cos(\psi))$$

$$+ \sum_{m=1}^{\infty} (2/m\pi)\sin(m\pi/2)\{u_o(A_{mo}\cos(\psi) + B_{mo}) - v_o(A_{mo} + B_{mo}\cos(\psi))\}]$$

$$(3.53)$$

In equation (3.53) the power radiated into the downstream duct has been split into two terms. The first on the right hand side is the power carried by the (0,0) mode and the second consists of an infinite sum representing the power carried by the higher order modes. In particular if one assumes that piston A and B have the same velocity

amplitudes i.e. $u_o = v_o$ then equation (3.53) reduces to

$$W_{u_o = v_o} = (\rho_o \omega/2)(h/2)[v_o(\cos(\psi) + 1)(A_{oo} + B_{oo}) + \sum_{m=1}^{\infty} (2/m\pi)\sin(m\pi/2)v_o(\cos(\psi) - 1)(A_{mo} - B_{mo})] \quad (3.54)$$

If $u_o = v_o$ equations (3.26) and (3.33) require that $A_{oo} = B_{oo}$ while equations (3.27) and (3.34) require that $A_{mo} = -B_{mo}$, thus equation (3.54) further reduces to

$$W_{u_o = v_o} = (\rho_o \omega h/2)[v_o A_{oo}(\cos(\psi) + 1) + \sum_{m=1}^{\infty} (2/m\pi)\sin(m\pi/2)v_o A_{mo}(\cos(\psi) - 1)] \quad (3.55)$$

If $\psi = 0$ the dipole source can be considered as a uniform piston over the whole duct cross section and the result of equation (3.55) reduces to plane wave radiation in the duct. Thus

$$W_{u_o = v_o} = (\rho_o \omega h) v_o A_{oo} + 0 \quad (3.56)$$

Now
$$A_{oo} = v_o/(2k_{oo}) = v_o/(2k_o) \quad (3.57)$$

hence
$$W_{\substack{u_o = v_o \\ \psi = 0}} = \rho_o c_o \frac{v_o^2}{2} h \quad (3.58)$$

Equation (3.58) is the relation for nett power flow of the (0,0) mode in a rectangular duct. Thus when $u_o = v_o$ and $\psi = 0$, all input power to the piston dipole source is radiated.

Radiation efficiency σ is defined as the ratio of the power radiated by the source to the power radiated by an equal area of an infinite plane wave. According to Cremer, Heckl & Ungar (1973) the power radiated by such a source of area A^* with velocity amplitude v_o is

$$W_{piston} = \rho_o c_o \frac{v_o^2}{2} A^* \tag{3.59}$$

In a two-dimensional system A^* can be replaced by h. Thus the radiation efficiency of the dipole piston source with velocity of piston A equal to piston B is

$$\sigma = (k_o/v_o)[A_{oo}(\cos(\psi) + 1) + \sum_{m=1}^{\infty} (2/m\pi) \sin(m\pi/2) A_{mo}(\cos(\psi) - 1)] \tag{3.60}$$

Substituting for A_{oo} and A_{mo} from equations (3.24) and (3.25) we obtain

$$\sigma = \frac{(\cos(\psi) + 1)}{2} - (\cos(\psi) - 1) \sum_{m=1}^{\infty} (2/m\pi)^2 \sin^2(m\pi/2)(k_o/k_{mo}) \tag{3.61}$$

As previously, the first term represents the radiation efficiency due to the (0,0) mode and the second term sums the radiation efficiency of all the higher modes. If $\psi = 0$ the radiation efficiency $\sigma = 1$ from equation (3.61).

This result is not surprising since equation (3.61) predicts that when $\psi = 0$ the sound power radiated will be identical to a piston of equivalent area. Thus when $\psi = 0$ the dipole piston source becomes a monopole source and is an extremely efficient radiator.

We now consider the transmission of sound power past a junction of two smaller ducts with one larger duct. The junctions of the small ducts to the larger form the pistons A and B where consistent with our earlier stated assumption we are concerned only with frequencies

below cut-off for the higher order modes.

In the case of $u_o \neq v_o$ the input power (or incident power) at the generating surface can be written as

$$W_i = \rho_o c_o h u_i^2 / 2 \tag{3.62}$$

If the input power is constant, then it can be written as

$$\rho_o c_o h W_i^2 / 2 = \frac{\rho_o c_o h}{4} (u_o^2 + v_o^2) \tag{3.63}$$

Hence the ratio of sound power radiated to the input power (more specifically the sound power transmission coefficient) is

$$\alpha_t = W_t / W_i \tag{3.64}$$

We substitute equations (3.53) and (3.63) into equation (3.64) to obtain

$$\alpha_t = (k_o/(u_o^2 + v_o^2))[u_o(A_{oo}\cos(\psi) + B_{oo}) + v_o(A_{oo} + B_{oo}\cos(\psi))$$

$$+ \sum_{m=1}^{\infty} (2/m\pi)\sin(m\pi/2)(u_o(A_{mo}\cos(\psi) + B_{mo}) - v_o(A_{mo} + B_{mo}\cos(\psi))] \tag{3.65}$$

For $u_o = v_o$ this relation reduces with the aid of equations (3.24), (3.25), (3.32) and (3.33) to

$$\alpha_t = \frac{\cos(\psi) + 1}{2} - \sum_{m=1}^{\infty} (2/m\pi)^2 \sin^2(m\pi/2)(k_o/k_{mo})(\cos(\psi) - 1) \tag{3.66}$$

which is identical to the expression for radiation efficiency given by equation (3.61).

The evaluation of the equations derived in the analysis is limited to frequencies below the cut-off of the (1,0) mode in the

downstream duct. The cut-off wave number for the (1,0) mode in a rigid walled duct is given by setting $k_{mo} = 0$ in equation (3.5), thus

$$(k_1)_c = \pi/h \tag{3.67}$$

and the modal wave number for waves below cut-off is

$$k_{mo} = \pm i[(m\pi/h)^2 - k_o^2]^{\frac{1}{2}} \tag{3.68}$$

Thus for frequencies below cut-off of the (1,0) mode, k_{oo} will be real, but k_{mo} will be imaginary for all higher modes. Thus the expression for radiation efficiency can be considered as separated into real and imaginary parts. The radiation efficiency is then

$$\sigma = \frac{(\cos(\psi)+1)}{2} - \sum_{m=1}^{\infty} (2/m\pi)^2 \sin^2(m\pi/2)(k_o/k_{mo})(\cos(\psi)-1) \tag{3.69}$$

where for the frequency range considered, the first term represents the resistive radiation efficiency and gives the actual power radiated while the second term is the reactive radiation efficiency and describes the fluid loading on the piston. If $\psi = \pi$ then equation (3.69) reduces to

$$\sigma = 0 + 2\sum_{m=1}^{\infty} (2/m\pi)^2 \sin^2(m\pi/2)(k_o/k_{mo}) \tag{3.70}$$

which is entirely reactive implying no actual radiation of sound power. The resistive radiation efficiency, from equation (3.69) is independent of frequency but is dependent on the phase difference ψ between pistons. The variation in resistive radiation efficiency with phase angle is shown in Figure 3.5.

It will be of interest to consider the reactive part of equation (3.69).

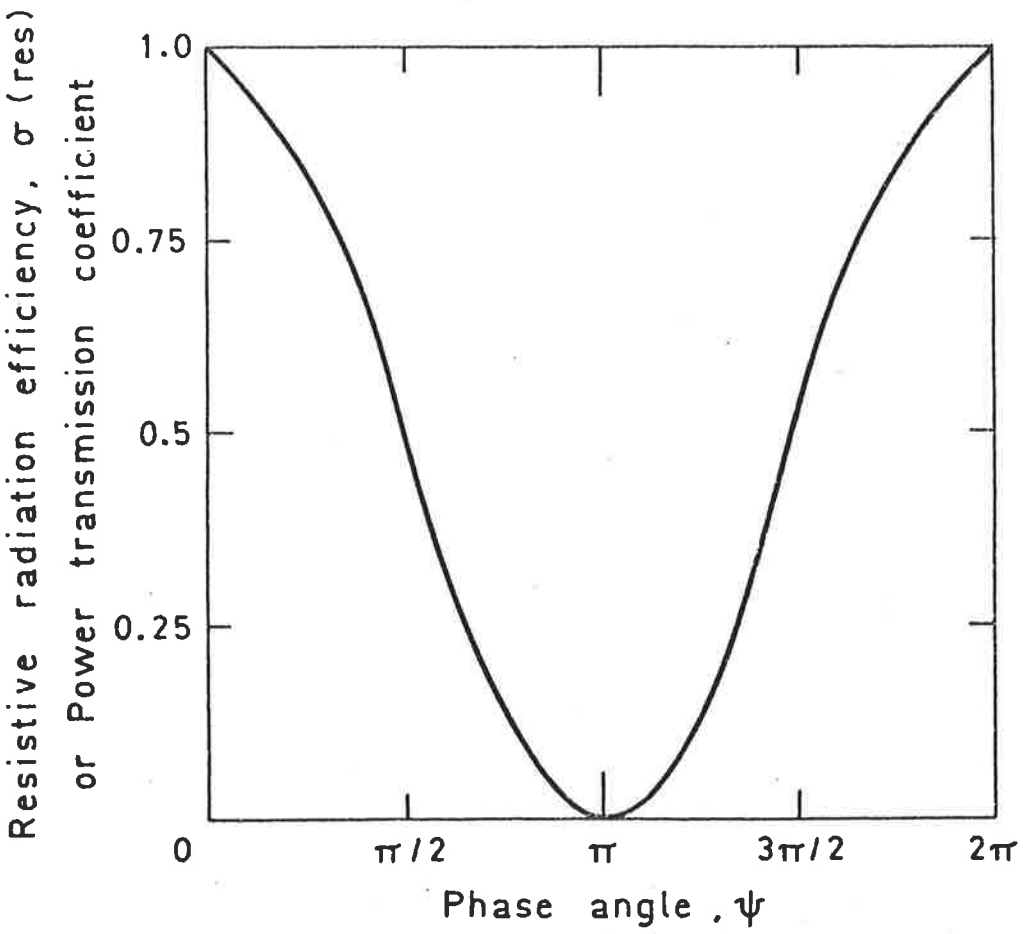

FIGURE 3.5. Resistive radiation efficiency or power transmission coefficient of the dipole piston source.

$$\sigma(\text{react}) = -\sum_{m=1}^{\infty} (2/m\pi)^2 \sin^2(m\pi/2)(k_o/k_{mo})(\cos(\psi) - 1) \tag{3.71}$$

For a first order modal solution (i.e. the infinite sum truncated at $m = 1$) equation (3.71) becomes

$$\sigma(\text{react})_{m=1} = \frac{4}{\pi^2} (k_o h/[\pi^2 - (k_o h)^2]^{\frac{1}{2}})(\cos(\psi) - 1) \tag{3.72}$$

Or alternatively writing the reactive radiation efficiency as a phase dependent factor we obtain

$$\sigma_{nd}(\text{react}) = (\cos(\psi) - 1) \tag{3.73}$$

where $$\sigma_{nd}(\text{react}) = \sigma(\text{react})/(\frac{4}{\pi^2} \frac{k_o h}{[\pi^2 - (k_o h)^2]^{\frac{1}{2}}}) \tag{3.74}$$

Values of reactive radiation efficiency factor are plotted in Figure 3.6.

The reactive radiation efficiency is dependent upon the frequency parameter (k_o/k_{mo}) as well as upon the phase angle ψ. For even values of m the reactive efficiency is seen to be equal to zero thus

$$\sigma(\text{react}) = -\sum_{m=1,3,5\cdots}^{\infty} (2/m\pi)^2 (k_o/k_{mo}) (\cos(\psi) - 1) \tag{3.75}$$

To determine the dependence of the accuracy of the final result of reactive radiation efficiency on modal truncation, the infinite sum of equation (3.75) was truncated at $m = 1$ and $m = 3$ and the results compared. Values of theoretical reactive radiation efficiency are plotted against phase angle for various non-dimensional

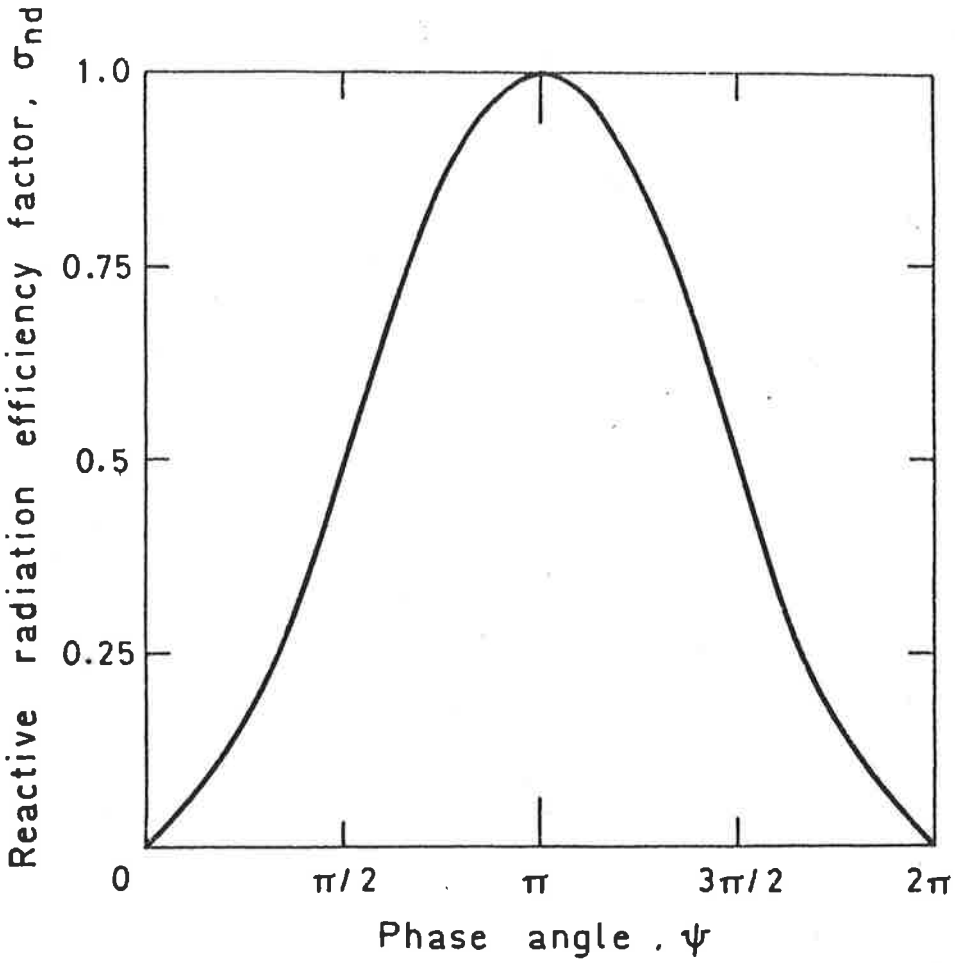

FIGURE 3.6. Reactive radiation efficiency factor of the dipole piston source for a first order modal solution.

frequencies, $k_o h$, in Figure 3.7 for the two different truncation values. Apparently the higher order terms contribute very little to the sum.

It has been demonstrated previously that the power transmission coefficient can be separated into two terms. The power transmitted by the second of these terms, represented by an infinite sum, now will be discussed. As the higher modes are below cut-off, the axial particle velocity and the pressure of these higher modes are in phase quadrature and they thus propagate no nett energy flux away from the generating surface. Thus one would expect the higher evanescent modes not to contribute to nett energy propagation. This will be proved in terms of the previous analysis.

For the non-propagating modes let $k_{mo} = -ik'_{mo}$. The general velocity potential for these modes will then be

$$\phi_{m>o} = \sum_{m=1}^{\infty} \cos(k_m y)[(A_{mo}\cos(\psi) + B_{mo})\sin(\omega t)\exp[-k'_{mo}x]$$

$$+ A_{mo}\sin(\psi)\cos(\omega t)\exp[-k'_{mo}x] \qquad (3.76)$$

and the acoustic pressure is thus

$$p = -\rho_o \omega \sum_{m=1}^{\infty} \cos(k_m y)[(A_{mo}\cos(\psi) + B_{mo})\cos(\omega t)\exp[-k'_{mo}x]$$

$$- A_{mo}\sin(\psi)\sin(\omega t)\exp[-k'_{mo}x] \qquad (3.77)$$

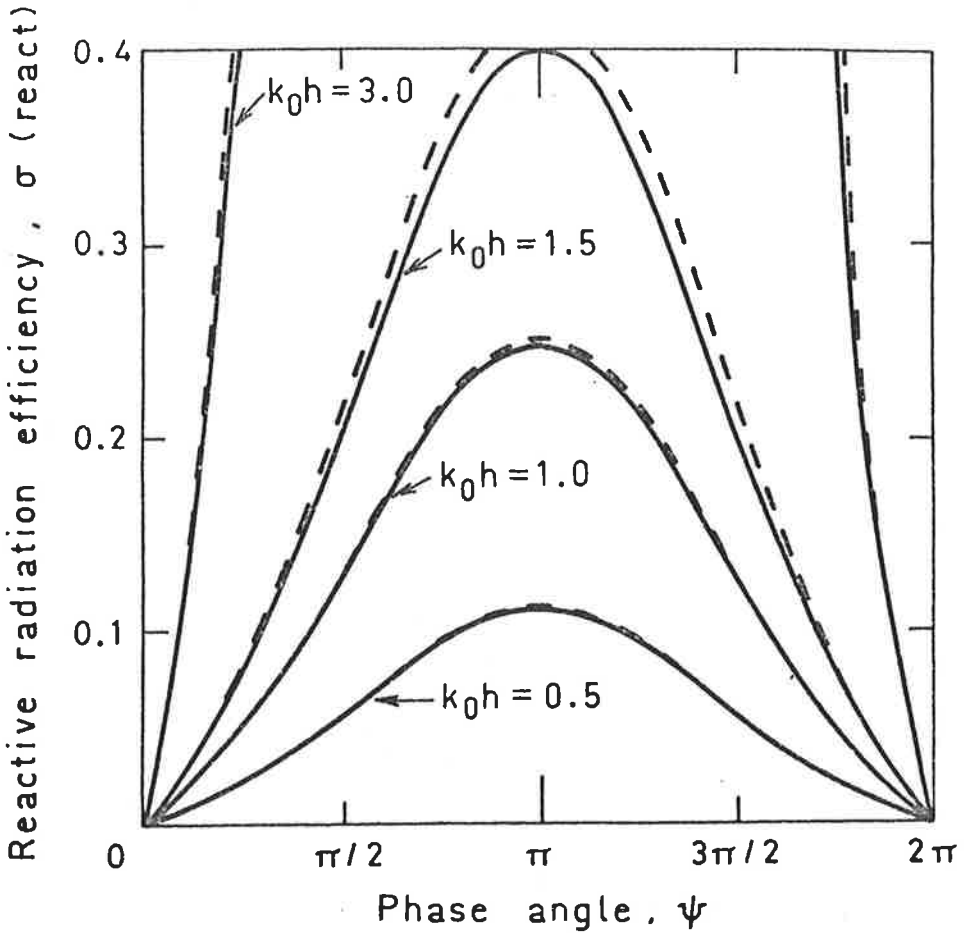

FIGURE 3.7. Reactive radiation efficiency of the dipole piston source. ——— , first order modal solution;— — — , third order modal solution.

Thus the power transmitted by higher modes

$$W_{m>o} = -1/T \int_o^T dt[\int_o^{h/2} \rho_o \omega u_o \sin(\omega t) \sum_{m=1}^{\infty} \cos(k_m y)[(A_{mo}\cos(\psi) + B_{mo}) \times$$

$$\times \cos(\omega t)\exp[-k'_{mo}x] - A_{mo}\sin(\psi)\sin(\omega t)\exp[-k'_{mo}x]\, dy$$

$$+ \int_{h/2}^{h} \rho_o \omega v_o \sin(\omega t + \psi) \sum_{m=1}^{\infty} \cos(k_m y)[(A_{mo}\cos(\psi) + B_{mo})\cos(\omega t)\exp[-k'_{mo}x]$$

$$- A_{mo}\sin(\psi)\sin(\omega t)\exp\{-k'_{mo}x\}\,]\,dy\,] \qquad (3.78)$$

$$\therefore W_{m>o} = -\tfrac{1}{2}\rho_o \omega u_o \sum_{m=1}^{\infty} A_{mo}\sin(\psi)\exp[-k'_{mo}x](h/m\pi)\sin(m\pi/2)$$

$$- \tfrac{1}{2}\rho_o \omega v_o \sum_{m=1}^{\infty} B_{mo}\sin(\psi)\exp[-k'_{mo}x](h/m\pi)\sin(m\pi/2) \qquad (3.79)$$

$$W_{m>o} = -\tfrac{1}{2}\rho_o \omega \sin(\psi)[\sum_{m=1}^{\infty} (u_o A_{mo} + B_{mo} v_o)\exp[-k'_{mo}x](h/m\pi)\sin(m\pi/2)\,] \qquad (3.80)$$

now from equations (3.25) and (3.33)

$$A_{mo} = -\frac{2v_o}{m\pi k_{mo}} \sin(m\pi/2)$$

and

$$B_{mo} = \frac{2u_o}{m\pi k_{mo}} \sin(m\pi/2)$$

Hence $W_{m>o} = -\tfrac{1}{2}\rho_o \omega \sin(\psi)[\sum_{m=1}^{\infty} \{-\frac{2u_o v_o}{m\pi k_{mo}} \sin(m\pi/2) + \frac{2u_o v_o}{m\pi k_{mo}} \sin(m\pi/2)\} \times$

$$\times \exp[-k'_{mo}x](h/m\pi)\sin(m\pi/2)\,]$$

$$= 0$$

The higher modes for frequencies below cut-off transmit no energy independent of u_o, v_o and ψ and the ratio of actual power radiated to input power of the dipole source can be written as

$$\alpha_t = \frac{(\cos(\psi) + 1)}{2} \tag{3.81}$$

The transmission coefficient of the source is therefore identical to the resistive radiation efficiency and thus is also plotted in Figure 3.5.

3.3 DISCUSSION

In the frequency range under consideration ($k_o h \lesssim \pi$) the resistive radiation efficiency and the power transmission coefficient are identical. This result follows from the definition of radiation efficiency. The discussion is thus limited to the parameters of radiation efficiency and characteristic impedance.

Equation (3.45) provides the characteristic impedance of the dipole source. If $\psi = 0$, or in other words the generating surface is a perfect piston, the radiation impedance is a positive real number equal to $\rho_o c_o$. Thus the resulting induced wave motion in the down-stream duct will be a plane wave. However if $\psi \neq 0$, the generating surface will not be a perfect piston, the characteristic impedance will be complex and a series of higher order evanescent modes will be generated. Although these modes do not carry nett power away from the source, nor propagate substantially into the duct, the evanescent modes effect the impedance of the source. As these modes are below cut-off, their axial wave number is imaginary and the characteristic impedance of the generating surface expressed by equation (3.45) will contain an imaginary part as well as a real part. The imaginary part is called the reactive impedance and is a measure of the fluid mass

reactance or loading on the driving surface. In physical terms the reactive impedance describes the "sloshing" of fluid or the transfer of energy back and forth from one part of the generating surface to another. The real part of the impedance on the other hand describes actual propagation of energy away from the generating surface.

The resistive and reactive parts of the impedance are plotted in Figures 3.3 and 3.4 respectively for different phase angles. It is interesting to note from Figure 3.3 when $\psi = 3\pi/2$ or piston B leads piston A the plot of resistive impedance implies that piston B "pushes" the air in front of it over to the part of the generating surface represented by piston A. In this region $(0.5 \leq y/h < 1.0)$ the resistive impedance is seen to be positive implying that piston A then does most of the work in radiating energy. Of course the converse is true when $\psi = \pi/2$. This phenomenon is also demonstrated by the reactive part of the impedance shown in Figure 3.4 where in the region of piston A for $\psi = 3\pi/2$ the plot demonstrates greater mass loading of air than the region represented by piston B.

When $\psi = \pi$ the characteristic impedance is seen from equation (3.45) to be entirely reactive. In this case there is no nett propagation of energy away from the source due to the phase quadrature between pressure and velocity and the acoustic motion consists entirely of a mass loading on the generating surface. Physically this means that the air in the near field of the generating surface will be entirely sloshing backwards and forwards between the regions of pistons A and B. Similarly when $\psi = \pi$, the resultant acoustic motion in the duct will consist of a series of evanescent modes and no plane wave mode is generated.

The resistive radiation efficiency (or transmission coefficient) is seen from Figure 3.5 to vary between zero and unity for different

phase angles between the motion of the pistons. As expected when $\psi = n\pi$, $n = 0,2,4...$ the resistive radiation efficiency is unity and the dipole source is an extremely efficient radiator of sound energy. This case of a perfect driving piston, as discussed previously, results in an excitation of a plane wave and no higher modes. When $\psi = n\pi$, $n = 1,3,5...$ the resistive radiation efficiency is zero and there is no power radiated into the downstream duct. In this case the dipole source is an extremely inefficient radiator of sound power. For intermediate phase angles the radiation efficiency predicts that some (but not all) input power will be radiated to the downstream duct as determined by equation (3.81).

Equation (3.45) shows that for frequencies less than the cut-off of the (1,0) mode the resistive radiation efficiency is entirely determined by the (0,0) mode of propagation (as evanescent modes carry no nett power). Thus in terms of real power flux away from the generating surface it is only necessary to consider the (0,0) mode for frequencies such that $k_o h \leq \pi$. However it must be remembered that the degree of excitation of the (0,0) mode is determined by the mass loading or reactive part of the characteristic impedance of the source.

The reactive radiation efficiency is seen from equation (3.75) to be dependent upon driving frequency as well as phase angle. Figure 3.6 demonstrates that when $\psi = n\pi$, $n = 0,2,4...$ the reactive radiation efficiency is zero and there is no mass loading on the source. This is the case of the perfect piston discussed previously. When $\psi = n\pi$, $n = 1,3,5...$ the reactive efficiency is seen to take a maximum value, while at the same time the resistive efficiency is zero. Thus the acoustic motion consists entirely of a localized mass loading on the pistons (or in other words a generation of only evanescent modes).

The degree of this mass loading is seen from Figure 3.7 to strongly increase with frequency. In fact equation (3.75) predicts that the reactive radiation efficiency becomes infinite as $k_o h \to \pi$ or in other words the (1,0) mode nears cut-on. Thus theoretically although there is no nett energy of propagation, an infinite force is needed to drive the mass loading in the infinitely long downstream duct. This can be thought of as an evanescent (1,0) mode excited to infinity in the downstream duct. Of course resistive losses, which have been neglected prevent this from occurring, however this result provides a reason why cut-off cannot be precisely observed experimentally, that is, the reactive term theoretically becomes infinite at cut-off!

Figure 3.7 also demonstrates that the reactive radiation efficiency is determined quite accurately by a first order modal solution, that is, the infinite sum of equation (3.75) truncated at $m = 1$. This result is also reflected in the relation for characteristic impedance. Physically, this result implies that the particular arrangement of dipole source considered results in a very strong driving of the (1,0) mode when there is a substantial phase difference between pistons. Of course when there is no substantial phase difference the result is a strong driving of the plane wave mode. Thus for a continuity condition involving an arrangement similar to Figure 3.1 it would be sufficiently accurate to truncate the modal sum of the downstream generated wave at $m = 1$. Although the evanescent mode does not contribute to nett power flow it must be included to take account of the mass loading on the generating surface and thus the degree of excitation of the (0,0) mode.

It is also interesting to note from equation (3.75) that only modes for which m is odd are excited. Thus the dipole source would theoretically only generate symmetric modes whether they be evanescent or propagating.

3.4 SUMMARY

Equations have been developed which theoretically predict the radiation efficiency and characteristic impedance of a dipole piston source mounted in the end of a hard walled semi-infinite rectangular duct. The relations have been used to investigate the behaviour of the source for different phase angles and non-dimensional driving frequencies. Explanations for the different radiation characteristics are given in terms of modal excitation and propagation.

The source is found to be an extremely efficient radiator for phase angle differences between pistons of $\psi = n\pi$, $n = 0,2,4...$ and an extremely poor radiator for phase angles of $\psi = n\pi$, $n = 1,3,5...$ and reasons for this behaviour are given. Nett power radiated has been shown to be due purely to the (0,0) mode while the role of the reactive or mass loading on the degree of excitation has been highlighted. The physical behaviour of the source near field at different phase angles has been discussed and related to the various parameters.

The analysis also demonstrates that for frequencies such that $k_o h \lesssim \pi$ a first order modal sum provides a sufficiently accurate description of the resultant sound field.

CHAPTER 4

PROPAGATION OF SOUND IN A CURVED BEND CONTAINING A CURVED AXIAL PARTITION

4.1. INTRODUCTION

In recent years attention has been focused on the problem of sound propagation in radial bends of rectangular cross section. Most of the early work in electromagnetic and acoustic waves is described in the introduction to Chapter 2. Work performed in the last ten years, relative to the problem of this chapter will be revised here.

Rostafinski (1974, 1976) has theoretically investigated the acoustic velocity distribution of propagating and evanescent modes within radial bends. Cummings (1974) has theoretically and experimentally investigated the acoustic discontinuity caused by a 180° radial bend of severe curvature in a straight duct system of rectangular cross section. He found that even for bends of severe curvature, near the cut-off frequency of the (1,0) mode in the curved section, the bends caused negligible reflection of sound. Osborne (1976) considered the more complex case of higher mode propagation in short curved bends, but still found no appreciable discontinuity in the acoustic propagation through the duct system. The main practical conclusion of these works is that curved duct bends, even of severe sharpness, have a low reflection coefficient. All the above work was based on a cylindrical coordinates solution to the wave equation. More recently, Fuller and Abell (1978) have approached the problem

differently, using conformal mapping to develop equations for the angular wavenumber of the (0,0) mode and higher evanescent modes in curved bends with and without mean flow. Their analysis is limited to low frequencies where the velocity potential solution of the wave equation is an approximate solution of Laplace's equation. Fuller and Bies (1978 A) have also investigated the case of sound propagation in a curved bend containing a curved axial partition and found that the partition profoundly alters the acoustic characteristics of the bend.

In this chapter the discontinuity and natural oscillations caused by a 180° bend divided by a curved partition are considered. This problem has been briefly discussed by Rostafinski (1976) to illustrate the dispersive nature of the (0,0) mode in curved ducts as opposed to the (0,0) mode in straight ducts with rigid walls. Three parameters, power reflection coefficient, characteristic impedance and transmission loss are investigated. Experimentally measured values of these parameters are given and compared with theoretical predictions. The presence of the partition is shown to drastically alter the acoustic properties of the bend and reasons for this different behaviour as opposed to a straight duct with a partition are given.

The partition effectively divides the curved bend into two concentric bends. The duct system containing the concentric bends is investigated theoretically by applying equations for sound propagation in straight and curved ducts of rectangular cross section to the respective parts. The propagating medium is assumed stationary. Continuity of acoustic pressure and axial particle velocities at adjoining interfaces between straight and curved sections is postulated to determine the Fourier coefficients of waves in each section. The analysis is limited to frequencies less than the cut-off frequency of

the (1,0) mode in both straight and curved ducts.

4.2 ANALYSIS

The arrangement of the compound bend to be investigated is shown in Figure 4.1. For analysis the bend has dimensions $R_1 = 0.127$ meters, $R_2 = 0.1905$ meters and $R_3 = 0.254$ meters and is to be analysed by dividing into sections with coordinate systems and adjoining interfaces as shown in Figure 4.1. Thus sound propagation in sections 1 and 4 is to be described by straight duct equations with no mean flow as derived in Chapter 1, while sound propagation in sections 2 and 3 is to be described by the curved duct, cylindrical equations with no mean flow of Chapter 2.

The Fourier coefficients of the incident and reflected waves in sections 1 to 4 as shown in Figure 4.1 are obtained by applying continuity conditions across interfaces A and B between the straight and curved ducts. Continuity implies that acoustic pressure and particle velocity are equal on the interface between respective duct sections. In this analysis continuity of axial particle velocity is postulated. This is supported by the fact that, as the frequencies to be considered are well below the cut-off frequency (1,0) mode, the radial particle velocities in the curved sections are very small. The validity of this assumption is borne out by experimental results. As there is no discontinuity in the z direction it is satisfactory to use a two dimensional coordinate system, i.e. $k_n = 0$.

Both sides of each equation, obtained by continuity of axial particle velocity and pressure, are mutliplied by $\cos[(m\pi y/h)]$ and integrated with respect to y, y' or r. The orthognality property of $\cos[(m\pi/h)y]$ allows determination of the coefficients of the waves necessary to determine the propagation characteristics of the bend.

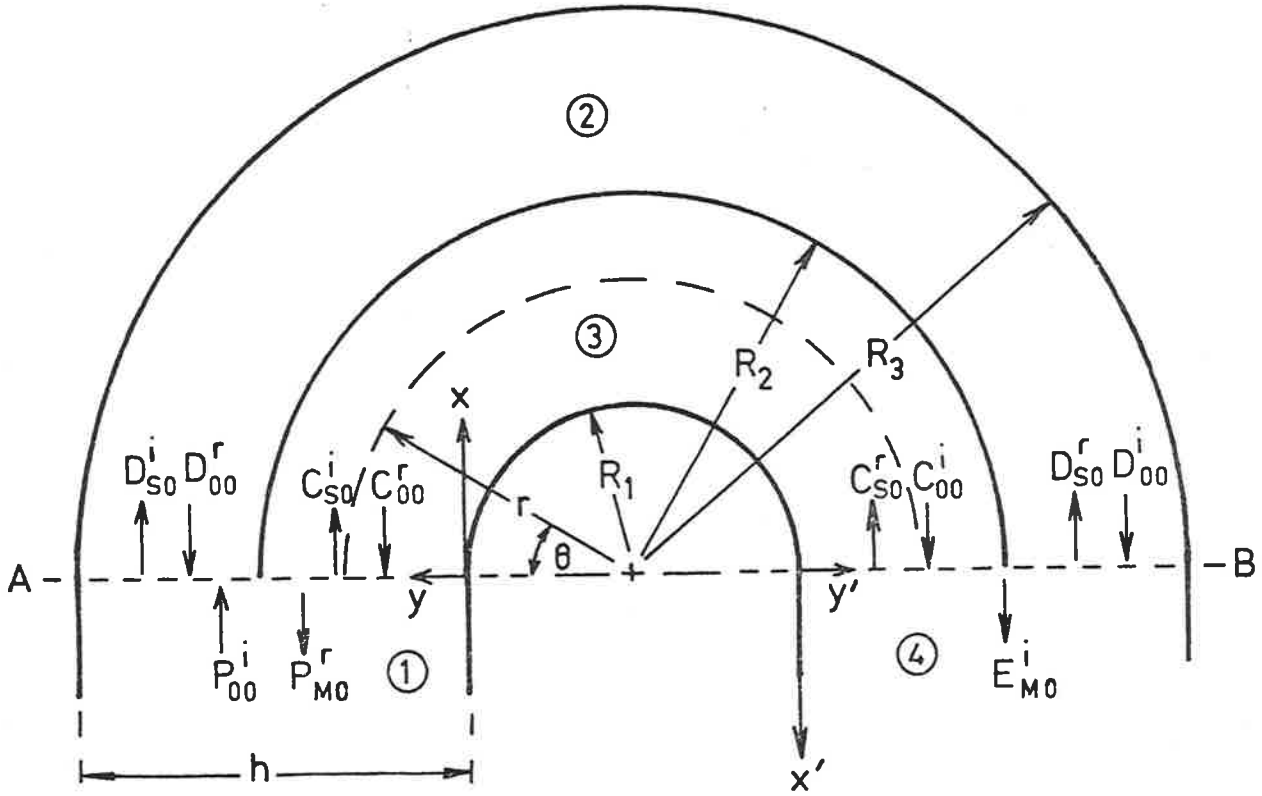

FIGURE 4.1. Arrangement and co-ordinate system of the compound bend.

Thus applying continuity of acoustic pressure at interface A where $x = 0$, $\theta = 0$ we obtain, assuming a pressure form solution of the wave equation

$$P^i_{oo} + \sum_{m=0}^{\infty} P^r_{mo} \cos[(m\pi/h)y] = \sum_{s=0}^{\infty} C^i_{so} \psi^c_{so} + C^r_{oo}\psi^c_{oo} \qquad (4.1)$$

for $R_1 < r \leq R_2$

and

$$P^i_{oo} + \sum_{m=0}^{\infty} P^r_{mo} \cos[(m\pi/h)y] = \sum_{s=0}^{\infty} D^i_{so}\psi^c_{so} + D^r_{oo}\psi^c_{oo} \qquad (4.2)$$

for $R_2 < r \leq R_3$ where superscripts i and r imply incident and reflected waves respectively.

Multiplying both sides by $\cos[(m\pi/h)y]$ and integrating over the duct interface we obtain

$m = 0$,

$$P^i_{oo}h + P^r_{oo}h = \sum_{s=0}^{\infty} C^i_{so} \int_{R_1}^{R_2} \psi^c_{so}dr + C^r_{oo} \int_{R_1}^{R_2} \psi^c_{oo}dr$$

$$+ \sum_{s=0}^{\infty} D^i_{so} \int_{R_2}^{R_3} \psi^c_{so}dr + D^r_{oo} \int_{R_2}^{R_3} \psi^c_{oo}dr \qquad (4.3)$$

$m \neq 0$,

$$P^r_{mo}(h/2) = \sum_{s=0}^{\infty} C^i_{so} \int_{R_1}^{R_2} \psi^c_{so} \cos[(m\pi/h)(r-R_1)]dr$$

$$+ C^r_{oo} \int_{R_1}^{R_2} \psi^c_{oo} \cos[(m\pi/h)(r-R_1)]dr$$

$$+ \sum_{s=0}^{\infty} D^i_{so} \int_{R_2}^{R_3} \psi^c_{so} \cos[(m\pi/h)(r-R_1)]dr$$

$$+ D^r_{oo} \int_{R_2}^{R_3} \psi^c_{oo} \cos[(m\pi/h)(r-R_1)]dr \qquad (4.4)$$

Similarly continuity of tangential particle velocity at interface A provides

$m = 0$,

$$P^i_{oo} k_{oo} h - P^r_{oo} k_{oo} h = \sum_{s=0}^{\infty} C^i_{so} \int_{R_1}^{R_2} \psi^c_{so}(\nu_s/r)dr - C^r_{oo} \int_{R_1}^{R_2} \psi^c_{oo}(\nu_o/r)dr$$

$$+ \sum_{s=0}^{\infty} D^i_{so} \int_{R_2}^{R_3} \psi^c_{so}(\nu_s/r)dr - D^r_{oo} \int_{R_2}^{R_3} \psi^c_{oo}(\nu_o/r)dr \qquad (4.5)$$

$m \neq 0$,

$$- P^r_{mo} k_{mo} h/2 = \sum_{s=0}^{\infty} C^i_{so} \int_{R_1}^{R_2} \psi^c_{so}(\nu_s/r)\cos[(m\pi/h)(r-R_1)]dr$$

$$- C^r_{oo} \int_{R_1}^{R_2} \psi^c_{oo}(\nu_o/r)\cos[(m\pi/h)(r-R_1)]dr$$

$$+ \sum_{s=0}^{\infty} D^i_{so} \int_{R_2}^{R_3} \psi^c_{so}(\nu_s/r)\cos[(m\pi/h)(r-R_1)]dr$$

$$- D^r_{oo} \int_{R_2}^{R_3} \psi^c_{oo}(\nu_o/r)\cos[(m\pi/h)(r-R_1)]dr \qquad (4.6)$$

The equations obtained by this method at interface B are given in Appendix 2. At both interfaces an infinite series of modes will be generated. As the frequency over which the bend will be investigated is limited to less than the cut-off frequency of the (1,0) mode in both straight and curved sections these infinite sets will consist of one propagating and an infinite number of evanescent

modes. In order to determine the coefficients it is necessary to truncate each infinite sum at a value determined by two factors: (1) Since the number of unknown coefficients generated must equal the number of equations, the number of modes considered in straight sections 1 and 4 is truncated at twice the number considered in curved sections 2 and 3 (this relation is derived in more detail in Chapter 5). (2) The accuracy of the analysis is determined by the number of modes considered.

Cummings (1974) and Osborne (1976) have both shown that non-propagating modes have only a small effect on the sound propagation in a curved bend. Thus in the equations developed previously from continuity conditions, the number of modes considered in the curved sections will be truncated at one while in the straight sections, one propagating and one non-propagating mode will be considered. This simplification is justified, as will be shown, by the comparison between theoretical and experimental results. The two modes considered in both straight sections are necessary to provide continuity across adjoining interfaces.

4.3 EXPERIMENTAL APPARATUS AND METHOD

The bend was investigated with the arrangement shown in Figure 4.2. The duct system has a 0.0635 x 0.127 meter cross section and was constructed from a 0.0254 meter thick wood lined with laminex. The compound bend was machined from laminated wood and the curved partition was rolled from 1.5mm aluminium sheet to the required dimensions and is shown in Plate 1. The sound source was positioned 1.7 meters upstream from the entrance to the bend at which distance any evanescent modes are sufficiently attenuated to be negligible. The straight duct downstream of the bend was terminated with an

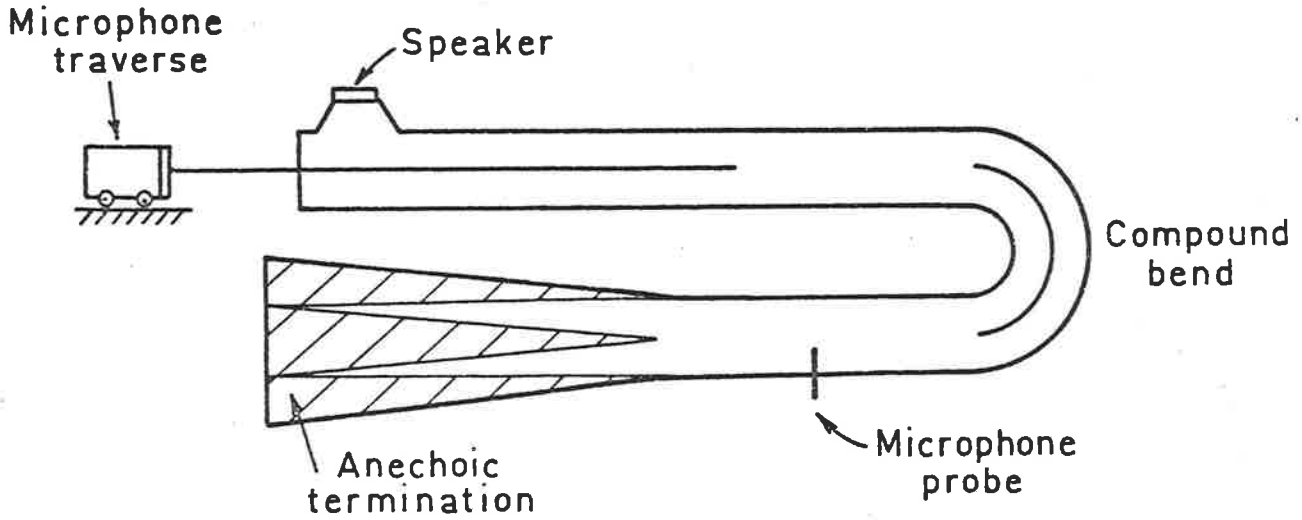

FIGURE 4.2. Arrangement of experimental apparatus.

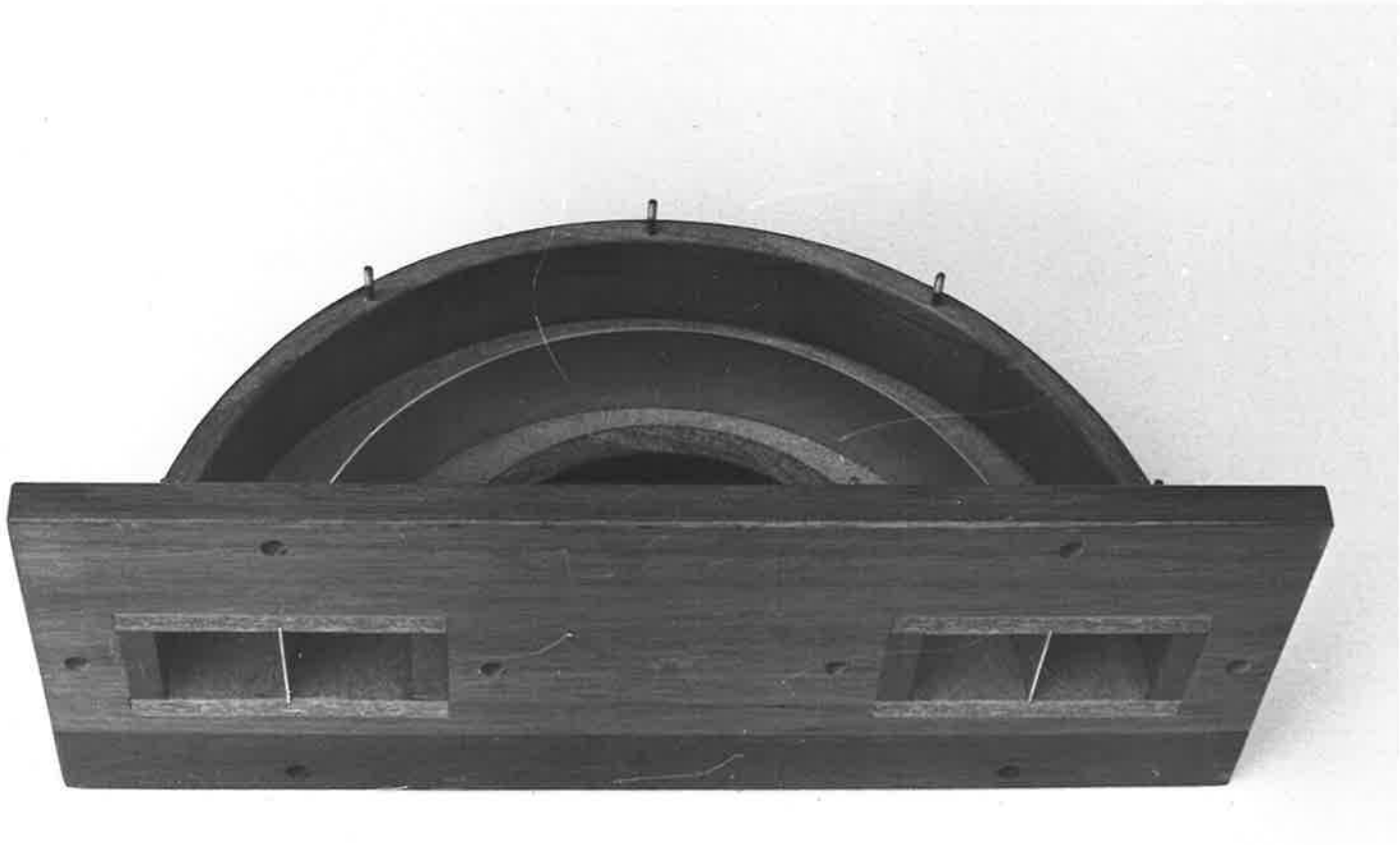

PLATE 1. The compound bend

anechoic muffler with a pressure reflection coefficient of less than 0.12.

The acoustic signal used was a pure tone and was measured using a Brüel and Kjaer One Third Octave Filter. Standing wave outputs from this instrument were fed to a Brüel and Kjaer Graphic Level Recorder for visual examination. Three parameters were measured. The power reflection coefficient, an indication of how much sound energy is reflected back towards the source, and the characteristic impedance, and indication of how severe a discontinuity the bend presents to acoustic propagation were obtained by measuring the standing wave in the upstream duct with a Brüel and Kjaer standing wave apparatus set, and applying standing wave theory as outlined in Beranek (1950). Values of experimental power reflection coefficient plotted against a non-dimensional frequency parameter $k_o h$ are shown in Figure 4.3. Since the analysis is limited to less than the cut-off frequency of the (1,0) mode in the straight duct section, for which $k_o h = \pi$, values of $k_o h$ are terminated at $k_o h = 3.02$. Experimental values of resistive impedance $R_i/\rho_o c_o$ are shown in Figure 4.4 while those of the reactive part $\chi_i/\rho_o c_o$ are shown in Figure 4.5.

The transmission loss, a measure of the attenuation in decibels of the incident wave, was measured by traversing a calibrated microphone in the upstream duct until a maximum in sound pressure level P_{oo}^{max}(dB) was recorded. The sound pressure level of the propagating wave E_{oo}^{i}(dB) in the downstream duct was measured with a calibrated microphone inserted through the duct wall at a distance of 1 meter from the bend exit. The transmission loss was then calculated from equation (4.7) and is plotted in Figure 4.6.

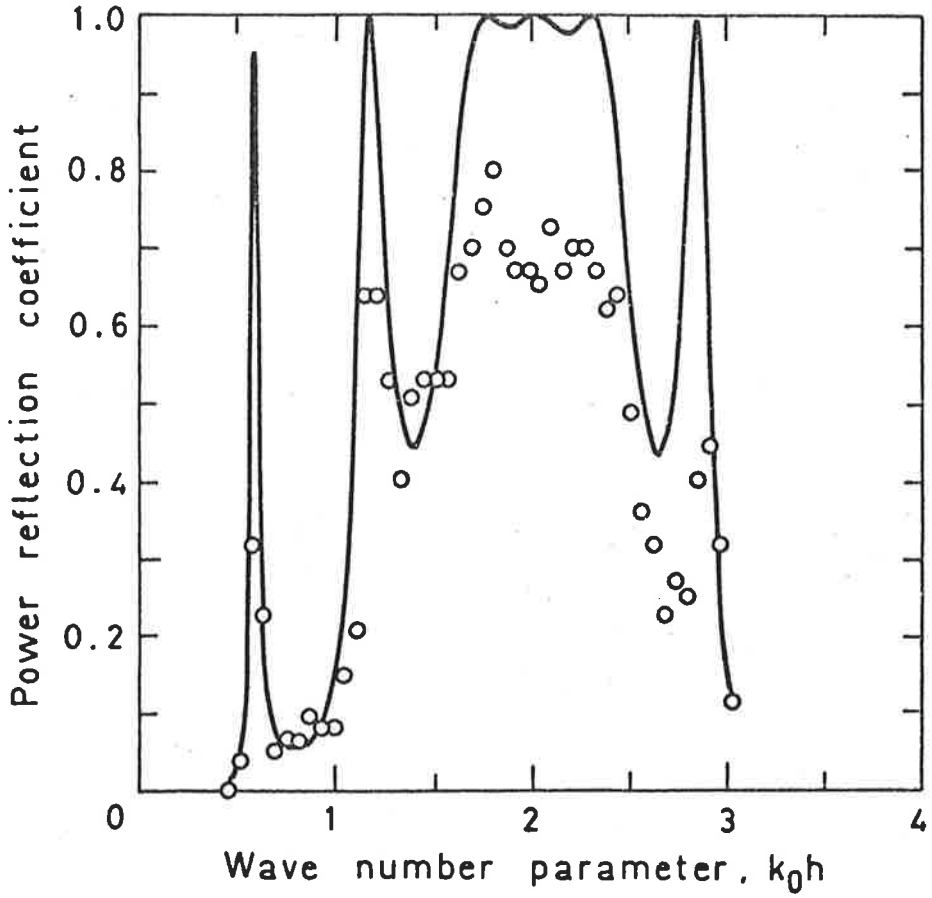

FIGURE 4.3. Sound power reflection coefficient of the compound bend. ———, theoretical; O , experimental.

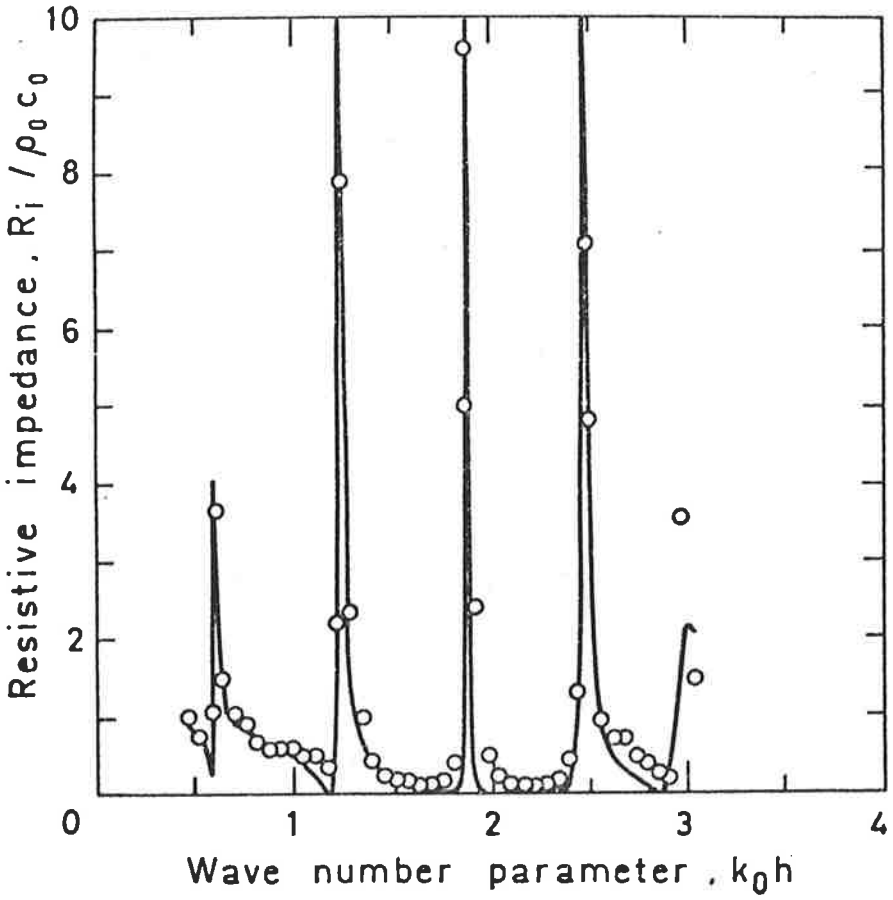

FIGURE 4.4. Resistive part of the characteristic impedance of the the compount bend. ——— , theoretical; o , experimental.

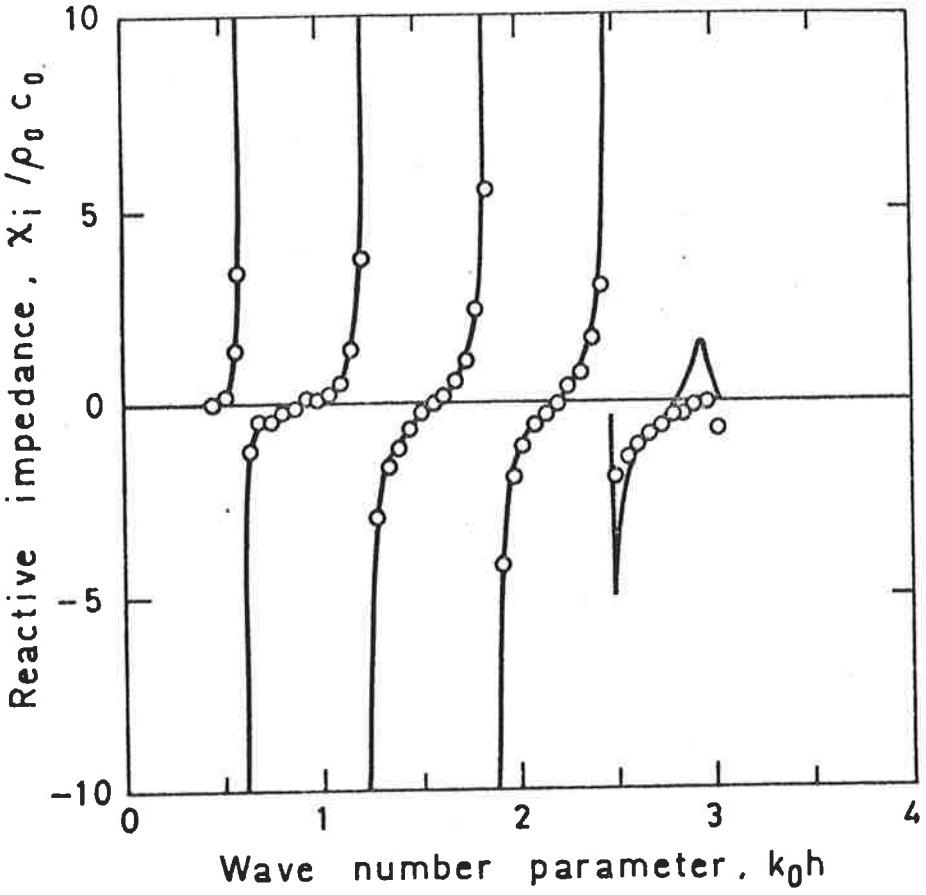

FIGURE 4.5. Reactive part of the characteristic impedance of the compound bend. ——— ,theoretical; O experimental.

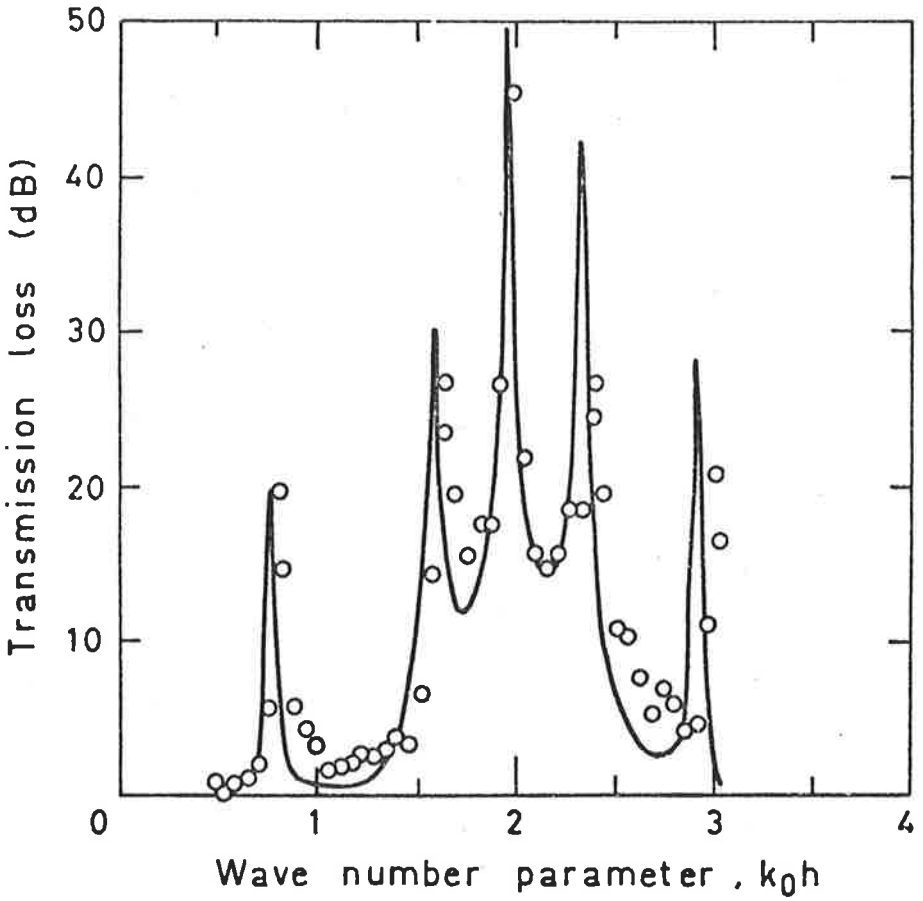

FIGURE 4.6. Transmission loss of the compound bend.
——— , theoretical; O , experimental.

$$P_{oo}^{max} = (1 + |R|)P_{oo}^{i}$$

$$\therefore \quad P_{oo}^{i}(dB) = P_{oo}^{max}(dB) - 20 \log_{10} [1 + |R|]$$

Hence transmission loss (dB) = $P_{oo}^{max}(dB) - 20 \log_{10} [1 + |R|]$

$$- E_{oo}^{i}(dB) \qquad (4.7)$$

In equation (4.7) R is the measured pressure reflection coefficient. It should be noted that equation (4.7) holds only for equal values of temperature and area of the inlet and outlet sections.

4.4 THEORETICAL PREDICTIONS

The radial terms of equations (4.3) to (4.6) and those of Appendix 2 were expressed as power series expansions of Bessell and Neumann functions from McLachlan (1941) and integrated using Simpson's rule by a CDC 6400 computer. The resulting coefficients of the equations were then set in an eight by eight matrix as given in Appendix 3 and the variables of the matrix were obtained by a computer program based on Crout's rule described in Fröberg (1970). For convenience a reference amplitude of $P_{oo}^{i} = 1 - 0i$ was assumed.

The theoretical power reflection coefficient is given by

$$\alpha_r = \left| \frac{P_{oo}^{r}}{P_{oo}^{i}} \right|^2 \qquad (4.8)$$

The characteristic impedance is

$$Z/\rho_o c_o = R_i/\rho_o c_o + (\chi_i/\rho_o c_o)i$$

$$= (P_{oo}^{i} + P_{oo}^{r})/(P_{oo}^{i} - P_{oo}^{r}) \qquad (4.9)$$

where P_{oo}^{i} and P_{oo}^{r} are complex amplitudes.

The theoretical transmission loss is

$$T.L. = -10 \log_{10} [1 - \alpha_r] \qquad (4.10)$$

All three parameters are shown with the respective experimental values for comparison in Figures 4.3 to 4.6.

4.5 DISCUSSION

4.5.1 Power Reflection Coefficient

As can be seen in Figure 4.3 there is close agreement between theoretical and experimentally measured values of the frequencies at which maxima occur. The small discrepancies are thought to be due to dimensional inaccuracies and variation in ambient temperature during the course of experimentation.

The magnitude of the experimental reflection coefficient is consistently less than predicted at the maxima. This was thought to be due to the difficulty of determining accurately the standing wave ratio when it is quite large. In the case of large standing wave ratio the minima are quite sharp and very easily obscured by, for example, overtones due to a small distortion in the signal. They are thus very difficult to measure and the measured magnitude of sound pressure level is always too high. The standing wave ratio and thus the corresponding power reflection coefficient in this case will always be too small.

As can be seen in Figure 4.3, a curved 180° bend with a partition positioned on its centreline provides a large disruption to sound propagation. In fact the theory developed here predicts that at the dimensionless frequencies given in Table 4.1, the power reflection coefficient is very close to unity. This is in direct contrast to a normal curved bend. Cummings (1974) studied two 180° bends, one of radius ratio $R_1/R_2 = 0.097$ representing a very sharp bend, at frequencies below the cut-off frequency of the (1,0) mode and

Table 4.1: Characteristic Frequencies of a Compound 180° Bend for $R_3/R_1 = 2$

Characteristic Freq. $(k_o h)$*					
0.6	1.18	1.80	2.08	2.25	2.86

* Only frequencies below cut-off ($k_o h = \pi$) for the (1,0) mode in the straight duct are included.

found that the pressure transmission coefficient of the (0,0) mode does not fall below 0.975. Thus it can be seen that positioning a splitter or turning vane in a curved bend of a duct system leads to drastically different acoustic behaviour for frequencies below the cut-off for the first cross mode.

The reason for the markedly different effect of a partition in a straight and curved duct is due to the resulting variation in path length and phase of the two parts of the acoustic disturbance propagating in the two parts of the compound curved duct. Without the partition the phase of the (0,0) mode will be maintained radially across the duct and will be determined approximately by the centre-line propagation distance. The partition effectively prevents the implied redistribution of the disturbance across the original bend, containing it to the two separate concentric bends formed by the partition.

The effect of curvature on sound propagation in a curved duct in contrast to propagation in a straight duct is reflected in the respective solutions of the characteristic equation in cylindrical coordinates and the straight duct characteristic equation. For the (0,0) mode in a straight duct the wavenumber is independent of duct dimensions, whereas in a curved duct the corresponding angular wave-number is strongly dependent on the radii of the curved section as discussed by Rostafinski (1976). Thus the waves travelling in the separate curved sections, shown in Figure 4.1, have the same amplitude but different relative phases at each angle θ of propagation, due to different values of angular wavenumber. Therein lies the explanation for the effect of the partition in a curved duct.

At interface B, shown in Figure 4.1, the two incident waves

in sections 2 and 3 have a phase difference induced by the different values of respective angular wavenumber. When these two waves recombine at B, the phase difference leads to generation of non-propagating cross modes and the resulting impedance mismatch causes reflection of sound. Interface B is very similar to the dipole piston source discussed in Chapter 3. Similarly reflected waves from B will have a phase difference at A and an impedance mismatch results here as well. When these phase differences are close to π, large reflection of sound occurs.

4.5.2. Characteristic Impedance

Theoretical and experimental values of resistive and reactive parts of the characteristic impedance are in excellent agreement as shown in Figure 4.4 and 4.5.

It can be seen that at the dimensionless frequencies of $k_o h$, given in Table 4.1, a large impedance mismatch relative to the characteristic impedance $\rho_o c_o$ of the incident wave is generated. Thus one would expect large reflection of sound at these frequencies. This is demonstrated in Figure 4.3, which shows high reflection of sound at the characteristic frequencies of Table 4.1.

At the intermediate frequencies the characteristic impedance $Z/\rho_o c_o$ of the bend is relatively closer to unity than at the bend characteristic frequencies and incident sound is thus mostly transmitted at these intermediate frequencies.

As the non-dimensional frequency $k_o h$ approaches π the reactive part of the characteristic impedance changes its general shape demonstrated at lower frequencies. This was thought to be due to the effect of evanescent (1,0) mode in the straight duct becoming predominant near cut-off.

4.5.3 Transmission Loss

Much closer agreement is demonstrated by comparison of experimental and theoretical values of transmission loss shown in Figure 4.6 than reflection coefficient shown previously in Figure 4.3. This observation supports the argument presented previously to explain the discrepancies shown in the latter figure.

At $k_o h = 2.0$ a transmission loss of 45.5 dB was measured. Thus an incident pure tone at this frequency would be virtually completely reflected. Such high levels of attenuation suggest the use of the discontinuity provided by the bend as a reactive attenuator. An attenuator based on the impedance mismatch generated by a center body placed in a 90° bend is discussed by Fuller and Bies (1978 B) and also in Chapter 6.

4.6 SUMMARY

Sound transmission in a duct system containing a curved 180° bend with a central partition has been discussed. Theoretical and experimental values have been given and good agreement is obtained.

The partition was found to significantly alter the sound propagation through the bend, resulting in high reflection of sound at a number of discrete frequencies.

The problem discussed illustrates the essential difference between sound propagation in straight and curved ducts. Namely, the angular wavenumber of the (0,0) mode in curved ducts is dependent on the boundary conditions, whereas in the straight duct the wavenumber is independent of duct geometry.

PART III: REACTIVE ATTENUATORS

CHAPTER 5

A REACTIVE ACOUSTIC ATTENUATOR

5.1 INTRODUCTION

Despite extensive previous investigations, the control of sound propagating in ducts continues to be a problem requiring research. One particular aspect of this problem, the control of low frequency sound, has until recently defied satisfactory solution. Proposed attenuators invariably suffer the disadvantage of excessive size or large pressure drop. Attenuators fall generally into two categories; reactive devices which trap acoustic energy and store it until it is dissipated by small losses inherent in the system and dissipative devices which encourage the propagation of sound into some medium, generally lining the walls of the device, in which the sound is subsequently dissipated.

Dissipative devices work well for sounds of medium or high frequencies, but are ineffective at low frequencies where the wavelength of sound is comparable to the duct dimensions. Reactive attenuators usually follow the well known form of either a quarter wave tube, a Hemholtz resonator or an expansion chamber. As well as having a narrow frequency response, these devices tend to be bulky and cause a high pressure drop to the flow through the duct.

In a paper by Fuller and Bies (1978 B) a reactive acoustic attenuator was described which combined high transmission loss over a fairly broad frequency band with a low pressure drop. The attenuator,

based upon a principle described by Rayleigh (1877) may be fitted into a 90° bend in the duct system. A similar attenuator has been investigated experimentally by Luxton (1968). Other work on reactive attenuation, apart from the traditional methods of resonators and plenum chambers, has largely been centred on the application of Swinbank's method for the control of sound in a duct. The basic idea of this method is to introduce an antiphase copy of the sound in the duct. Ideally the added sound does not cancel the incident sound in an energy sense but causes an impedance mismatch and thus reflection of sound. The limiting factor is to generate the antiphase signal such that it propagates only in the direction of propagation of the original sound. Poole and Leventhall (1976) have, with limited success, developed a reactive attenuator based on Swinbank's proposal. They constructed a suitable source with omnidirectional characteristics as proposed by Swinbank (1973) and measured the attenuation of incident pure tones and band-limited noise. The test was carried out for low frequencies and stationary medium of propagation. Poole and Leventhall measured attenuation of pure tones of greater than 50 dB but found that the band-limited noise tests gave far less encouraging results. However, they concluded that the system proposed was not a practical replacement for a passive silencer as the attenuation achieved was over a very narrow frequency range. In conclusion Pool and Leventhall stated that for Swinbank's method to work two requirements have to be satisfied: (1) no sound propagation from the cancelling sources towards the actual noise source, (2) the sound introduced must be an accurate, but phase inverted copy of the noise to be cancelled.

Patrick (1967) has considered the transmission loss of duct systems containing a series of ducts aligned in parallel, either

with lined or unlined walls. He applies matrix techniques usually used in the analysis of electrical circuits to develop a systematic method for determining the acoustical characteristics of complicated duct arrays.

In this chapter, a reactive acoustic attenuator is investigated which makes use of inherent differences in path lengths of the inner and outer portions of a bend fitted with a splitter to generate an impedance mismatch at the inlet and exit of the device, causing reflection of sound. The attenuator, when fitted into any convenient bend in the duct system, combines high rejection of low frequency sound over a frequency range of three quarters of an octave with a low pressure drop coefficient (0.46). The attenuator also provides very high attenuation in the order of 30 to 50 dB at a number of discrete frequencies.

Equations characterizing sound propagation in straight and curved ducts (cylindrical coordinates solution) are used to describe the device without flow. The effect of flow on the performance of the attenuator is considered in Chapter 6. The predicted results agree well with those measured experimentally. An understanding of the performance of the attenuator has allowed a redesign of its shape to optimize its performance. By the nature of the device the analysis is necessarily limited to frequencies less than the cut-off frequency of the (1,0) mode in the incident duct. Two parameters, power transmission coefficient and transmission loss are investigated and small discrepancies between theoretical and experimental results are discussed.

5.2 DESIGN

The arrangement of the attenuator fitted into a right angled bend in the duct system is shown in Figure 5.1. The frequency range over which the attenuator is expected to be useful lies below the cut-off frequency of the (1,0) mode in the straight sections of the duct upstream of interface A and downstream of interface D. An impedance mismatch is generated at interface D by the phase difference between the propagating waves in the two separate duct sytems. The phase difference is achieved by placing a profiled center body in the duct bend which divides the incident acoustic plane wave at interface A into two halves that recombine at D. The relative phase of the two separate propagating waves at D is approximately determined by the mean path difference of the two separate channels. At the design frequency, for which the mean path difference between the inner and outer channels is one half wave length, a plane wave incident at interface A will be converted to a series of non-propagating cross modes at interface D and at this frequency all incident sound energy to the attenuator will be reflected.

As the center body is shaped with gradual bends it acts as a turning vane and a low pressure drop results across the device.

The design frequency of the attenuator was chosen to be 844 Hz corresponding to a 0.2 meter path difference in the experimental duct. This was achieved with the crescent shaped center body of the shape shown in Figure 5.1, of which two variations were investigated.

5.3 ANALYSIS

The theory of Chapter 3 provides an approximate indication of the power transmitted and reflected at interface D of the attenuator. The analysis accurately described the reflection of sound power at the

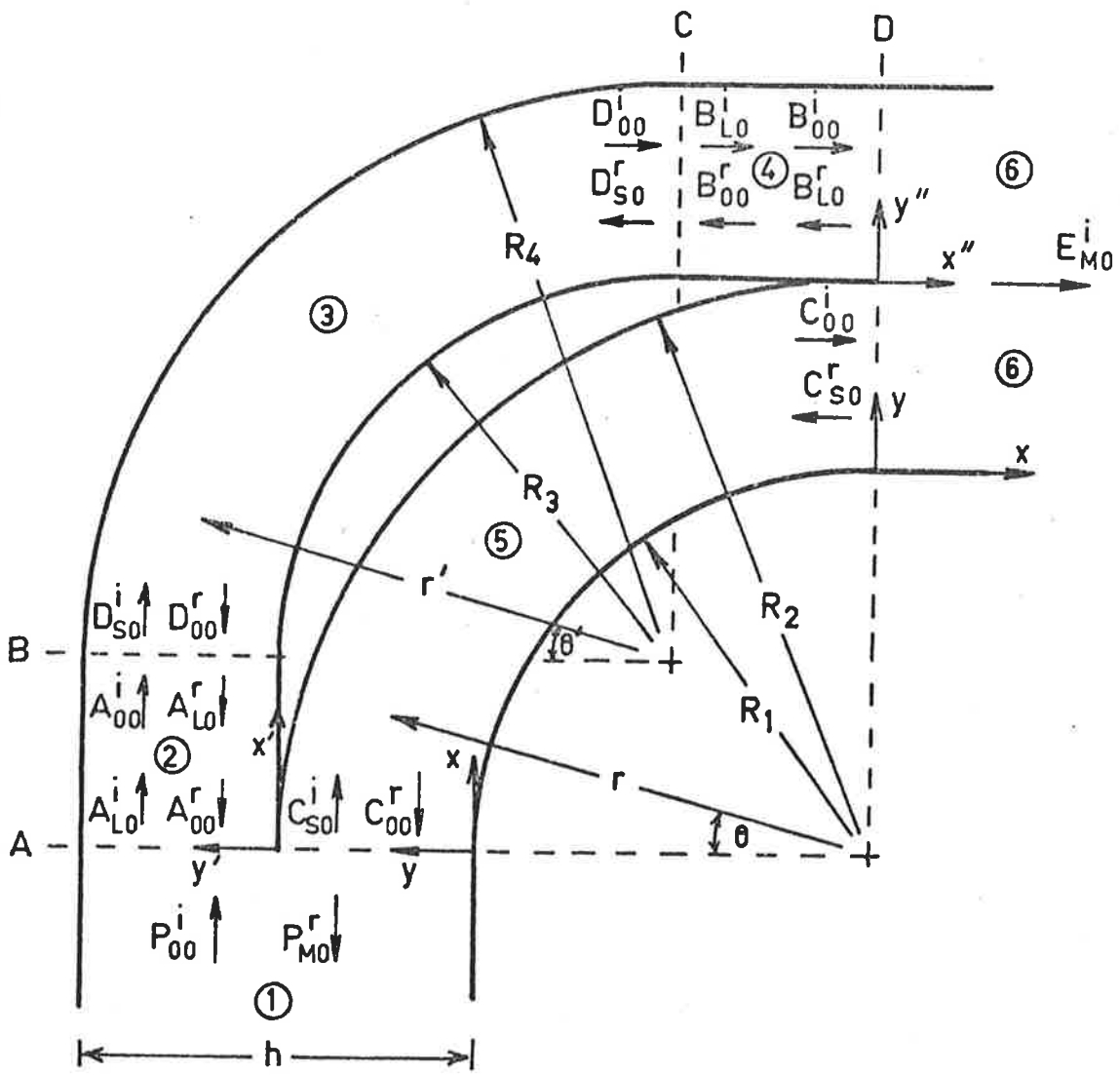

FIGURE 5.1. Arrangement and co-ordinate system of the attenuator.

design frequency but failed to account for observed major reflections at other frequencies also in the range considered. The theory of Chapter 3 also revealed the mechanism that causes reflection of sound, namely an impedance mismatch generated by a series of non-propagating cross modes. Thus the attenuator was described by dividing it into sections and considering propagation and reflection of acoustic waves in each. With the coordinate systems and joining interfaces shown in Figure 5.1, sound propagation may then be described by straight duct equations in sections 1, 2, 4 and 6 and by curved duct equations in sections 3 and 5.

The coefficients of each wave were obtained by applying continuity conditions across each interface. Continuity implies that acoustic pressure and particle velocity must be continuous across the plane joining the two duct systems. Since there is no discontinuity in the z direction it is satisfactory to use a two dimensional co-ordinate system i.e. $k_n = 0$. For convenience a reference amplitude of $P^i_{oo} = 1 - 0i$ will be used for the incident wave in the upstream duct.

At each discontinuity (interface) an infinite set of higher order modes will be generated. As the frequency is limited to less than the cut-off frequency of the (1,0) mode in all straight duct sections, the higher modes in the straight ducts will decay and only the (0,0) mode will propagate without attenuation. Similarly the frequencies considered are well below the cut-off frequency of the (1,0) mode in both curved sections and only the (0,0) mode will propagate in the curved sections 3 and 5 without attenuation. Hence the waves *arriving* at each interface will be limited to the (0,0) mode as all other modes will have decayed to be negligible, however the waves *leaving* each interface will consist of an infinite series

of higher modes as well as the (0,0) mode.

The requirement for continuity of particle velocity will be simplified to continuity of tangential particle velocity along the direction of the duct centerline. This simplification is supported by the consideration that no cross modes propagate and thus cannot contribute to the nett power flow. However ultimate justification for the simplification rests with the agreement between the results of experiment and predictions of theory. On this basis the simplification is justified and thus continuity of acoustic pressure and tangential particle velocity at each interface is postulated.

The Fourier coefficients are obtained by multiplying both sides of the equations by $\cos(m\pi y/h)$ and integrating with respect to y, y', y" or r as applies. Since the functions $\cos(m\pi y/h)$ are orthogonal the P^r_{mo} coefficients can be separated.

Thus continuity of acoustic pressure at interface A where $x = 0$, $x' = 0$ and $\theta = 0$ provides

$$P^i_{oo} + P^r_{oo} \cos[(m\pi y/h)] = \sum_{s=0}^{\infty} C^i_{so}\psi^c_{so} + C^r_{oo}\psi^c_{oo} \qquad (5.1)$$

for $R_1 < r \leq R_2$

and

$$P^i_{oo} + P^r_{oo} \cos[(m\pi y/h)] = \sum_{\ell=0}^{\infty} A^i_{\ell o}\psi^s_{\ell o} + A^r_{oo}\psi^s_{oo} \qquad (5.2)$$

for $0 \leq y' < h/2$

Multiplying both sides of equations (5.1) and (5.2) by $\cos(m\pi y/h)$ and integrating with respect to y, y' and r leads to

$m = 0$,

$$P_{oo}^{i}h + P_{oo}^{r}h = \sum_{s=0}^{\infty} C_{so}^{i} \int_{R_1}^{R_2} \psi_{so}^{c} dr + C_{oo}^{r} \int_{R_1}^{R_2} \psi_{oo}^{c} dr$$

$$+ \sum_{\ell=0}^{\infty} A_{\ell o}^{i} \int_{0}^{h/2} \psi_{\ell o}^{s} dy' + A_{oo}^{r} h/2 \qquad (5.3)$$

$m \neq 0$,

$$P_{mo}^{r}(h/2) = \sum_{s=0}^{\infty} C_{so}^{i} \int_{R_1}^{R_2} \psi_{so}^{c} \cos[(m\pi/h)(r - R_1)]dr$$

$$+ C_{oo}^{r} \int_{R_1}^{R_2} \psi_{oo}^{c} \cos[(m\pi/h)(r - R_1)]dr$$

$$+ \sum_{\ell=0}^{\infty} A_{\ell o}^{i} \int_{0}^{h/2} \psi_{\ell o}^{s} \cos[(m\pi/h)(y' + h/2)]dy'$$

$$- A_{oo}^{r}\left(\frac{h}{2m\pi}\right) [1 - (-1)^{m}] \qquad (5.4)$$

Similarly continuity of tangential velocity at interface A provides

$m = 0$,

$$P_{oo}^{i}k_{oo}h - P_{oo}^{r}k_{oo}h = \sum_{s=0}^{\infty} C_{so}^{i} \int_{R_1}^{R_2} \psi_{so}^{c}(\nu_s/r)dr - C_{oo}^{r} \int_{R_1}^{R_2} \psi_{oo}^{c}(\nu_o/r)dr$$

$$+ \sum_{\ell=0}^{\infty} A_{\ell o}^{i} k_{\ell o} \int_{0}^{h/2} \psi_{\ell o}^{s} dy' - A_{oo}^{r} k_{oo} h/2 \qquad (5.5)$$

$m \neq 0$,

$$-P_{mo}^{r}k_{mo}h/2 = \sum_{s=0}^{\infty} C_{so}^{i} \int_{R_1}^{R_2} \psi_{so}^{c}(\nu_s/r)\cos[(m\pi/h)(r - R_1)]dr$$

$$- C^{r}_{oo} \int_{R_1}^{R_2} \psi^{c}_{oo}(\nu_o/r)\cos[(m\pi/h)(r - R_1)]dr$$

$$+ \sum_{\ell=0}^{\infty} A^{i}_{\ell o} k_{\ell o} \int_{0}^{h/2} \psi^{s}_{\ell o} \cos[(m\pi/h)(y' + h/2)]dy'$$

$$+ A^{r}_{oo} k_{oo} (\frac{h}{2m\pi})[1 - (-1)^{m}] \qquad (5.6)$$

The equations derived by continuity conditions at interfaces B, C, and D are given in Appendix 2.

The above system of equations constitute an infinite set with an infinite number of unknowns. In order to proceed, it is necessary to truncate the various infinite series. Truncation of each series is determined by two considerations. Firstly, the accuracy of the resulting mathematical expression which is desired when compared with experimental results and, secondly the number of equations necessary to determine all of the unknown coefficients in the several truncated series.

Let the number of modes in straight sections 1 and 6 truncate at L, in straight sections 2 and 4 at Q and in curved sections 5 and 3 at N. In this case the total number of unknown coefficients U is

$$U = 2L = 4N = 4Q \qquad (5.7)$$

while the total number of equations G is

$$G = 4L = 4Q \qquad (5.8)$$

Cummings (1974) has shown for an interface between a straight and curved cut the number of modes in each duct section must be equal for solution, hence

$$N = Q \qquad (5.9)$$

Therefore equating the number of unknowns U and equations G gives

$$L = 2N = 2Q \tag{5.10}$$

Hence the series describing propagation in sections 1 and 6 must be truncated at twice the number of terms of the series describing sections 2, 3, 4 and 5.

At each discontinuity in the duct system an infinite number of higher order modes are generated. Cummings (1974) has shown that at frequencies well below the cut-off frequency of the (1,0) mode, non-propagating modes have only a small effect on sound propagation through a curved duct-straight duct interface. On comparing the theoretical and experimentally measured impedance (assumed entirely reactive) of a 180° curved bend terminated by an infinite impedance, Cummings found good agreement with prediction when the analysis was truncated at the (0,0) mode. For this reason and in the interest of economy of computing time, the present analysis is limited to consideration only of the (0,0) mode. Hence we set N and Q of equation (5.9) equal to unity and thus L of equation (5.10) equal to two. Therefore the number of modes considered in straight sections 1 and 6 will be limited to two, one propagating and one evanescent mode, while only one propagating mode will be considered in all other sections of the attenuator.

This simplification is also supported by the analysis of Chapter 3, where it was shown a first order modal truncation gave a very accurate prediction of the reactive radiation impedance of a surface similar to interfaces A and D.

5.4 EXPERIMENTAL APPARATUS AND METHOD

The attenuator was investigated with the arrangement shown

in Figure 5.2. The duct system basically consisted of the apparatus used to test the compound bend of Chapter 4, having a 0.0635 x 0.127 meter rectangular cross section. The attenuator was constructed from machined laminated wood painted on the inside with a hard estapol varnish to approximate the rigid wall conditions. As in Chapter 4 the sound source was positioned 1.7 meters upstream from the entrance to the attenuator at which distance all cross modes generated locally by the speakers would have decayed to be negligible. Thus the incident wave at interface A of the attenuator was plane with constant pressure and velocity amplitude across the duct.

The downstream duct was terminated with an anechoic termination of the arrangement shown in Figure 5.2. The pressure reflection coefficient of this termination was measured separately over the frequency range considered and found to be less than 0.1. Hence the downstream duct appears infinite to the exit of the attenuator and only one wave with coefficient E^{i}_{oo} need be assumed to be propagating in the straight duct section 6.

The original attenuator investigated consists of a crescent shaped center body and surrounding duct with dimensions $R_1 = 0.229$ meters, $R_2 = 0.292$ meters, $R_3 = 0.051$ meters and $R_4 = 0.114$ meters where the corresponding radii are shown in Figure 5.1. This arrangement results in a path difference of 0.2 meters between the mean center lines of the two separate ducts. The corresponding design frequency, assuming plane wave propagation in all sections is 844 Hz.

When the analysis of the present chapter had been completed and verified a second, optimum, attenuator was constructed and tested. It had dimensions $R_1 = .0184$ meters, $R_2 = 0.248$ meters, $R_3 = 0.006$ meters and $R_4 = 0.07$ meters and is shown in Plate 2.

Two parameters, sound power transmission coefficient and

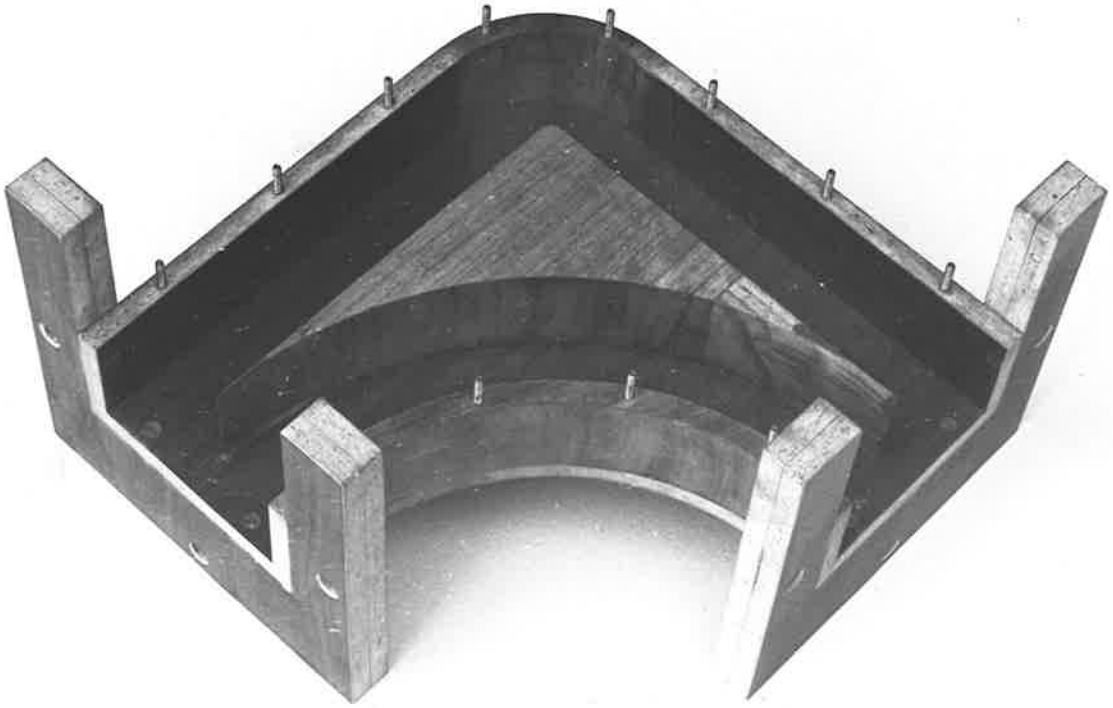

PLATE 2. The optimum attenuator

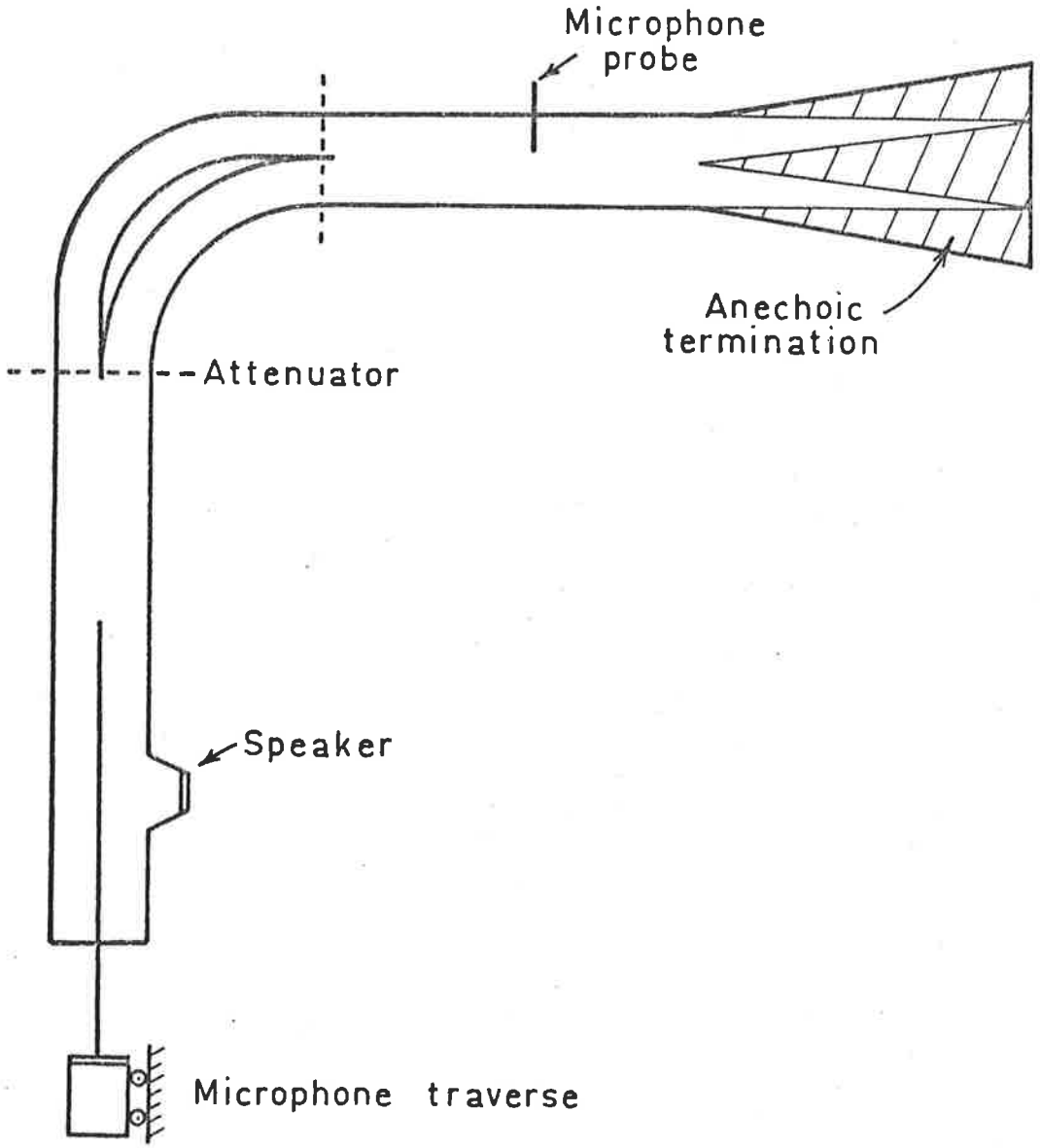

FIGURE 5.2. Arrangement of the experimental apparatus.

transmission loss were measured. The sound power transmission coefficient provides a measure of how much energy the attenuator will reflect and was obtained by measuring the acoustic standing wave in the upstream duct with a probe as indicated in Figure 5.2. Maximum and minimum pressures were measured and recorded as in Chapter 4 using a Brüel and Kjaer Spectrometer set to a one-third octave filtering band and a Graphic Level Recorder. The transmission coefficient was obtained from the measured standing wave ratio n_s using equation (5.11) and is shown plotted in Figure 5.3 for the original attenuator.

$$\alpha_t = 1 - \left[\frac{n_s - 1}{n_s + 1}\right] \tag{5.11}$$

The transmission loss of the attenuator is defined as the reduction in decibels between the sound pressure level of the incident wave P^i_{oo} and the transmitted wave E^i_{oo}. Transmission loss provides an indication of the performance of the attenuator as it shows to what degree the sound pressure level in the duct will be reduced by its installations. As the duct downstream of the attenuator is terminated anechoically, and thus appears infinite, values of transmission loss in this case will be identical to values of insertion loss for the same arrangement. The procedure of Chapter 4 was used to determine the experimental transmission loss. A calibrated microphone was traversed in the upstream duct until a maximum in sound pressure level P^{max}_{oo} was reached. The sound pressure level of the transmitted wave E^i_{oo} was measured with a calibrated microphone positioned midstream in the acoustic flow 0.3 meters from the exit of the attenuator. The transmission loss of the attenuator is then given by equation (4.7) of Chapter 4, repeated here.

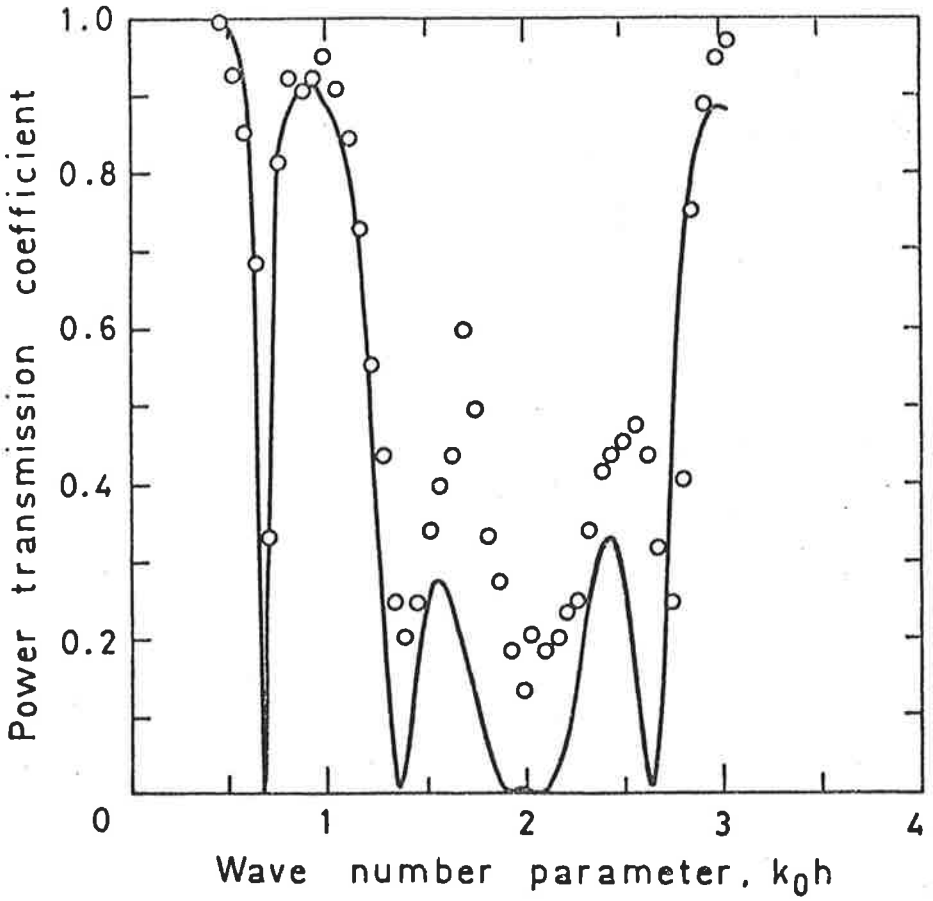

FIGURE 5.3. Power transmission coefficient of the original attenuator. ——— , theoretical; O , experimental.

$$\text{Transmission Loss} = P_{oo}^{max}(dB) - 20 \log_{10} [1 + |R|] - E_{oo}^{i}(dB) \quad (5.12)$$

where R is the measured pressure reflection coefficient. Values of experimental transmission loss determined from equation (5.12) for the original attenuator are plotted in Figure 5.4.

The transmission loss of the attenuator was also measured using broad band noise in one-third octave bands. To determine the transmission loss in this case, sound pressure levels were measured in the incident straight duct terminated directly with the anechoic termination. The input voltage level to the speaker was recorded in each one-third octave band for later use. The attenuator was then placed in position between the incident duct and the anechoic termination, the input voltage level to the speaker was set to the identical value as used previously in each one-third octave band, and the sound pressure level was recorded downstream of the attenuator. The transmission loss (for broad band noise) was then, directly the difference between the two measured values of sound pressure level. This technique overcomes the difficulty in determining the incident sound pressure level from the recorded sound pressure level in the upstream duct with the attenuator in position. Experimental values of transmission loss with band limited broad band noise determined by this method are shown in Figure 5.5.

5.5 THEORETICAL PREDICTIONS

The radial terms in equations (5.3) to (5.6) and of Appendix 2 were expressed as power series expansions of Bessel and Neumann functions from McLachlan (1934) and integrated using Simpson's rule on the computer as in section 4.4 of Chapter 4 for the compound

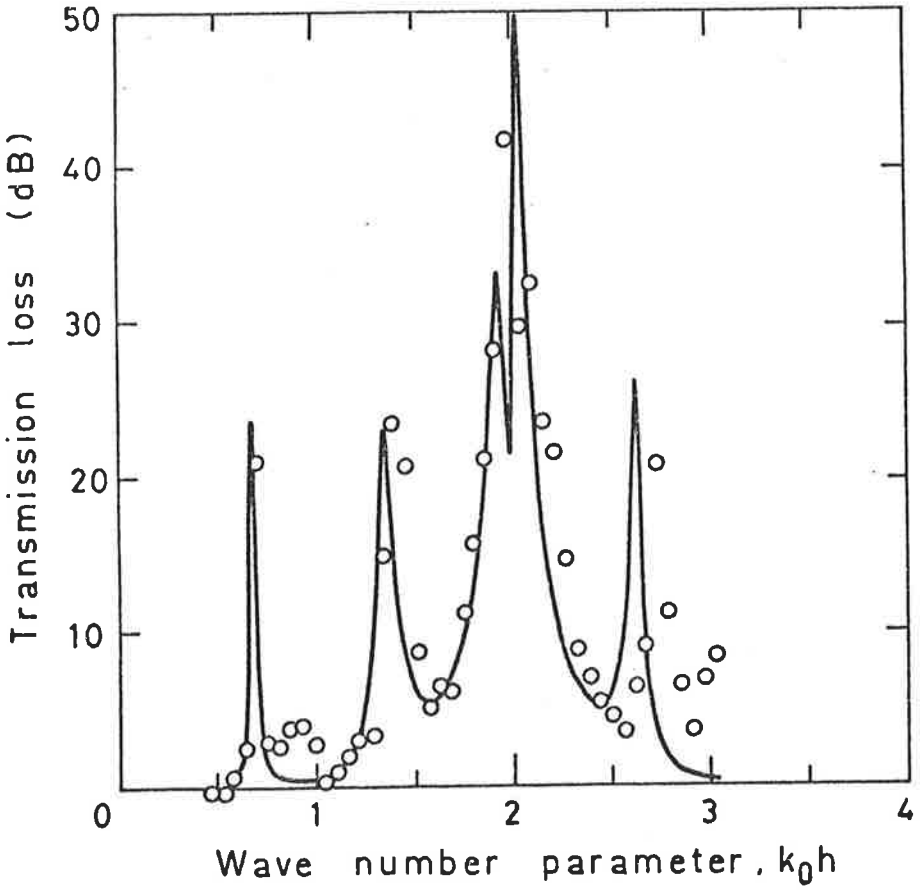

FIGURE 5.4. Transmission loss of the original attenuator. ——— , theoretical; O , experimental.

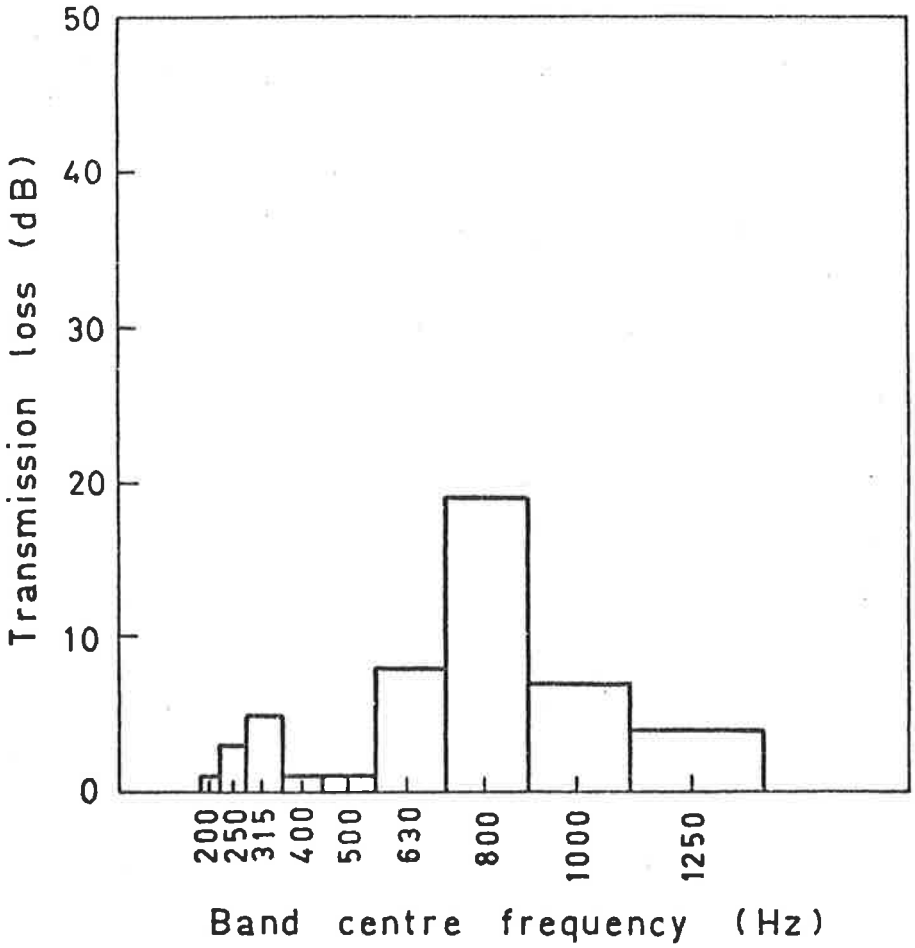

FIGURE 5.5. Experimental transmission loss of the original attenuator in 1/3 octave bands with a broad band noise source.

bend. Each series was summed until an error of less than 10^{-4} was obtained. The resulting constants for each equation were then set in a 12 x 12 complex matrix, shown in Appendix 3, and the variables of each wave (Fourier coefficients) were obtained by solving the matrix using a computer program based on Crout's rule. The predicted values of power transmission coefficient were then evaluated from the obtained coefficients by

$$\alpha_t = 1 - \left[\frac{P^r_{oo}}{P^i_{oo}}\right]^2 \qquad (5.13)$$

The theoretical values obtained for the original attenuator are shown in Figure 5.3 where sound power transmission coefficient is plotted against a nondimensional frequency parameter, $k_o h$. Experimental values are also shown in the figure for comparison.

The theoretical transmission loss is evaluated as in Chapter 4 as

$$T.L. = -10 \log (\alpha_t) \qquad (5.14)$$

where α_t is the theoretical power transmission coefficient.

5.6 DISCUSSION OF RESULTS

5.6.1 Power Transmission Coefficient

As shown in Figure 5.3, close agreement is observed between the predicted and measured frequencies at which minima in the transmission coefficient are observed, especially at lower frequencies. Slight discrepancies between the theoretical and experimental frequencies of minimum transmission coefficient are thought to be due to dimensional inaccuracies in the geometry of the attenuator affecting the mean path difference, between the two ducts. At low frequencies the wavelength of the incident sound is very much larger than the duct small scale dimensions and small discrepancies result. However, at

high frequencies ($k_o h \rightarrow 3.0$) this is no longer true and the discrepancies are larger. Another possible cause of discrepancy may have been ambient temperature fluctuation during the course of experimentation.

The magnitude of the transmission coefficient which agrees closely at low frequencies is progressively greater than predicted at increasing frequencies. Three possible reasons for this behaviour are suggested as follows:

(1) The walls of the experimental duct are not absolutely rigid as supposed by theory. In fact they were found to vibrate and radiate sound. Thus vibration through the walls acts as a flanking path to increase the apparent transmission through the attenuator (as detected by measurement of the upstream standing wave).

(2) The minima of the standing wave measured in the upstream duct becomes sharper with increasing frequency, particularly for large values of standing wave ratio n_s. Large increases or decreases in measured sound pressure level in this case were found to occur in very small changes in position of the standing wave probe. Thus the accuracy of the minima detected is limited by the size of the probe end hole (some end effect is apparent) plus small distortions in the signal causing the actual position of the minima to fluctuate slightly. This effect obviously becomes worse with increasing frequency as the minima of the standing wave becomes sharper. The detection of the maxima of the standing wave is much more accurate as it is characterized by a gradual change in sound pressure level with distance x in the duct.

(3) The duct dimensions are not exactly as described by theory.

Minimum transmission at the design frequency may be fully accounted for in terms of reflection at the bends exit plane, interface D of Figure 5.1. In fact, the theory of Chapter 3 which describes the exit plane as composed of two vibrating pistons (air) but with variable

relative phase, dependent upon the wavelength to path difference ratio describes quite well the overall transmission of the attenuator. However the presence of additional minima in the experimentally determined transmission coefficient that occur at values of $k_o h = 0.6$, 1.3, 2.6...shown in Figure 5.3 cannot be explained by considering reflection at the exit interface D alone. The additional minima are due to multi-reflections at interfaces A and D and are fully accounted for by the more exact theory presented in this chapter. The frequencies at which additional minima occur depend upon the magnitude of the path difference relative to the mean lengths of either of the ducts in the compound bend. For convenience we will take the inside mean length as the standard length for comparison. Thus the ratio of the inside duct mean length to path difference determines the frequencies of additional minima.

The following strategy is now possible. Choice of the path difference determines the design frequency while independent choice of the mean inside path length to path difference ratio determines the frequencies of additional minima. Thus for a given design frequency the ratio can be chosen to optimize the rejection characteristics of the attenuator by appropriate adjustment of the frequencies of the additional minima. Optimum performance in this particular case is taken as a ten decibel transmission loss over as wide as possible a frequency range. Figure 5.4 shows that the transmission loss of the original attenuator is characterized by a series of high rejection peaks interspaced by low rejection of sound at a number of discrete frequencies. If the peaks could be moved closer to each other, centred on the design frequency then the minima between peaks may be increased to greater or equal to ten decibels.

In practice one proceeds by keeping the path length difference

between the inside and outside ducts in the bend constant and varying their total lengths or equivalently the ratio of their lengths. The ratio of lengths of the original attenuator whose transmission coefficient is shown in Figure 5.4 is 2.00, however the optimum ratio of lengths for a crescent shaped center body with a design frequency of 844 Hz has been determined by these investigations to be 1.67. With this choice the position of the extra minima are moved closer to the design frequency and a continuous rejection band of greater than ten decibels over three quarters of an octave is achieved.

The attenuator designed for optimal attenuation characteristics has the following dimensions. Referring to Figure 5.1 its radii are R_1 = 0.184 meters, R_2 = 0.248 meters, R_3 = 0.006 meters and R_4 = 0.07 meters.

The theoretical and experimentally measured transmission coefficient values of this attenuator are shown in Figure 5.6. It can be seen that the extra minima have indeed moved closer to the design frequency than those shown in Figure 5.3. In the model attenuator a rejection band of 430 Hz centered at a design frequency of 844 Hz was achieved.

Closer agreement is obtained in the position of theoretical and experimentally measured minima produced by the optimum attenuator. This is due to more accurate machining of components in the attenuator thus achieving the correct mean path lengths.

5.6.2 Transmission Loss

Theoretical and experimentally measured values of transmission loss for the optimum attenuator are shown in Figure 5.7 for a pure tone, while the transmission loss of the optimum attenuator with broad band noise source is shown in Figure 5.8.

At the design frequency the rejection of sound is very

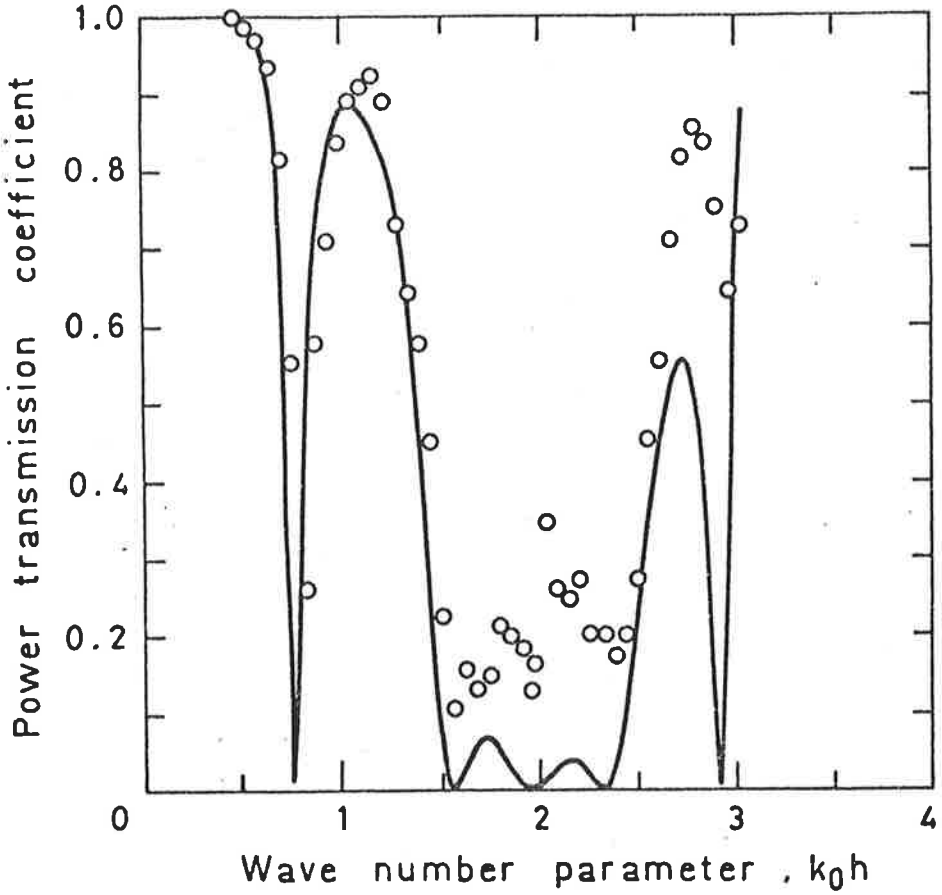

FIGURE 5.6. Power transmission coefficient of the optimum attenuator. ——— , theoretical; O , experimental.

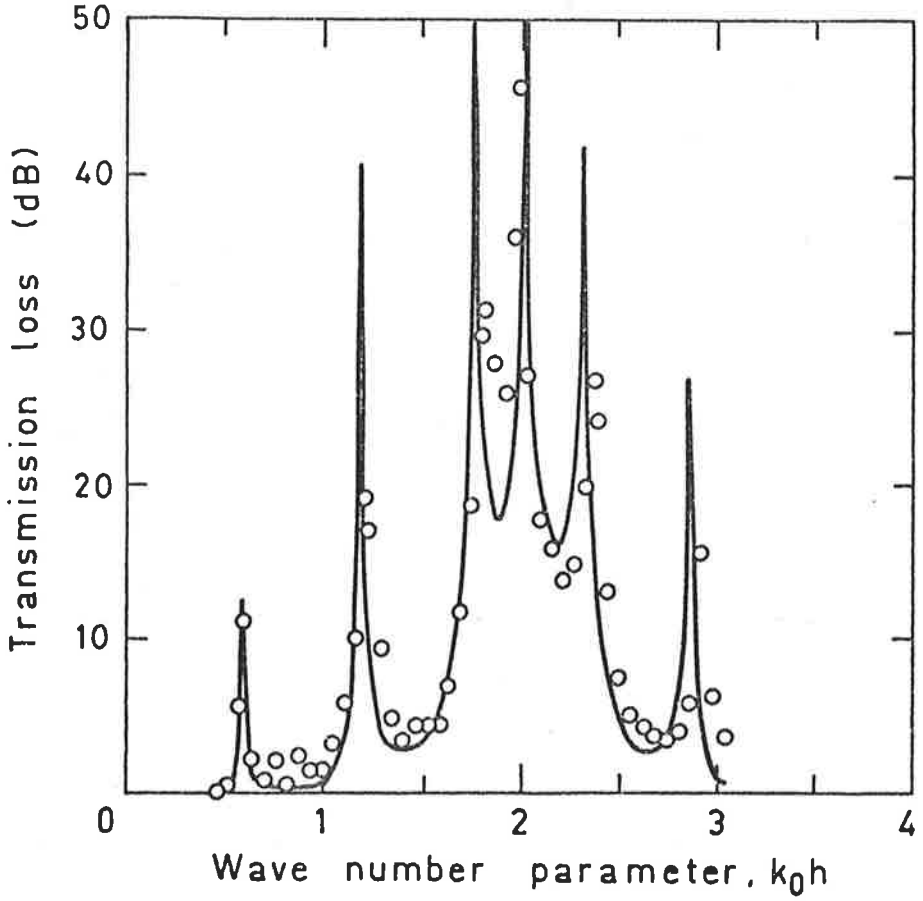

FIGURE 5.7. Transmission loss of the optimum attenuator. ——— , theoretical; O , experimental.

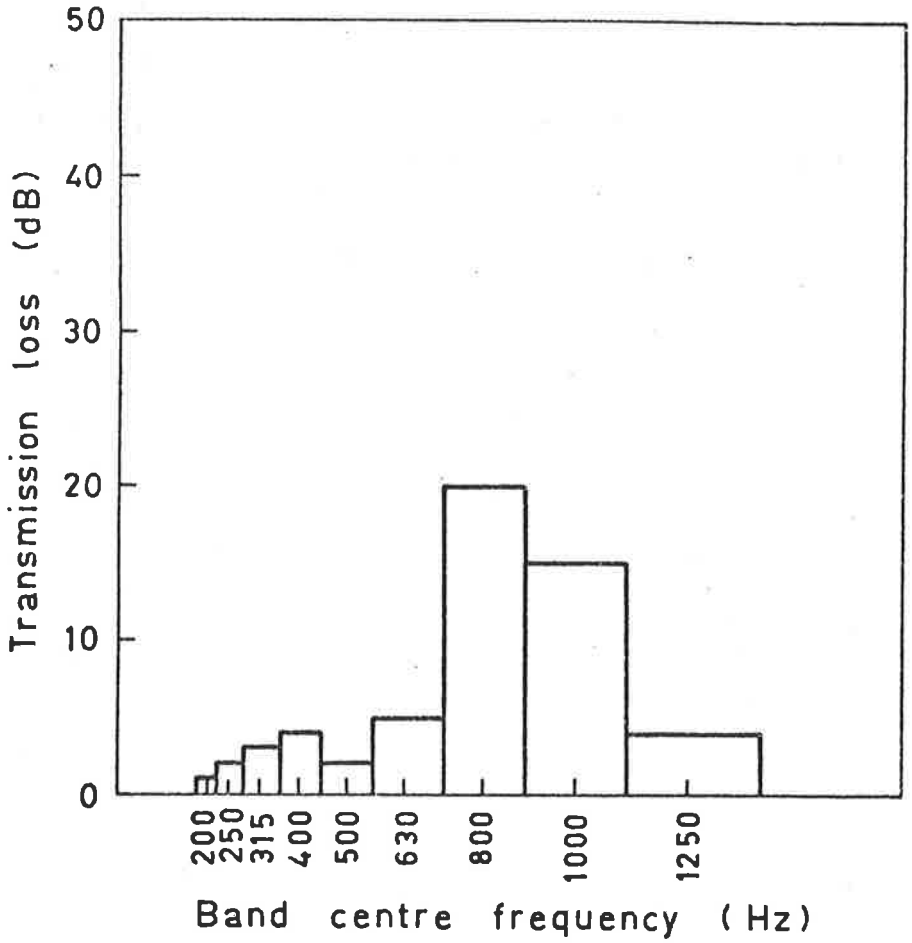

FIGURE 5.8. Experimental transmission loss of the optimum attenuator in 1/3 octave bands with a broad band noise source.

nearly complete so that the transmission loss in a narrow frequency band about the design frequency depends upon the bandwidth. The narrower the bandwidth the greater the transmission loss. The peaks shown in Figures 5.4 and 5.7 approach infinity (dB) for a narrowing frequency band. In the analysis used to derive the theoretical transmission losses of Figure 5.4 and 5.7 a bandwidth of 25 Hz has been used but as pure tones were used for measurement of the transmission loss, occasionally very much greater rejection levels than predicted were observed. Subsequent investigations with narrower theoretical bandwidth increments showed that these high anomolous values could always be accounted for on the basis of the analysis presented here.

Small discrepancies between the theoretical predictions and the experimental measurements are thought to be due to small dimensional inaccuracies in the models as previously discussed. However, much closer agreement is obtained between the actual magnitude of the theoretical transmission loss and that measured experimentally, than that shown by the transmission coefficients in Figures 5.3 and 5.6. Thus the attenuator performs far better than shown by measuring the standing wave alone. For example, the power transmission coefficient of the optimum attenuator was measured to be 0.13 at the design frequency. Interpolating the experimental transmission loss from this value, using equation (5.14) one obtains an interpolated experimental transmission loss of 15.6 dB. However the actually measured transmission loss at the design frequency of the optimum attenuator is seen from Figure 5.7 to be 45 dB. This result tends to support reason number (2) presented previously to explain the discrepancies between the magnitude of experimental and theoretical transmission coefficient. Hence measurement of the

standing wave alone is a poor indication of the performance of an attenuator, unless special precautions are undertaken to increase the sensitivity of the microphone probe with distance and increase the stability of the acoustic signal. This especially applies at higher frequencies.

Figure 5.7 shows that the optimum attenuator achieves a high transmission loss at a number of characteristic frequencies corresponding to the natural reflections between interfaces A and D of the attenuator. At these frequencies, a pure tone would be virtually completely reflected. As well as this a continuous rejection band of ten decibels over three quarters of an octave is obtained by careful choice of the attenuator dimensions as discussed previously. This result should be compared to the much narrower operating band of the original attenuator.

The transmission losses measured for the original and optimum attenuators with a broad band noise source, shown in Figures 5.5 and 5.8, also indicates the wider operating band of the optimum attenuator. For the optimum attenuator greater than ten decibels transmission loss is obtained over two one-third octave bands. It is also interesting to note from these figures that by superimposing the corresponding pure tone transmission loss the broad band transmission loss is seen to be approximately a logarithmic sum of the pure tone transmission loss, as one would expect. The figures also show that the attenuator substantially reduces broad band noise.

5.6.3 Curved Duct Radial Pressure Distribution

It is appropriate to the understanding of the performance of the attenuator to introduce the concept of curved duct radial pressure distribution. Values of theoretical and experimentally measured curved duct pressure amplitude distribution for a duct of

aspect ratio a = 2.25, which corresponds to curved section 3 of the original attenuator have been discussed in Chapter 2 and are shown in Figure 2.5. It can be seen that at low frequencies, corresponding to values of the dimensionless frequency $k_o h \leq 1.5$ acoustic waves propagate with only a small variation in pressure amplitude across the duct for a bend of aspect ratio a = 2.25. However as the frequency increases, the variation in sound pressure amplitude across the duct becomes more marked. If one had assumed plane wave propagation in the attenuator at all frequencies (below the cut-off frequency of the (1,0) mode) it would appear that this assumption would hold at lower frequencies but be inaccurate at higher frequencies due to non plane propagation in the curved sections. However later work has shown this not to be the case. The actual variation in pressure or velocity amplitude of the (0,0) mode has little effect on the impedance of the curved duct. The effect the curved duct *does* have is to change the effective path length of the wave slightly as discussed by Cummings (1974). For the frequencies and aspect ratios used here this effect is considered marginal.

5.7 GENERAL DESIGN GUIDE OF ATTENUATOR

The design guide proposed is intended to be approximate and apply only for low flow velocities in the duct system. Flow effects at higher velocities will be considered in the next chapter. The basic assumption is that the acoustic waves propagate as plane waves with phases determined approximately by the mean path length of the duct in all sections of the attenuator. In this case, any shape as well as the crescent shaped center body may be used to give the required dimensions.

The basic design steps are:

(1) Calculate the path difference necessary to give the required deisgn frequency.

(2) Optimize the bandwidth by careful choice of duct dimensions using a trial and error method based on this analysis.*

(3) Adjust the shape of the center body to give the combination of most compact shape required with the least sharp bends to give the lowest pressure drop.

* This step may be changed if for instance it is desired to cancel fan harmonics, then the frequencies at which maxima occur may be adjusted by choice of dimensions to correspond to the frequencies of the fan harmonics.

5.8 SUMMARY

An attenuator with an inherently low pressure drop coefficient which may be installed in a duct bend has been described. The attenuator when optimally designed is capable of providing a transmission loss of greater than ten decibels over a frequency range of three quarters of an octave in the very low frequency range. Optimization of design is facilitated by a theoretical description that has provided good agreement between theory and experiment.

The attenuator also provides large transmission losses at a series of discrete frequencies all below the cut-off frequency for the first cross mode in the duct. The presence of these discrete frequencies is explained by reflection of incident sound at the exit and entrance of the attenuator. Their relative distribution is determined by the geometry of the attenuator.

It is found that measurement of the standing wave alone gives a poor indication of the performance of the attenuator due to difficulty in measuring accurately the minima of the generated standing wave when rejection is high.

CHAPTER 6

THE EFFECT OF FLOW ON THE PERFORMANCE OF A REACTIVE ACOUSTIC ATTENUATOR

6.1 INTRODUCTION

In Chapter 5 a reactive acoustic attenuator was described which combined high transmission loss with low pressure drop. Although the latter chapter established that high levels of attenuation can be combined with good aerodynamic properties, it did not consider convection of the propagating medium.

Previous investigations into the effect of flow in the attenuation obtained in lined ducts and ducts with side branch resonators have shown that flow can significantly alter the performance of an attenuator. Mechel (1962) and Kurze and Allen (1971) found that flow in the direction of propagation of sound in a lined duct reduced the attenuation obtained while flow in the direction opposite to the direction of propagation of sound increased the attenuation. Theory shows that to a first approximation the effect may be accounted for by an increase or decrease in wave speed due to convection.

Lambert (1956) calculated theoretically the insertion loss of a side branch resonator as a function of Mach number in the main duct and found the theoretical insertion loss characteristics sensitive to flow especially at frequencies near resonance. He found that small changes in Mach number could considerably alter the insertion loss obtained near resonance and showed this to be due to flow induced changes in impedance at the various junctions. It is

also interesting to note that Lambert could not confirm these results experimentally due to noise generated by the air flow exciting the air column in the quarter wave tube. This result points out that a simplified approach to the problem of fluid convection may lead to misleading theoretical results.

In this chapter the effect of Mach number on the performance of the attenuator discussed previously in Chapter 5 is considered. The effects of flow have been previously discussed by Fuller and Bies (1978 C) and (1978 D). As the performance of the attenuator is based upon impedance mismatches generated by differences in arrival times of propagating waves, and is thus critically dependent upon wave-number, it is expected that flow will significantly affect the operating characteristics of the device.

Equations recently developed by conformal mapping techniques described in Chapter 2 which describe low frequency sound propagation in the curved ducts with flow are used to analyse sound propagation in the curved parts of the attenuator. Equations for sound propagation in straight ducts with flow are used to describe the straight parts of the attenuator. The analysis closely follows the procedure of Chapter 5 except that flow of the propagating medium is considered. As described in Chapter 2, flow is expected to modify the energy as well as wavenumber dependent properties of the attenuator.

Four parameters, pressure reflection coefficient, power reflection coefficient, power transmission coefficient and transmission loss are investigated theoretically and experimentally for varying Mach numbers. Good agreement is obtained and small discrepancies between prediction and measurement are discussed. These four parameters

are all necessary to show the varied effect of flow on the operating characteristics of the attenuator. The two cases of sound propagating with and against flow through the attenuator are considered. By the nature of the device the analysis is necessarily limited to frequencies less than the cutoff frequency of the (1,0) mode in the upstream incident duct at the highest value of Mach number considered. The fluid flow is assumed to be uniform, homogenous and irrotational and due to practical experimental considerations is limited to values of Mach number less than 0.1. Convection of the propagating medium is found to alter the performance of the attenuator significantly due to both wavenumber and energy propagation effects.

6.2 ANALYSIS

The equations to be used in the analysis for sound propagation in straight ducts and curved ducts with flow have been previously discussed in Chapters 1 and 2. It is worth noting at this stage that the modes considered in each section will be exactly as the no-flow case i.e. one mode, the (0,0), in each sub-section of the attenuator and two modes in the incident and exit duct of the attenuator. Thus the curved duct equations will be limited to those describing the (0,0) mode. If one considers equations (2.86) and (2.89), which described sound propagation in curved ducts with mean flow by conformal mapping techniques, in relation to a curved duct of angle θ it can be shown that these equations for downstream propagation of sound reduce to

$$p^c = C_{oo}\exp[k_o R_m \frac{X}{R_m} \frac{1}{(1+M)}] \tag{6.1}$$

$$u_\theta = C_{oo}k_o \frac{1}{\omega\rho_o(1+M)} \exp[k_o R_m \frac{X}{R_m} \frac{1}{(1+M)}] \tag{6.2}$$

In both these equations the harmonic function exp[-iωt] has been omitted, R_m (=X/θ) is the mean radius of the curved section and X is the mean centerline distance of the curved duct. Thus in the case of only the (0,0) mode, equations (6.1) and (6.2) show that one is effectively considering the curved duct section as an equivalent straight duct. Hence by considering only the exit and inlet interfaces of the attenuator and applying straight duct equations with flow and with relative phase determined by the mean centerline distance one would arrive at exactly the same answer as the analysis proposed here. However use of the conformal mapping equations has the advantage of enabling the analysis to be extended to include higher non-propagating modes generated at the interfaces of straight and curved ducts with flow, if a greater accuracy of the analytical result is required. Due to the low frequencies and gradual bends considered, the small change in radial position from the mean radius at which the angular wavespeed equals the phase speed of the (0,0) mode in the straight duct is thought to have only a marginal effect on the analysis.

The method of analysis follows very closely that outlined in Chapter 5 except that equations describing sound propagation in ducts with convection of the propagating medium are used. The procedure is to: (1) divide the attenuator into sections with relative coordinate systems; (2) match pressure and acoustic velocities of propagating and evanescent waves across interfaces of each section using continuity conditions; (3) obtain the required Fourier coefficients for determination of transmission coefficients and transmission loss by using the orthognality property of the cos(mπy/h) function.

Condition (2) implies continuity of pressure and particle velocity at each interface. In the case of flow of the propagating

medium, the particle velocity must include the convection term normally ignored in the no-flow case. As both wave systems on either side of a particular interface are travelling in a medium convecting at the same velocity vector, then this continuity condition is correct. However for the case of a wave striking a boundary between two fluids moving at different velocities then continuity of particle displacement rather than velocity must be used (Ingard (1959)).

As described by equations (1.63) and (1.64) of Chapter 1 the particle velocities are related to the acoustic pressure by

$$u_x^d = \frac{p}{\rho_o \omega} \xi_{mo}^d \tag{6.3}$$

and

$$u_x^u = \frac{p}{\rho_o \omega} \xi_{mo}^u \tag{6.4}$$

where $\xi_{mo}^d = k_o(\varepsilon - M)/(1-\varepsilon M)$ and $\xi_{mo}^u = k_o(\varepsilon + M)/(1+\varepsilon M)$. These symbols will be used in the following analysis. For the (0,0) mode $\xi^u = \xi^d = k_o$.

The arrangement of the attenuator, with coordinate systems and acoustic waves considered, is shown in Figure 6.1. As mentioned previously the number of modes considered will be exactly as the no-flow case. Thus only the (0,0) mode is shown in the sub-sections of the attenuator. Two variations of the attenuator shown in Figure 6.1 will be investigated. These are the optimum attenuator with dimensions $R_1 = 0.184$ meters, $R_2 = 0.284$ meters, $R_3 = 0.006$ meters and $R_4 = 0.076$ meters and the original attenuator with dimensions $R_1 = 0.229$ meters, $R_2 = 0.292$ meters, $R_3 = 0.051$ meters and $R_4 = 0.114$ meters. The attenuator is acoustically described by dividing it into sections with suitable coordinate systems as shown and considering sound propagation and reflection of travelling waves in each section. As there is no discontinuity in the z direction, a

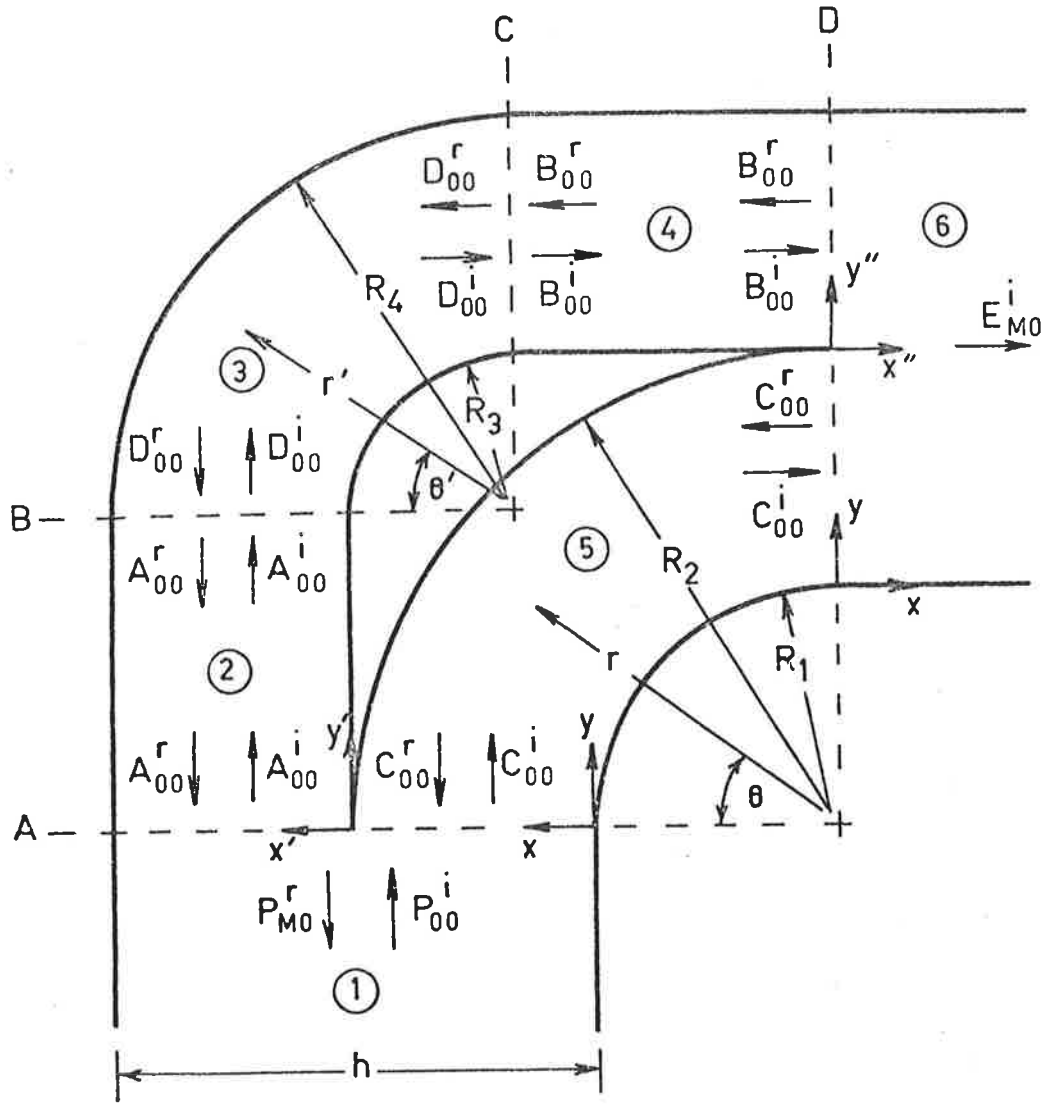

FIGURE 6.1. Arrangement of the attenuator with co-ordinate systems and modes considered in the analysis.

two dimensional coordinate system is used.

Since the frequencies considered are well below the cut-off frequency of the (1,0) mode in the curved sections only the (0,0) mode is considered in these parts of the attenuator. Evanescent curved duct modes generated at the interfaces are also ignored. This simplification gave an accurate result in the no-flow case of Chapter 5 and is used again here. As explained in Chapter 5 since the number of modes considered in the curved sections is limited to one, for a solution to be obtained at interfaces B and C then the number of modes considered in straight subsections 2 and 4 will also be one each. Similarly as in Chapter 5 continuity of axial and tangential particle at the interfaces is postulated. This approximation gave an accurate result in the no-flow case and will be used again here.

Hence at interface A, where $x = 0$, $\theta = 0$, $x' = 0$ continuity of acoustic pressure provides equations (6.5) and (6.6)

$$P^i_{oo} \exp[i(\omega t - k^d_{oo}x)] + \sum_{m=0}^{\infty} P^r_{mo} \cos[(m\pi/h)y] \exp[i(\omega t + k^u_{mo}x)]$$

$$= C^i_{oo} \exp[i(\omega t - \nu^d_o\theta)] + C^r_{oo} \exp[i(\omega t + \nu^u_o\theta)] \qquad (6.5)$$

$$\text{for } 0 < y \leq h/2$$

and $$P^i_{oo} \exp[i(\omega t - k^d_{oo}x)] + \sum_{m=0}^{\infty} P^r_{mo} \cos[(m\pi/h)y] \exp[i(\omega t + k^u_{mo}x)]$$

$$= A^i_{oo} \exp[i(\omega t - k^d_{oo}x')] + A^r_{oo} \exp[i(\omega t - k^u_{oo}x')] \qquad (6.6)$$

$$\text{for } h/2 < y \leq h$$

In equations (6.5) and (6.6) and equations to follow superscript i and r denote incident and reflected wave amplitudes in the attenuator respectively, while superscripts d and u denote down-stream and upstream propagation of sound respectively.

The Fourier coefficients are obtained by multiplying both sides of the continuity equations by $\cos[(m\pi/h)y]$ and integrating over the interface surface with respect to y, y' or r. The orthognality property of the latter function allows determination of the P^r_{mo} and E^i_{mo} coefficients for m = 0, 1, 2... as given in equations (6.7) and (6.8).

m = 0,

$$P^i_{oo}h + P^r_{oo}h = C^i_{oo}h/2 + C^r_{oo}h/2 + A^i_{oo}h/2 + A^r_{oo}h/2 \qquad (6.7)$$

$m \neq 0$,

$$P^r_{mo}h/2 = C^i_{oo}\left(\frac{h}{2m\pi}\right)[1 - (-1)^m] + C^r_{oo}\left(\frac{h}{2m\pi}\right)[1 - (-1)^m]$$

$$- A^i_{oo}\left(\frac{h}{2m\pi}\right)[1 - (-1)^m] - A^r_{oo}\left(\frac{h}{2m\pi}\right)[1 - (-1)^m] \qquad (6.8)$$

Similarly continuity of tangential particle velocity at A provides

m = 0,

$$P^i_{oo}k_{oo}h - P^r_{oo}k_{oo}h = C^i_{oo}k_{oo}(h/2) - C^r_{oo}k_{oo}(h/2)$$

$$+ A^i_{oo}k_{oo}(h/2) - A^r_{oo}k_{oo}(h/2) \qquad (6.9)$$

$m \neq 0$,

$$-P^r_{mo}\xi^u_{mo}(h/2) = C^i_{oo}k_{oo}\left(\frac{h}{2m\pi}\right)[1 - (-1)^m] - C^r_{oo}k_{oo}\left(\frac{h}{2m\pi}\right)[1 - (-1)^m]$$

$$- A^i_{oo}k_{oo}\left(\frac{h}{2m\pi}\right)[1 - (-1)^m] + A^r_{oo}k_{oo}\left(\frac{h}{2m\pi}\right)[1 - (-1)^m]$$

(6.10)

The equations derived for continuity of pressure and axial particle velocity at interfaces B, C and D are given in Appendix 2. It can be seen that these equations consist of an infinite set with an infinite number of unknowns. In order to proceed we shall truncate the series so that the number of unknowns equals the number of

of equations. As already stated the number of modes considered in Sections 2, 3, 4 and 5 are limited to one each. Thus to solve the problem two modes must be considered in Sections 1 and 6, as described in the previous chapter. The two modes considered in Sections 1 and 6 are necessary to provide continuity across interfaces A and D when the propagating waves in the minor ducts are out of phase.

6.3 EXPERIMENTAL APPARATUS AND METHOD

The performance of the attenuator with flow was investigated with the arrangement shown in Figure 6.2. The duct system is basically the apparatus used for previous investigations into sound propagation in ducts, having a 0.0635 x 0.127 meter cross section fabricated in removable sections from 0.0254 meter thick wood. A centrifugal fan driven by a variable speed D.C. motor provides air flow through the duct system at different Mach numbers. Flow velocities were measured midstream using a pitot-static tube positioned as in Figure 6.2. Due to flow separation in the attenuator it was not thought necessary to measure the flow velocity using a more accurate method than at midstream. At the maximum rating of the motor a flow rate of $M = 0.08$ was measured in the upstream duct. A muffler was positioned downstream of the fan to reduce fan generated harmonics and attenuate negative travelling waves.

For measurements of sound propagating with flow the sound source was positioned 1.7 meters from the entrance to the attenuator. To eliminate reflections from the exit plane of the straight duct section, the downstream duct was anechoically terminated. For measurements of sound propagating against flow the anechoic termination

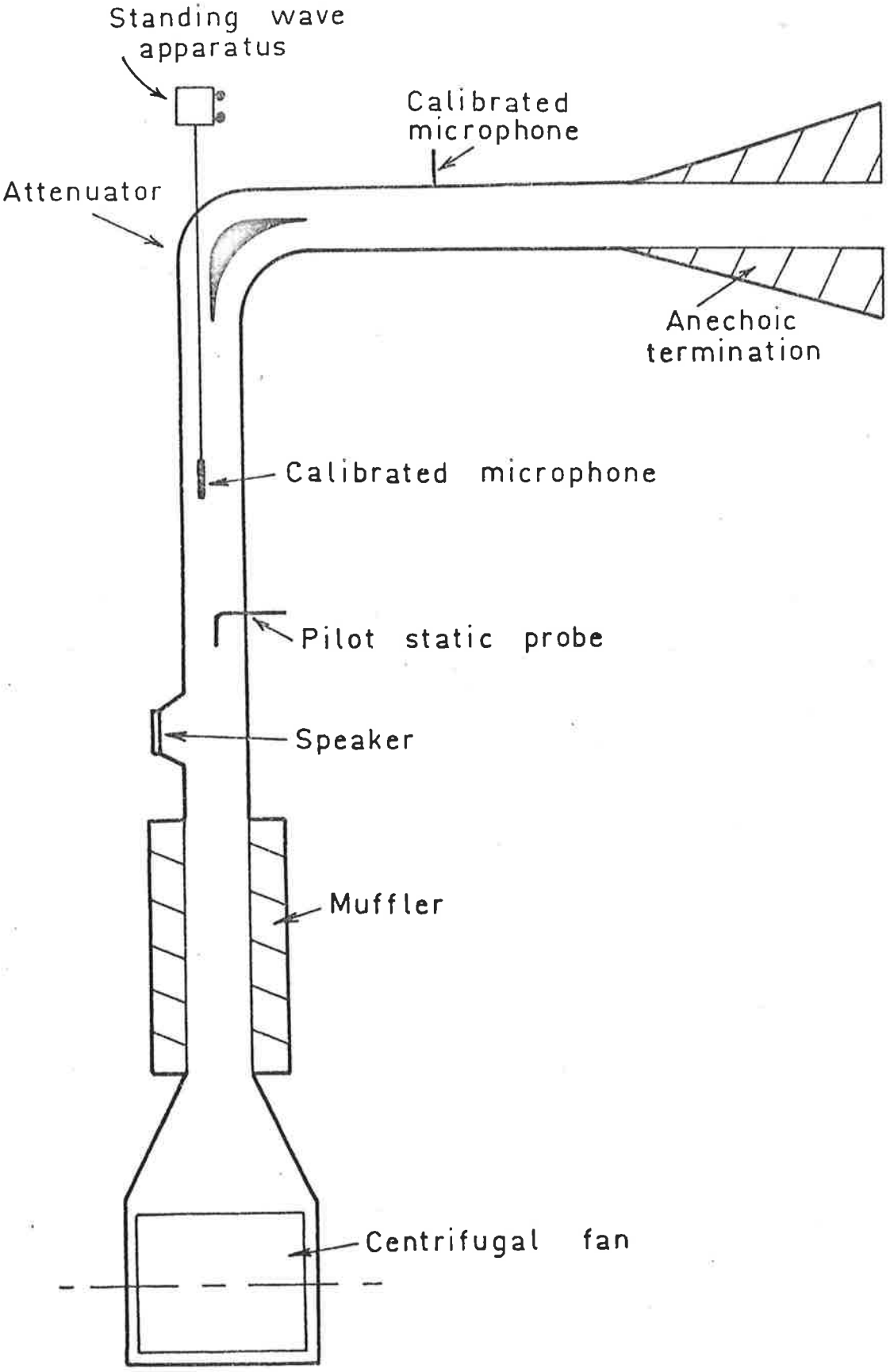

FIGURE 6.2. Arrangement of the experimental apparatus.

was removed and the sound source positioned 1.7 meters downstream. In this case the fan muffler acts as an anechoic termination to waves leaving the attenuator. The experimental apparatus arranged for measurement of the upstream case is shown in Plate 3.

A pure tone was used as the acoustic signal and when measured with a Brüel and Kjaer Heterodyne Analyser with a 3.16 Hz bandwidth provided a signal to noise ratio greater than 50 dB at maximum flow. A large signal to noise ratio is necessary to detect maxima of transmission loss. The frequency range investigated was from 200 to 1200 Hz which is less than the evanescent cut-off frequency of the (1,0) mode at M = 0.3. Four parameters were measured which were pressure reflection coefficient, power reflection and transmission coefficients and transmission loss.

The pressure reflection coefficient defined as the ratio of the reflected pressure amplitude to the incident pressure amplitude was obtained by measuring the acoustic standing wave in the incident duct. As discussed by Alfredson (1970) it is possible with mean downstream flow to measure a pressure reflection coefficient of greater than unity. In this case the usual standing wave theory (Beranek (1950)) is modified to keep the nett energy flux in the correct direction.

Thus for the reflection coefficient R greater than unity, the standing wave ratio n_s is given by

$$n_s = (1 + R)/(R - 1) \tag{6.11}$$

and for R less than unity

$$n_s = (1 + R)/(1 - R) \tag{6.12}$$

Whether R is greater or less than unity can be determined by observing the minima of the standing waves. If R > 1 the minima

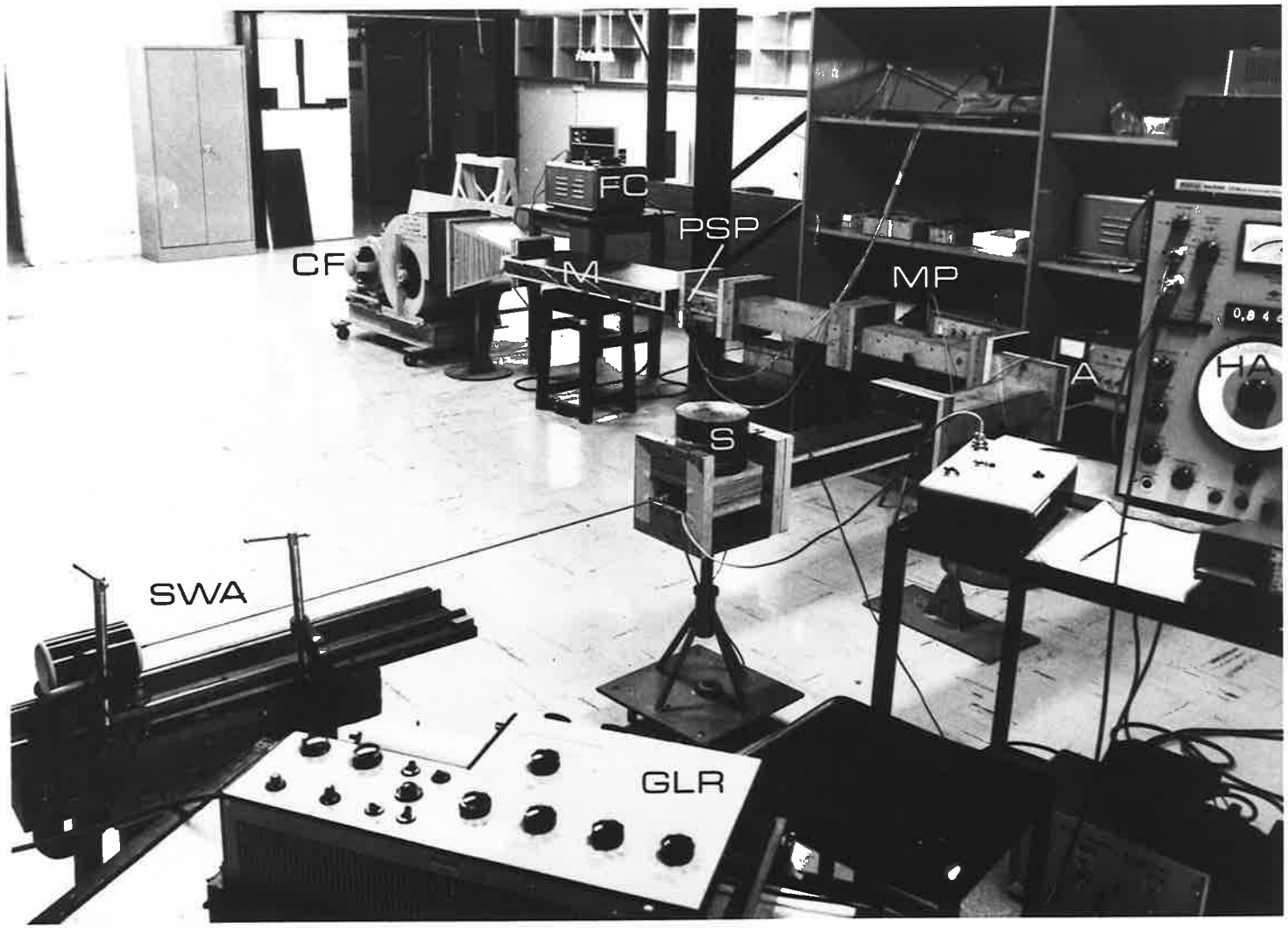

PLATE 3. The experimental apparatus for upstream propagation of sound, (SWA) standing wave apparatus, (S) speaker, (A) attenuator, (HA) heterodyne analyser, (GLR) graphic level recorder, (MP) microphone, (PSP) pitot static probe, (M) muffler, (CF) centrifugal fan, (FC) fan control.

will *decrease* as the probe moves towards the source and equation (6.11) must be used to determine R. If $R < 1$ the minima will *increase* as the probe moves towards the source and equation (6.12) must be used.

Values of experimental pressure reflection coefficient for the optimum attenuator are plotted in Figures 6.3(a), 6.3(b) and 6.3(c) for both upstream and downstream propagation of sound for flow speeds of M = 0, 0.04 and 0.08 respectively.

The experimental power reflection and transmission coefficient were determined from measured values of pressure reflection coefficient. In the no-flow case the power reflection coefficient is simply the square of the pressure reflection coefficient. However with mean flow as discussed previously the power reflection and transmission coefficients are related for both upstream and downstream cases to the pressure reflection coefficient by

$$\alpha_r^d = R^2\left(\frac{1-M}{1+M}\right)^2 \tag{6.13}$$

$$\alpha_r^u = R^2\left(\frac{1+M}{1-M}\right)^2 \tag{6.14}$$

and

$$\alpha_t = 1 - \alpha_r \tag{6.15}$$

Values of experimental power reflection coefficient for the optimum attenuator are plotted in Figures 6.4(a), 6.4(b) and 6.4(c) for M = 0, 0.04 and 0.08 and values of experimental power transmission coefficient are plotted in Figures 6.5(a), 6.5(b) and 6.5(c) for the same flow conditions.

The transmission loss was measured as in the no-flow case

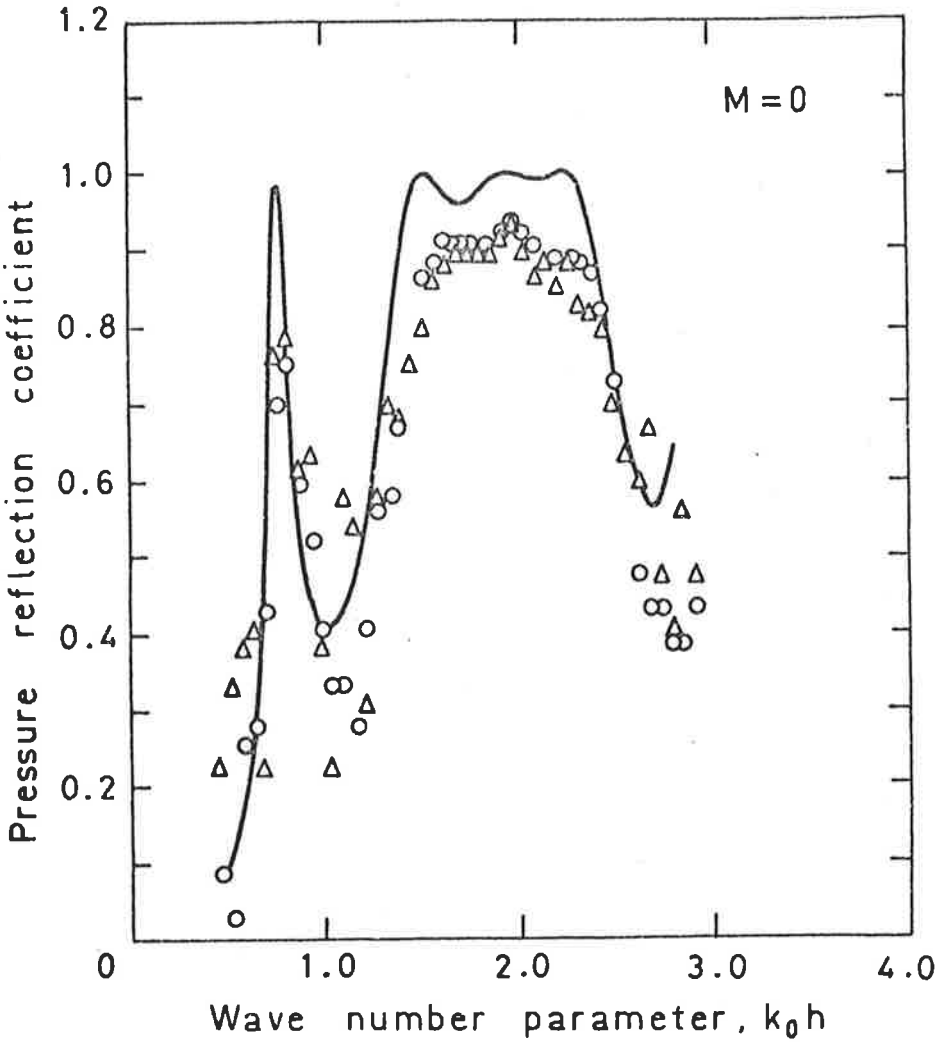

FIGURE 6.3(A). Pressure reflection coefficient of the optimum attenuator with flow. M = 0. ———— , theoretical curve for downstream propagation of sound; — — — , theoretical curve for upstream propagation; O , experimental values for downstream propagation; Δ , experimental values for upstream propagation.

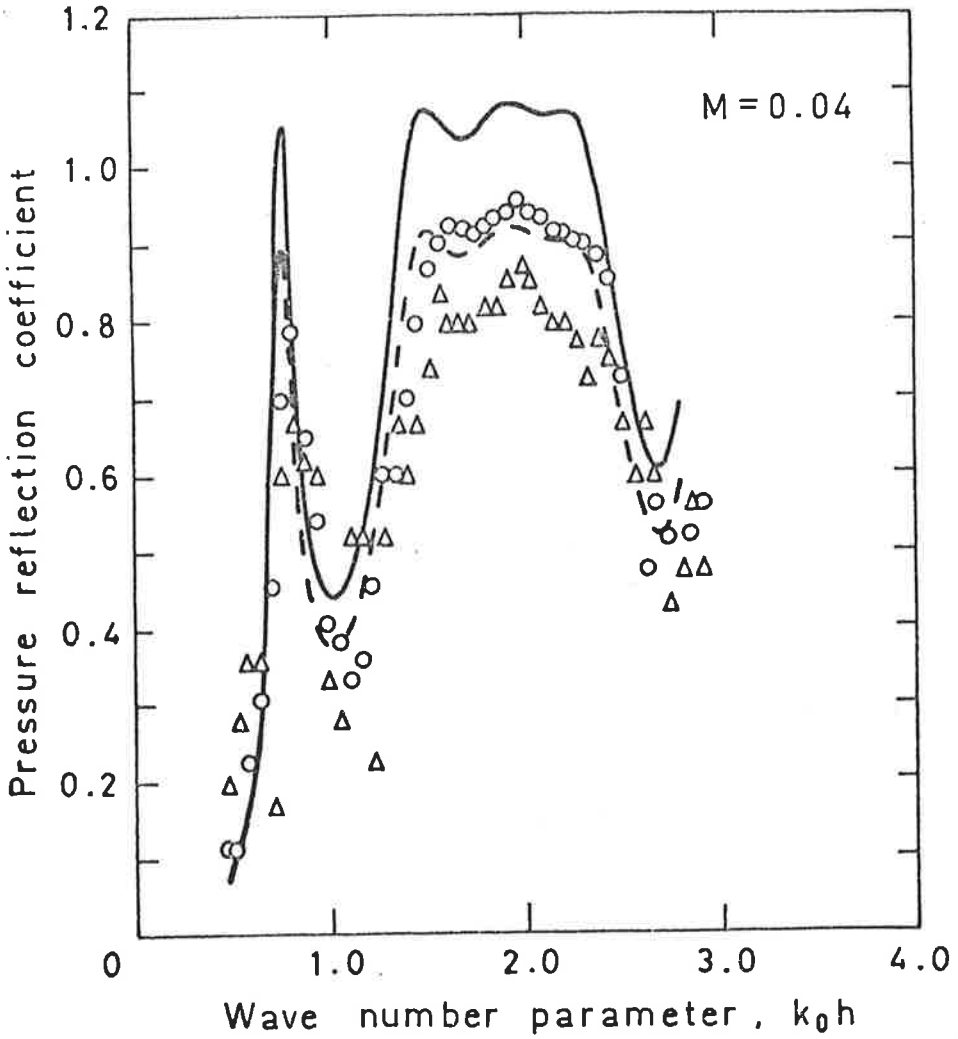

FIGURE 6.3 (B). M = 0.04.

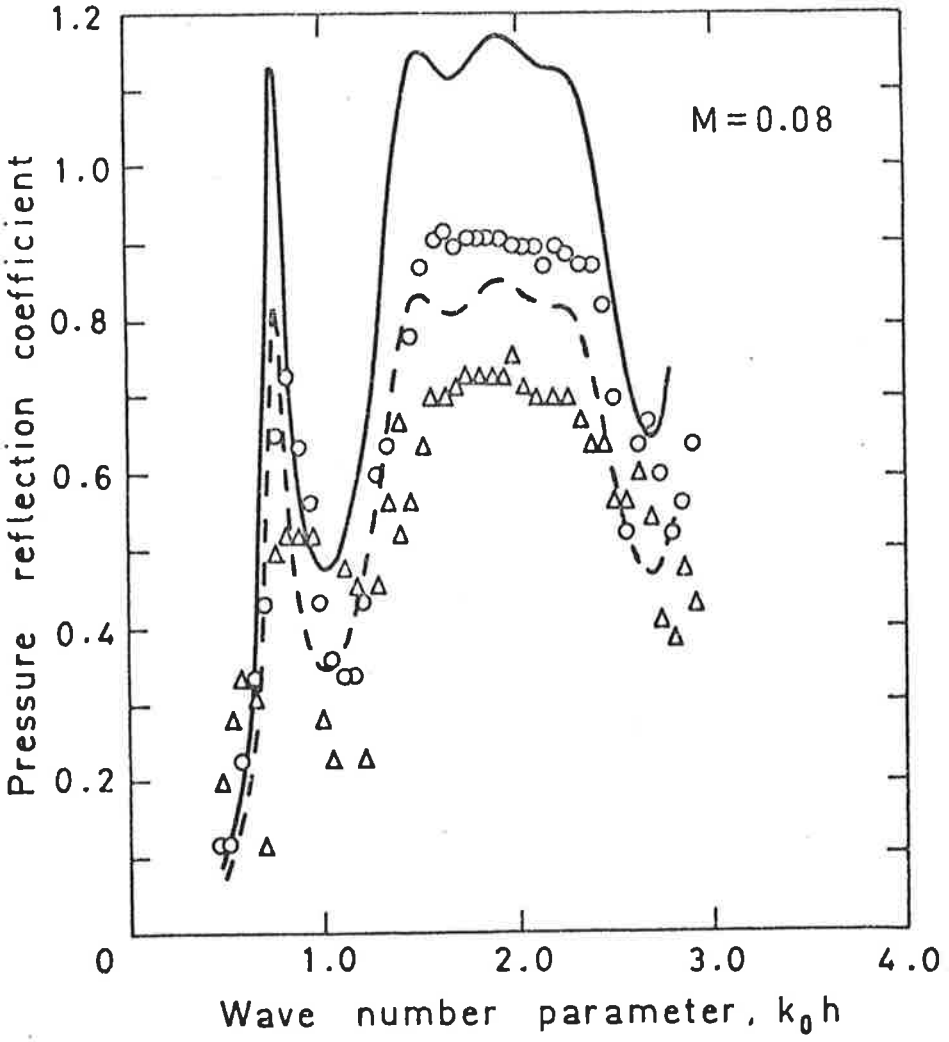

FIGURE 6.3 (c). M = 0.08.

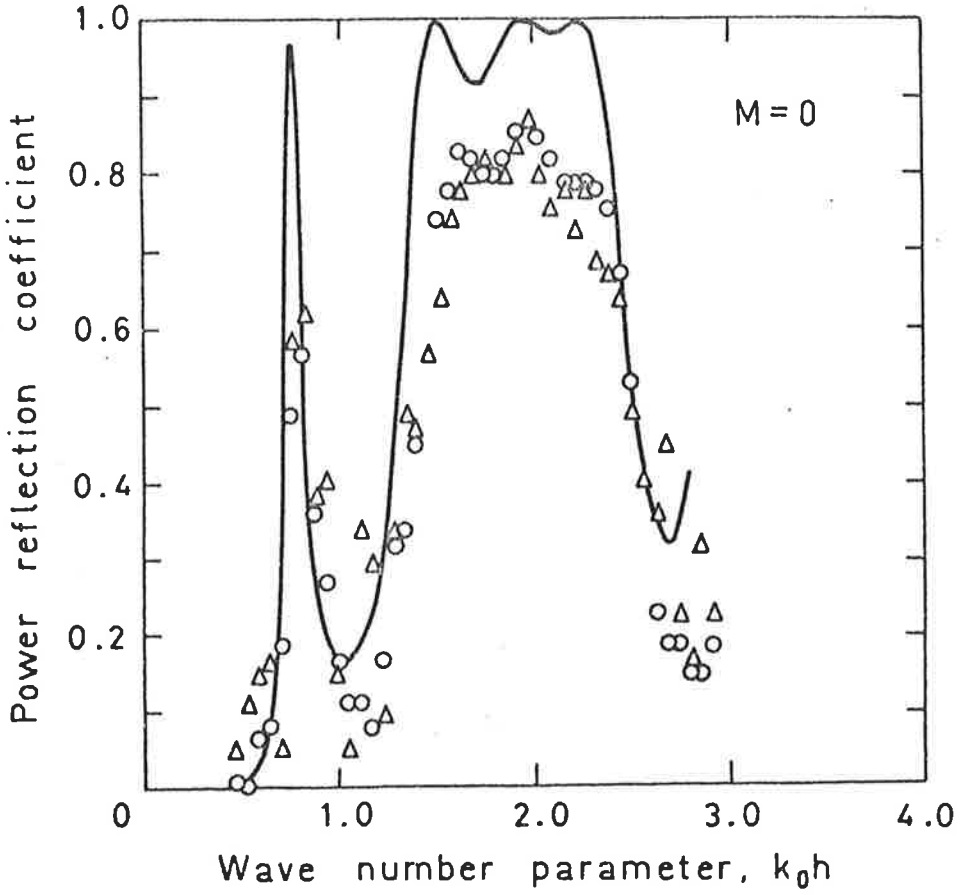

FIGURE 6.4. (A). Power reflection coefficient of the optimum attenuator with flow. M = 0. ——— , theoretical curve; O , experimental values for downstream propagation of sound; Δ , experimental values for upstream propagation.

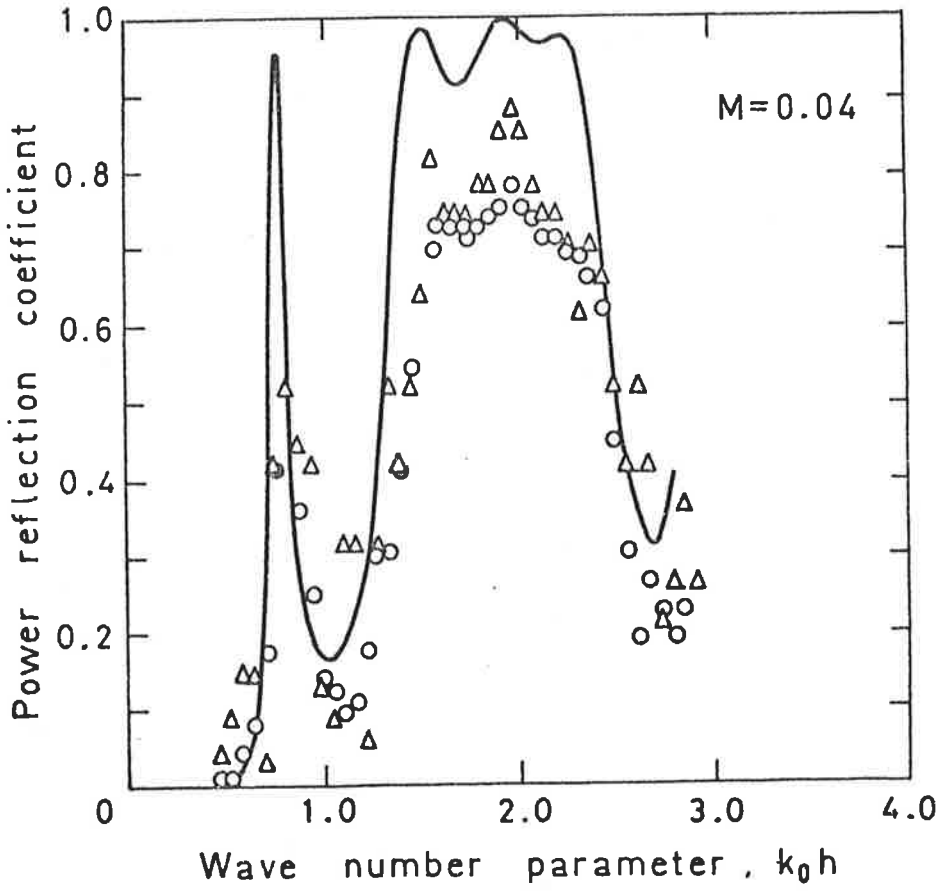

FIGURE 6.4 (B). M = 0.04.

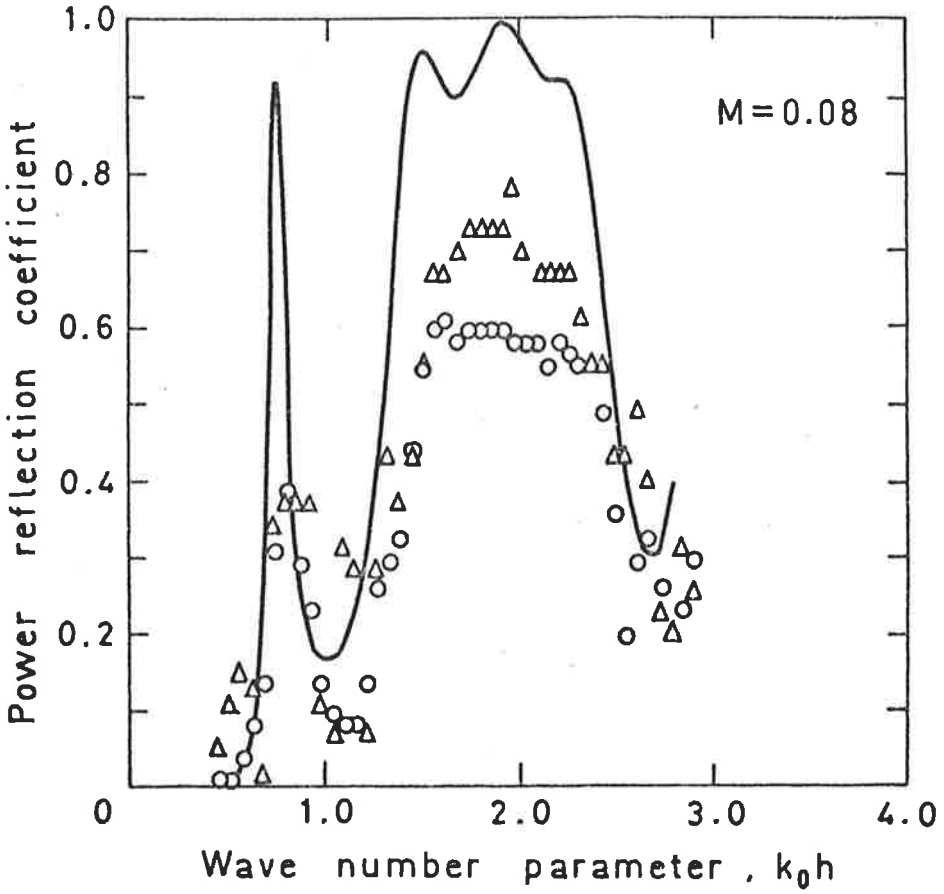

FIGURE 6.4 (c). M = 0.08.

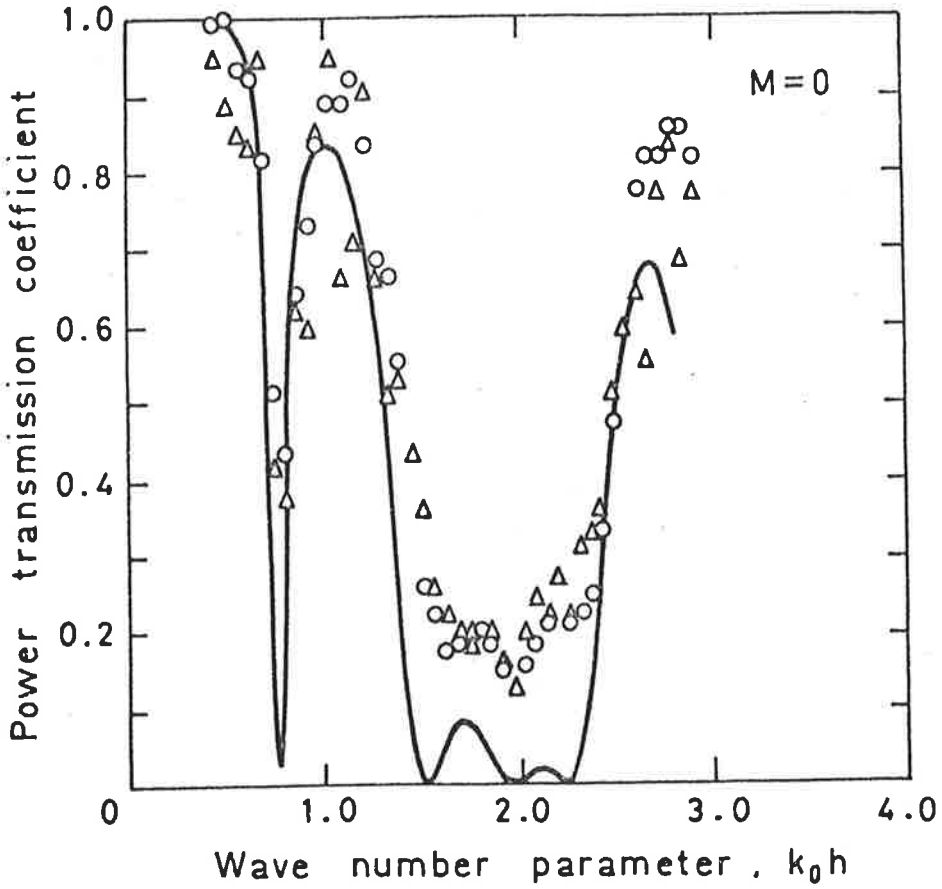

FIGURE 6.5 (A). Power transmission coefficient of the optimum attenuator with flow. M = 0. ——— , theoretical curve; O , experimental values for downstream propagation of sound; Δ , experimental values for upstream propagation.

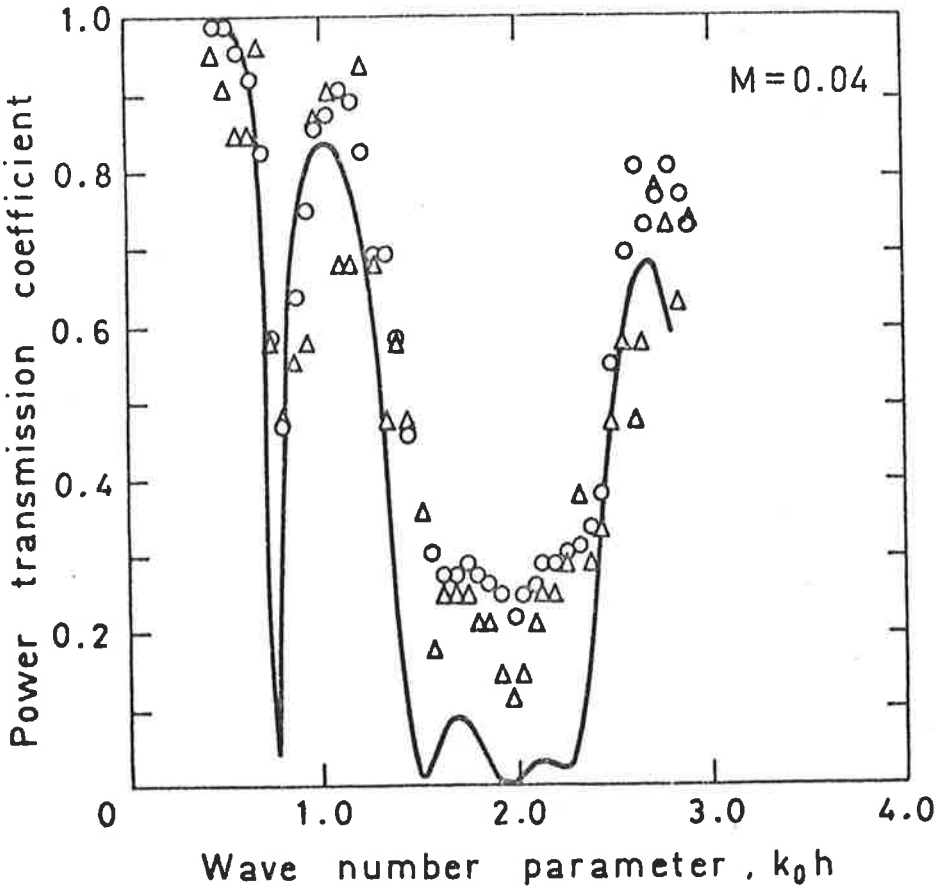

FIGURE 6.5 (B). M = 0.04.

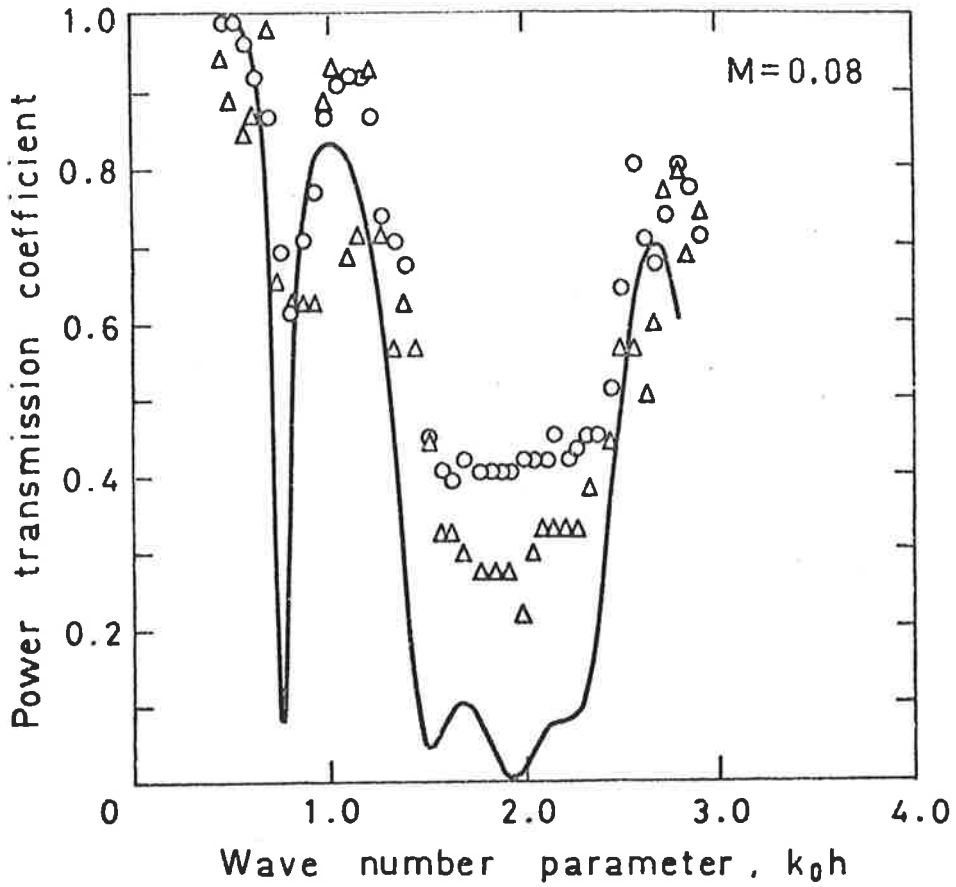

FIGURE 6.5 (c). M = 0.08.

by traversing a Brüel and Kjaer one-quarter inch calibrated microphone in the incident duct until a maximum in sound pressure level was recorded. A nose cone was fitted to the microphone to minimize noise generated due to flow turbulence. The sound pressure level of the plane wave leaving the attenuator was measured by a calibrated microphone mounted flush with the duct inside wall and perpendicular to the flow. The transmission loss was then calculated from equation (5.12) of Chapter 5 and is plotted in Figures 6.6(a), 6.6(b) and 6.6(c) for the optimum attenuator and in Figures 6.7(a), 6.7(b) and 6.7(c) for the original attenuator for flow speeds of M = 0, 0.04 and 0.08 and upstream and downstream propagation of sound.

6.4 THEORETICAL PREDICTIONS

The coefficients of equations (6.7) to (6.10) and of Appendix 2 were obtained using the procedure outlined in Chapter 5. The constants of the equations were evaluated simply (as no Bessel functions were present) and set into a matrix given in Appendix 3. The complex matrix was solved as in Chapter 5 using a program based on Crout's rule.

The theoretical power reflection coefficient is given simply by

$$R = \left| \frac{P_{oo}^{r}}{P_{oo}^{i}} \right| \qquad (6.16)$$

for both upstream and downstream cases. The theoretical power reflection coefficient for downstream and upstream propagation is related to the theoretical reflection coefficient by equations (6.13) and (6.14) respectively.

The theoretical power transmission coefficient is

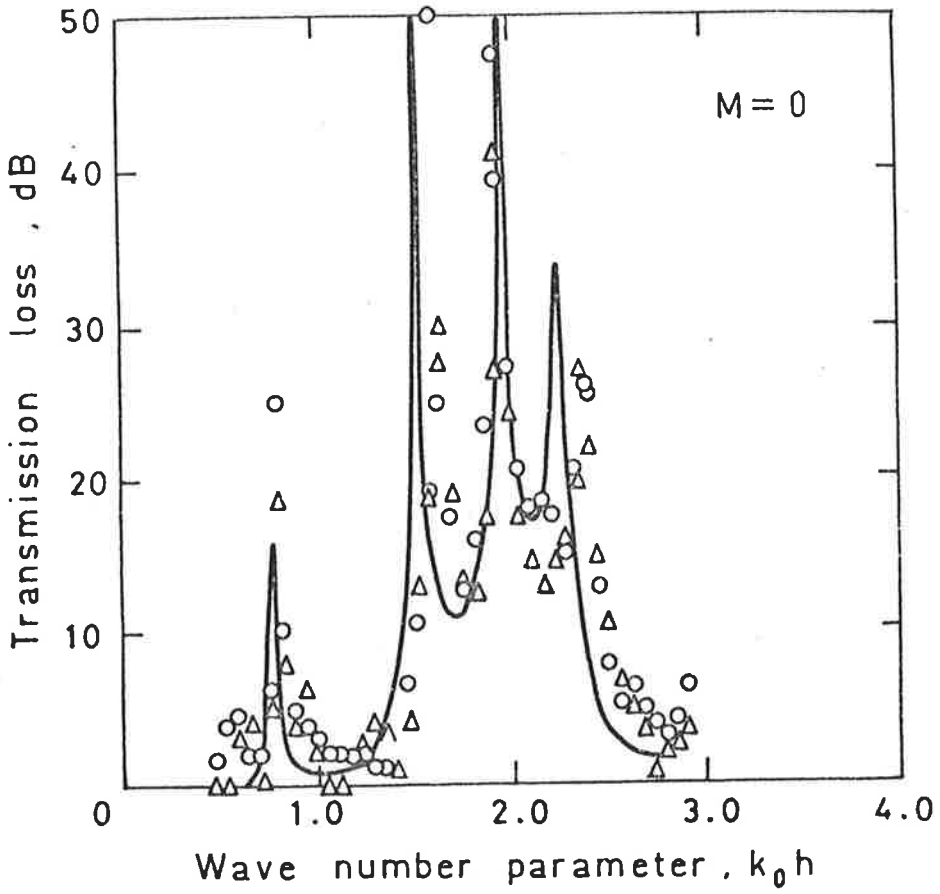

FIGURE 6.6 (A). Transmission loss of the optimum attenuator with flow. M = 0. ——— , theoretical curve; O , experimental values for downstream propagation of sound; Δ , experimental values for upstream propagation.

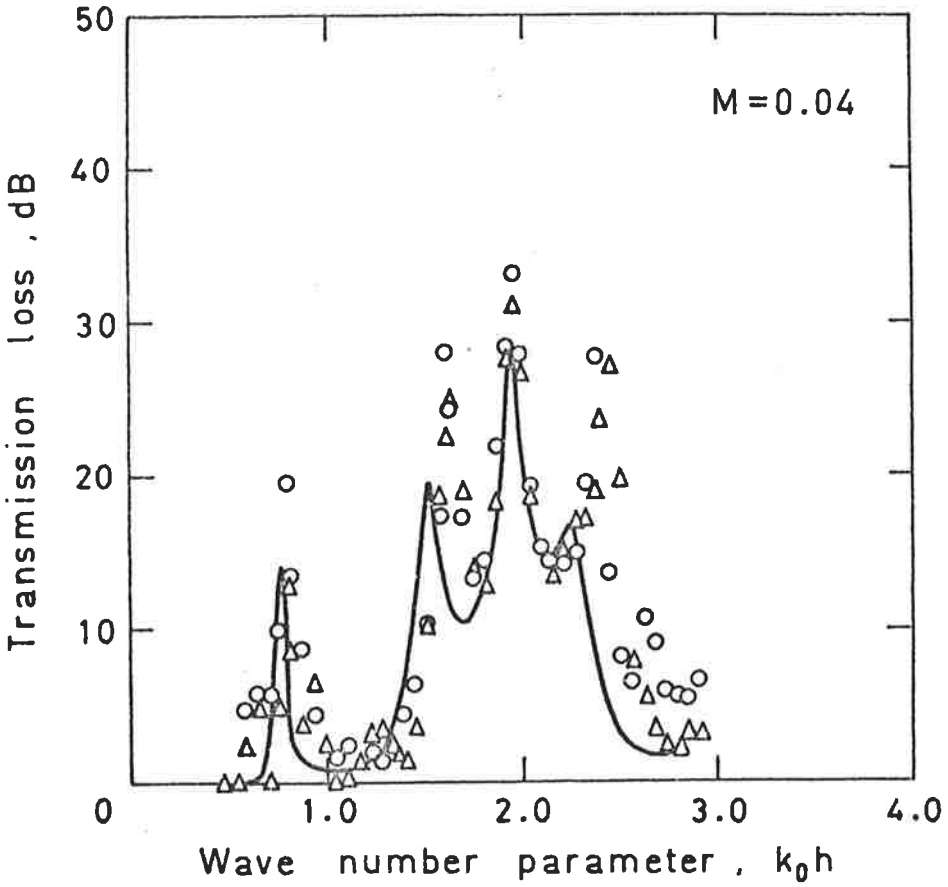

FIGURE 6.6 (B). M = 0.04.

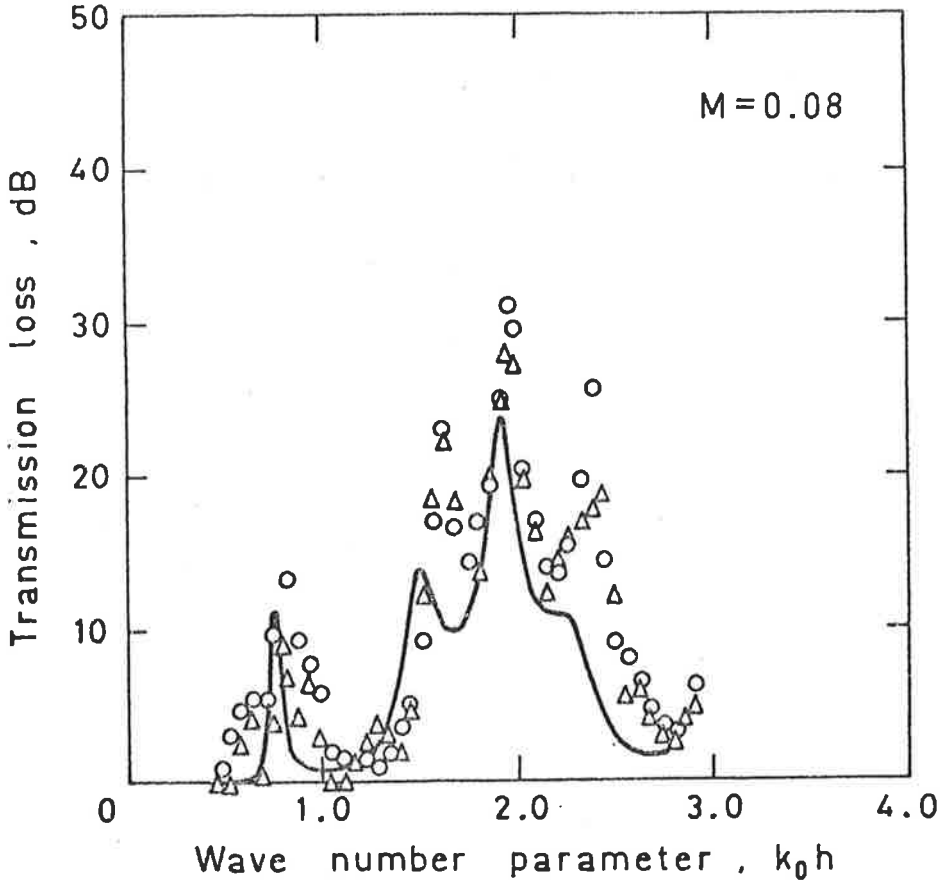

FIGURE 6.6 (c). M = 0.08.

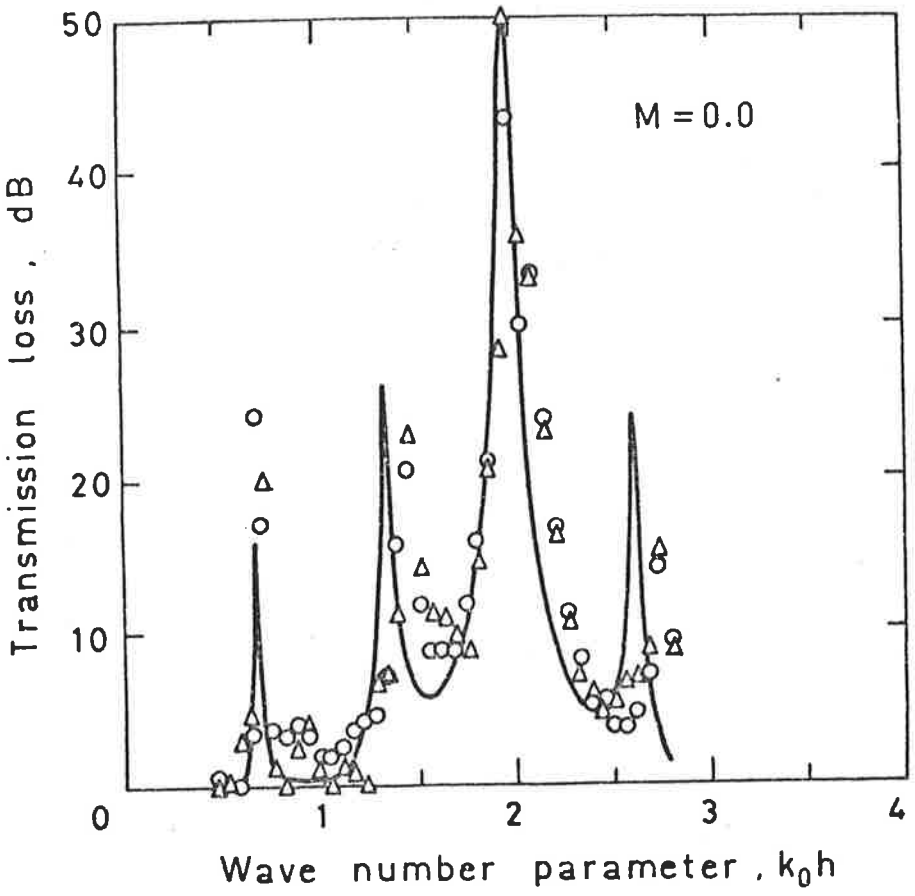

FIGURE 6.7.(A) Transmission loss of the original attenuator with flow. M = 0. ——— , theoretical curve, O , experimental values for downstream propagation of sound; Δ , experimental values for upstream propagation.

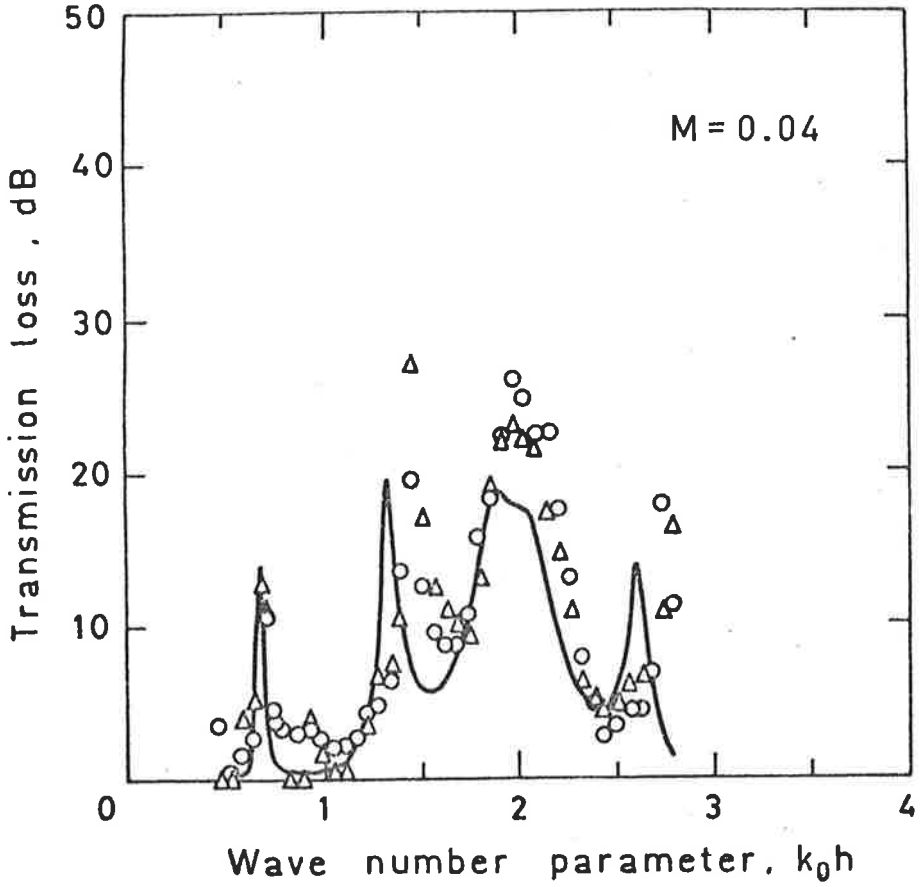

FIGURE 6.7. (B). M = 0.04.

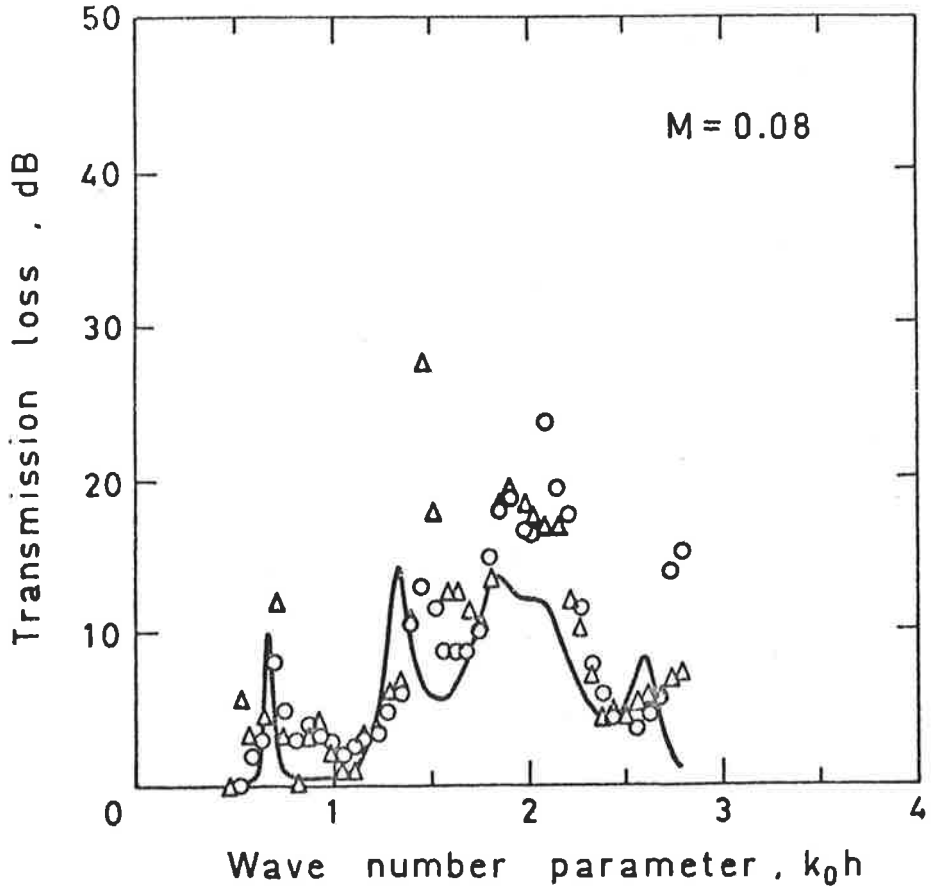

FIGURE 6.7. (c). M = 0.08.

$$\alpha_t = \left| \frac{E_{oo}^{\,i}}{P_{oo}^{\,i}} \right|^2 \qquad (6.17)$$

for both downstream and upstream cases. Finally the theoretical transmission loss is related to the theoretical transmission coefficient by

$$T.L. = -10 \log (\alpha_t) \qquad (6.18)$$

for both downstream and upstream cases.

The four theoretical parameters are plotted in Figures 6.3 to 6.7 for comparison with the respective experimental results.

Figures 6.8 and 6.9 show theoretical transmission losses for flow rates up to M = 0.3 for the optimum and original attenuator respectively.

6.5 DISCUSSION OF RESULTS

6.5.1 Pressure Reflection Coefficient

As can be seen in Figures 6.3(a), 6.3(b) and 6.3(c) there is reasonable agreement between experiment and theory. The main reason for error in the experimentally measured reflection coefficient is due to difficulty in measuring standing wave minima. As encountered in the no-flow case of Chapter 5, if the standing wave ratio is large, the minima are quite sharp and very easily obscured by, for example, overtones due to small distortion in the signal. The minima are thus very difficult to measure accurately and the measured magnitude of sound pressure level is always too high. The standing wave ratio and thus the corresponding reflection coefficient in this case will always be too small.

Figures 6.3(b) and 6.3(c) demonstrate a theoretically predicted pressure reflection coefficient greater than unity for

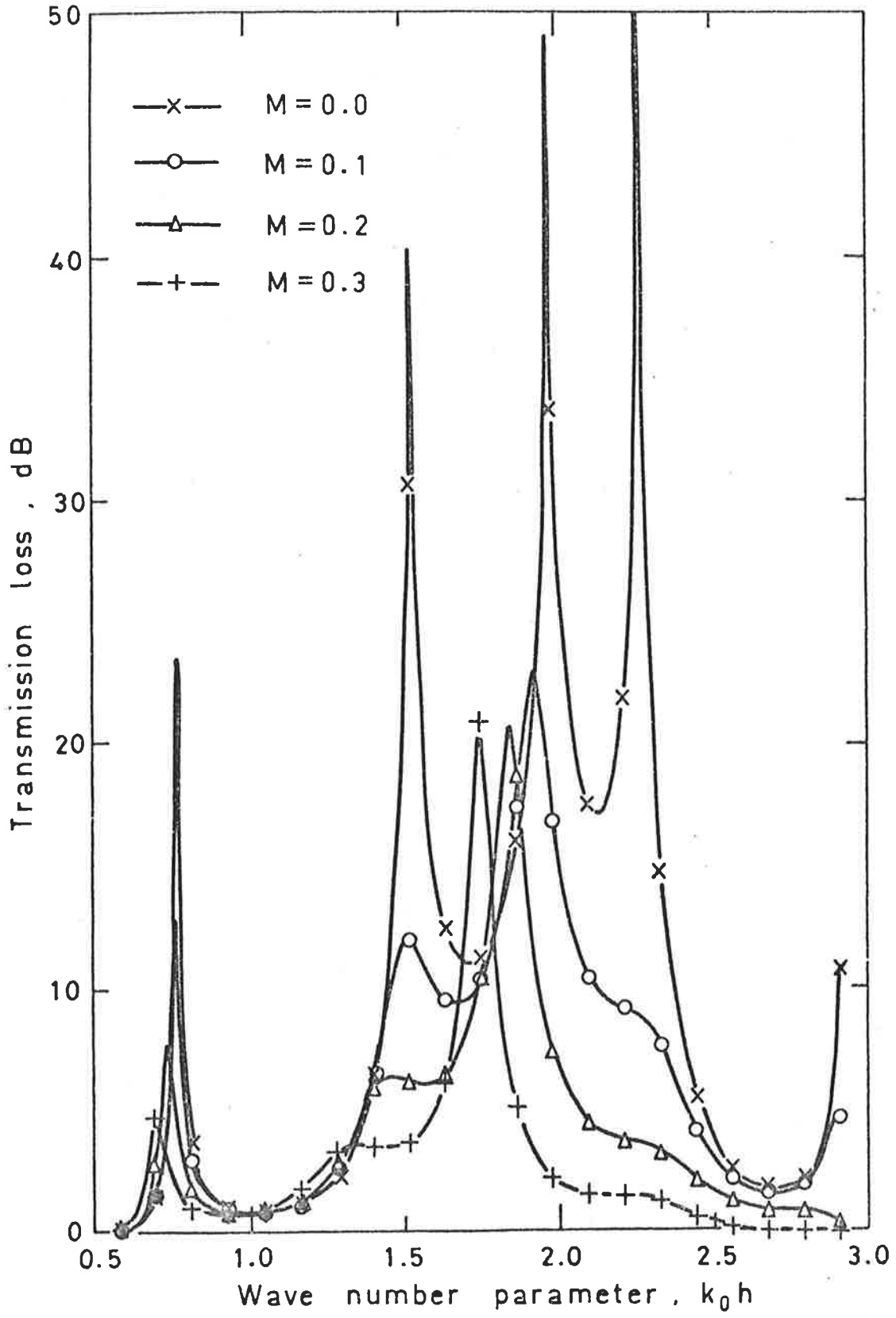

FIGURE 6.8. Theoretical transmission loss of the optimum attenuator with high speed flow.

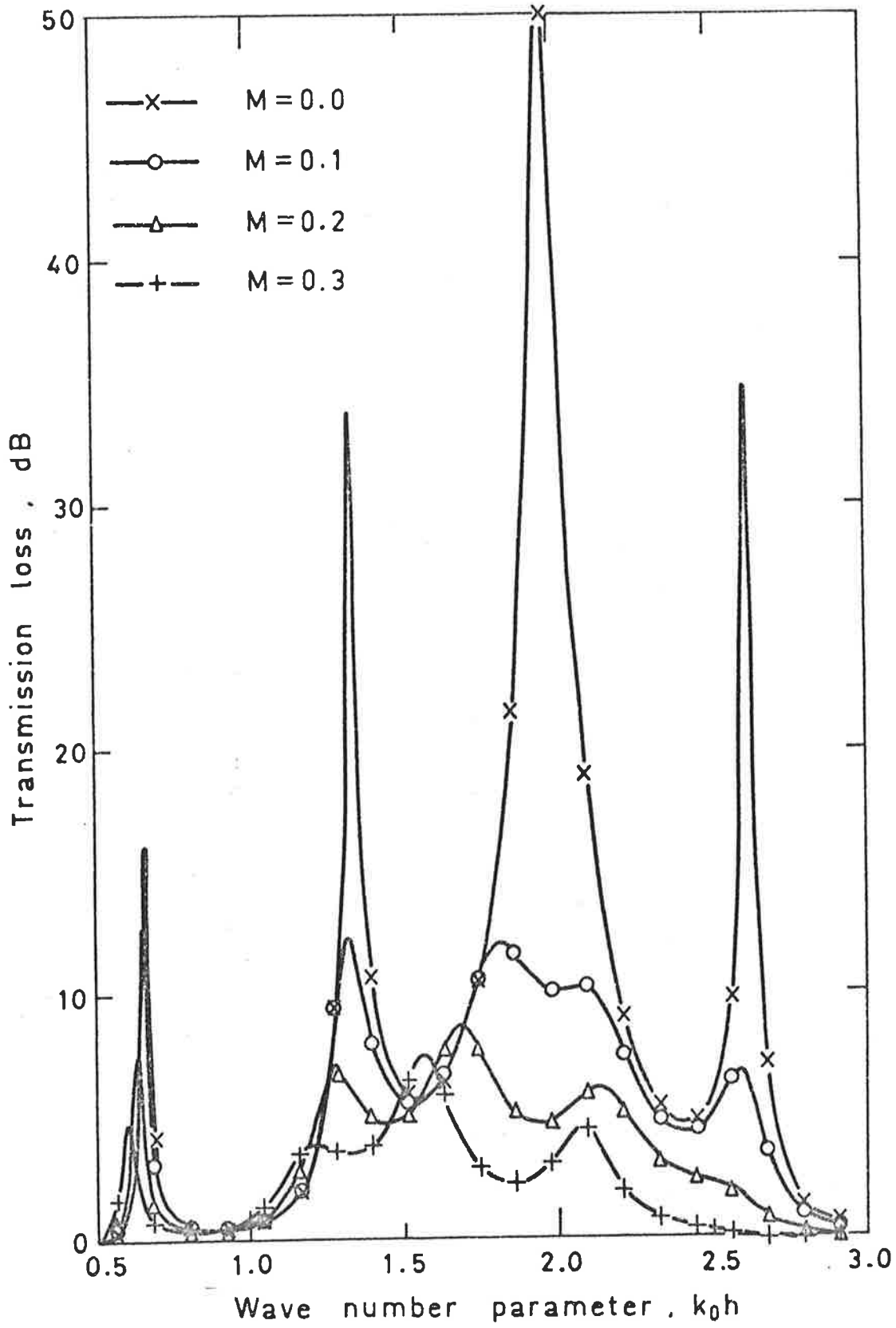

FIGURE 6.9. Theoretical transmission loss of the original attenuator with high speed flow.

downstream propagation. The ratio of the maximum reflection coefficient at M = 0.08 to the maximum reflection coefficient at M = 0 from Figures 6.3(c) and 6.3(a) is approximately 1.16. Using the relationship discussed in Chapter 1 that R_{max} before flux reversal occurs is given by

$$R_{max} = R(1+M)/(1 - M) \tag{6.19}$$

we thus obtain theoretically for M = 0.08, R = 1,

$$R_{max} = 1.174$$

Similarly for the upstream case from Figure 6.3(c) and 6.3(a) a ratio is determined to be approximately 0.84 while for M = 0.08, R = 1 we theoretically obtain

$$R_{max} = R(1 - M)/(1+M) \tag{6.20}$$
$$= 0.852$$

Thus ignoring slight changes in performance due to convected wave number effects, the major effect of convection of the propagating medium on the pressure reflection coefficient is to increase it by a factor of $(1 + M)/(1 - M)$ for the downstream case and decrease it by a factor of $(1 - M)/(1 + M)$ for the upstream case.

The experimental pressure reflection coefficients measured for the upstream and downstream cases confirm the effect that flow has on the pressure reflection coefficient. Measurements for the upstream case show a definite trend to reduction with increasing flow rates. The downstream case however does not agree quite as well. The evaluation of the downstream pressure reflection coefficient for R > 1 depends upon detection of the change in magnitude of the minima with distance traversed by the probe. As discussed previously the minima

are difficult to measure accurately and thus this information was obscured.

6.5.2 Power Reflection and Transmission Coefficients

The theoretical power reflection coefficient plotted in Figures 6.4(a), 6.4(b) and 6.4(c) is shown to be the same for both upstream and downstream propagation of sound. This supports the theoretical predictions of Section 1.3.2 of Chapter 1. The experimental values agree well with the theoretical predictions. However the downstream experimental power reflection coefficient is found to be consistently less than the upstream coefficient. The discrepancy between upstream and downstream experimental values was thought to be due to flow separation in the attenuator and is discussed in more detail later.

The theoretical power transmission coefficient in Figures 6.5(a), 6.5(b) and 6.5(c) demonstrates similar agreement with experimental results. Although the power transmission coefficient was theoretically evaluated independently it can be seen that for the same flow rates the power transmission coefficient plus the power reflection coefficient equals unity.

Thus although flow has the effect of increasing or decreasing the pressure reflection coefficient markedly due to convection of energy the same effect is not shown in the power reflection and transmission coefficients. The small changes in the theoretical power coefficients are due to changes in the convected wavenumbers thus altering the relative phases at interfaces A and D of reflected and incident waves. Wavenumber effects are more apparent in a reduction of tranmission loss and will be discussed in the next section.

6.5.3 Transmission Loss

Figure 6.6(a) demonstrates that the analysis provides a very accurate description of the performance of the optimum attenuator without flow. This figure should be compared to the corresponding Figure 5.6 of Chapter 5 where the theoretical curve was derived more exactly using cylindrical co-ordinates for sound propagation in the curved sections. A comparison of these two figures shows that they are nearly identical and that the conformal mapping equations give a very good result in the case of no flow. In Figure 6.6(a) the small discrepancies between theoretical and experimentally measured values of the frequencies at which maxima occur were thought to be due, as previously, to dimensional inaccuracies and variations in ambient temperature during the course of experimentation. However, for increasing Mach number, the theoretical prediction shown in Figures 6.6(b) and 6.6(c) is decreasingly reliable at the maxima. At $M = 0.08$ good agreement is obtained at all frequencies except at the peaks where theory underestimates the measured transmission loss.

The discrepancy may be due to flow separation in the curved sections of the attenuator. The theory assumes that flow is uniform at the interfaces and boundary layers are ignored. However, at flow velocities of $M \geq 0.04$ the flow is likely to separate from the curved sections of the attenuator and thus effectively "slow" the wave propagation over a part of the reflecting interfaces of the attenuator. This explanation is supported by the experimental results of transmission loss of the original attenuator shown in Figures 6.7(a), 6.7(b) and 6.7(c) which demonstrate better agreement between theory and experiment than the optimum attenuator, especially at $M = 0.04$. The original attenuator has less severe curved sections

than the optimum attenuator and separation is thus likely to occur at a higher flow velocity leading to improved agreement due to more uniform flow over the exit and inlet surfaces.

The theory predicts that convection of the propagating medium will reduce the magnitude of the transmission loss peaks with increasing Mach number. This can be understood by considering that the rejection peaks are critically dependent on the arrival times of waves at interfaces A and D. Flow is found to disturb the sensitive phase balance needed for high reflection of sound. This reduction in maxima of transmission loss is demonstrated in the experimental values of Figure 6.6(c) but not to the magnitude predicted.

A theoretical comparison of transmission loss values for flow rates up to M = 0.3 for the optimum attenuator is shown in Figure 6.8. At M = 0.3 rejection is reduced to a single narrow peak centered on the design frequency. At this velocity the attenuator would theoretically only have a satisfactory transmission loss over a very narrow frequency band. Figure 6.8 also shows that the design frequency has reduced with increasing Mach number independent of direction of propagation of sound. As the design frequency is determined in the no-flow case by wavelength considerations, one would intuitively expect the design frequency to increase with sound propagating with the flow and decrease with sound propagating against the flow. However, this reduction is similar to a reduction in resonant frequency of a tube open at both ends with the propagating medium convecting at Mach number M. The new resonant frequency of the tube is given by $f' = (1 - M^2)f$. Similarly if the design frequency of the attenuator without flow is 844 Hz then a flow velocity of M = 0.3 would theoretically reduce it to 769 Hz. This value agrees well with the new design frequency determined theoretically

by the analysis and shown in Figure 6.8 for a flow rate of M = 0.3.

This also explains why the attenuator theoretically provides the same transmission loss independent of the direction of the flow. In either case the travelling waves are slowed or increased in speed on one leg and vice versa on the return leg of the round trip between interfaces. Similarly as discussed in Chapter 1 the theoretical transmission loss is unaffected by the direction of convection of the propagating medium. Experimental values of transmission loss differ however, depending on the direction of flow. The effect was most likely due to separation. For downstream propagation of sound separation occurs near the acoustic exit of the attenuator and interferes with the major reflecting interface A. For upstream propagation of sound separation occurs at the acoustic inlet interface and thus has a secondary effect. The velocity profile at the acoustic exit interface in this case, would be close to uniform.

Figure 6.9 demonstrates that a flow rate of M = 0.3 has virtually destroyed all theoretical attenuation obtained using the original attenuator. Thus it is important to optimize the design of the attenuator to reduce the effects of flow on the magnitude of transmission loss to be expected as well as providing the broadest operating band possible of useful (10 dB) transmission loss.

In the velocity range considered experimentally, the results show that although flow severely reduces the magnitude of the rejection peaks a continuous band of at least 10 dB transmission loss is still obtained over three quarters of an octave when using the optimum attenuator,largely due to separation in the bend. Thus the attenuator still performs well for incident duct velocities of $M \lesssim 0.08$. Different configuration attenuators with different radii

may lead to different separation characteristics and altered experimental values but at the flow velocities for which the attenuator is most likely to be used this is unlikely to reduce the effectiveness of the attenuator.

6.6 SUMMARY

The investigation demonstrates clearly that convection of the propagating medium affects the operating characteristics of the attenuator quite markedly. Even at low values of Mach number ($M \lesssim 0.04$) the high levels of attenuation obtained at the peaks in the no-flow case are reduced substantially.

Flow has been shown to increase the pressure reflection coefficient by a factor of $(1 + M)/(1 - M)$ for downstream propagation of sound and decrease the coefficient by a factor of $(1 - M)/(1 + M)$ for the upstream case.

Theory predicts that the attenuator performs identically from an energy point of view with sound propagating with or against the flow. Changes in energy transmission are found to be due to changes in wavenumber arising from increased or decreased phase speed with flow. Experiments, however, show that flow has a greater detrimental effect when sound propagates against the flow through the attenuator.

Flow also has the effect of lowering the design frequency by a factor of $(1 - M^2)$ independent of direction of propagation of sound relative to flow.

Although the maxima of transmission loss are reduced, for flow speeds of $M \lesssim 0.08$ a continuous band of at least 10 dB transmission loss is still measured over three quarters of an octave when using an optimized attenuator.

CHAPTER 7

A DELAY LINE REACTIVE ATTENUATOR FOR USE IN FLOW DUCTS OF CIRCULAR CROSS SECTION

7.1 INTRODUCTION

The investigations of Chapters 5 and 6 have established that the principle of reactive attenuation can be applied very successfully to low frequency sound in ducts with and without flow of the propagating medium. However the arrangement of the attenuator discussed in Chapters 5 and 6 must be fitted into a bend in the duct system to obtain the necessary path difference for reflection of sound, hence this arrangement is unsuitable for use in straight ducts. As many duct systems are straight and are usually of circular cross section it would be useful to develop a reactive attenuator based upon the same principles applied to the attenuator of Chapters 5 and 6 but applicable to straight ducts of circular cross section.

It can be seen from Chapter 5 that the high levels of attenuation obtained are achieved by impedance mismatches generated at the exit and inlet surfaces of the attenuator. Multi-reflections between the inlet and exit surfaces have also been shown to give rise to a broad operating band as opposed to the narrow frequency response obtained by the more conventional forms of reactive attenuators such as a quarter wave tube or a Helmholtz resonator. As discussed previously the impedance mismatch results from the generation of non-propagating cross modes at the exit and inlet of the attenuator due to phase differences between the sound waves propagating in the separate duct sections of the attenuator. At the design frequency the

impedance at the exit surface is purely reactive and the wave motion of sound leaving the attenuator consists entirely of a series of evanescent modes. Thus at this frequency all incident sound to the attenuator is theoretically reflected.

In this chapter a reactive attenuator suitable for application in straight ducts of circular cross section and based upon the principles of the attenuator discussed in Chapter 5 is investigated experimentally and theoretically with and without flow. The principle aim of the investigation is to establish whether high levels of attenuation can be obtained with the proposed arrangement and thus the investigation concentrates on the experimental side. However the attenuator may be modelled in terms of an equivalent electrical circuit at very low frequencies and by this means it is analysed theoretically at very low frequencies, using the lumped elements approach for the case without flow of the propagating medium. Analysis at higher frequencies and in the presence of flow is not attempted.

The two parameters of pressure transmission coefficient and transmission loss are investigated experimentally for flow speeds of $M = 0$, $M = 0.22$ and $M = 0.37$ for sound propagating downstream and $M = 0$, $M = 0.22$ for sound propagating upstream against the flow. The investigation is limited to frequencies less than the cut-off frequency of the (1,0) mode in the incident duct.

It is proposed to obtain attenuation by creating an impedance mismatch over a cross section of the duct. The resulting impedance mismatch will generate a series of evanescent modes and will cause high reflection of low frequency sound. This approach to reactive attenuation should be compared to that of Poole and Leventhall (1976) who introduced an antiphase "copy" of the incident sound in a

rectangular duct by means of an arrangement of speakers mounted in the duct wall and driven from an amplified, electronically phase shifted signal from a microphone positioned so as to sense the incident sound field. As Poole and Leventhall explained, the sound field generated by the speakers does not cancel or destroy the energy of the incident waves but causes an impedance mismatch and hence reflection of sound.

Poole and Leventhall met with limited success in the experimental implementation of their idea, a major problem being that the introduced sound field tended to propagate upstream towards the sensing microphone. Poole and Leventhall obtained reasonably high attenuation of sound, however the attenuation was limited to a very narrow frequency band. Furthermore the device was complicated by the need for electronics to obtain the necessary delay in phase. Any change in the speed of propagation of the wave due to flow of the propagating medium or variation in ambient temperature required an adjustment of the delay necessary to keep the required frequency centered on the narrow frequency band where satisfactory attenuation was obtained. Poole and Leventhall did not investigate the effect of flow on their attenuator.

It is expected that the attenuator discussed in this chapter will overcome the problems of narrow band width and thus sensitivity to wave speed. It is also intended to obtain the delay by purely physical means (without changing the cross sectional shape of the pipe), thereby eliminating the need for electronic support equipment.

7.2 DESIGN OF THE ATTENUATOR

The basic arrangement of the attenuator is shown diagramatically in a section view in Figure 7.1. The attenuator is designed to operate as follows. When incident plane wave sound reaches interface A some of the incident sound propagates through a series of slots in the duct wall while the remainder travels on with phase speed c_o downstream. The sound that passes through the slots and out of the main duct travels through a series of volumes and orifices contained in a tube positioned on the same centerline on the major duct, as shown. The orifices and capacitances form an acoustic delay line (Morse and Ingard, (1968)) so that the sound travelling through them is delayed and hence the speed of propagation of sound in this part of the attenuator is less than c_o. When the waves in the outside (delay) section of the attenuator reach interface B they are substantially out of phase with the waves that have travelled in the main duct to interface B. The amount of phase shift can be adjusted by varying the size of the volumes and orifices. The actual delay in phase in simple delay lines similar to that of the attenuator of Figure 7.1 can be calculated using an analogous electrical circuit approach as described by Morse and Ingard (1968). However this procedure is limited to very low frequencies and at higher frequencies transmission line theory should be used. Due to the complicated physical shape of the attenuator, transmission line theory is not attempted here.

The sound that travels in the delay line section of the attenuator is out of phase with the sound in the duct when it reaches the secondary slots at interface B. The sound that has travelled in the delay line radiates through the slots at interface B and induces a pressure field over a portion of the inside periphery of the major

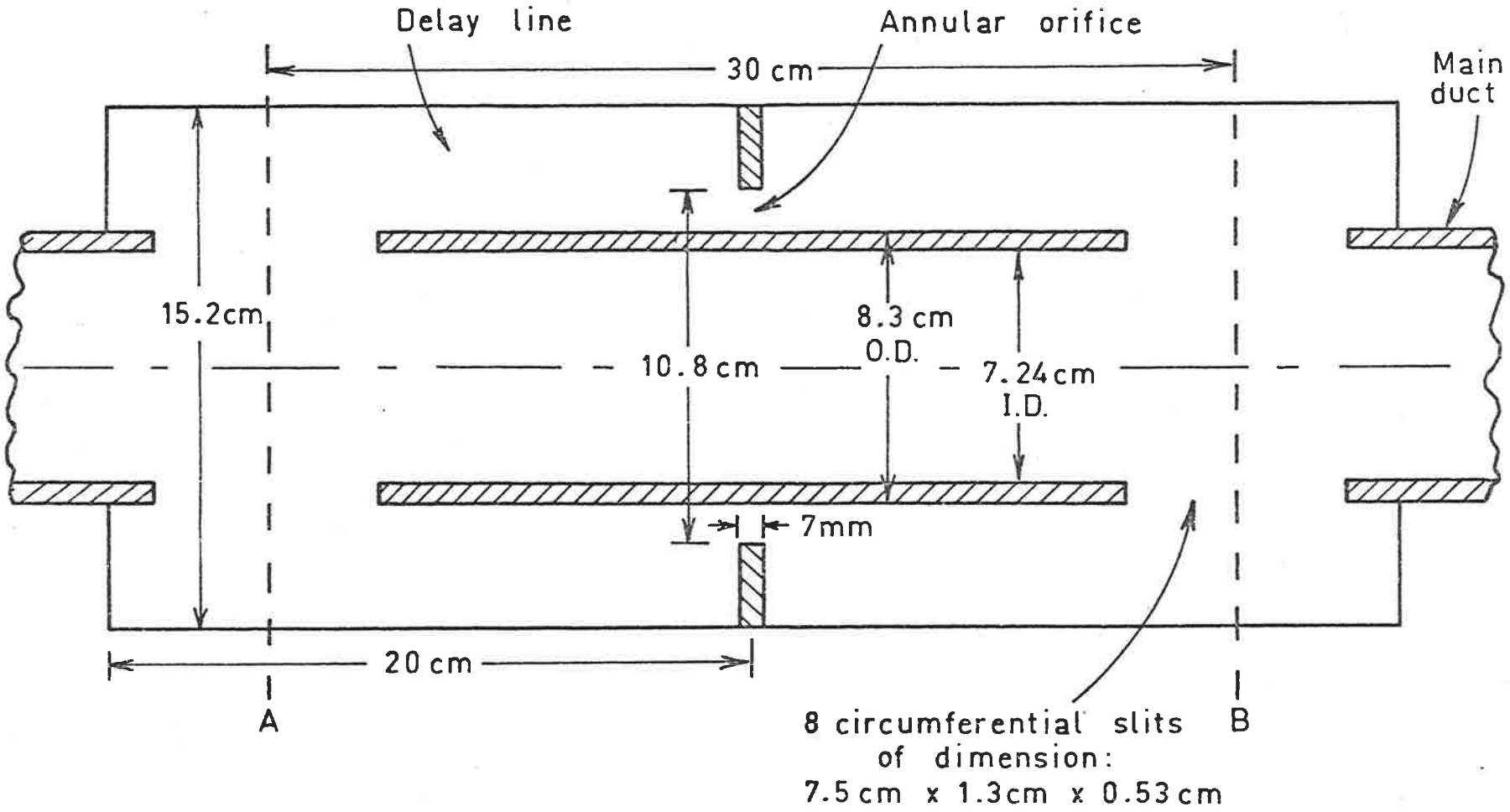

FIGURE 7.1. Arrangement and dimensions of the delay line attenuator.

duct. The induced pressure field is thus out of phase with the incident pressure field over the remainder of the duct cross section at B. The slots can be thought of as similar to loud speakers positioned radially on the duct wall. The approximate pressure distribution induced in the main duct corresponds to that of the (0,1) mode in a circular duct with rigid walls (Rschevkin (1963)). This mode, illustrated in Figure 7.2, has a cut-on frequency much greater than the frequencies over which this attenuator is to be investigated. If the phase and pressure distribution of the (0,1) mode is faithfully induced at interface B then high reflection of sound should be achieved. Similarly it is expected that multi-reflections will be set up between interfaces A and B of the attenuator, and these will cause high reflection of sound at a number of frequencies and thus provide a broad operating band.

7.3 CONSTRUCTION OF THE ATTENUATOR

The dimensions of the attenuator were chosen nominally except for the internal diameter of the main duct which was chosen to be 0.0724 m to correspond to the inside diameter of the "suck down" flow rig tubing already in use at the University of Adelaide. The size of the annular orifice plates was fixed for all tests at R_1 = .054 m and R_2 = .076 m. Variation in phase delay through the delay section of the attenuator and corresponding changes in design frequency were to be investigated by varying the number of orifice plates used and hence the volume between orifice plates.

All parts of the attenuator were constructed from mild steel. The eight rectangular slots in the wall of the main duct at interfaces A and B were milled at equidistant circumferential positions. Each slot was chosen to have dimensions of .075m x .013 m, which presented

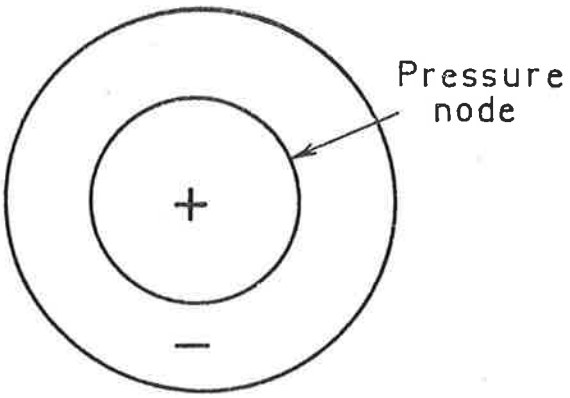

FIGURE 7.2. Pressure distribution of the (0,1) mode in a hard walled circular duct.

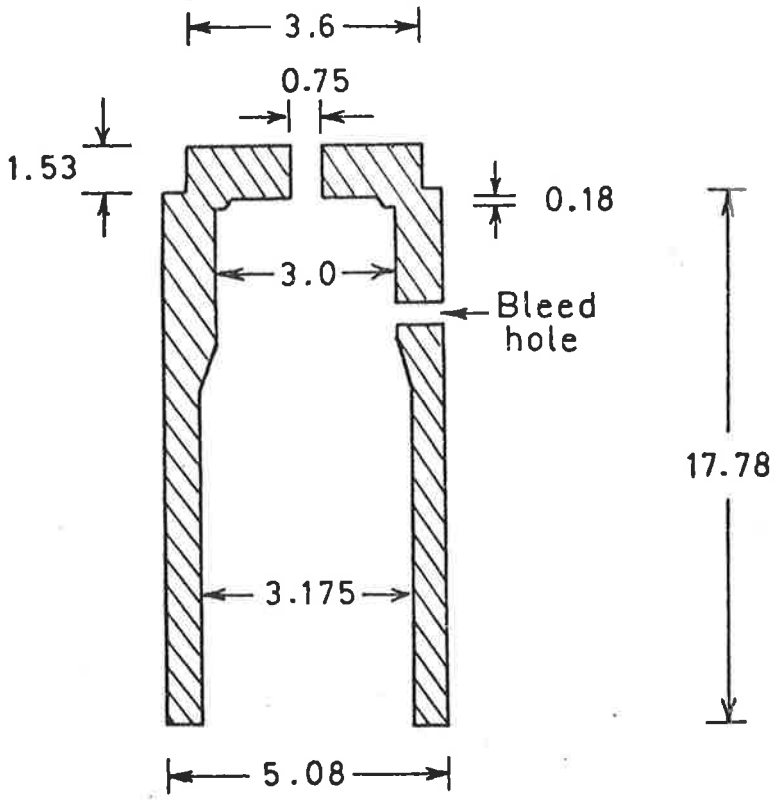

FIGURE 7.3. The perspex tip used on the microphone of the standing wave apparatus - dimensions in mm.

equal open area to incident sound to the attenuator as the main duct itself. For ease of insertion of the orifice plates the delay line center casing was split into two halves. Each orifice plate was fitted with an O' ring in its outside periphery to ensure tight sealing with the inside surface of the casing. When placed in position the orifice plate forms an annular, symmetrical orifice with the outside diameter of the major duct. The position of the orifice plates can be adjusted by sliding the plate backwards or forwards on the bore of the delay line casing. For all tests the orifice plates were positioned such that the distance between plates and the distance between the end plates and the center of the interface slots were equal.

To seal the whole attenuator the halves of the attenuator casing were threaded. The major duct was attached permanently to one half of the casing and when the other half of the casing was screwed into position an O' ring at the other end of the major duct provided the necessary seal. The whole arrangement constitutes a robust,compact and simple attenuator. The arrangement is also seen likely to cause little disturbance and hence negligible pressure drop to high speed flows in the major duct. The finished attenuator split into two halves, for adjustment of the orifice plates, is shown in Plate 4.

7.4 EXPERIMENTAL EQUIPMENT AND PROCEDURE

7.4.1. The Standing Wave Apparatus

As the attenuator was to be investigated for relatively high speeds of flow of the propagating medium a special standing wave apparatus was constructed. The requirements of this standing wave device were that it be: (1) quick acting, (2) provide no disturbance to the flow in the duct system and (3) be able to withstand low static wall pressures induced by high speed flows.

PLATE 4. The delay line attenuator (split into two halves for adjustments of the orifice plates)

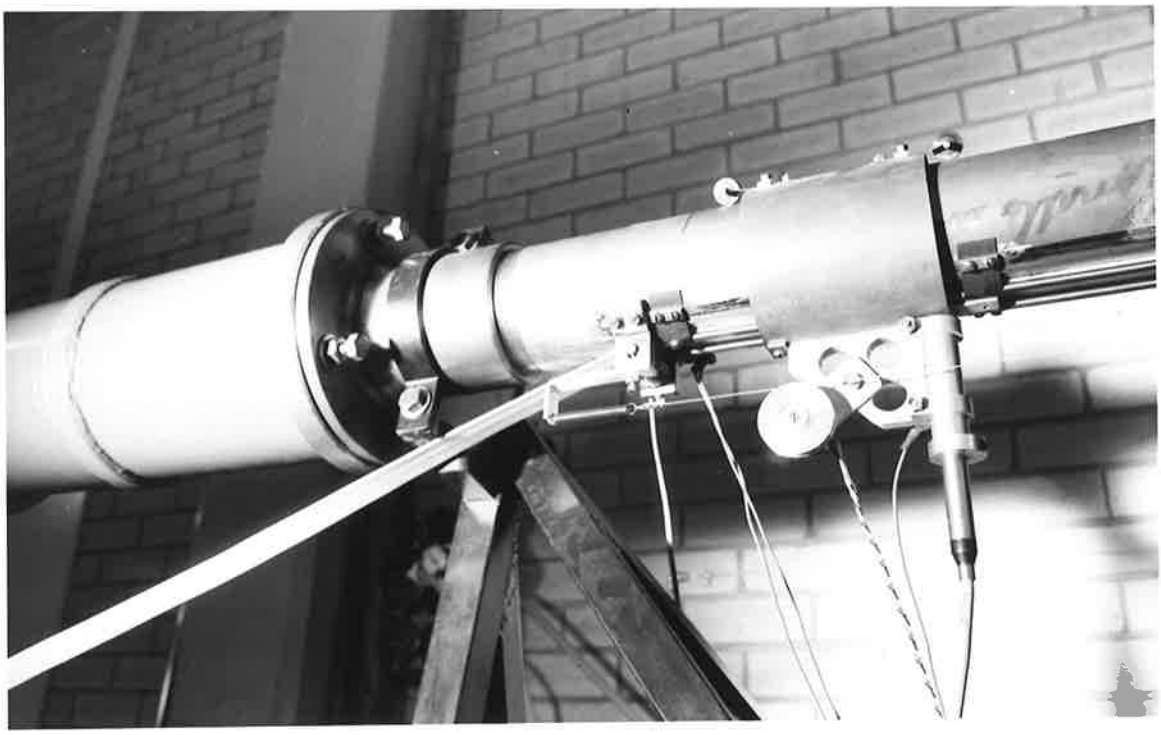

PLATE 5. The microphone carriage of the standing wave apparatus

The apparatus was constructed from a 1.4 meter length of mild steel circular duct with the same internal radius as the attenuator and the flow rig. A .7mm wide slot was machined over a distance of 1 meter in the duct wall to enable the traversing of a microphone carriage. To seal the duct at positions other than where the carriage was located, the microphone carriage was connected to a long piece of "Teflon" strip on either end, which was chosen to fit tightly in the slot yet slide easily when pulled. The strip was sealed by two rods positioned lengthways on both outside edges. One end of the "Teflon" strip was connected to a toothed rubber belt which could be fed into a matching drive pulley driven through a reduction gear box by a variable speed three-phase motor. Thus to perform an investigation of the standing wave in the duct automatically, the toothed belt was disengaged from the drive pulley and the microphone carriage pulled back manually to its starting position. The toothed belt was then engaged with the drive pulley and when required, the microphone carriage was traversed under power by switching on the drive motor. The motor was switched off automatically when the carriage had reached the maximum traverse distance by a fixed micro-switch. Different traversing speeds could be obtained by varying the input voltage to the drive motor. At high voltages, fast traversing speeds (of the order of 20 cm/sec) could be obtained. The total distance traversed was .84 meter which limited the lowest usable frequency of the apparatus to 204 Hz.

For measurements of sound pressure level in the standing wave tube, a Brüel and Kjaer one eighth inch microphone was used. The normal diaphragm cover was removed and replaced with a perspex tip, the arrangement of which is shown in Figure 7.3. A very small hole was used as a pressure inlet to increase the accuracy of detection

of the minima of the standing wave. A small bleed hole was drilled in the side of the tip to connect to a small channel in the microphone carriage and equalize the static pressure over the back and front of the microphone diaphragm. The cavity between the diaphragm and inside of the tip was kept to .1 mm in height to reduce the possibility of resonances affecting the measured values. The microphone and probe tip were mounted in the microphone carriage with the probe tip sitting in a machined metal holder mounted in the "Teflon" strip. The top surface of the probe tip was flush with the inside surface of the "Teflon" strip. Plate 5 shows the microphone carriage and the "Teflon" strip.

The arrangement allowed fast detection of the standing waves without disturbances to the flow in the duct. As the probe hole was aligned perpendicular to the flow, the noise due to turbulent fluctuations in the flow was minimized.

7.4.2. The "Suck Down" Flow Rig

To obtain flow through the test section, the "suck down" flow pipe facility at the University of Adelaide was used. The flow rig was designed to investigate the coupling of pipes, excited with internal flow, with the acoustic response of the surrounding medium (Rennison (1976)), as well as more recently the sound generated by flow through bends and orifice plates. The arrangement of the flow rig is shown diagramatically in Figure 7.4. The piping system consists of steel circular sections with an internal diameter of .724 meter. Each section has a male and female flange at either end which enables close alignment of the bore. Sealing at the flanges was achieved by O' rings mounted in each female flange.

The downstream end of the rig was connected to a system of

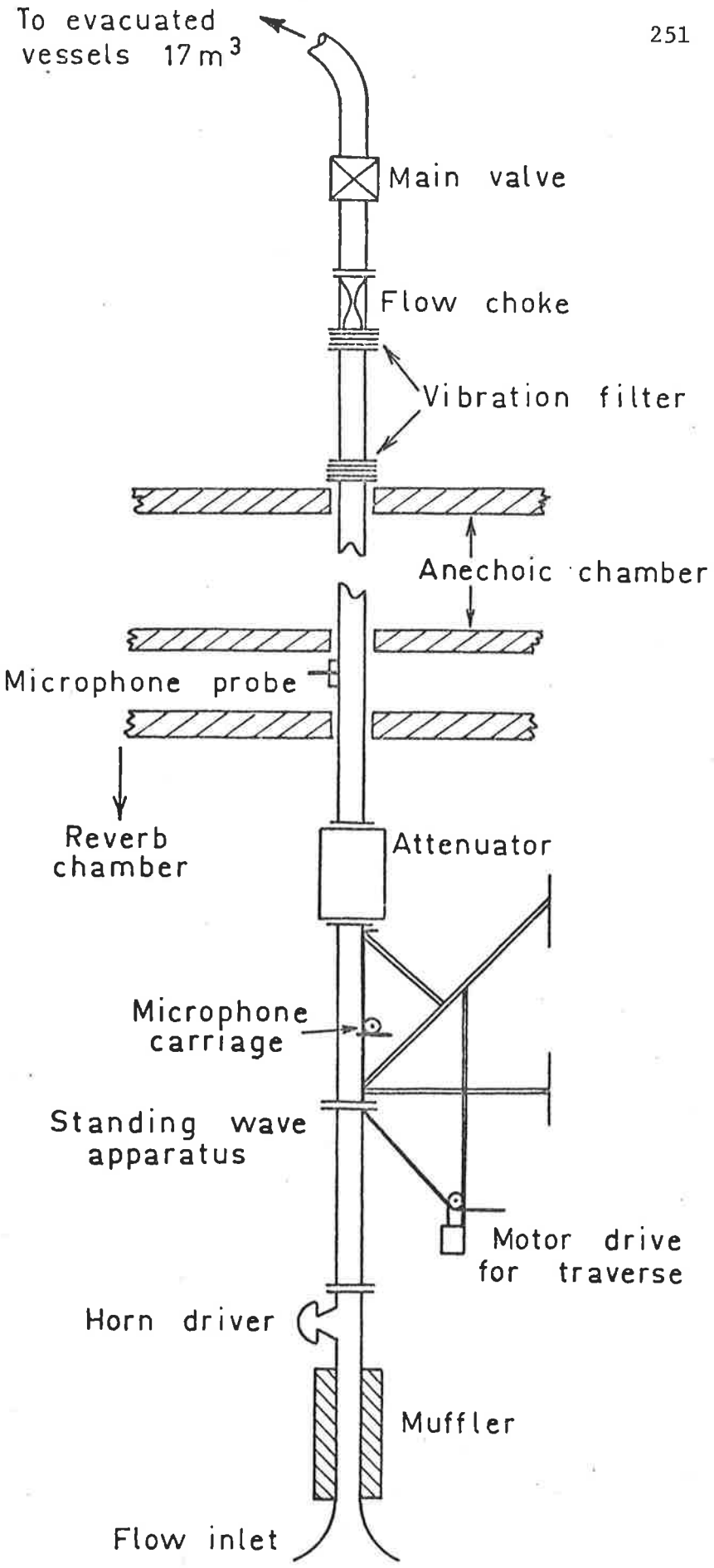

FIGURE 7.4. The "suck down" flow rig and the experimental apparatus used to investigate the performance of the delay line attenuator with flow.

tanks of total volume equal to $75m^3$ which were slowly evacuated to a pressure of 25 kPa. During the evacuation procedure the tanks are isolated from the test section by a butterfly valve. The butterfly valve can be operated remotely by an electric switch. To start the flow the butterfly valve is opened and air is drawn into the pipe through a smooth bell-shaped inlet. The flow speed in the test section is controlled by use of various choked nozzles of different throat areas which are mounted in the pipe system upstream of the butterfly valve. The flow speed in the test section was measured by traversing a pitot tube across the pipe (Rennison (1976)). The static pressure was measured at the pipe wall. The mean velocity in the test section was then calculated from the measured profiles. For this investigation the sonic chokes which induced a mean flow speed of M = 0.22 (which is the lowest speed of flow possible) and M = 0.37 were used. Higher values of flow speed were impracticable due to a poor signal to noise ratio. Since the flow speed nozzles were choked, no sound can propagate upstream through the throat into the test section. Similarly the nozzle was found to have a low reflection coefficient to sound propagating downstream. Mechanical noise transmitted through the pipe walls is isolated from the test section by a series of vibration isolators as shown in Figure 7.4.

Measurements of the flow velocity in the test section showed that steady flow conditions are obtained within one second of opening the butterfly valve. The length of running time is dependent on the choice of the choked nozzle used. For M = 0.22 the running time was approximately 15 seconds while for M = 0.37 the running time was approximately 8 seconds. The time taken to re-evacuate the tanks between runs is of the order of 10 to 15 minutes depending upon the

test conditions. Hence a series of tests at different frequencies using this rig is a lengthy procedure.

7.4.3 Experimental Procedure

To test the performance of the attenuator with flow, the device was mounted in the flow rig as shown in Figure 7.4. For sound propagating downstream with the flow the standing wave apparatus was positioned directly upstream of the attenuator. The acoustic signal was achieved by using a Tao 35 watt horn driver positioned 2.25 meters upstream from the entrance to the attenuator. A muffler was positioned between the sound source and the flow inlet to attenuate sound travelling upstream and radiating out of the inlet. The pressure reflection coefficient of the muffler was measured separately and found to be less than 0.2. Use of the muffler allowed the sound source to be driven at high levels without endangering the hearing of the person operating the apparatus. The apparatus arranged for the testing of downstream propagation of sound is shown in Plate 6.

For sound propagating upstream, the standing wave apparatus was positioned downstream of the attenuator. In this case the muffler acts as an anechoic termination to waves leaving the attenuator. For $M = 0$ the attenuator was tested in the upstream position due to the nature of the sonic choke, as discussed previously.

The standing wave in the upstream duct was measured with a Brüel and Kjaer one-eighth inch microphone. The signal from the microphone preamplifier was filtered using a Brüel and Kjaer Heterodyne Analyser (H.A.) set to a 3.16 Hz bandwidth. As used in the experimental investigation of Chapter 6, the Beat Frequency Oscillator section of the analyser was employed as the acoustic signal, thus the filter center frequency and the acoustic signal were always locked. The

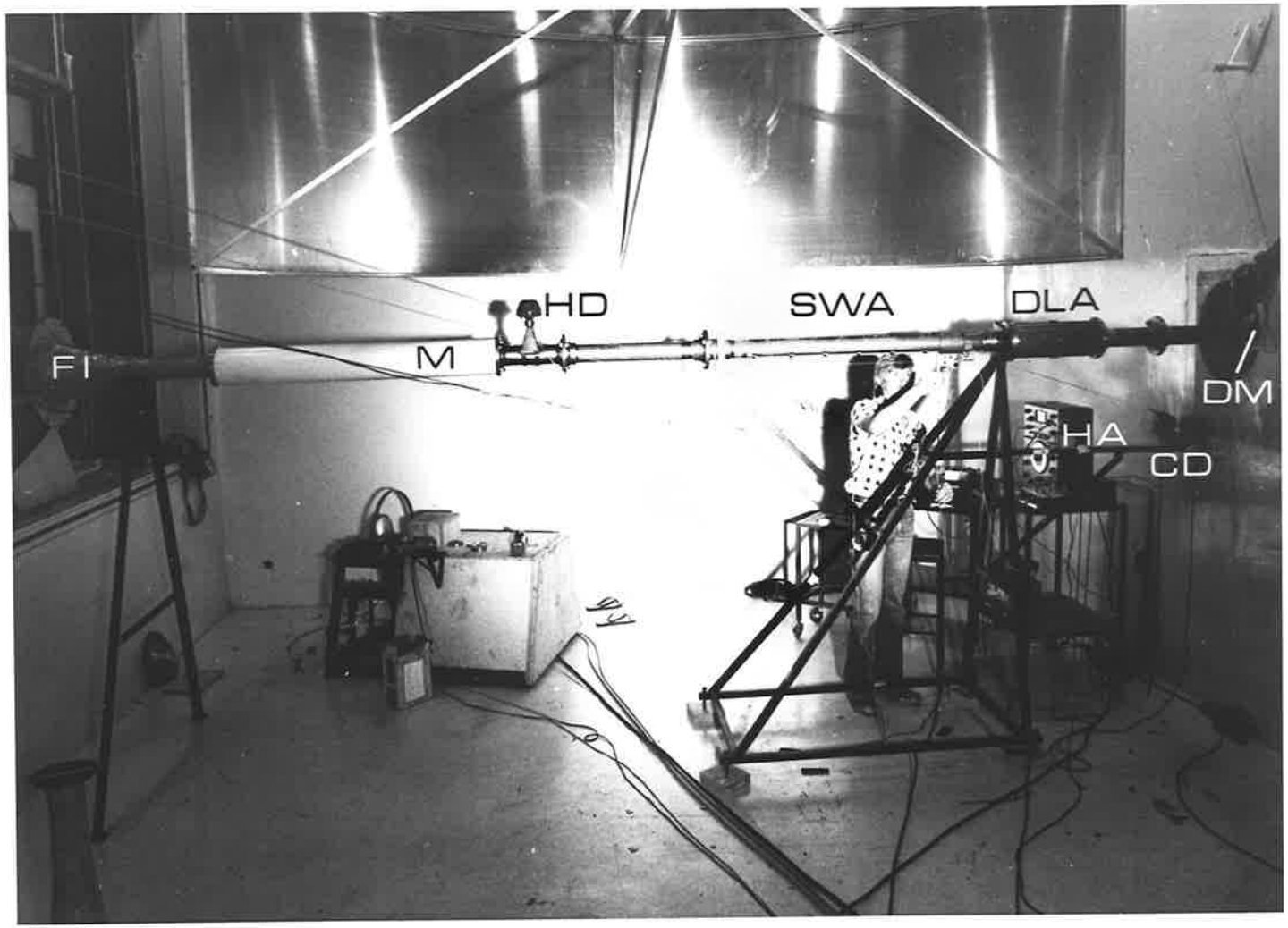

PLATE 6. The experimental apparatus for downstream propagation of sound, (FI) flow inlet, (M) muffler, (HD) horn driver, (SWA) standing wave apparatus, (DLA) delay line attenuator, (DM) downstream microphone, (HA) heterodyne analyser, (CD) carriage drive.

output of the analyser was recorded graphically with a Brüel and Kjaer Level Recorder for later evaluation. The sound levels of waves leaving the attenuator were measured with a Brüel and Kjaer one quarter inch microphone mounted flush with the pipe inside wall, 1.5 meters from the exit of the device. Due to the short running time of the flow rig and the fact that only one signal could be measured by the H.A. at any one time, the input voltage to the horn driver was kept constant at each frequency investigated and the standing wave distribution and sound pressure level of waves leaving the attenuator were measured separately on two consecutive runs. However, the results obtained were still consistent due to the very stable flow conditions in the test section.

Two parameters were investigated. The power transmission coefficient was obtained by measuring the standing wave in the upstream duct and applying the standing wave theory developed by Alfredson (1970) for flow and described in Chapter 6. However measurement of the standing wave minima were found to be inaccurate above 1200 Hz and only the case of 5 orifice plates and M = 0 is presented in Figure 7.5, where power transmission coefficient is plotted against the dimensionless quantity wave number multiplied by the main duct internal diameter. This result will be discussed in more detail later.

The transmission loss was obtained from the standing wave maximum and the transmitted sound pressure level using the method of Chapter 5 and given by equation (5.12), and is plotted in Figures 7.6 to 7.10 for 1 to 5 orifice plates and M = 0. The investigation was limited to 5 plates due to the "effective length" of orifices used. This will be discussed in more detail later. For the case of flow the arrangement of the attenuator with 5 plates alone (due

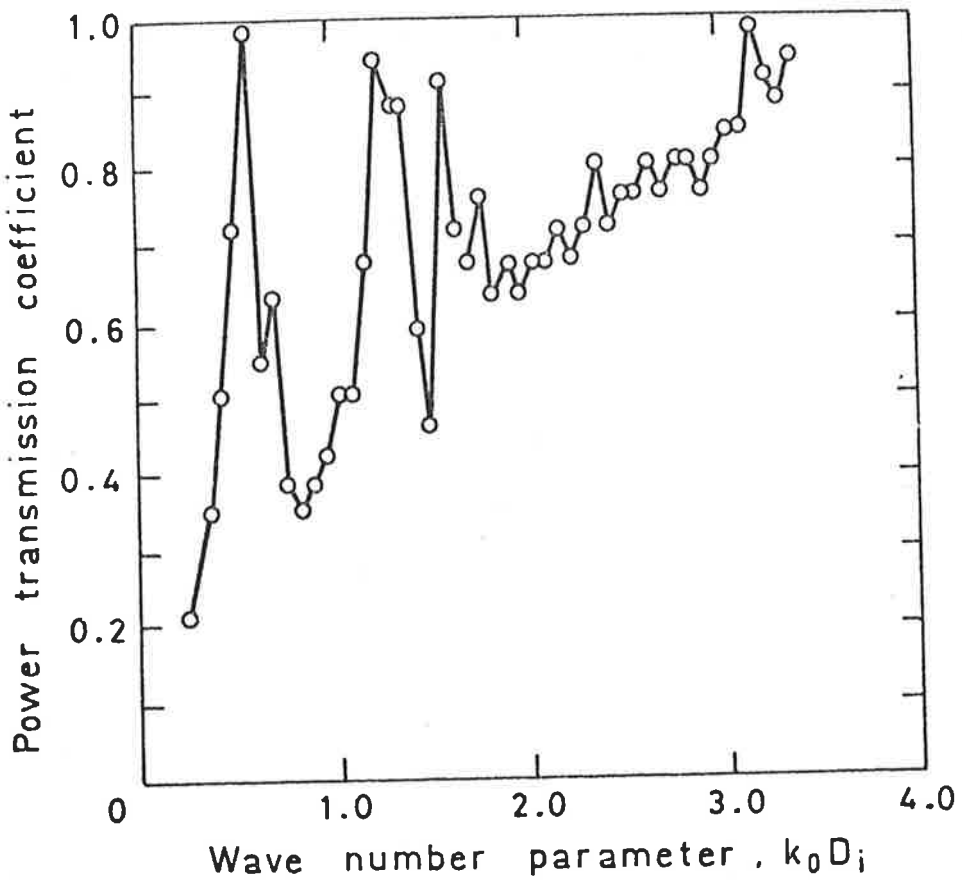

FIGURE 7.5. Experimental power transmission coefficient of the delay line attenuator with five orifice plates.

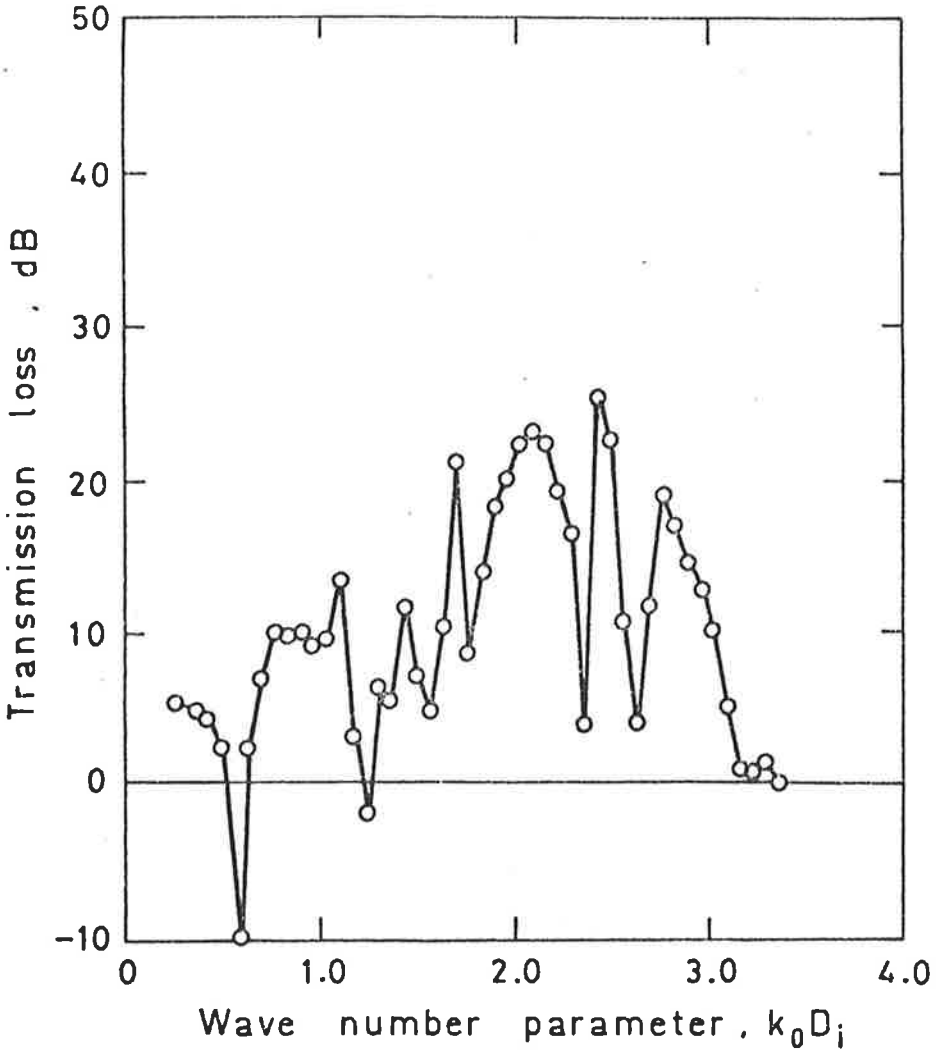

FIGURE 7.6. Experimental transmission loss of the delay line attenuator with one orifice plate.

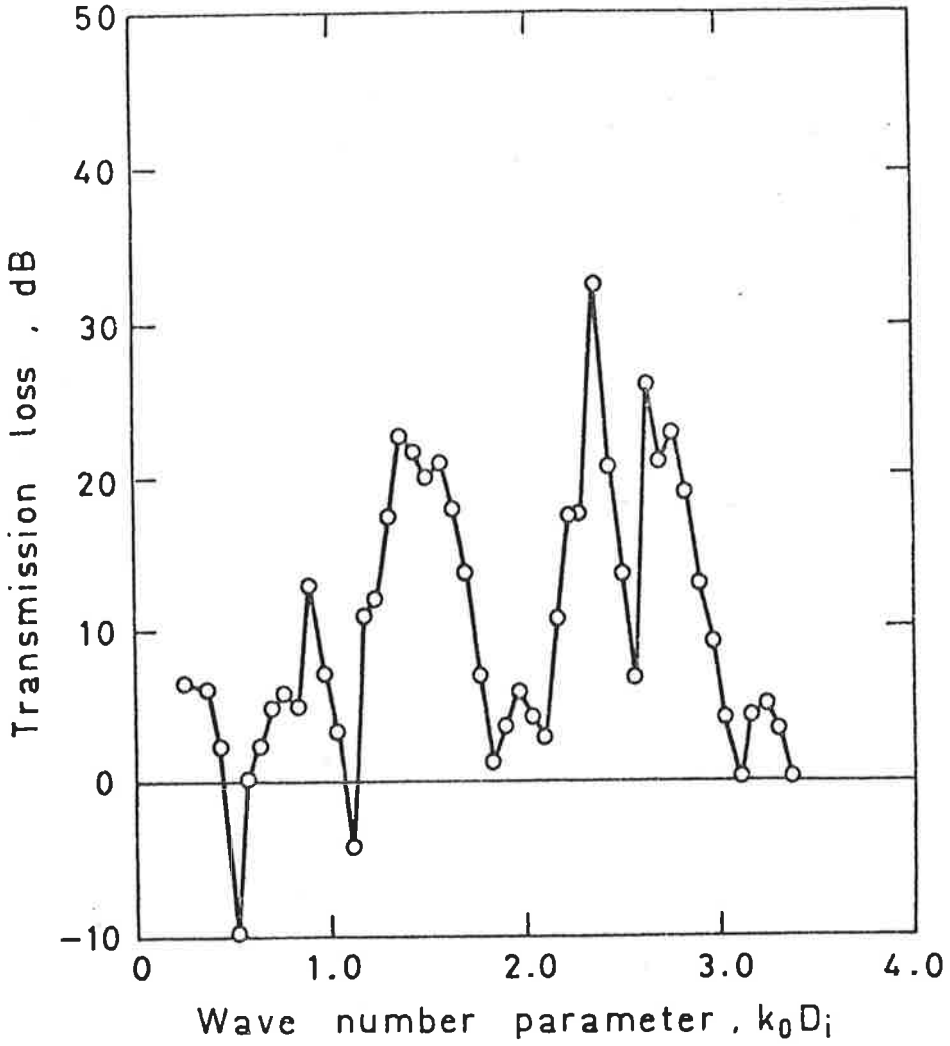

FIGURE 7.7. Experimental transmission loss of the delay line attenuator with two orifice plates.

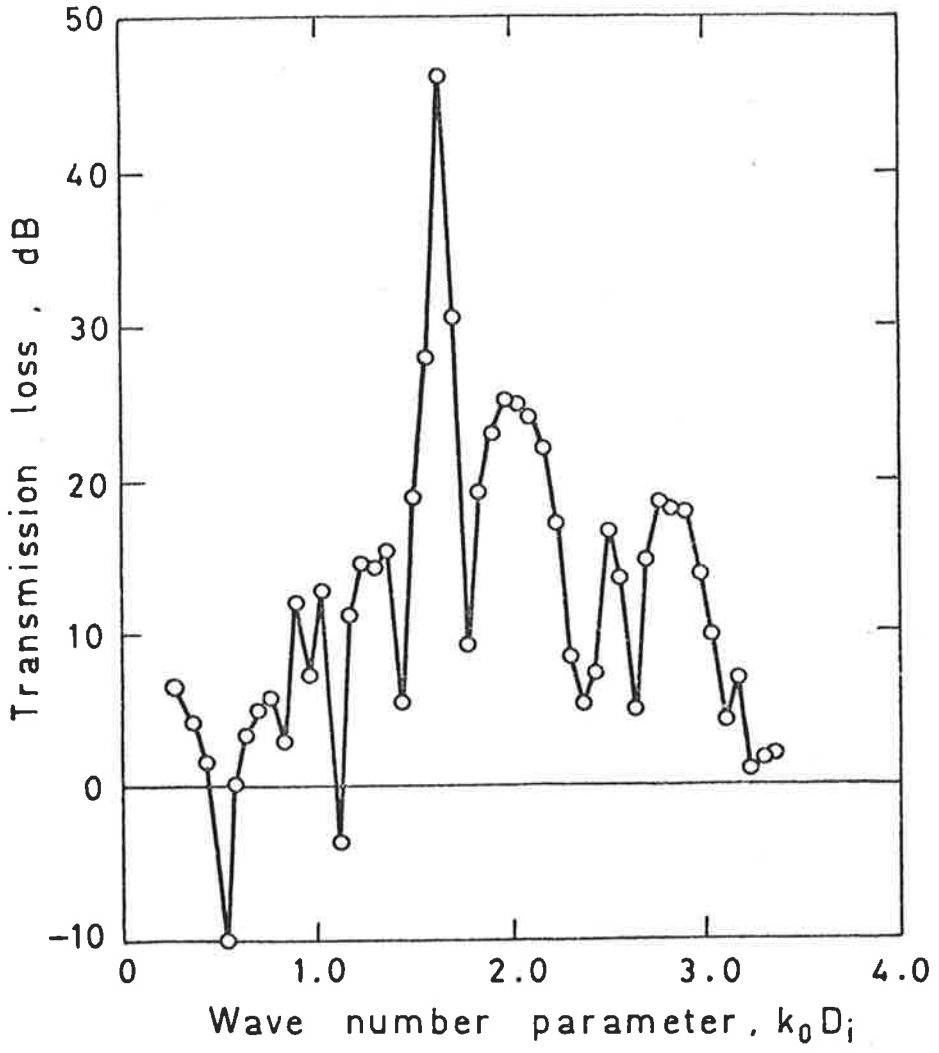

FIGURE 7.8. Experimental transmission loss of the delay line attenuator with three orifice plates.

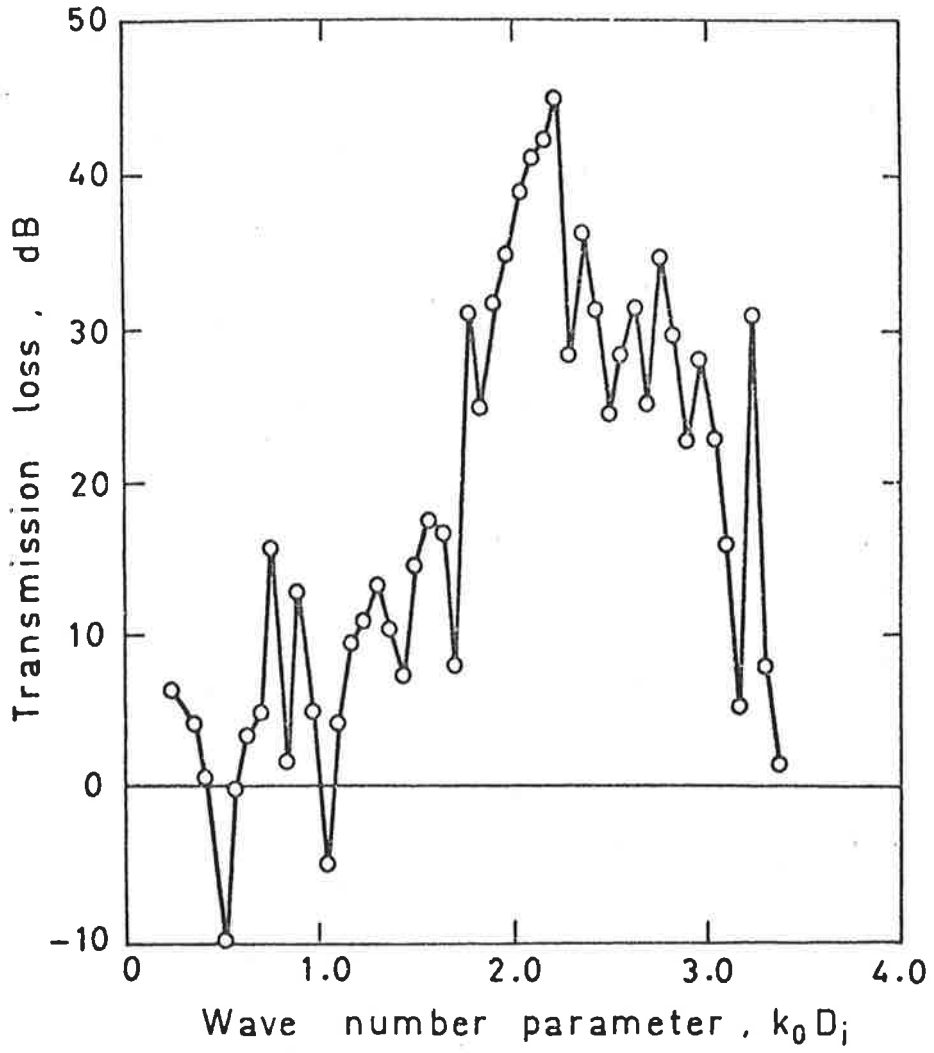

FIGURE 7.9. Experimental transmission loss of the delay line attenuator with four orifice plates.

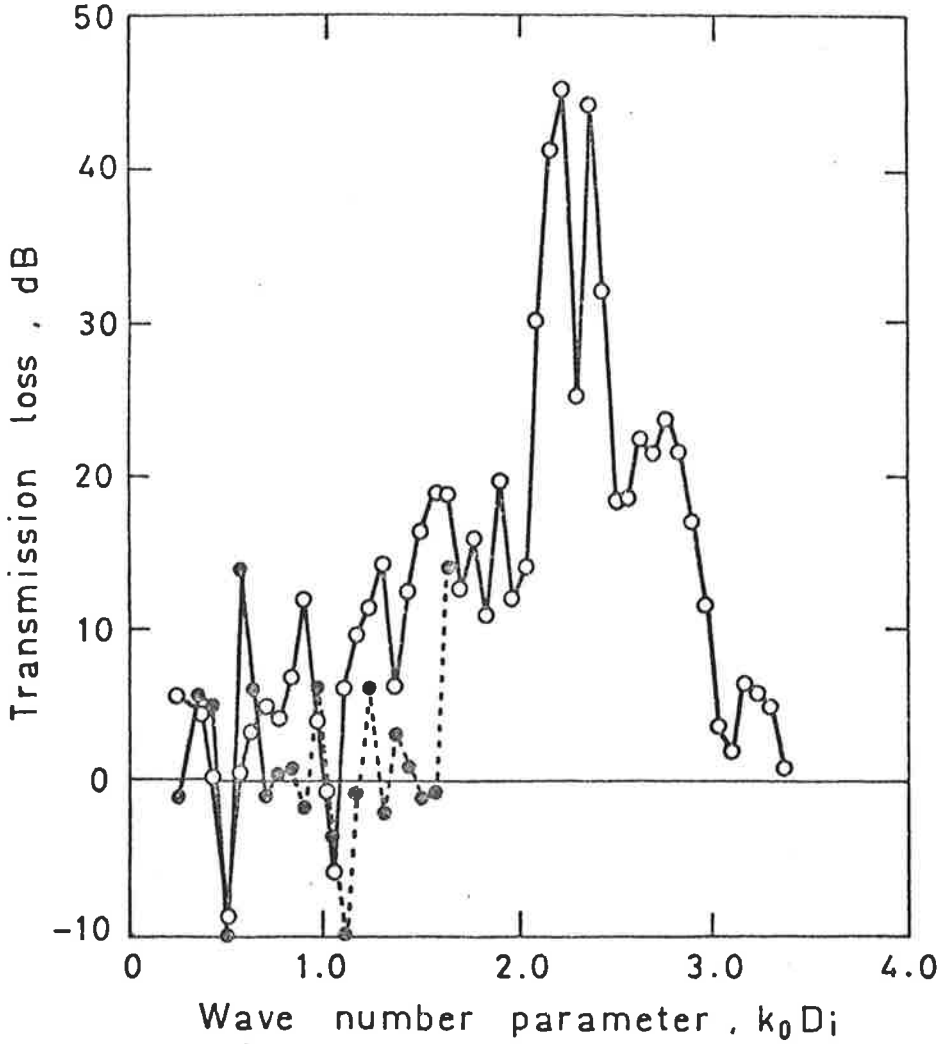

FIGURE 7.10. Transmission loss of the delay line attenuator with five orifice plates. —○— , experimental; —●— , electrical analogy theory. (--●-- , theory becomes inaccurate).

to the length of time between runs) was investigated for both upstream and downstream propagation of sound. Figure 7.11 shows the transmission loss of the 5 plate attenuator for a flow rate of M = 0.22 and the upstream and downstream cases. Figure 7.12 shows the transmission loss of the same attenuator for M = 0.37 and sound propagating downstream. The upstream case was not presented for M = 0.37 due to a poor signal to noise ratio.

The frequencies investigated were limited to less than the cut-off frequency of the (1,0) mode. For a circular pipe of internal diameter of .0724 m with rigid walls, the cut-off frequency of the (1,0) mode was calculated to be 2771 Hz (Morse and Ingard (1968)) hence frequencies investigated were limited to less than 2500 Hz.

7.5 ANALYSIS

In many cases of sound propagating in tubes the dimensions of the various parts of the tube are small compared with the wavelength of sound. In this case the behaviour of the sound in the tube is analogous to the behaviour of an electric circuit with suitable lumped circuit elements of capacitance, inductance and resistance. For higher frequencies transmission effects must be taken into account; the duct system must be described by transmission line theory. In lumped circuit analysis, acoustic pressure is analogous to the voltage drop across the corresponding part of the equivalent electrical circuit while acoustic volume velocity is the analogue of current. Duct systems or attenuators basically consist of constrictions and volumes. To correctly analyse the resulting circuit it is necessary to develop expressions for the electrical analogues of volumes and constrictions (orifices). The appropriate derivation of these relations is well explained by Morse and Ingard (1968).

Cavities or volumes are analogous to electrical capacitors as an additional volume of fluid introduced into the volume causes an

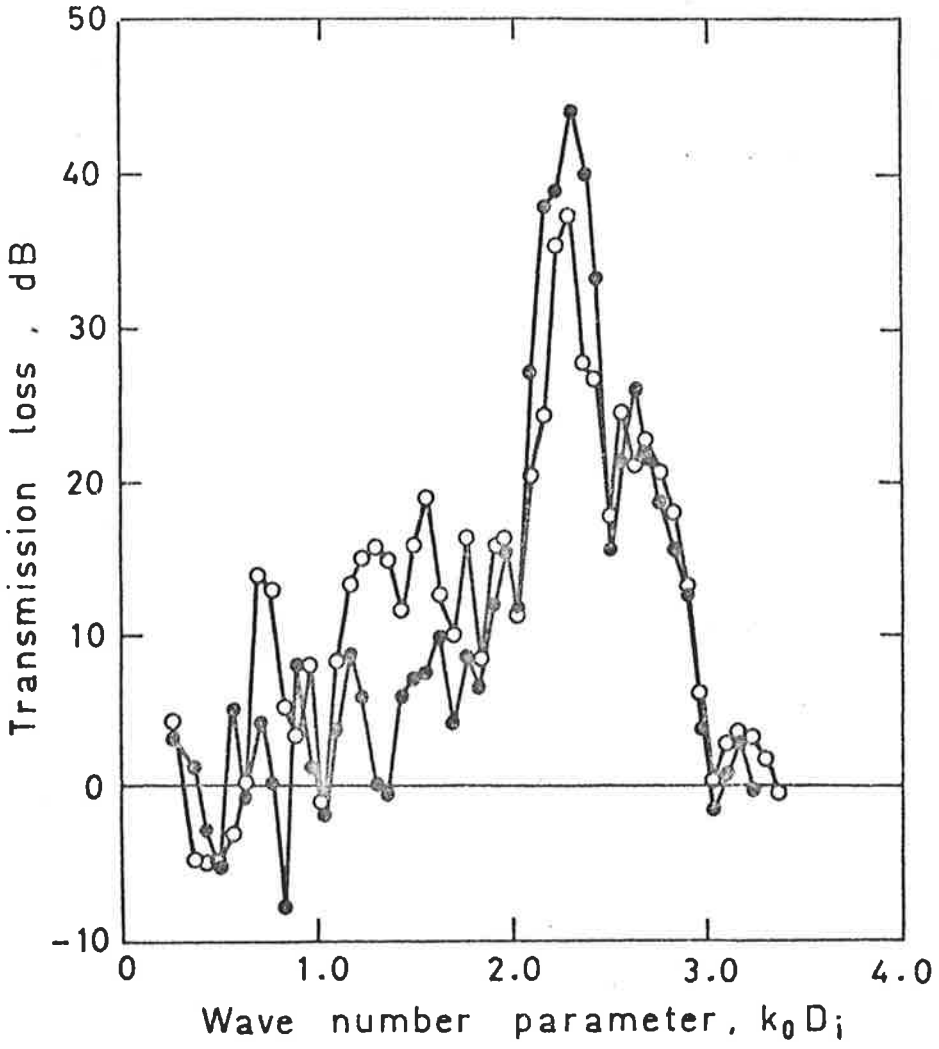

FIGURE 7.11. Experimental transmission loss of the delay line attenuator with five orifice plates and a flow rate of M = 0.22. —○— , downstream propagation of sound; —●— , upstream propagation of sound.

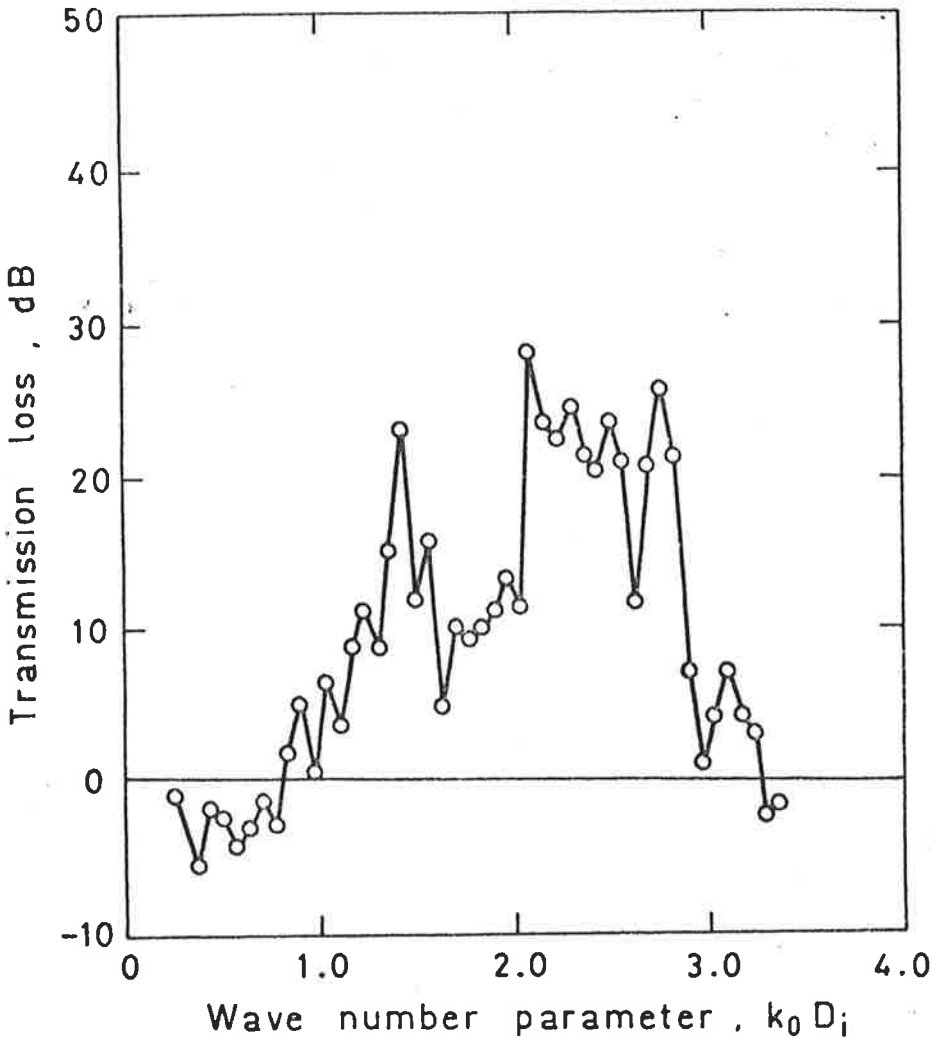

FIGURE 7.12. Experimental transmission loss of the delay line attenuator with five orifice plates, a flow rate of M = 0.37 and downstream propagation of sound.

increase in pressure. Thus cavities or volumes store energy in potential form. If one considers the acoustically induced cyclic flow through a constriction or orifice in the duct system it is apparent that the acoustic energy will pass through the orifice largely in the form of kinetic energy. The impedance of such an orifice for low sound pressure levels and zero flow of the propagating medium is essentially inductive. When there is an energy loss in the duct system due to radiation of sound from an outlet or losses due to viscosity, the analogous electrical element used is resistance.

Lumped circuit analysis is only applicable to low frequencies such that the wavelength of sound is much longer than the filter element major dimensions. Estimates of the maximum ratio of major device dimension to wavelength allowable, range from 1/8 to 1/2 a wavelength. In this analysis the proposed frequency limit of the analysis will be taken as when the ratio of the major attenuator dimension to wavelength is 0.5. The major dimension of the attenuator is 0.4 m thus the upper limiting frequency of the analysis will approximately be 430 Hz or $k_o D_i = 0.58$, however as will be shown the theoretical predictions agree quite well for frequencies above this upper limiting frequency.

The attenuator of Figure 7.1, modelled in terms of analogous electrical elements of capacitance and inductance is shown in Figure 7.13 for a 5 plate arrangement. As shown in Figure 7.13 a small 1 ohm resistor is inserted in the main duct line (between nodes 1 and 9) to avoid a loop of inductances, a condition under which analysis of the circuit is not possible. The value of resistor used, although it makes analysis possible, does not affect the result substantially. Viscosity effects at all orifices are ignored and thus the impedance of the orifices is assumed purely inductive. The

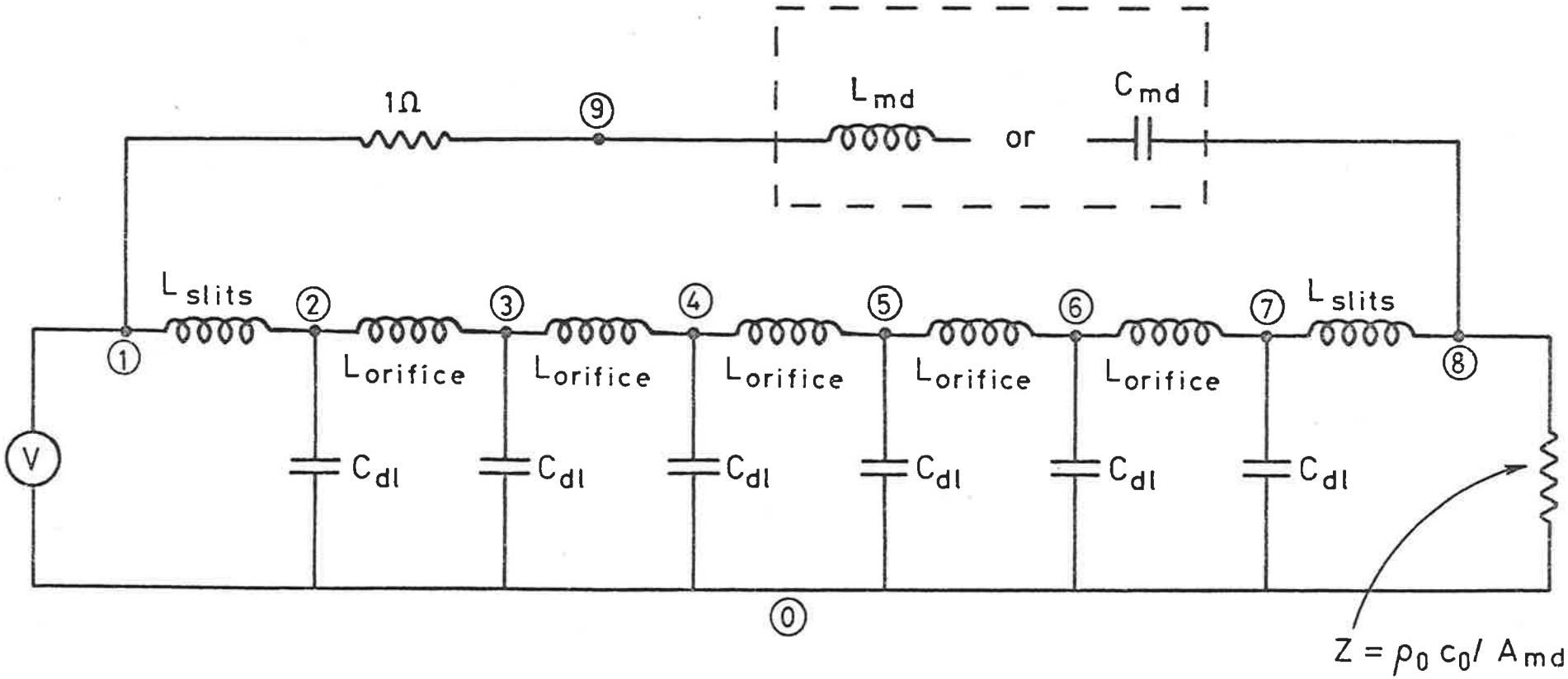

FIGURE 7.13. Equivalent electrical circuit of the delay line attenuator with five orifice plates.

downstream duct is assumed to look infinite to waves leaving the attenuator and can be represented as an impedance with a value of $Z = \rho_o c/A_{md}$ where A_{md} is the cross sectional area of the main duct. The impedance of the main duct is represented by either an inductance or capacitance, depending upon the driving frequency and is in parallel with the delay line duct. This will be discussed in more detail later.

The equivalent electrical capacitance values of the cavities between orifices in the delay line are given by

$$C_{eq} = A_{d\ell} X_{d\ell}/\rho_o c_o^2 \tag{7.1}$$

where $A_{d\ell}$ is the cross sectional area of the delay line and $X_{d\ell}$ is the length between plates. Thus for the 5 plate attenuator of the dimensions of Figure 7.1 spaced evenly apart the value of equivalent capacitance is

$$C_{eq} = 4.473 \text{ n Farads}$$

The inductance of the orifices or constriction is given by an equivalent inductance such that

$$L_{eq} = \frac{\rho_o \ell_e}{A_o} \tag{7.2}$$

where A_o is the area and ℓ_e is the "effective length" of the orifice and is given by

$$\ell_e = t_o + .8\sqrt{A_o} \tag{7.3}$$

and t_o is the orifice thickness. The "effective length" allows for the fact that there will be a small volume of air somewhat larger than the actual orifice which will participate in the induced motion. For the orifice plates of Figure 7.1, the effective length is thus

$$\ell_e = .007 + 0.04899$$

$$= 0.056 \text{ m}$$

Thus for the main casing of .4 m in length the maximum number of plates used in the investigation was limited to 5 to ensure that adjacent orifices did not acoustically interact with each other, therefore affecting the delay line. Equation (7.3) is ideally derived for a circular orifice in a circular plate but was thought to approximately apply at very low frequencies to the annular orifices used here. The inductance of the orifice openings in the delay line is thus

$$L_{eq} = 18.069 \text{ Henrys}$$

Morse and Ingard (1968) give an expression, shown in equation (7.4) for the equivalent electrical inductance of rectangular holes or circular orifices. In the lack of other information this expression is used to describe approximately the impedance of the slits in the main duct wall leading to the delay line. As 8 slits were used at the same position, arranged circumferentially, the total inductance of the arrangement can be considered as all 8 inductances in parallel. Viscosity effects through the slits were ignored. This assumption was thought to be justified as the slits are reasonably wide (.07 m).

Thus,

$$\text{Equivalent Inductance of one slit} = \frac{\rho_o X_s}{4A_s} \qquad (7.4)$$

where X_s is the circumferential length of the orifice and A_s is the area of the slit. Thus the total inductance of each arrangement of 8 slits is

$$L_{eq} = (1/8)\ (27.3025)$$

$$= 3.1428 \text{ Henrys}$$

Harris (1957) gives the impedance of a section of duct with an open end as

$$Z = i\frac{\rho_o c_o}{A_{md}} \tan\ [k_o(X + 2\alpha^*)] \qquad (7.5)$$

where in this case α^* is the end correction factor given by

$$\alpha^* = 0.82R_2 \qquad (7.6)$$

X is the length of duct, A_{md} is the cross sectional area of the main duct and R_2 the outside diameter of the duct. Thus the effective length of the main duct of the attenuator is

$$\ell_e = .375 + .059$$

$$= 0.434 \text{ m}$$

It can be seen that for varying frequencies equation (7.5) will be either positive or negative and thus the impedance of the main duct will be either inductive or capacitive depending upon the driving frequency. For $0 < k_o\ell_e < \pi/2$ the impedance is inductive and the analogous electrical value of the main duct of the attenuator can be determined from

$$L_{eq} = \frac{\rho_o}{A_{md}k_o} \tan\ (k_o\ell_e) \qquad (7.7)$$

When the wavelength of sound is much larger than the length of the main duct, $\tan(k_o\ell_e) \simeq k_o\ell_e$ and equation (7.7) reduces to

$$L_{eq} \simeq \frac{\rho_o\ell_e}{A_{md}} \qquad (7.8)$$

which is identical to equation (7.2). Thus for very low frequencies the impedance of the main duct is approximately constant and inductive and its value is

Inductance of main duct $\simeq$ 127.56 Henrys

while for higher frequencies such that $k_o \ell_e < \pi/2$ the inductance will be given by equation (7.7).

When $\pi/2 < k_o \ell_e < \pi$ the impedance of the main duct given by equation (7.5) is negative and is thus capacitive. In this case the equivalent electrical value is given by

$$C_{eq} = -\frac{A_{md}}{\rho_o c_o^2 k_o} \cot(k\ell_e) \qquad (7.9)$$

Values of equivalent inductance and capacitance for frequencies from 200 to 1400 Hz were derived from equations (7.7) and (7.9) to be used in the later analysis. The performance of the analogous electrical circuit of Figure 7.13 was analysed using a computer library program "SPICE" and a Cyber 6400 computer.

"SPICE" is a general purpose circuit simulation program for nonlinear D.C., nonlinear transient and linear A.C. analyses. Circuits may contain resistors, capacitors, inductors, independent voltage and current sources and other electrical parameters. "SPICE" uses a dynamic memory management to store elements, models and output values and can thus be used for very complex circuits with up to 500 nodes.

The driving voltage across the input to the equivalent circuit was assumed to be 1 volt. Thus without any attenuator the current through the impedance which represents the downstream duct will be 1/Res where Res = $\rho_o c_o / A_{md}$ and the power radiated downstream

will be 1/Res Watts. With the attenuator in position the voltage drop across the impedance representing the downstream duct is calculated from "SPICE" to be V_{80} (where the subscripts imply nodal position in the equivalent electrical circuit). Thus the power radiated downstream with the attenuator in position is V_{80}^{2}Res. The theoretical transmission loss of the attenuator given by the lumped circuit analysis is

$$\text{Transmission Loss} = -20 \log_{10} \left(\frac{V_{80}}{1} \right) \qquad (7.10)$$

For the case of infinite downstream duct the theoretical transmission loss is identical to insertion loss. Values of theoretical transmission loss derived using the lumped circuit analysis for the 5 plate attenuator with no flow are plotted in Figure 7.10 for comparison with experimental results. The broken line at higher frequencies indicates when the theory tends to be increasingly unreliable due to a shortening of wavelength relative to the major attenuator dimensions. The theory was not derived for other arrangements of the attenuator with fewer orifice plates due to length of computing time.

For the very low frequency range (0 to 200 Hz) the 5 plate attenuator was analysed theoretically using equation (7.8) for the inductance of the main duct of the device and was found to provide negligible transmission loss in this frequency range.

7.6 DISCUSSION OF RESULTS

7.6.1. No Flow of the Propagating Medium

Figures 7.6 to 7.10 which show the transmission loss of the attenuator with no flow and with 1 to 5 orifice plates demonstrate that the attenuator provides excellent rejection of sound over a

broad frequency range. Increasing the number of plates is seen both to increase the attenuation obtained at the maximum and increase the bandwidth over which a minimum of 10 dB transmission loss is obtained. The best transmission loss characteristics shown in Figure 7.10 were obtained with a 5 plate arrangement of the attenuator, where a continuous rejection band of greater than 10 dB was obtained from $k_o D_i = 1.4$ to $k_o D_i = 2.95$ which corresponds to a bandwidth of greater than an octave. As well as this high levels of rejection of greater than 20 dB were measured over 322 Hz centered on a frequency of maximum rejection of 1640 Hz. Figures 7.6 to 7.10 show that increasing the number of orifice plates increases the design frequency until the design frequency stabilizes when four orifice plates are used. Further increases in design frequency are probably limited by the end effect of the orifice in the delay line.

As stated previously the rejection of sound of the delay line attenuator is dependent upon an impedance mismatch generated at the device exit by a series of evanescent cross modes. Thus the performance of the attenuator is independent of the impedance of the termination of the downstream duct, as opposed to reactive devices such as an expansion tube muffler where performance depends upon the length of the downstream duct. To verify this the transmission loss of the attenuator with a .83 m length of open duct as a termination was measured experimentally. In this case the standing waves upstream and downstream of the attenuator were measured separately and the transmission loss calculated from the measured maxima and reflection coefficient. The experimental transmission loss of the 5 plate attenuator is shown in Figure 7.14 without flow. As can be seen the measured values are very similar to those shown in Figure

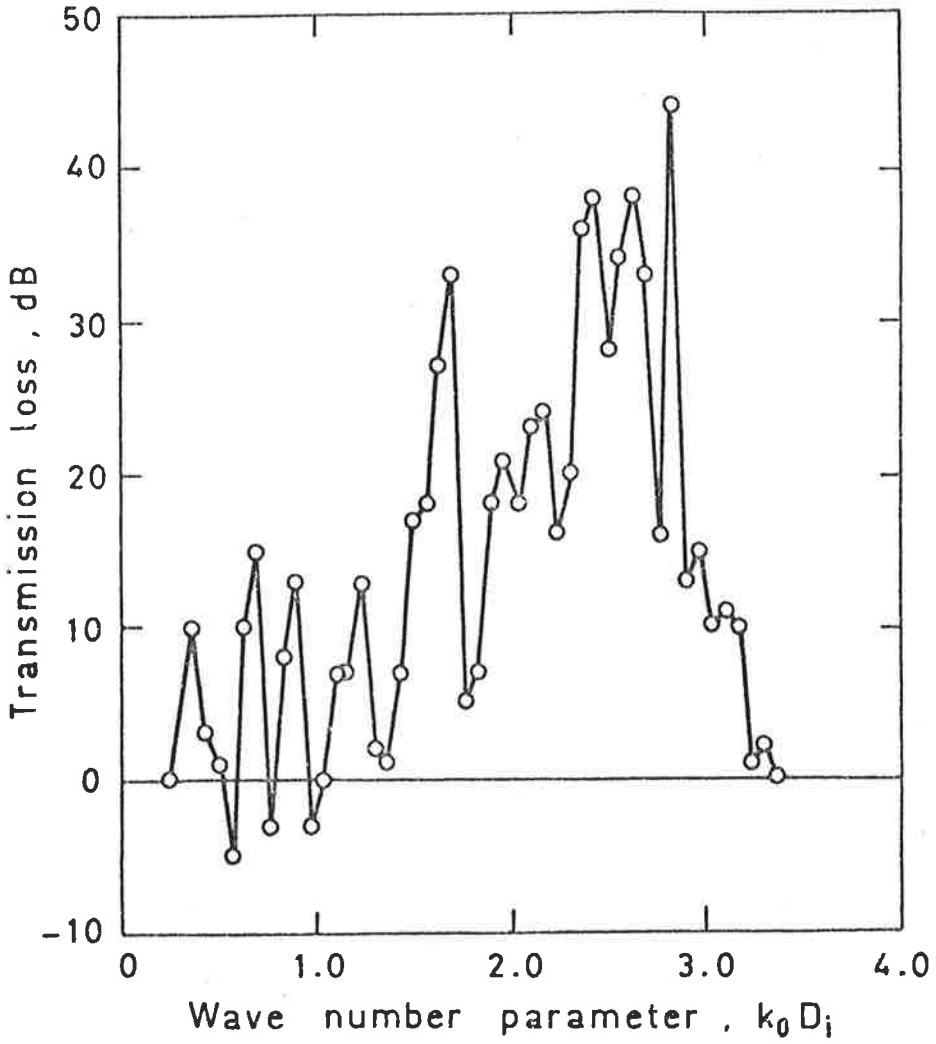

FIGURE 7.14. Experimental transmission loss of the delay line attenuator with five orifice plates and a semi-reflecting termination.

7.10 which are for the 5 plate attenuator with a downstream anechoic termination. This result confirms that the performance of the attenuator is independent of the impedance of the downstream duct termination.

The electrical analogy of the transmission loss of the attenuator shown for the 5 plate arrangement in Figure 7.10 is found to provide a reasonably accurate prediction of the performance of the attenuator at low frequencies ($k_o D_i < 1.75$). The analysis in fact is found to agree for frequencies well in excess of the half-wavelength limit proposed. This was thought to be due to the use of the frequency dependent impedance of the main duct of the attenuator. As discussed previously the expression used approximately describes resonance in this duct section. Hence this section of the attenuator is actually modelled as a transmission line element.

The theory shown in Figure 7.10 appears to be displaced to higher frequencies with respect to experimental results. This could be due to variation in effective length of the main duct. If a longer effective length was used in the theoretical analysis the theoretical curve would agree very closely to experimental values.

It can be seen from Figure 7.10 that at higher frequencies the theory does not match peaks displayed in the experimentally measured transmission loss. These peaks are due to resonant conditions in sections of the attenuator and the values of transmission loss obtained are limited by viscosity effects through the orifices. Viscosity has been ignored in the lumped circuit analysis and this may lead to inaccuracies at resonant conditions.

Figure 7.10 shows that when $k_o D_i = 0.5$ and $k_o D_i = 1.1$ a negative transmission loss was measured. This result was also

indicated by the theoretical result as well, at values close to these frequencies. The amplification of sound at particular frequencies is characteristic of reactive mufflers and is due to resonances in elements of the attenuator.

The theoretical result is seen to be inaccurate at higher frequencies ($k_o D_i > 1.7$) and to fully describe the theoretical performance of the attenuator, transmission line methods must be used in this higher frequency range. It was proposed to model the attenuator in the higher frequency range by calculating the phase speeds of waves through the delay line section at different frequencies using transmission line theory. By using a "black box" approach and only considering the inlet and exit interfaces of the attenuator and using the effective phase speed of waves in the delay line section one could determine the relative phases of travelling waves at each interface. The theoretical transmission loss could then be derived using a procedure of matching continuity conditions as in Chapters 5 and 6. In this case the equations used would be for sound propagation in straight circular ducts and the pressure distribution assumed at both interfaces would be that of Figure 7.2 with relative phase determined by the delay line theory. However due to time limitations and lack of knowledge of the inductances of the annular orifices (as opposed to circular orifices) and the inlet slits, this was not attempted.

Referring to Figure 7.13 which is the equivalent electrical circuit of the attenuator, it can be seen that when the impedance of the main duct is zero then the delay line section will be completely shorted out and zero transmission loss will occur. The frequencies at which this should theoretically occur are given by $k_o \ell_e = n\pi$,

n = 0, 1, 2 .... One can thus conclude that to optimize the bandwidth of the attenuator, i.e. move the minima to lower frequencies, the main duct of the attenuator should be made as long as possible. However length considerations are also determined by the desired compactness of the attenuator and a compromise must be sought.

The power transmission coefficient of the attenuator measured from the standing wave is seen to give a reasonably accurate prediction of the performance of the device up to 1200 Hz. However above this frequency, as discussed in Chapters 5 and 6, the minima of the standing wave are too sharp to detect accurately.

7.6.2 With Flow of the Propagating Medium

Due to the length of time of experiments involved with flow, the investigation was limited to the attenuator with 5 orifice plates. This arrangement provided the best performance in the no-flow case. Flow of the propagating medium at M = 0.22 is seen to affect the lower frequencies more than the higher frequencies. Figure 7.11 shows that at M = 0.22 the 10 dB bandwidth is reduced substantially to 0.7 of an octave. However high levels of attenuation are still obtained at $k_o D_i$ = 2.2 as for the no flow case. Flow was thus found not to lower the design frequency as occurred in the investigation of Chapter 6. Figure 6.11 also shows that the attenuator amplifies the incident sound at some particular frequencies (indicated by a negative transmission loss). While some of this amplification is undoubtedly due to resonance within the attenuator, the noise generated by the fluid flow over the slits in the main duct wall was thought to contribute significantly also. This problem could be reduced by careful design of the slits with thought to the fluid flow.

Figure 7.11 demonstrates that the attenuator performance is

basically independent of direction of sound propagation relative to flow. This can be understood by assuming there is no flow in the delay line section of the attenuator. As discussed previously the impedance of the main duct is governed by natural oscillations. Flow has the effect of lowering the natural frequencies of such a tube by a factor of $(1-M^2)$ independent of direction. Thus in this case flow is likely to have an identical effect on the impedance of the main duct for either direction of propagation.

Figures 7.10 and 7.11 show clearly that flow also has the effect of decreasing the magnitude of the negative transmission losses obtained at low frequencies. This effect is most likely caused by the flow "blowing away" the masses of air contained in the slits in the duct wall which provide the necessary inductance.

The main difference between experimental upstream and downstream values occurs at lower frequencies where downstream flow reduces the attenuation obtained by a greater amount than for the upstream case. The reduction in attenuation at low frequencies may also be due to the flow reducing the masses of air contained in the slits in the duct wall and consequently affecting the slit inductance.

The flow rate of M = 0.37 substantially reduces the attenuation obtained at the peaks but provides a broader operating band. The reduction in the attenuation at the peaks may be due to flow regenerated noise but is most likely due to the changes in inductance of the slits and orifices as discussed previously. The broader bandwidth is due to a reduction in resonant frequency of the main duct due to flow and a corresponding decrease in frequency at which zero transmission loss occurs. The flow thus effectively lengthens the main duct. The attenuator was also found to perform better at lower frequencies for a flow rate of M = 0.37 but an increase

in amplification of sound was apparent.

7.7 SUMMARY

A reactive acoustic attenuator for use in straight ducts of circular cross section has been investigated experimentally and theoretically. The attenuator is found to provide excellent rejection of low frequency sound over a broad operating band with and without the presence of high speed flows (M = 0.37). The attenuator is robust, compact and cheap to manufacture.

CHAPTER 8

GENERAL CONCLUSIONS

Propagation and reactive attenuation of low frequency sound in hard-walled ducts have been studied. The investigation has established that reactive attenuation can be employed to control low frequency sound without the usual disadvantages of low pressure drop, excessive size or narrow operating band. The effect of flow on the performance of the attenuators has been investigated and it has been shown that the devices perform well in the presence of a convecting propagating medium. The proposed attenuators are simple in concept and thus should be cheap to manufacture.

The effects of flow on the cut-off frequencies and propagation of energy of higher modes have been investigated. The independence of cut-off frequency from direction of sound propagation relative to flow has been clarified.

A dipole piston source is studied and the theoretical results provide insight into some of the physical aspects of the performance of the attenuator and the effect of flow on modal propagation. This investigation establishes that reflection of sound at an interface similar to the exit plane of the attenuator is entirely due to generation of a series of evanescent modes. Likewise the investigation demonstrates that the reactive impedance of such a surface, which closely approximates the phase distribution of a (1,0) mode when the phase discrepancy between pistons is π radians, becomes infinite at cut-on of the (1,0) mode. This

result is impossible in practice and explains why the cut-on frequency of an evanescent mode is always difficult to determine and cannot be measured with the precision implied by the analysis.

A simple method for analysing propagation of low frequency sound in curved bends has been developed. This method, although it relies on an approximation, accurately and simply predicts the variables necessary to analyse curved duct systems in the low frequency range with and without flow. It eliminates the need to consider complicated Bessell and Neumann functions in its range of application. The analysis is subsequently used to analyse an attenuator with flow.

The difference between sound propagation in curved bends and straight ducts is highlighted by an analysis which considers the effect of a partition in a curved bend. The partition is found to cause high reflection of sound at a number of frequencies due to the dependence of the curved duct wavenumber on the bend geometry, whereas the corresponding straight duct wavenumber is independent of duct dimensions.

The thesis leaves unanswered many questions. Of those areas needing more research, perhaps the theoretical analysis of the attenuator of Chapter 7 takes priority. To fully understand the performance of the delay line attenuator some preliminary investigations into the phase speed through the annular delay line would have to be undertaken. Combined with the "black box" model proposed in Chapter 7, this knowledge would provide a theoretical description of the attenuator, without which it is hard to predict design frequencies and optimize band widths. However due to time limitations this was not attempted.

It would be of interest to experimentally study the effect of flow on the cut-off frequencies of higher order modes. A particularly clear demonstration of this effect might be possible in a ripple tank.

The mode under study could be driven by two "dabbers" exciting the surface of the water at the required frequency near cut-on, while convection could be simulated by means of a steady flow of water through the tank. It would be extremely interesting to see the angle of propagation of wavefronts for the downstream case as the mode approaches cut-on.

These and other problems uncovered in the work of this thesis remain as research work for the future.

APPENDIX 1

THE WAVE EQUATION

As all propagation theory stems from solutions of the wave equation in different coordinate systems it is appropriate here to describe the different forms of the wave equation used and the assumptions made in their derivations.

Perhaps the most complete derivation of the wave equation is given by Morse and Feshbach (1953). In terms of the velocity potential, whose partial derivatives with respect to the axis of the chosen coordinate system are the components of velocity in those directions, it can be written as

$$\nabla^2\phi = (1/c_o^2)\,\partial^2\phi/\partial t^2 \qquad (A.1)$$

where $c_o^2 = \chi_m/\rho_o$. χ_m is the bulk modulus and ρ_o is the undisturbed density of the propagating medium.

The wave equation can be interpreted as physically stating (from Rschevkin (1963)) "an excess concentration causes a decrease in the rate at which concentration increases, and a defect in concentration results in an increase in this rate."

The assumptions made in the deriviation of the wave equation are well documented in Rschevkin (1963). The main points, relevant to the following analyses, are summarized here.

Main assumptions made in the derivation of the wave equation

1. The medium is assumed inviscid.
2. The mean pressure and density are assumed constant.

3. Spatial forces are neglected.

4. The steady velocity components and their gradients are assumed small.

5. The oscillatory velocity components and their gradients are assumed small.

6. The motion is assumed to be irrotational.

7. Only small deformations of the medium are assumed to occur, with deformations being linear.

8. The propagating medium is assumed uniform.

Some of the major implications of these assumptions are:

1. Assumption (1) implies that viscosity is ignored, thus acoustic energy is not dissipated through conversion to heat.

2. Assumption (5) implies that the wave equation is only applicable to slowly (relatively) oscillating pressures and not to sudden disturbances such as shock waves.

3. Assumption (5) implies that the convected velocity terms in the case of no flow of the propagating medium is small and that this part of the momentum balance can be ignored.

4. Assumption (7) limits the application of the wave equation to small deformations of the particles and thus places an upper bound in terms of sound pressure level ($\simeq$ 160 dB in air) at which the wave equation can still be considered linear.

If the particle oscillatory motion is harmonic, the time component can be separated. For example the solution in terms of the potential function may be written as

$$\phi(x,y,z,t) = \psi(x,y,z)e^{i\omega t} \qquad (A.2)$$

where ψ is a characteristic function solely of the coordinates and ω is the angular frequency of oscillation. In this case equation (A.1) reduces to the well known Hemholtz equation

$$\nabla^2\psi + k_o^2\psi = 0 \qquad (A.3)$$

where k_o is equal to ω/c_o and is called the wave number.

From the definition of the velocity potential expressions for the particle velocity of the acoustic motion follow:

$$\underset{\sim}{u} = +\nabla\phi \tag{A.4}$$

When the convected velocity term is small the acoustic pressure is given by the following:

$$p = -\rho_o \partial\phi/\partial t \tag{A.5}$$

In this case according to equation (A.5), the wave equation can be written in the alternative well used form

$$\nabla^2 p = (1/c_o^2)\partial^2 p/\partial t^2 \tag{A.6}$$

The form of vector operators in the coordinate systems used in the analysis of the text are as follows:

Rectangular coordinates

$$\nabla\phi_x = \partial\phi/\partial x, \quad \nabla\phi_y = \partial\phi/\partial y, \quad \nabla\phi_z = \partial\phi/\partial z \tag{A.7}$$

and $$\nabla^2\phi = \partial^2\phi/\partial x^2 + \partial^2\phi/\partial y^2 + \partial^2\phi/\partial z^2 \tag{A.8}$$

Clyindrical coordinates

$$\nabla\phi_r = \partial\phi/\partial r, \quad \nabla\phi_\theta = (1/r)\partial\phi/\partial\theta, \quad \nabla\phi_z = \partial\phi/\partial z \tag{A.9}$$

and $$\nabla^2\phi = \partial^2\phi/\partial r^2 + (1/r)\partial\phi/\partial r + (1/r^2)\partial^2\phi/\partial\theta^2 \tag{A.10}$$

If a pressure form of the wave equation as given by equation (A.6) is used then the particle velocities in terms of the pressure solution are

$$\underset{\sim}{u} = -(1/i\rho_o c_o k_o)\nabla p . \tag{A.11}$$

The Wave Equation with Convection of the Propagating Medium

The derivation of the wave equation with uniform flow is well explained by Morse and Ingard (1968). In addition to the assumptions previously made, the medium is assumed to travel with uniform velocity independent of the direction of sound propagation. However it must be noted that assumption (5) cannot be applied here. Whereas in the no flow case the convected velocity of the particles is the acoustic particle velocity and therefore very small, in the case of flow of the propagating medium this convected velocity term will be replaced by the velocity of the medium and therefore cannot be ignored.

Assumption (1) also has important implications in the case of flow of the propagating medium. Due to the lack of viscosity such fluid properties as boundary layers and separation are ignored and the flow is assumed uniform (potential).

Thus the linearized momentum equation relating particle velocity and acoustic pressure for flow of the medium is

$$\rho_o(\partial/\partial t + \underset{\sim}{V}.\nabla)u = -\partial p/\partial x \qquad (A.12)$$

where $\underset{\sim}{V} = V_x\underset{\sim}{i} + V_y\underset{\sim}{j} + V_z\underset{\sim}{z}$ is the vector describing velocity magnitude and direction of the medium.

The wave equation with flow can thus be written in velocity potential form as (from Morse and Ingard (1968))

$$(1/c_o^2)(\partial/\partial t + \underset{\sim}{V}.\nabla)^2\phi = \nabla^2\phi \qquad (A.13)$$

The acoustic particle velocity is given simply by

$$\underset{\sim}{u} = +\nabla\phi \qquad (A.14)$$

However, since the convective acceleration is not negligible,

in the one dimensional case equation (A.12) becomes for fluid flow in the x direction

$$-\partial p/\partial x = \rho_o \partial u_x/\partial t + \rho_o V_x \partial u_x/\partial x$$

Now $$u_x = +\partial\phi/\partial x$$

then $$\partial p/\partial x = -\rho_o \partial^2\phi/\partial t\partial x - \rho_o(\partial\phi/\partial x)(\partial^2\phi/\partial x^2)$$

Since $$(1/2)\partial(\partial\phi/\partial x)^2/\partial x = (\partial\phi/\partial x)(\partial^2\phi/\partial x^2)$$

then $$\partial/\partial x\,[p + \rho_o \partial\phi/\partial t + (1/2)\rho_o(\partial\phi/\partial x)^2] = 0$$

Letting the constant of integration equal zero this becomes

$$p = -\rho_o \partial\phi/\partial t - (1/2)\rho_o(\partial\phi/\partial x)^2 \qquad (A.15)$$

More generally in three dimensions

$$p = -\rho_o\, \partial\phi/\partial t - (1/2)\rho_o \nabla^2\phi \qquad (A.16)$$

Hence if V_x is large then $u = V_x + u_x$ is large and in this case

$$p = -\rho_o \partial\phi/\partial t - \rho_o V_x \partial\phi/\partial x \qquad (A.17)$$

The wave equation can also be written in terms of a pressure solution as for the no flow case. This well used form (Morse and Ingard (1968))

$$(1/c_o^2)(\partial/\partial t + \underset{\sim}{V}.\nabla)^2 p = \nabla^2 p \qquad (A.18)$$

When the motion is governed by a harmonic time dependence, the Hemholtz equation with flow follows.

$$\nabla^2 p + (\omega/c_o)^2(1 + i(1/\omega)\underset{\sim}{V}.\nabla)^2 p = 0 \qquad (A.19)$$

The form of the wave equation in terms of the pressure solution is identical to the form of the wave equation in terms of the potential function as may be seen by comparing equations (A.13) and (A.18), thus p and ϕ must differ by a multiplicative constant. Hence we conclude that the particle velocity may again be determined from the pressure solution using equation (A.11).

The convection terms introduced by flow will be found to significantly modify the solutions of the wave equation.

APPENDIX 2

CONTINUITY EQUATIONS OF THE ANALYSES OF CHAPTERS 4, 5, AND 6

2.A CONTINUITY EQUATIONS AT INTERFACE B OF THE ANALYSIS OF CHAPTER 4

Continuity of pressure at B where $x' = 0$, $\theta = \pi$

provides

$m = 0$,

$$E^i_{oo}h = C^i_{oo}\int_{R_1}^{R_2}\psi^c_{oo}\exp[-i\nu_o\pi]dr + \sum_{s=0}^{\infty} C^r_{so}\int_{R_1}^{R_2}\psi^c_{so}\exp[i\nu_s\pi]dr$$

$$+ D^i_{oo}\int_{R_2}^{R_3}\psi^c_{oo}\exp[-i\nu_o\pi]dr + \sum_{s=0}^{\infty} D^r_{so}\int_{R_2}^{R_3}\psi^c_{so}\exp[i\nu_s\pi]dr \qquad (A.20)$$

$m \neq 0$,

$$E^i_{oo}h/2 = C^i_{oo}\int_{R_1}^{R_2}\psi^c_{oo}\exp[-i\nu_o\pi]\cos[(m\pi/h)(r-R_1)]dr$$

$$+\sum_{s=0}^{\infty} C^r_{so}\int_{R_1}^{R_2}\psi^c_{so}\exp[i\nu_s\pi]\cos[(m\pi/h)(r-R_1)]dr$$

$$+ D^i_{oo}\int_{R_2}^{R_3}\psi^c_{oo}\exp[-i\nu_o\pi]\cos[(m\pi/h)(r-R_1)]dr$$

$$+\sum_{s=0}^{\infty} D^r_{so}\int_{R_2}^{R_3}\psi^c_{so}\exp[i\nu_s\pi]\cos[(m\pi/h)(r-R_1)]dr \qquad (A.21)$$

Continuity of tangential particle velocity at B provides,

$m = 0$,

$$E^i_{oo} k_{oo} h = C^i_{oo} \int_{R_1}^{R_2} \psi^c_{oo}(\nu_o/r) \exp[-i\nu_o\pi]dr$$

$$- \sum_{s=0}^{\infty} C^r_{so} \int_{R_1}^{R_2} \psi^c_{so}(\nu_s/r) \exp[i\nu_s\pi]dr$$

$$+ D^i_{oo} \int_{R_2}^{R_3} \psi^c_{oo}(\nu_o/r) \exp[-i\nu_o\pi]dr$$

$$- \sum_{s=0}^{\infty} D^r_{so} \int_{R_2}^{R_3} \psi^c_{so}(\nu_s/r) \exp[i\nu_s\pi]dr \qquad (A.22)$$

$m \neq 0$,

$$E^i_{mo} k_{mo} h/2 = C^i_{oo} \int_{R_1}^{R_2} \psi^c_{oo}(\nu_o/r) \exp[-i\nu_o\pi]\cos[(m\pi/h)(r-R_1)]dr$$

$$- \sum_{s=0}^{\infty} C^r_{so} \int_{R_1}^{R_2} \psi^c_{so}(\nu_s/r) \exp[i\nu_s\pi]\cos[(m\pi/h)(r-R_1)]dr$$

$$+ D^i_{oo} \int_{R_2}^{R_3} \psi^c_{oo}(\nu_o/r) \exp[-i\nu_o\pi]\cos[(m\pi/h)(r-R_1)]dr$$

$$- \sum_{s=0}^{\infty} D^r_{so} \int_{R_2}^{R_3} \psi^c_{so}(\nu_s/r) \exp[i\nu_s\pi]\cos[(m\pi/h)(r-R_1)]dr \qquad (A.23)$$

2.B CONTINUITY EQUATIONS AT INTERFACES B, C AND D OF THE ANALYSIS OF CHAPTER 5

Continuity of pressure at B where $x' = X$ and $\theta' = 0$ provides,

$\ell = 0$,

$$A^i_{oo}(h/2) \exp[-ik_{oo}X] + A^r_{oo}(h/2) \exp[ik_{oo}X]$$

$$= \sum_{s=0}^{\infty} D^i_{so} \int_{R_3}^{R_4} \psi^c_{so} dr' + D^r_{oo} \int_{R_3}^{R_4} \psi^c_{oo} dr' \qquad (A.24)$$

$\ell \neq 0$,

$$A^r_{\ell o}(h/4)\exp[ik_{\ell o}X] = \sum_{s=0}^{\infty} D^i_{so} \int_{R_3}^{R_4} \psi^c_{so}\cos[(2\ell\pi/h)(r'-R_3)]dr'$$

$$+ D^r_{oo} \int_{R_3}^{R_4} \psi^c_{oo}\cos[(2\ell\pi/h)(r'-R_3)]dr' \qquad (A.25)$$

Continuity of tangential particle velocity at B provides,

$\ell = 0$,

$$A^i_{oo}k_{oo}(h/2)\exp[-ik_{oo}X] - A^r_{oo}k_{oo}(h/2)\exp[ik_{oo}X]$$

$$= \sum_{s=0}^{\infty} D^i_{so} \int_{R_3}^{R_4} \psi^c_{so}(\nu_s/r')dr' - D^r_{oo} \int_{R_3}^{R_4} \psi^c_{oo}(\nu_o/r')dr' \qquad (A.26)$$

$\ell \neq 0$,

$$-A_{\ell o}k_{\ell o}(h/4)\exp[ik_{\ell o}X] = \sum_{s=0}^{\infty} D^i_{so} \int_{R_3}^{R_4} \psi^c_{so}(\nu_s/r')\cos[(2\ell\pi/h)(r'-R_3)]dr'$$

$$- D^r_{oo} \int_{R_3}^{R_4} \psi^c_{oo}(\nu_o/r')\cos[(2\ell\pi/h)(r'-R_3)]dr' \qquad (A.27)$$

Continuity of pressure at C where $x'' = -X$ and $\theta' = \pi/2$ provides,

$\ell = 0$,

$$B^i_{oo}(h/2)\exp[ik_{oo}X] + B^r_{oo}(h/2)\exp[-ik_{oo}X]$$

$$= D^i_{oo} \int_{R_3}^{R_4} \psi^c_{oo}\exp[-i\nu_o\pi/2]dr' + \sum_{s=0}^{\infty} D^r_{so} \int_{R_3}^{R_4} \psi^c_{so}\exp[i\nu_s\pi/2]dr' \qquad (A.28)$$

$\ell \neq 0$,

$$B^i_{\ell o}(h/4)\ \exp[ik_{\ell o}X]$$

$$= D^i_{oo} \int_{R_3}^{R_4} \psi^c_{oo}\ \exp[-i\nu_o\pi/2]\cos[(2\pi\ell/h)(r'-R_3)]dr'$$

$$+\sum_{s=0}^{\infty} D^r_{so} \int_{R_3}^{R_4} \psi^c_{so}\ \exp[i\nu_s\pi/2]\cos[(2\pi\ell/h)(r'-R_3)]dr' \qquad (A.29)$$

Continuity of tangential particle velocity at C provides,

$\ell = 0$,

$$B^i_{oo}k_{oo}(h/2)\exp[ik_{oo}X] - B^r_{oo}k_{oo}(h/2)\exp[-ik_{oo}X]$$

$$= D^i_{oo} \int_{R_3}^{R_4} \psi^c_{oo}(\nu_o/r')\exp[-i\nu_o\pi/2]dr'$$

$$-\sum_{s=0}^{\infty} D^r_{so} \int_{R_3}^{R_4} \psi^c_{so}(\nu_s/r')\exp[i\nu_s\pi/2]dr' \qquad (A.30)$$

$\ell \neq 0$

$$B^i_{\ell o}k_{\ell o}(h/4)\exp[ik_{\ell o}X]$$

$$= D^i_{oo} \int_{R_3}^{R_4} \psi^c_{oo}(\nu_o/r')\exp[-i\nu_o\pi/2]\cos[(2\ell\pi/h)(r'-R_3)]dr'$$

$$-\sum_{s=0}^{\infty} D^r_{so} \int_{R_3}^{R_4} \psi^c_{so}(\nu_s/r')\exp[i\nu_s\pi/2]\cos[(2\ell\pi/h)(r'-R_3)]dr' \qquad (A.31)$$

Continuity of pressure at D where $x'' = 0$ and $\theta = \pi/2$ provides,

$m = 0$,

$$E^i_{oo}h = C^i_{oo} \int_{R_1}^{R_2} \psi^c_{oo}\exp[-i\nu_o\pi/2]dr + \sum_{s=0}^{\infty} C^r_{so} \int_{R_1}^{R_2} \psi^c_{so}\exp[i\nu_s\pi/2]dr$$

$$+ B^i_{oo}h/2 + \sum_{\ell=0}^{\infty} B^r_{\ell o} \int_o^{h/2} \psi^s_{\ell o}\, dy'' \qquad (A.32)$$

$m \neq 0$,

$$E^i_{mo} h/2 = C^i_{oo} \int_{R_1}^{R_2} \psi^c_{oo} \exp[-i\nu_o \pi/2] \cos[(m\pi/h)(r-R_1)]dr$$

$$+ \sum_{s=0}^{\infty} C^r_{so} \int_{R_1}^{R_2} \psi^c_{so} \exp[i\nu_s \pi/2] \cos[(m\pi/h)(r-R_1)]dr$$

$$- B^i_{oo} \left(\frac{h}{2m\pi}\right)[1 - (-1)^m]$$

$$+ \sum_{\ell=0}^{\infty} B^r_{\ell o} \int_{o}^{h/2} \psi^s_{\ell o} \cos[(m\pi/h)(y'' + h/2)]dy'' \qquad (A.33)$$

Continuity of tangential particle velocity at D provides,

$m = 0$,

$$E^i_{oo} k_{oo} h = C^i_{oo} \int_{R_1}^{R_2} \psi^c_{oo} (\nu_o/r) \exp[-i\nu_o \pi/2]dr$$

$$- \sum_{s=0}^{\infty} C_{so} \int_{R_1}^{R_2} \psi^c_{so} (\nu_s/r) \exp[i\nu_s \pi/2]dr$$

$$+ B^i_{oo} k_{oo} h/2 - \sum_{\ell=0}^{\infty} B^r_{\ell o} k_{\ell o} \int_{o}^{h/2} \psi^s_{\ell o} \, dy'' \qquad (A.34)$$

$m \neq 0$,

$$E^i_{mo} k_{mo} h/2 = C^i_{oo} \int_{R_1}^{R_2} \psi^c_{oo} (\nu_o/r) \exp[-i\nu_o \pi/2] \cos[(m\pi/h)(r-R_1)]dr$$

$$- \sum_{s=0}^{\infty} \int_{R_1}^{R_2} \psi^c_{so} (\nu_s/r) \exp[i\nu_s \pi/2] \cos[(m\pi/h)(r-R_1)]dr$$

$$- B^i_{oo} k_{oo} \left(\frac{h}{2m\pi}\right)[1 - (-1)^m]$$

$$- \sum_{\ell=0}^{\infty} B^r_{\ell o} k_{\ell o} \int_{o}^{h/2} \psi^s_{\ell o} \cos[(m\pi/h)(y'' + h/2)]dy'' \qquad (A.35)$$

2.C CONTINUITY EQUATIONS AT INTERFACES B, C AND D OF THE ANALYSIS OF CHAPTER 6

Continuity of pressure at B where $x' = X$ and $\theta' = 0$ provides

$$A^i_{oo}(h/2)\ \exp[-ik^d_{oo}X] + A^r_{oo}(h/2)\ \exp[ik^u_{oo}X]$$

$$= D^i_{oo}(h/2) + D^r_{oo}(h/2) \qquad \text{(A.36)}$$

Continuity of tangential particle velocity at B provides

$$A^i_{oo}k_{oo}(h/2)\ \exp[-ik^d_{oo}X] - A^r_{oo}(h/2)\ \exp[ik^u_{oo}X]$$

$$= D^i_{oo}k_{oo}(h/2) - D^r_{oo}k_{oo}(h/2) \qquad \text{(A.37)}$$

Continuity of pressure at C where $x'' = -X$ and $\theta' = \pi/2$ provides,

$$B^i_{oo}(h/2)\ \exp[ik^d_{oo}X] + B^r_{oo}(h/2)\ \exp[-ik^u_{oo}X]$$

$$= D^i_{oo}(h/2)\ \exp[-i\nu^d_o\pi/2] + D^r_{oo}(h/2)\ \exp[i\nu^u_o\pi/2] \qquad \text{(A.38)}$$

Continuity of tangential particle velocity at C provides

$$B^i_{oo}k_{oo}(h/2)\ \exp[ik^d_{oo}X] - B^r_{oo}k_{oo}(h/2)\ \exp[-ik^u_{oo}X]$$

$$= D^i_{oo}k_{oo}(h/2)\ \exp[-i\nu^d_o\pi/2] - D^r_{oo}k_{oo}(h/2)\ \exp[i\nu^u_o\pi/2] \qquad \text{(A.39)}$$

Continuity of pressure at D where $x'' = 0$, $x = 0$ and $\theta = \pi/2$ provides $m = 0$,

$$E^i_{oo}h = C^i_{oo}(h/2)\ \exp[-i\nu^d_o\pi/2] + C^r_{oo}(h/2)\ \exp[i\nu^u_o\pi/2]$$

$$+ B^i_{oo}(h/2) + B^r_{oo}(h/2) \qquad \text{(A.40)}$$

$m \neq 0$,

$$E^i_{mo}(h/2) = C^i_{oo} \exp[-i\nu^d_o \pi/2](\frac{h}{2m\pi})[1-(-1)^m]$$

$$+ C^r_{oo} \exp[i\nu^u_o \pi/2](\frac{h}{2m\pi})[1-(-1)^m]$$

$$- B^i_{oo}(\frac{h}{2m\pi})[1-(-1)^m] - B^r_{oo}(\frac{h}{2m\pi})[1-(-1)^m] \qquad (A.41)$$

Continuity of tangential particle velocity at D provides,

$m = 0$,

$$E^i_{oo}k_{oo}h = C^i_{oo}k_{oo}(h/2) \exp[-i\nu^d_o \pi/2] - C^r_{oo}k_{oo}(h/2) \exp[i\nu^u_o \pi/2]$$

$$+ B^i_{oo}k_{oo}(h/2) - B^r_{oo}k_{oo}(h/2) \qquad (A.42)$$

$m \neq 0$,

$$E^i_{mo}\xi^d_{mo}(h/2) = C^i_{oo}k_{oo}(h/2) \exp[-i\nu^d_o \pi/2](\frac{h}{2m\pi})[1-(-1)^m]$$

$$- C^r_{oo}k_{oo}(h/2) \exp[i\nu^u_o \pi/2](\frac{h}{2m\pi})[1-(-1)^m]$$

$$- B^i_{oo}k_{oo}(\frac{h}{2m\pi})[1-(-1)^m]$$

$$+ B^r_{oo}k_{oo}(\frac{h}{2m\pi})[1-(-1)^m] \qquad (A.43)$$

APPENDIX 3

MATRICES OF THE ANALYSES OF CHAPTERS 4, 5 AND 6

The equations obtained by continuity at the interfaces of straight and curved sections for the analyses of Chapters 4, 5 and 6 were set into a complex matrix system such that $A_m \times X_m = B_m$. A_m is the matrix of the complex variables of each Fourier coefficient, X_m is the matrix of Fourier coefficients or the complex amplitude of each acoustic wave considered and B_m is the matrix of coefficients obtained by moving the coefficient P^i_{oo} to one side of the equations.

Thus at each particular frequency the coefficients of each wave were evaluated and the matrix system solved for the Fourier constants X_m, by a computer program based on Crout's rule.

For simplification of the matrices the following symbols will be used:

$$I_1 = \int_{R_1}^{R_2} \psi^c_{oo}\, dr \tag{A.44}$$

$$I_2 = \int_{R_1}^{R_2} \psi^c_{oo} \cos[(m\pi/h)(r-R_1)]dr \tag{A.45}$$

$$I_3 = \int_{R_1}^{R_2} \psi^c_{oo}(\nu_o/r)dr \tag{A.46}$$

$$I_4 = \int_{R_1}^{R_2} \psi^c_{oo}(\nu_o/r) \cos[(m\pi/h)(r-R_1)]dr \tag{A.47}$$

Where the integral notation refers to the outside or inside curved section of the bend or attenuator is indicated by marking the matrix column.

$$A_m = \begin{bmatrix} & & \text{Inside Section} & & \text{Outside Section} & & & \\ -h & 0 & I_1 & I_1 & I_1 & I_1 & 0 & 0 \\ 0 & -h/2 & I_2 & I_2 & I_2 & I_2 & 0 & 0 \\ k_o h & 0 & I_3 & -I_3 & I_3 & -I_3 & 0 & 0 \\ 0 & k_{lo} h/2 & I_4 & -I_4 & I_4 & -I_4 & 0 & 0 \\ 0 & 0 & e^{-i\nu_o\pi} I_1 & e^{i\nu_o\pi} I_1 & e^{-i\nu_o\pi} I_1 & e^{i\nu_o\pi} I_1 & -h & 0 \\ 0 & 0 & e^{-i\nu_o\pi} I_2 & e^{i\nu_o\pi} I_2 & e^{-i\nu_o\pi} I_2 & e^{i\nu_o\pi} I_2 & 0 & -h/2 \\ 0 & 0 & e^{-i\nu_o\pi} I_3 & -e^{i\nu_o\pi} I_3 & e^{-i\nu_o\pi} I_3 & -e^{i\nu_o\pi} I_3 & -k_o h & 0 \\ 0 & 0 & e^{-i\nu_o\pi} I_4 & -e^{i\nu_o\pi} I_4 & e^{-i\nu_o\pi} I_4 & -e^{i\nu_o\pi} I_4 & 0 & k_{lo} h/2 \end{bmatrix}$$

$$X_m = \begin{bmatrix} P^r_{oo} \\ P^r_{lo} \\ C^i_{oo} \\ C^r_{oo} \\ D^i_{oo} \\ D^r_{oo} \\ E^i_{oo} \\ E^i_{lo} \end{bmatrix}$$

$$B_m = \begin{bmatrix} P^i_{oo}{}_h \\ 0 \\ P^i_{oo}{}_{k_o}{}_h \\ 0 \\ 0 \\ 0 \\ 0 \\ 0 \end{bmatrix}$$

$A_m =$

				Inside Section		Outside Section					
$-h$	0	$h/2$	$h/2$	I_1	I_1	0	0	0	0	0	0
0	$h/2$	$-h/\pi$	$-h/\pi$	I_2	I_2	0	0	0	0	0	0
$k_o h$	0	$k_o h/2$	$-k_o h/2$	I_3	$-I_3$	0	0	0	0	0	0
0	$k_{1o} h/2$	$-k_o h/\pi$	$k_o h/\pi$	I_4	$-I_4$	0	0	0	0	0	0
0	0	$e^{-ik_o X} h/2$	$e^{ik_o X} h/2$	0	0	I_1	I_1	0	0	0	0
0	0	0	$e^{ik_o X} k_o h/4$	0	0	I_3	$-I_3$	0	0	0	0
0	0	0	0	0	0	$e^{-i\nu_o \pi/2} I_1$	$e^{i\nu_o \pi/2} I_1$	$e^{ik_o X} h/2$	$e^{-ik_o X} h/2$	0	0
0	0	0	0	0	0	$e^{-i\nu_o \pi/2} I_3$	$-e^{i\nu_o \pi/2} I_3$	0	$-e^{-ik_{1o} X} h/4$	0	0
0	0	0	0	$e^{-i\nu_o \pi/2} I_1$	$e^{i\nu_o \pi/2} I_1$	0	0	$h/2$	$h/2$	$-h$	0
0	0	0	0	$e^{-i\nu_o \pi/2} I_2$	$e^{i\nu_o \pi/2} I_2$	0	0	$-h/\pi$	$-h/\pi$	0	$-h/2$
0	0	0	0	$e^{-i\nu_o \pi/2} I_3$	$-e^{i\nu_o \pi/2} I_3$	0	0	$k_o h/2$	$-k_o h/2$	$-k_o h$	0
0	0	0	0	$e^{-i\nu_o \pi/2} I_4$	$-e^{i\nu_o \pi/2} I_4$	0	0	$-k_o h/\pi$	$k_o h/\pi$	0	$-k_{1o} h/2$

$$X_m = \begin{bmatrix} P^r_{oo} \\ P^r_{lo} \\ A^i_{oo} \\ A^r_{oo} \\ C^i_{oo} \\ C^r_{oo} \\ D^i_{oo} \\ D^r_{oo} \\ B^i_{oo} \\ B^r_{oo} \\ E^i_{oo} \\ E^i_{lo} \end{bmatrix}$$

$$B_m = \begin{bmatrix} P^i_{oo}h \\ 0 \\ P^i_{oo}k_oh \\ 0 \\ 0 \\ 0 \\ 0 \\ 0 \\ 0 \\ 0 \\ 0 \\ 0 \\ 0 \end{bmatrix}$$

$$
A_m = \begin{bmatrix}
-h & 0 & h/2 & h/2 & h/2 & h/2 & 0 & 0 & 0 & 0 & 0 & 0 \\
0 & -h/2 & h/\pi & h/\pi & -h/\pi & -h/\pi & 0 & 0 & 0 & 0 & 0 & 0 \\
k_o h & 0 & k_o h/2 & -k_o h/2 & k_o h/2 & -k_o h/2 & 0 & 0 & 0 & 0 & 0 & 0 \\
0 & \xi_{lo}^{u} h/2 & k_o h/\pi & -k_o h/\pi & -k_o h/\pi & k_o h/\pi & 0 & 0 & 0 & 0 & 0 & 0 \\
0 & 0 & e^{-ik_o^d x} h/2 & e^{ik_o^u x} h/2 & 0 & 0 & h/2 & h/2 & 0 & 0 & 0 & 0 \\
0 & 0 & k_o e^{-ik_o^d x} h/2 & -k_o e^{ik_o^u x} h/2 & 0 & 0 & k_o h/2 & -k_o h/2 & 0 & 0 & 0 & 0 \\
0 & 0 & 0 & 0 & 0 & 0 & e^{-i\nu_o^d \pi/2} h/2 & e^{i\nu_o^u \pi/2} h/2 & e^{ik_o^d x} h/2 & e^{-ik_o^u x} h/2 & 0 & 0 \\
0 & 0 & 0 & 0 & 0 & 0 & e^{-i\nu_o^d \pi/2} k_o h/2 & -e^{i\nu_o^u \pi/2} k_o h/2 & e^{ik_o^d x} k_o h/2 & e^{-ik_o^u x} k_o h/2 & 0 & 0 \\
0 & 0 & 0 & 0 & e^{-i\nu_o^d \pi/2} h/2 & e^{i\nu_o^u \pi/2} h/2 & 0 & 0 & h/2 & h/2 & -h & 0 \\
0 & 0 & 0 & 0 & e^{-i\nu_o^d \pi/2} h/\pi & e^{i\nu_o^u \pi/2} h/\pi & 0 & 0 & -h/\pi & -h/\pi & 0 & -h/2 \\
0 & 0 & 0 & 0 & k_o e^{-i\nu_o^d \pi/2} h/2 & -k_o e^{i\nu_o^u \pi/2} h/2 & 0 & 0 & k_o h/2 & -k_o h/2 & -k_o h & 0 \\
0 & 0 & 0 & 0 & k_o e^{-i\nu_o^d \pi/2} h/\pi & -k_o e^{i\nu_o^u \pi/2} h/\pi & 0 & 0 & -k_o h/\pi & k_o h/\pi & 0 & -\xi_{lo}^{d} h/2
\end{bmatrix}
$$

$$X_m = \begin{bmatrix} P^r_{oo} \\ P^r_{1o} \\ A^i_{oo} \\ C^i_{oo} \\ C^r_{oo} \\ D^i_{oo} \\ D^r_{oo} \\ B^i_{oo} \\ B^r_{oo} \\ E^i_{oo} \\ E^i_{10} \end{bmatrix}$$

$$B_m = \begin{bmatrix} P^i_{oo}h \\ 0 \\ P^i_{oo}k_oh \\ 0 \\ 0 \\ 0 \\ 0 \\ 0 \\ 0 \\ 0 \\ 0 \\ 0 \end{bmatrix}$$

APPENDIX 4

REDUCTION OF HARMONIC NOISE GENERATED BY A CENTRIFUGAL FAN

4.A INTRODUCTION

Fans are a necessary part of every ventilating and air-conditioning system. However as the demand for faster flow in such ducts increases so does the noise generated by the fan. This noise generally can be divided into two parts: (1) the harmonic noise generated by interaction between the airstream and the rotating impeller, and (2) broad band noise most likely generated by flow interaction with the fan and housing. Many attempts have been made to reduce both these causes of noise and the major works have been well summarized by Neise (1976). Due to the more obvious nature of the harmonic part of the noise generated most work has been concentrated on reducing this part. In this case stated simply, the fan blades chop the air stream causing regions of low and high pressure and corresponding radiation of sound. The frequency of the radiated sound is thus determined by the number of blades and the angular speed of the rotor.

The most effective reduction of the harmonic part has been gained by varying the distance between the fan rotor blade tip and the scroll cut-off. The reduction in level at the blade passing frequency was found to be sensitive to the shape of the cut-off as well as the clearance (Ploner and Herz (1969)). In general the reduction obtained by varying the cut-off clearance varied between 6 and 20 dB depending upon the shape of the cut-off and the operating condition of the fan

(Embleton (1963), Smith (1974), Leidel (1969)). Increasing the cut-off clearance was shown to have an insignificant effect on the broad band noise (Leidel (1969)).

Embleton (1963) investigated inclined blades for multivane impellers and also rotors with backward curved blades. For multivane rotors Embleton measured a reduction of 12 dB in the noise generated at the blade passing frequency. For backward curved blades the reduction was far less, in the order of 2 to 3 dB. Khoroshev and Petrov (1971) obtained a reduction of 16 dB by angling the cut-off through 70 degrees. They also obtained a reduction of 8 to 10 dB in the broad band noise.

Wollherr (1973) investigated the effect of different outlet duct lengths on the sound radiated into the inlet duct. He found that varying the fan outlet duct length caused a 17 dB variation in the sound level at the blade passing frequency in the inlet duct. Changing the length of the outlet duct effectively changes the internal impedance of the fan including the outlet duct. Likewise Baade (1977) has shown that varying the length of the outlet duct strongly affects the sound radiated into free space at a particular frequency.

Finally Lyons and Platter (1963) investigated a configuration of double inlet fans. The blades of each rotor were angularly displaced so that the blades of one rotor lay half way between the blades of the other rotor. With this arrangement Lyons and Platter measured a reduction of the noise generated at the blade passing frequency of 10 dB due to local cancellation of pressures generated at the cut-off edges.

In this appendix the effect of a skewed (or angled) cut-off on the sound generated in a centrifugal fan is considered. The fan

has four backward curved blades and the skewed cut-off is arranged to cover two blades simultaneously. No attempt is made to reduce the broad band noise. The results obtained are compared to those obtained by other workers. A method of impedance loading of the fan outlet is proposed which can be used with fans with two rotors. Theoretically the proposed arrangement should completely attenuate all sound at the blade passing frequency.

4.B THE SKEWED CUT-OFF

Experimental Equipment and Procedure

The fan to be investigated is shown in Plate 7 with inlet section and part of the fan casing removed. The skewed cut-off is shown in position. The fan has four backward curved blades with inside and outside diameters of .22 m and .52 m respectively. The skewed cut-off was designed to cover at least two blades and thus had a total angle of 90°. The skewed cut-off was mounted in position as shown in Plate 7 by bolts through slotted tabs on the edge of the cut-off. Thus the radial clearance of the cut-off to the tip of the fan rotor could be varied through approximately 8 centimeters.

The fan inlet duct was of circular cross section of diameter .206 m and was 2 m in length. The fan outlet duct was a .132 m × .33 m rectangular cross section. The outlet duct length was chosen to be .9 m which approximately corresponds to the half wave length of the blade passing frequency. Thus the noise generated at the blade passing frequency should be radiated well from the outlet duct to examine effects of the harmonic noise at this particular frequency. The fan rotated at 304 radians/sec. The corresponding theoretical blade passing frequency for this fan is thus 193.5 Hz.

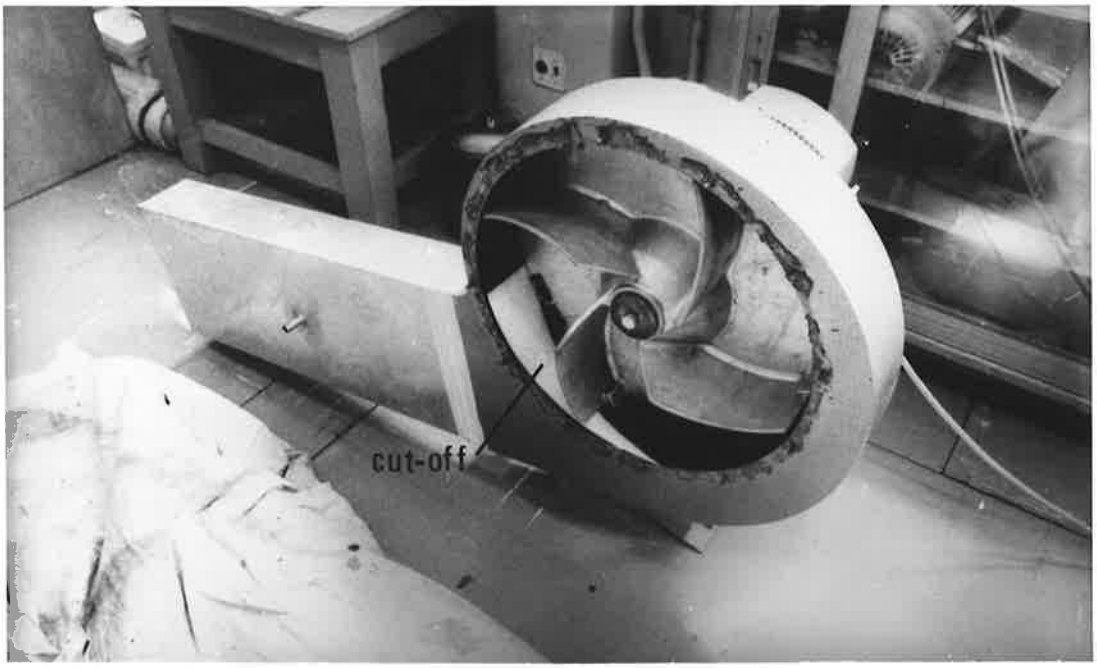

PLATE 7. The skewed fan cut-off

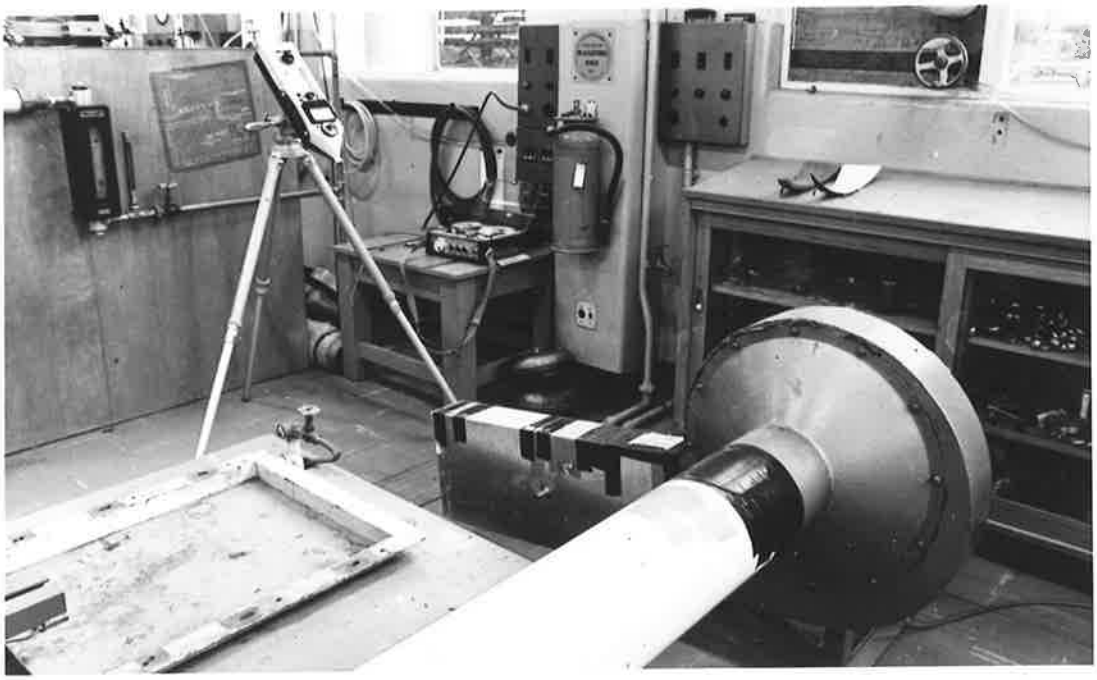

PLATE 8. Position of experimental apparatus for investigation of fan noise.

Measurements were made at a position one meter from the exit of the fan using a Brüel and Kjaer Sound Level Meter and 1/3 Octave Band Analyser as shown in Plate 8. It can be seen from Plate 8 that the exit duct does not radiate into free space due to several reflecting surfaces nearby. However the investigation is of a comparative nature and not absolute, so that the test condition was thought satisfactory. The two cases of the fan with a straight cut-off and with an angled cut-off were analysed in 1/3 octave bands and in narrow constant frequency bandwidths. For the 1/3 octave analysis the Sound Level Meter was set to slow and the readings taken as the fan was running. The two cases of sound levels with a straight cut-off and with a skewed cut-off are shown in Figure A.1 for 1/3 octave bands.

For narrow band analysis the output of the Brüel and Kjaer Sound Level Meter was recorded on a Nagra tape recorder. From this recording continuous tape loops were made to obtain a consistent level. The output of the Nagra recorder when played back with the tape loops fitted was fed into a Brüel and Kjaer Heterodyne Analyser. The narrow band Heterodyne Analyser was set to a 10 Hz bandwidth and the input was averaged over 3 secs. Thus with this averaging time and the tape loop arrangement an averaged reading was achieved. The Analyser was connected to a Brüel and Kjaer Graphic Level Recorder by means of a mechanical drive cable which enabled synchronized sweeping of frequency (at a 10 Hz bandwidth) to be achieved. The output of the Analyser was set to a D.C. current (and the level recorder set to D.C. accordingly) thus the output of the analyser was averaged by 3 secs. The narrow band frequency analysis of the fan noise with a straight cut-off and skewed cut-off using

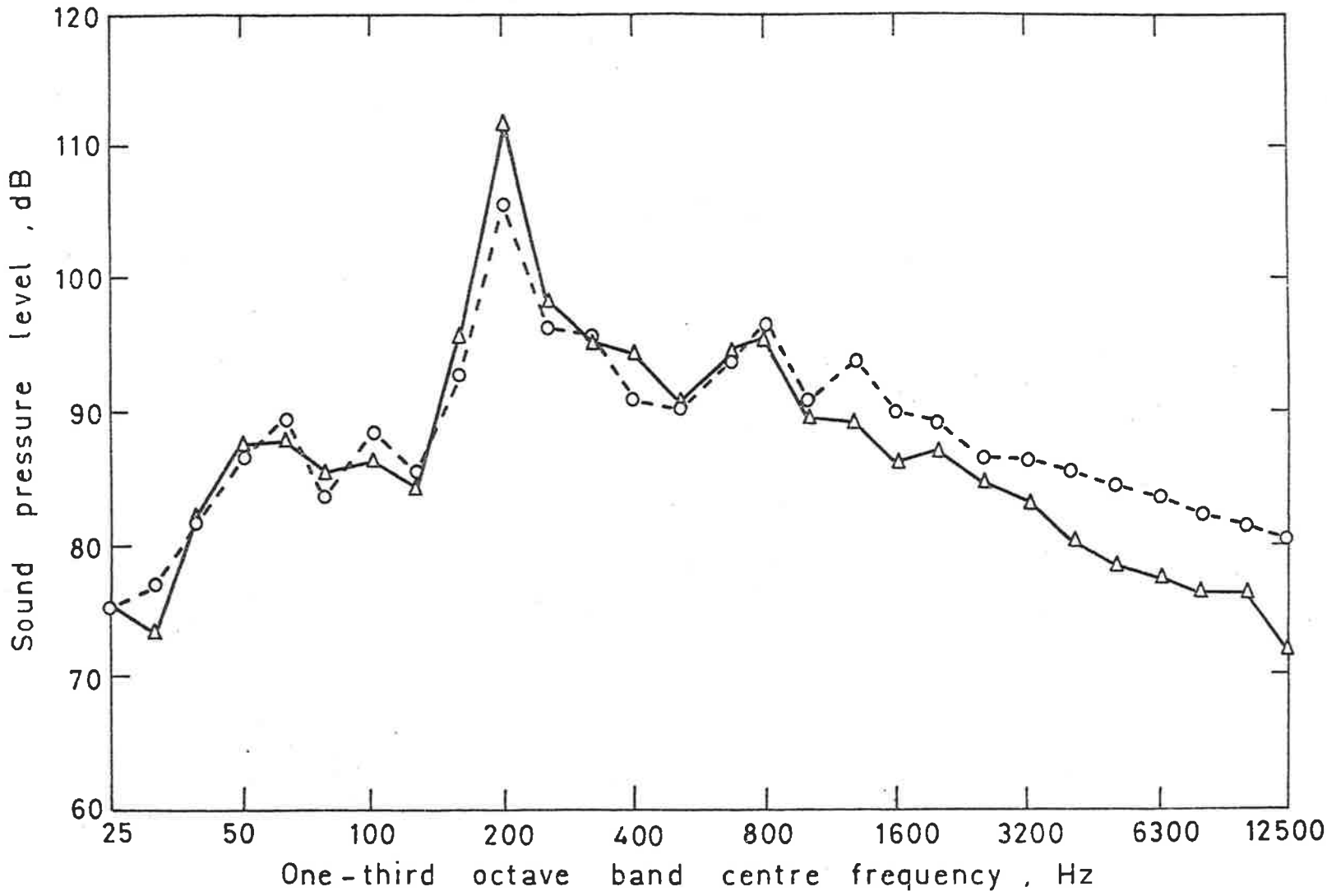

FIGURE A.1. One-third octave spectra of the fan noise. —△—, straight cut off; —○—, skewed cut-off.

the above method are shown in Figures A.2 and A.3 respectively.

The sound pressure level of the fan noise was also recorded during running at the 1 meter position using a sound level meter set to "slow". For the case of straight cut-off edge the level was 112 dB(lin) and with a skewed cut-off edge the level at the same position was 107 dB(lin) giving a reduction in overall sound pressure level of 5 dB(lin).

The effect of radial clearance of the cut-off was investigated by relocating the cut-off as required but was found to insignificantly effect the results. Thus results for a clearance of 5mm between the rotor tips and cut-off are presented in the figures.

4.C DISCUSSION OF SKEWED CUT-OFF EXPERIMENTAL RESULTS

Figure A.2 which is a narrow band analysis of the fan noise with a straight cut-off fitted shows that the fan noise is characterized by a broad band noise with a series of much louder discrete peaks. The first major peak is seen to occur at a frequency of approximately 196 Hz which corresponds closely to the theoretical blade passing frequency of the fan. The other peaks occur at multiples of the blade passing frequency and are thus thought to be harmonics. Thus as one would expect, the major contributor to fan noise is that part caused by the blade-flow interaction at the cut-off edge of the fan scroll.

The narrow band frequency spectrum of the fan with a skewed or angled cut-off is shown in Figure A.3. With the skewed cut-off fitted the sound pressure level generated at the blade passing frequency is seen to be substantially reduced by 9.5 dB, and the harmonics are reduced in the order of 4 to 5 dB. The same reduction is reflected in the 1/3 octave analysis of the same cut-off conditions.

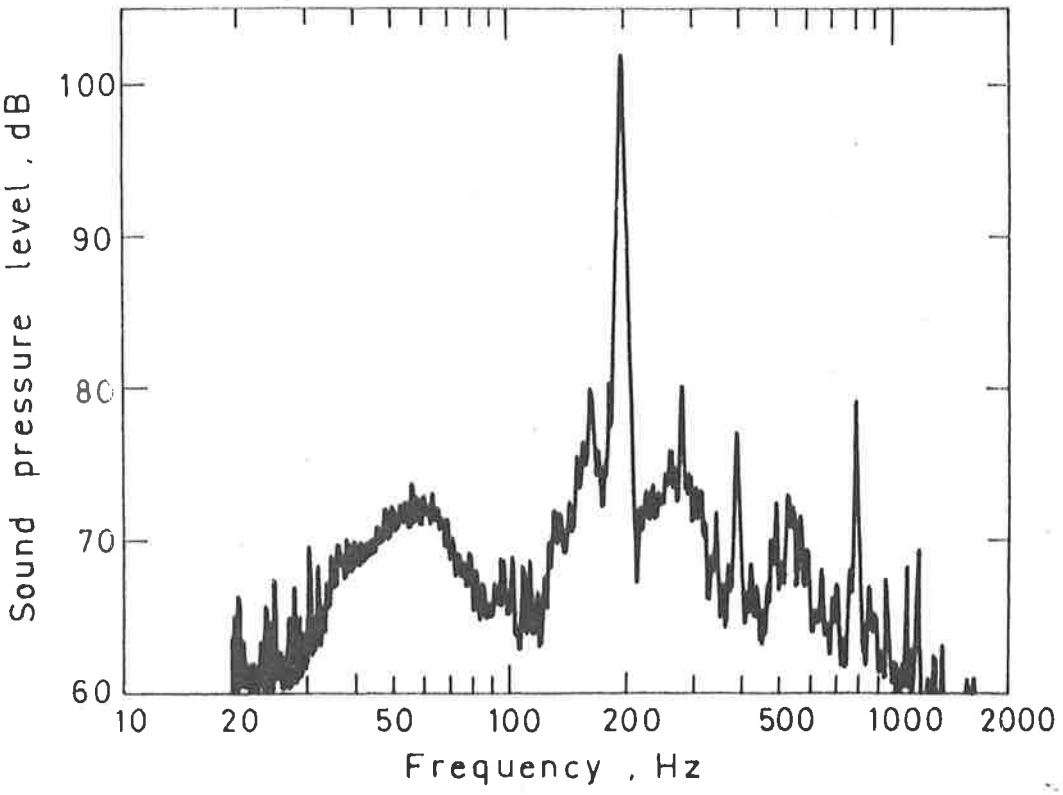

FIGURE A.2. Narrow band analysis of the fan noise with a straight cut-off.

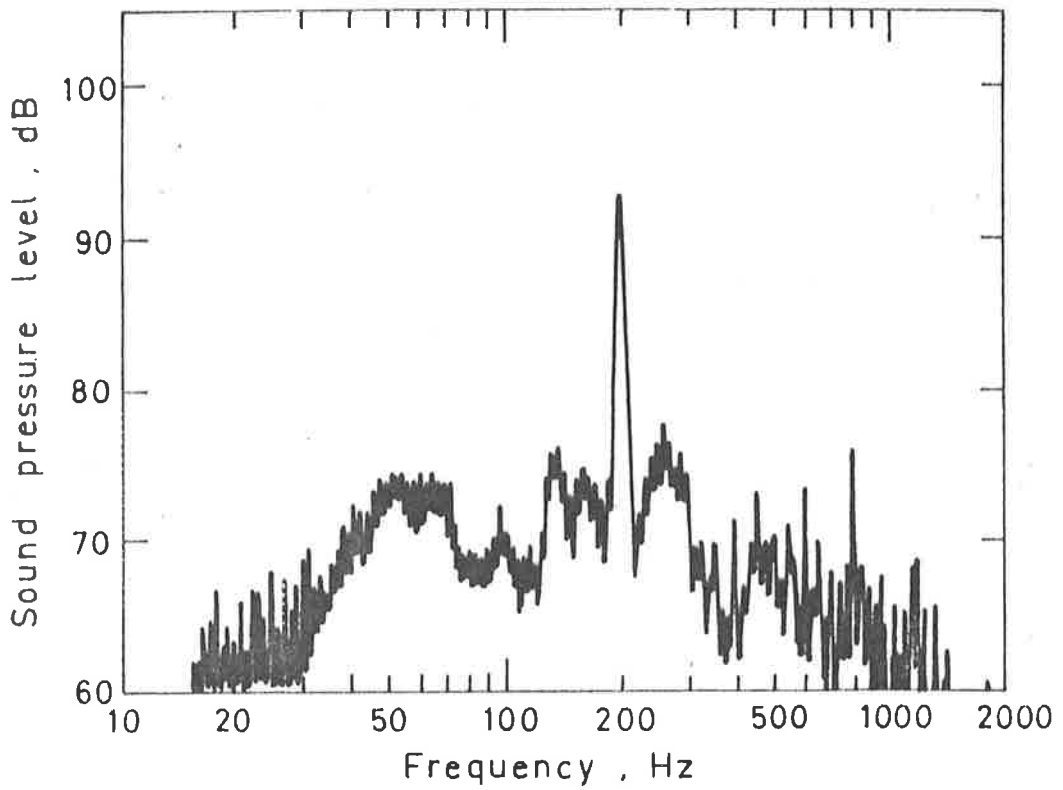

FIGURE A.3. Narrow band analysis of the fan noise with a skewed cut-off.

At the blade passing frequency Figure A.1 shows a reduction 6 dB in the sound pressure level when a skewed cut-off is fitted.

Thus the fitting of a skewed cut-off is seen to substantially reduce the noise generated by centrifugal fans at the blade passing frequency. The values of reduction in level obtained here should be compared to those of 2 to 3 dB obtained by Embleton (1963) for fans with backward curved blades. However it is not clear what type of frequency analysis Embleton used.

The values of dB (lin) measured with a straight cut-off and a skewed cut-off show a 5 dB reduction. Thus even though the sound pressure level at the blade passing frequency is substantially reduced, the overall level is only reduced by 5 dB when an angled cut-off is fitted. This was thought to be due to an increase in broad band noise when a skewed cut-off is used.

4.D IMPEDANCE LOADING OF THE FAN

Figure A.4 shows the arrangement by which this method could be used. It is only suitable for application to twin rotor fans. The rotors are separated by a solid partition which is placed parallel to the flow. The rotor blades are arranged such that one set of blades lie half way between the blades of the other rotor. Thus the sound generated at the blade passing frequency of one rotor would be close to being 180° out of phase with the other rotor. The dimensions of the separate ducts formed by the subpartitions are adjusted such that only the (0,0) mode will propagate at the blade passing frequency. This method is likely to be limited to multi-bladed fans in order to maintain reasonable duct dimensions. The partition is long enough such that all evanescent modes generated at the cut-off have decayed and are negligible. Thus at the exit of the

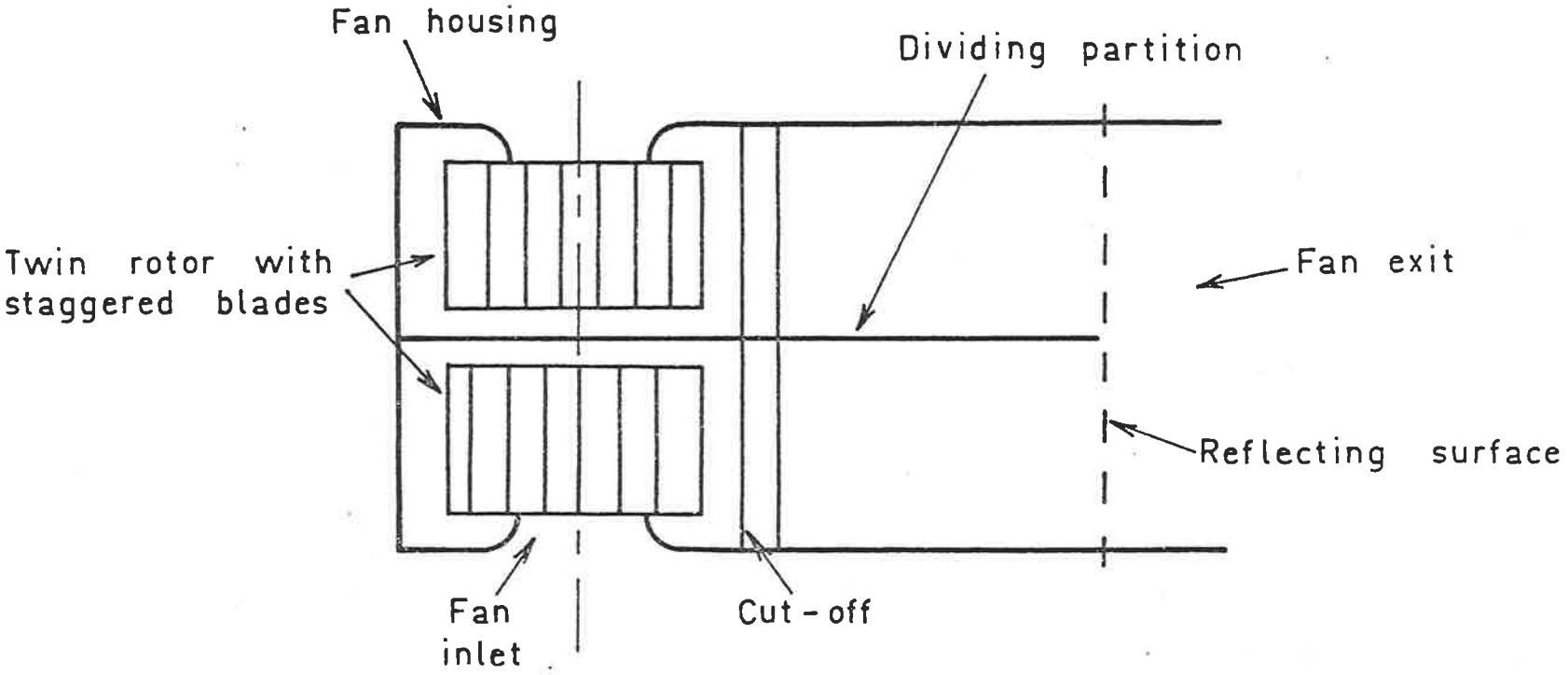

FIGURE A.4. Proposed arrangement to impedance load the fan.

partition, at the blade passing frequency, there are two vibrating pistons, 180° out of phase. By the theory of Chapter 3, for this arrangement, all sound would theoretically be reflected at this frequency.

Due to the fact that partition is parallel to the flow it is not likely to modify the performance characteristics of the fan.

APPENDIX 5

PUBLICATIONS

Journal of Sound and Vibration (1978) 56(1), 45–59

5.A A REACTIVE ACOUSTIC ATTENUATOR

C. R. FULLER AND D. A. BIES

Department of Mechanical Engineering, University of Adelaide, Adelaide, South Australia 5000

(*Received* 9 *May* 1977, *and in revised form* 24 *August* 1977)

A reactive acoustic attenuator that combines high reflection of low frequency sound with low pressure drop coefficient is investigated experimentally and theoretically by using equations for sound propagation in straight and curved ducts. Good agreement is obtained and the theory is used to redesign the device to give a minimum transmission loss of ten decibels over a frequency range of three-quarters of an octave. Small discrepancies between theoretical and experimental results are discussed.

1. INTRODUCTION

As the demand for faster flow in air conditioning duct systems increases so does the noise generated by the fan and the fluid flow. The noise generated by the fan and flow is usually of long wavelength relative to the dimensions of the duct, rendering it unsuitable to attenuation by lining the walls with acoustic absorbent material, and the level of this low frequency noise is often unacceptable in such applications as libraries or sound studios. In the usual method of control a system of resonators or lined expansion chambers may be employed but these devices have the disadvantage of excessive size or large pressure drop and usually operate over a narrow frequency range.

In this paper, an attenuator described by Luxton [1] is investigated. This attenuator, when fitted into any convenient bend in a duct system, combines high rejection of low frequency sound over a broad frequency range of three-quarters of an octave with a low pressure drop coefficient (0·46). The attenuator makes use of the inherent difference in path lengths of the inner and outer portions of a bend fitted with a splitter to generate an impedance mismatch at the inlet and exit of the device, causing reflection of sound.

Equations characterizing sound propagation in straight and curved ducts are used to describe the device without flow. The predicted results agree well with those measured experimentally. An understanding of the performance of the attenuator has allowed re-design of its shape to optimize its performance.

2. SOUND PROPAGATION IN RECTANGULAR SECTION DUCTS

2.1. INFINITE RECTANGULAR STRAIGHT DUCTS

Equations for sound propagating in an infinite rectangular straight duct have been well discussed [2]. As the more important conclusions will be of importance to the understanding of this paper and can also serve as a guide to the less familiar propagation in curved ducts they will be briefly reviewed and summarized here.

The general solution of the wave equation $(\nabla^2 + (\omega/c)^2)p = 0$ in separable rectangular co-ordinates is

$$p(x, y, z, t) = \sum_{m=0}^{\infty} \sum_{n=0}^{\infty} P_{mn} \psi^s_{mn}(y, z) \exp [i(\omega t - k_{mn} x)], \tag{1}$$

where the x axis is parallel to the direction of propagation of sound.

The characteristic function describing variation in pressure amplitude in the duct over a surface in the y–z plane is

$$\psi^s_{mn}(y,z) = \cos[m\pi y/h_1]\cos[n\pi z/h_2], \tag{2}$$

where h_1 and h_2 are dimensions of the duct in the y and z directions, respectively.

The wave number k_{mn} which describes sound propagation in the duct in the x direction is given by

$$k^2_{mn} = [(\omega/c)^2 - (m\pi/h_1)^2 - (n\pi/h_2)^2]. \tag{3}$$

If k_{mn} is real then propagation will occur without attenuation. If m and n are zero then k_{00} is always real and the corresponding wave will have constant amplitude across the duct. The (0,0) mode is a plane wave which propagates at all frequencies. However if either or both m and n are not zero there will always be a frequency below which k_{mn} is imaginary and the corresponding (m,n) mode will not propagate. Thus if k_{mn} is imaginary the corresponding disturbance will decay exponentially along the duct axis. The discrete frequency for cut-off of such modes, below which they are non-propagating and above which they are propagating, is given by

$$f_{mn} = (c/2)[(m/h_1)^2 + (n/h_2)^2]^{1/2}. \tag{4}$$

As the acoustic axial (x) particle velocity of a non-propagating mode is always in phase quadrature with the acoustic pressure, non-propagating modes carry no nett power away from the generating surface.

2.2. INFINITE RECTANGULAR RADIAL BENDS

The equations for sound propagation in radial bends with rectangular cross-sections are obtained from the wave equation in separable cylindrical co-ordinates. The sound pressure distribution in the curved duct may be described as follows:

$$p(r,\theta,z,t) = \sum_{n=0}^{\infty}\sum_{m=0}^{\infty} C_{nm}\,\psi^c_{nm}(r,z)\exp[\mathrm{i}(\omega t - \nu_n\theta)], \tag{5}$$

where the characteristic function is

$$\psi^c_{nm}(r,z) = [\mathrm{J}_{\nu_n}(k_m r) - A\mathrm{Y}_{\nu_n}(k_m r)]\cos[m\pi z/h_2], \quad k^2_m = k^2 - k^2_z. \tag{6}$$

We suppose the walls of the duct are rigid; thus the normal acoustic velocity at the walls is zero.

Using the general relation

$$v_r = -(1/\mathrm{i}\rho ck)\,\partial p/\partial r \tag{7}$$

one obtains, at $r = R_1$,

$$A = \mathrm{J}'_{\nu_n}(k_m R_1)/\mathrm{Y}'_{\nu_n}(k_m R_1), \tag{8}$$

where the prime (′) implies differentiation with respect to r.

The variable ν_n, called the angular wave number, is obtained by applying the boundary condition at $r = R_2$ and solving the resulting characteristic equation:

$$\mathrm{J}'_{\nu_n}(k_m R_2)\,\mathrm{Y}'_{\nu_n}(k_m R_1) - \mathrm{J}'_{\nu_n}(k_m R_1)\,\mathrm{Y}'_{\nu_n}(k_m R_2) = 0. \tag{9}$$

Values of the angular wave number were obtained from the characteristic equation (9) by an iterative process on a computer, power series expansions for the Bessel and Neumann functions [3] being used. Representative values obtained are shown in Figure 1. They agree well with the values interpolated from a solution by Rostafinski [4] who used a closed form of the Bessel function of order $(n + 1/2)$.

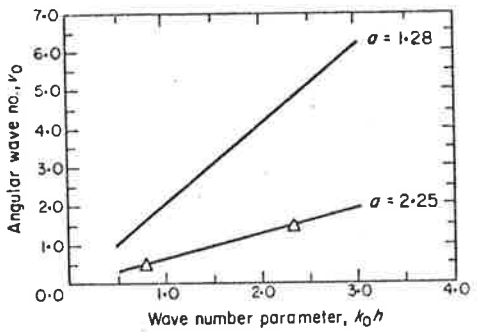

Figure 1. Solutions of the curved duct characteristic equation. $a = R_2/R_1$. ——, Iterative solution: △, Rostafinski's values.

One assumes that ν_n follows the form of k_{mn} in straight ducts; then if the value of ν_n obtained by solving equation (9) is real, the wave will propagate with constant amplitude. If ν_n is imaginary the wave corresponding to that mode will not propagate; rather the disturbance will rapidly decay with distance along the curved duct. Differences in propagation in straight and curved ducts are to be expected, however. The main difference occurs with the (0,0) mode. In a straight duct the wave number is independent of duct dimensions and the acoustic amplitude is constant across the duct. However in a curved duct the angular wave number depends upon the magnitudes of the inside and outside radii as well as on frequency.

Rostafinski [4] has shown that the tangential velocity distribution for the (0,0) mode follows closely that of a potential vortex for low frequencies ($kR_1 < 1$) and is close to that of a forced vortex at higher frequencies ($kR_1 \simeq 3{\cdot}0$). At low frequencies in gradual bends, however, the pressure amplitude does not vary markedly across the duct in a radial direction and is close to that of a plane wave. This has been confirmed experimentally by Cummings [5].

3. THE ATTENUATOR

3.1. DESIGN

The arrangement of the attenuator fitted into a right-angled bend in the duct system is shown in Figure 2. The frequency range over which the attenuator is expected to be useful lies below the cut-off frequency of the (1,0) mode in the straight sections of duct upstream of interface A and downstream of interface D. An impedance mismatch is generated at interface D by the phase difference between the propagating waves in the two separate duct systems. The phase difference is achieved by placing a profiled center-body in the duct bend which divides the incident acoustic plane wave at interface A into two halves that recombine at D. The relative phase of the two separate propagating waves at D is approximately determined by the mean path difference of the two separate channels. At the design frequency, for which the mean path difference between the inner and outer channel is one-half wave length, a plane wave incident at interface A will be converted to a series of non-propagating cross modes at interface D and at this frequency all sound will be reflected.

As the center-body is shaped with gradual bends it acts as a turning vane and a low pressure drop results across the device.

Various shapes were constructed to this design requirement at different design frequencies and tested experimentally. However only two variations of the crescent shaped center-body with 0·2 meter mean path difference, corresponding to a design frequency of 844 Hz in the experimental duct, were amenable to the analysis presented here. Thus discussion will be confined to the latter configuration.

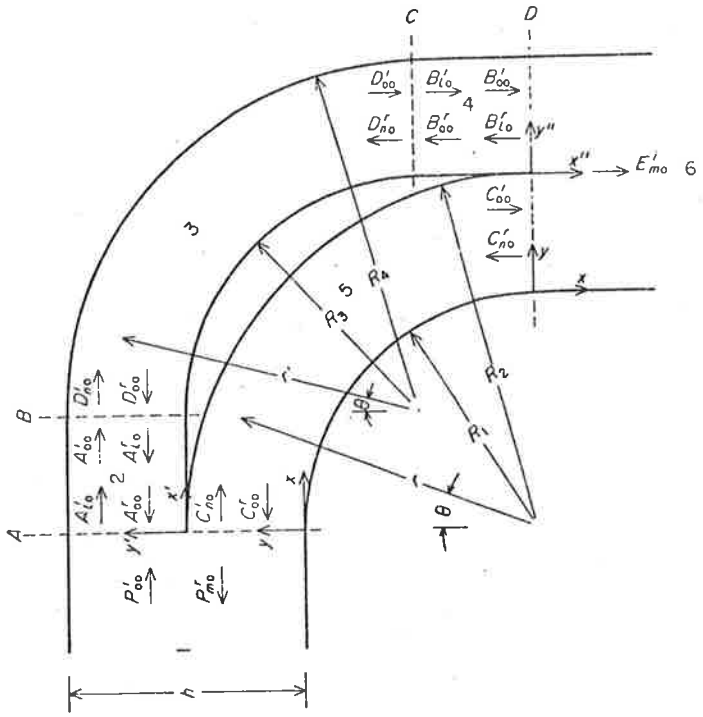

Figure 2. Arrangement and co-ordinate system of attenuator.

3.2. ANALYSIS

The attenuator was first investigated by considering only the power transmitted and reflected at interface D. The analysis accurately described the reflection of sound power at the design frequency but failed to account for observed major reflections at other frequencies also in the range considered. The attenuator was then described by dividing it into sections and considering propagation and reflection in each. With the co-ordinate systems and joining interfaces shown in Figure 2, sound propagation may then be described by straight duct equations in sections 1, 2, 4 and 6 and by curved duct equations in sections 3 and 5.

The coefficients of each wave were obtained by applying continuity conditions across each interface. Continuity implies that acoustic pressure and particle velocity must be continuous across the plane joining the two duct systems. Since there is no discontinuity in the z direction it is satisfactory to use a two-dimensional co-ordinate system: i.e., $k_z = 0$. For convenience a reference amplitude of $P^I_{00} = 1 - 0\mathrm{i}$ will be used for the incident wave in the upstream duct.

At each discontinuity an infinite set of higher order modes will be generated. As the frequency is limited to less than the cut-off frequency of the (1,0) mode in all straight duct sections, the higher modes in the straight ducts will decay and only the (0,0) mode will propagate without attenuation. Similarly it can be shown by solving characteristic equation (9) that only the (0,0) mode will propagate in the curved sections 3 and 5 without attenuation in the frequency range considered.

The requirement for continuity of particle velocity will be simplified to continuity of tangential particle velocity along the direction of the duct center line. This simplification is supported by the consideration that no cross-modes propagate and thus cannot contribute to the nett power flow. However ultimate justification for the simplification rests with the agreement between the results of experiment and predictions of theory. On this basis the

simplification is justified and thus continuity of acoustic pressure and tangential particle velocity at each interface is postulated.

Hence at interface A, where $x = 0$, $\theta = 0$, $x' = 0$, continuity of acoustic pressure provides

$$P^I_{00}\exp[\mathrm{i}(\omega t - k_{00}x)] + \sum_{m=0}^{\infty} P^r_{m0}\cos[(m\pi/h)y]\exp[\mathrm{i}(\omega t + k_{m0}x)]$$

$$= \sum_{n=0}^{\infty} C^I_{n0}\psi^c_{n0}\exp[\mathrm{i}(\omega t - \nu_n\theta)] + C^r_{00}\psi^c_{00}\exp[\mathrm{i}(\omega t + \nu_0\theta)] \qquad \text{for } 0 < y \leqslant h/2 \quad (10)$$

and

$$P^I_{00}\exp[\mathrm{i}(\omega t - k_{00}x)] + \sum_{m=0}^{\infty} P^r_{m0}\cos[(m\pi/h)y]\exp[\mathrm{i}(\omega t + k_{m0}x)]$$

$$= \sum_{l=0}^{\infty} A^I_{l0}\cos[(2m\pi/h)y']\exp[\mathrm{i}(\omega t - k_{l0}x')] + A^r_{00}\exp[\mathrm{i}(\omega t + k_{00}x')] \qquad \text{for } h/2 \leqslant y < h. \quad (11)$$

The Fourier coefficients are obtained by multiplying both sides of the equation by $\cos[(m\pi/h)y]$ and integrating over the interface surface with respect to y, y' or r. The orthognality property of the latter function allows determination of the P^r_{m0} coefficients for $m = 0$, 1, 2,..., as follows:

$m = 0$:

$$P^I_{00}h + P^r_{00}h = \sum_{n=0}^{\infty} C^I_{n0}\int_{R_1}^{R_2}\psi^c_{n0}\,\mathrm{d}r + C^r_{00}\int_{R_1}^{R_2}\psi^c_{00}\,\mathrm{d}r + \sum_{l=0}^{\infty} A^I_{l0}\int_0^{h/2}\psi^s_{l0}\,\mathrm{d}y' + A^r_{00}h/2, \quad (12)$$

$m \neq 0$:

$$P^r_{m0}h/2 = \sum_{n=0}^{\infty} C^I_{n0}\int_{R_1}^{R_2}\psi^c_{n0}\cos[(m\pi/h)(r - R_1)]\,\mathrm{d}r + C^r_{00}\int_{R_1}^{R_2}\psi^c_{00}\cos[(m\pi/h)(r - R_1)]\,\mathrm{d}r$$

$$+ \sum_{l=0}^{\infty} A^I_{l0}\int_0^{h/2}\psi^s_{l0}\cos[(m\pi/h)(y' + h/2)]\,\mathrm{d}y' - A^r_{00}(h/2m\pi)[1 - (-1)^m]. \quad (13)$$

Similarly, continuity of tangential particle velocity at A provides

$m = 0$:

$$P^I_{00}k_{00}h - P^r_{00}k_{00}h = \sum_{n=0}^{\infty} C^I_{n0}\int_{R_1}^{R_2}\psi^c_{n0}(\nu_n/r)\,\mathrm{d}r - C^r_{00}\int_{R_1}^{R_2}\psi^c_{00}(\nu_0/r)\,\mathrm{d}r +$$

$$+ \sum_{l=0}^{\infty} A^I_{l0}k_{l0}\int_0^{h/2}\psi^s_{l0}\,\mathrm{d}y' - A^r_{00}k_{00}h/2, \quad (14)$$

$m \neq 0$:

$$-P^r_{m0}k_{m0}h/2 = \sum_{n=0}^{\infty} C^I_{n0}\int_{R_1}^{R_2}\psi^c_{n0}(\nu_n/r)\cos[(m\pi/h)(r - R_1)]\,\mathrm{d}r -$$

$$- C^r_{00}\int_{R_1}^{R_2}\psi^c_{00}(\nu_0/r)\cos[(m\pi/h)(r - R_1)]\,\mathrm{d}r +$$

$$+ \sum_{l=0}^{\infty} A^I_{l0}k_{l0}\int_0^{h/2}\psi^s_{l0}\cos[(m\pi/h)(y' + h/2)]\,\mathrm{d}y' +$$

$$+ A^r_{00}k_{00}(h/2m\pi)[1 - (-1)^m]. \quad (15)$$

The equations derived by continuity of pressure and particle velocity at interfaces B, C and D are given in the Appendix.

The above system of equations (12) to (15), and equations (A1) to (A12), constitute an infinite set with an infinite number of unknowns. In order to proceed, it is necessary to truncate the various infinite series. Truncation of each series is determined by two considerations: firstly the accuracy of the resulting mathematical expression which is desired when compared with experimental results, and secondly the number of equations necessary to determine all of the unknown coefficients in the several truncated series.

Let the number of modes in straight sections 1 and 6 truncate at L, in straight sections 2 and 4 at M and in curved sections 5 and 3 at N. In this case the total number of unknown coefficients U is

$$U = 2L + 4N + 4M, \tag{16}$$

while the total number of equations V is

$$V = 4L + 4M. \tag{17}$$

Cummings [5] has shown for an interface between a straight and curved duct that the number of modes in each duct section must be equal for solution: hence

$$N = M. \tag{18}$$

Therefore, equating the number of unknowns U and equations V gives

$$L = 2N = 2M. \tag{19}$$

Hence the series describing sections 1 and 6 must be truncated at twice the number of terms of the series describing sections 2, 3, 4 and 5.

At each discontinuity in the duct system an infinite number of higher order modes are generated. Cummings has shown that at frequencies well below the cut-off frequency of the (1,0) mode, non-propagating modes have only a small effect on sound propagation in a curved duct. On comparing the theoretical and experimentally measured impedance (assumed to be entirely reactive) of a 180° bend, Cummings found good agreement with prediction in the curved section when the analysis was truncated at the (0,0) mode. For this reason and in the interest of economy of computing time, the present analysis is limited to consideration only of the (0,0) mode. Hence we set N and M of equation (18) equal to unity and L of equation (19) equal to two. Therefore the number of modes in straight sections 1 and 6 will be limited to two, one propagating and one non-propagating mode.

4. EXPERIMENTAL APPARATUS AND METHOD

The attenuator was investigated with the arrangement shown in Figure 3. The duct system consisted of a 0·0635 × 0·127 meter rectangular section and was constructed from 0·0254 meter thick wood lined with Laminex on the inside to fulfill the rigid wall boundary condition.

The sound source shown schematically in Figure 3 was placed in the duct side wall 1·7 meters upstream from the attenuator. At this distance, all locally generated cross-modes will be sufficiently attenuated to be negligible at the entrance to the attenuator. Thus the incident wave at interface A was plane with constant pressure and velocity amplitude across the duct.

The downstream duct was terminated with an anechoic termination of the arrangement shown in Figure 3. The pressure reflection coefficient of this termination was measured separately over the frequency range considered and found to be less than 0·1. Hence the downstream duct appears infinite to the exit of the attenuator and only one E_{00}^{t} wave need be assumed to be propagating in the section 6 straight duct.

The original attenuator investigated consists of a crescent-shaped center-body and surrounding duct with dimensions $R_1 = 0{\cdot}229$ meters, $R_2 = 0{\cdot}292$ meters, $R_3 = 0{\cdot}051$ meters and

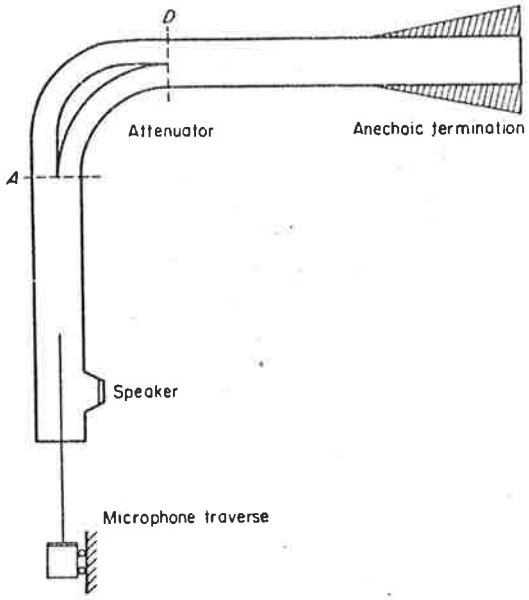

Figure 3. Experimental apparatus.

$R_4 = 0{\cdot}114$ meters, where the corresponding radii are shown in Figure 2. This arrangement results in a path difference of 0·2 meters between the mean center-lines of the two separate ducts. The corresponding design frequency, for plane waves propagating in all sections, is 844 Hz.

The three parameters sound power transmission coefficient, transmission loss and variation in pressure amplitude across the curved duct were measured.

The sound power transmission coefficient provides a measure of how much energy the attenuator will reflect and was obtained by measuring the acoustic standing wave in the upstream duct with a probe as indicated in Figure 3. Maximum and minimum pressures were measured and recorded by using a spectrometer and a level recorder. The transmission coefficient was obtained from the measured standing wave ratio, n, by using

$$\alpha_t = 1 - [(n-1)/(n+1)]^2. \tag{20}$$

The transmission loss of the attenuator is defined as the reduction in decibels between the sound pressure level of the incident wave P_{00}^i and the transmitted wave E_{00}^t. Transmission loss provides an indication of the performance of the attenuator as it shows to what degree the sound pressure level in the duct will be reduced by its installation. Experimental values of transmission loss were obtained by measuring the maximum pressure level of the standing wave in the upstream duct with a calibrated microphone, traversed until a maximum was reached. The sound pressure level of the transmitted wave E_{00}^t was measured by using a calibrated microphone positioned midstream in the acoustic flow 0·3 meters from the exit of the attenuator. The transmission loss of the attenuator is then given by

$$\text{transmission loss} = (P_{max})\,\text{dB} - 20\log_{10}(1 + \alpha_R^{1/2}) - (E_{00}^t)\,\text{dB}, \tag{21}$$

where α_R is the sound power reflection coefficient measured from the standing wave.

Variation in pressure amplitude across the curved duct sections indicates the degree to which non-plane propagation occurs in these sections, and was measured in the outside duct curved section by traversing a probe from the inside to the outside radius. The values obtained were normalized relative to that on the inside wall.

5. THEORETICAL AND EXPERIMENTAL RESULTS

5.1. SOUND POWER TRANSMISSION COEFFICIENT

The radial terms in equations (12) to (15) and (A1) to (A12) were expressed as power series and integrated by using Simpson's rule on a computer. Each series was summed until an error of less than 10^{-4} was obtained. The resulting constants for each equation were then set in a 12×12 matrix and the coefficients of each wave were obtained by solving the matrix by using a program based on Crout's rule. The predicted values of transmission coefficient were then evaluated from

$$\alpha_t = 1 - |P^r_{00}/P^i_{00}|^2.$$

The theoretical values obtained for the original attenuator are shown in Figure 4, where sound power transmission coefficient is plotted against a non-dimensional frequency parameter, $k_0 h$. Measured values are also shown in the figure for comparison.

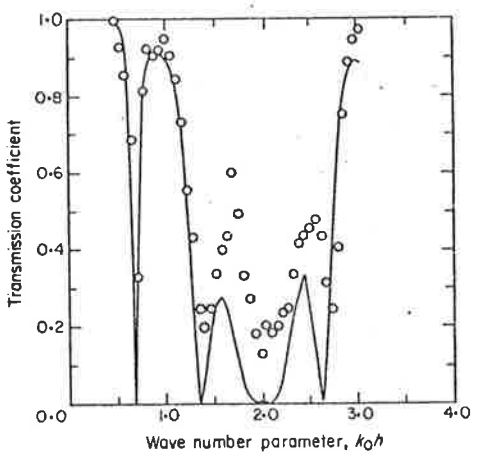

Figure 4. Power transmission coefficient of original attenuator. ——, Theoretical curve; o, experimental value.

As shown in Figure 4 close agreement is observed between the predicted and measured frequencies at which minima in the transmission coefficient are observed, especially at lower frequencies. Slight discrepancies between the theoretical and experimental frequencies of minimum transmission are thought to be due to dimensional inaccuracies in the geometry of the attenuator, affecting the mean path difference between the two ducts. At low frequencies the wavelength of the incident sound is very much larger than the duct's small scale dimensions and thus only a small discrepancy results. However, at high frequencies this is no longer true and the discrepancies are larger.

The magnitude of the measured transmission coefficient, which agrees closely with that predicted at low frequencies, is progressively greater than predicted at increasing frequencies. Three possible reasons for this observation are suggested, as follows.

(1) The walls of the experimental duct are not absolutely rigid as supposed by theory. In fact they were found to vibrate and radiate sound. Thus vibration through the walls acts as a flanking path to increase the apparent transmission through the attenuator. (2) The minima of the standing wave measured in the upstream duct become sharper with increasing frequency, particularly at large values of the standing wave ratio n. This leads to error in evaluating the magnitude of the minimum pressure and results in a higher value of transmission coefficient than predicted. (3) The duct dimensions are not exactly described by the theory.

Minimum transmission at the design frequency may be fully accounted for in terms of reflection at the bend exit plane, interface D of Figure 2. In fact a simple theory which described the exit plane as composed of two vibrating pistons but with variable phase, dependent upon the wavelength to path difference ratio, describes quite well the overall transmission of the attenuator. However the presence of the additional minima in the experimentally determined transmission coefficient that occur at values of $k_0h = 0{\cdot}6$, $1{\cdot}3$, $2{\cdot}6, \ldots$, as shown in Figure 4, cannot be explained by considering reflections at the exit plane alone. The additional minima are due to multi-reflections at interfaces A and D and are fully accounted for by the more exact theory presented here. The frequencies at which additional minima occur depend upon the magnitude of the path difference relative to the mean lengths of either of the

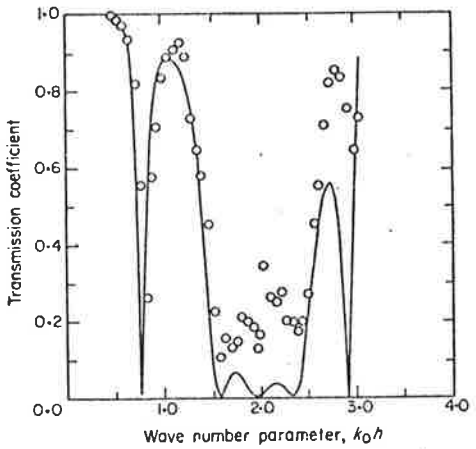

Figure 5. Power transmission coefficient of optimum attenuator. ——, Theoretical curve; o, experimental values.

ducts in the compound bend. For convenience we will take the inside duct mean length as the standard length for comparison. Thus the ratio of the inside duct length to path difference determines the frequencies of additional minima.

The following strategy is now possible. Choice of the path difference determines the design frequency while independent choice of the mean inside path length to path difference ratio determines the frequencies of additional minima. Thus for a given design frequency the ratio can be chosen to optimize the rejection characteristics of the attenuator by appropriate adjustment of the frequencies of the additional minima. For the purpose of this paper optimal attenuation has been taken to mean at least 10 dB transmission loss over as wide a continuous frequency range as possible, centered on the design frequency. In practice one proceeds by keeping the path length difference between the inside and outside ducts in the bend constant and varying their total lengths, or equivalently the ratio of their lengths. The ratio of lengths of the attenuator whose transmission coefficient is shown in Figure 4 is $2{\cdot}00$; however the optimum ratio of lengths for a crescent-shaped center-body has been determined by these investigations to be $1{\cdot}67$. With this choice the position of the extra minima are moved closer to the design frequency and a continuous rejection band of greater than ten decibels over three-quarters of an octave is achieved.

An attenuator designed for optimal attenuation characteristics has the following dimensions: with reference to Figure 2 its radii are $R_1 = 0{\cdot}184$ meters, $R_2 = 0{\cdot}248$ meters, $R_3 = 0{\cdot}006$ meters and $R_4 = 0{\cdot}070$ meters.

The theoretical and experimentally measured transmission coefficient values of this attenuator are shown in Figure 5. It can be seen that the extra minima have indeed moved

closer to the design frequency than those shown in Figure 4. In the model attenuator a rejection band of 430 Hz centered at a design frequency of 844 Hz has been achieved.

Closer agreement is obtained in the position of theoretical and experimentally measured minima produced by the optimum attenuator. This is due to more accurate machining of components in the attenuator, thus achieving the correct mean path lengths.

5.2. INSERTION LOSS

The theoretical transmission loss is predicted by

$$\text{transmission loss} = -10\log(\alpha_t). \tag{23}$$

Theoretical and experimentally measured values of transmission loss for the original attenuator are shown in Figure 6 while those for the optimum attenuator are shown in Figure 7.

At the design frequency the rejection of sound is very nearly complete so that the transmission loss in a narrow frequency band about the design frequency depends upon the band width. The narrower the band width the greater the transmission loss. In the analysis shown in Figures 6 and 7 a band width of 25 Hz has been used but as pure tones were used for the measurement of the transmission loss, occasionally very much greater rejection levels than predicted were observed. Subsequent investigation with narrower band width increments

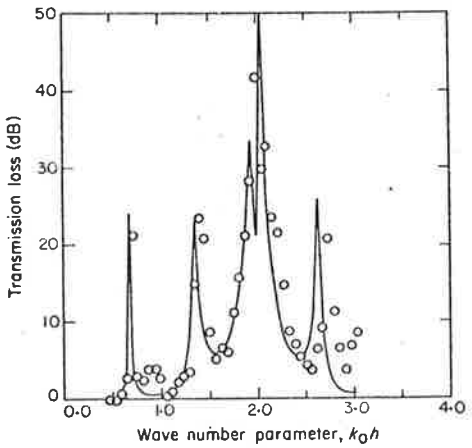

Figure 6. Transmission loss of original attenuator. ——, Theoretical curve; o, experimental values.

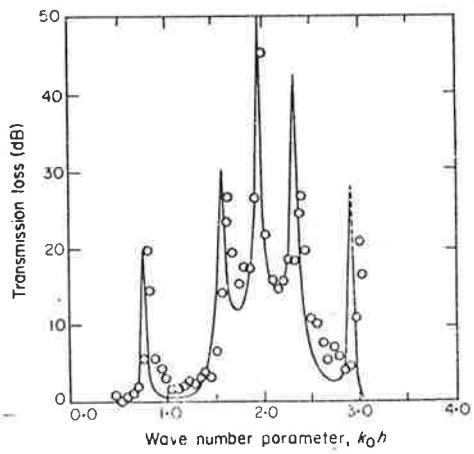

Figure 7. Transmission loss of optimum attenuator. ——, Theoretical curve; o, experimental values.

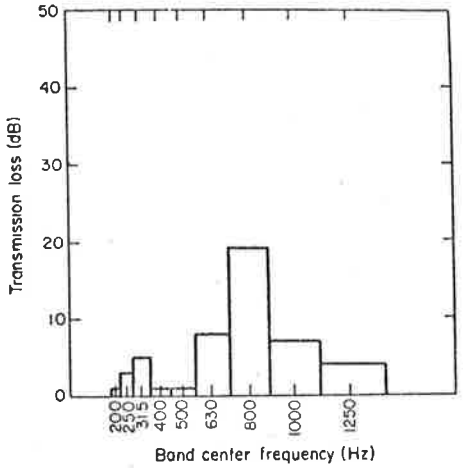

Figure 8. Experimentally measured transmission loss of original attenuator in 1/3-octave bands with white noise source.

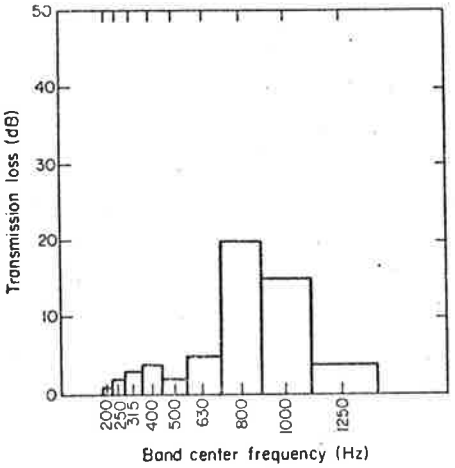

Figure 9. Experimental measured transmission loss of optimum attenuator in 1/3-octave bands with white noise source.

showed that these high anomalous values could always be accounted for on the basis presented here.

Small discrepancies between the theoretical predictions and the measurements are thought to be due to small dimensional inaccuracies in the models as previously discussed. However, much closer agreement is obtained, between the actual magnitude of the theoretical transmission loss and that measured experimentally, than that shown by the transmission coefficients in Figures 4 and 5. Thus the attenuator performs far better than shown by measuring the standing wave alone. This supports the argument presented for discrepancies between the magnitude of experimental and theoretical transmission coefficient.

The experimentally measured transmission losses of the original and optimum attenuator in one-third octave bands with a white noise source are shown in Figures 8 and 9, respectively.

5.3. CURVED DUCT RADIAL PRESSURE DISTRIBUTION

The theoretical variation in pressure amplitude across the duct was evaluated by using the following expression:

$$\text{relative sound pressure} = (\psi_{00}^{\xi})_r/(\psi_{00}^{\xi})_{R_1}, \tag{24}$$

where ψ_{00}^{ξ} is the characteristic function of the (0,0) mode.

In equation (24) the radial pressure amplitude distribution across the duct has been normalized to that at the inner wall. Representative values for the inside bend of radius ratio $a = R_2/R_1 = 1{\cdot}28$ are shown in Figure 10 while those for the outside bend, $a = 2{\cdot}25$, are shown in Figure 11.

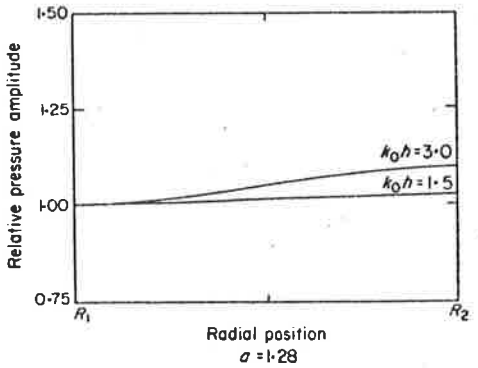

Figure 10. Variation in pressure amplitude for bend $a = 1{\cdot}28$. ——, Theoretical values.

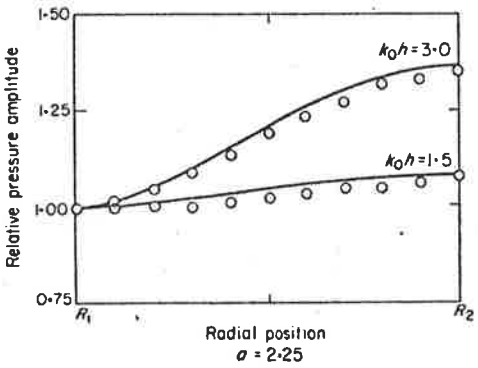

Figure 11. Variation in pressure amplitude for bend $a = 2{\cdot}25$. ——, Theoretical; o, experimental.

Experimental values for the variation in pressure amplitude across the outer bend, $a = 2{\cdot}25$, are shown in Figure 11 for comparison with the predicted values. The agreement is considered to be good. The small error apparent at high frequencies is thought to be due to dimensional inaccuracies in the radii of the curved sections.

It can be seen that at low frequencies, corresponding to values of the dimensionless frequency $k_0h \leqslant 1{\cdot}5$, acoustic waves propagate with only a small variation in pressure amplitude across the duct, for bends of radius ratio shown in Figures 10 and 11. Hence at low frequencies the basic design assumption that acoustic waves propagate as plane waves in all sections of the attenuator would lead to a negligible error. However as the frequency increases, the variation in sound pressure amplitude across the duct becomes more pronounced, particularly in the sharper bend. Thus for sharp bends at high frequencies the assumption of plane wave propagation does not hold. This conclusion is in agreement with results obtained by Cummings [5].

6. CONCLUSIONS

An attenuator with an inherently low pressure drop coefficient has been described which may be installed in a duct bend. The attenuator when optimally designed is capable of providing a transmission loss greater than ten decibels over a frequency range of three-quarters

of an octave in the very low frequency range. Optimization of design is facilitated by a theoretical description that has provided good agreement between theory and experiment.

The attenuator provides large transmission loss at a series of discrete frequencies all below the cut-off frequency for the first cross-mode in the duct. The presence of these discrete frequencies is explained by reflection of incident sound at the exit and entrance to the attenuator. Their relative distribution is determined by the geometry of the attenuator.

The variation of sound pressure amplitude of a travelling wave in a curved duct is adequately described by the theory. Large departure from uniform pressure amplitude is predicted and observed for curved ducts of small radius near but still below cut-off of the lowest order mode for straight ducts of the same cross-section. Thus in the latter case the assumption of plane wave propagation in the curved duct is inadequate; curved duct equations must be used to describe the sound propagation.

REFERENCES

1. R. E. Luxton 1968 *The 6th International Congress on Acoustics, Tokyo.* A low pressure loss attenuating bend for air flow ducts.
2. S. Rschevkin 1963 *The Theory of Sound.* New York: Pergamon Press.
3. N. W. McLachlan 1934 *Bessel Functions for Engineers.* London: Oxford University Press.
4. W. Rostafinski 1974 *Journal of the Acoustical Society of America* **56**, 11–15. Analysis of propagation of waves of acoustic frequencies in curved ducts.
5. A. Cummings 1974 *Journal of Sound and Vibration* **35**, 451–477, Sound transmission in curved duct bends.

APPENDIX: CONTINUITY EQUATIONS AT INTERFACES *B*, *C* AND *D*

At interface B, $x' = X$ and $\theta' = 0$, continuity of pressure provides

$l = 0$:

$$A^l_{00}(h/2)\exp[-ik_{00}X] + A^r_{00}(h/2)\exp[ik_{00}X] = \sum_{n=0}^{\infty} D^l_{n0}\int_{R_3}^{R_4}\psi^c_{n0}\,dr' + D^r_{00}\int_{R_3}^{R_4}\psi^c_{00}\,dr', \tag{A1}$$

$l \neq 0$:

$$A^r_{l0}(h/4)\exp[ik_{l0}X] = \sum_{n=0}^{\infty} D^l_{n0}\int_{R_3}^{R_4}\psi^c_{n0}\cos[(2l\pi/h)(r'-R_3)]\,dr' + D^r_{00}\int_{R_3}^{R_4}\psi^c_{00}\cos[(2l\pi/h)(r'-R_3)]\,dr'. \tag{A2}$$

Continuity of tangential velocity at B provides

$l = 0$:

$$A^l_{00}k_{00}(h/2)\exp[-ik_{00}X] - A^r_{00}k_{00}(h/2)\exp[ik_{00}X] = \sum_{n=0}^{\infty} D^l_{n0}\int_{R_3}^{R_4}\psi^c_{n0}(\nu_n/r')\,dr' - D^r_{00}\int_{R_3}^{R_4}\psi^c_{00}(\nu_0/r')\,dr', \tag{A3}$$

$l \neq 0$:

$$-A^r_{l0}k_{l0}(h/4)\exp[ik_{l0}X] = \sum_{n=0}^{\infty} D^l_{n0}\int_{R_3}^{R_4}\psi^c_{n0}(\nu_n/r')\cos[(2l\pi/h)(r'-R_3)]\,dr' - D^r_{00}\int_{R_3}^{R_4}\psi^c_{00}(\nu_0/r')\cos[(2l\pi/h)(r'-R_3)]\,dr'. \tag{A4}$$

At interface C, $x'' = -X$ and $\theta' = \pi/2$, continuity of pressure provides

$l = 0$:

$$B^l_{00}(h/2)\exp[ik_{00}X] + B^r_{00}(h/2)\exp[-ik_{00}X] = D^l_{00}\int_{R_3}^{R_4}\psi^c_{00}\exp[-iv_0\pi/2]\,dr' + \sum_{n=0}^{\infty} D^r_{n0}\int_{R_3}^{R_4}\psi^c_{n0}\exp[iv_n\pi/2]\,dr', \quad \text{(A5)}$$

$l \neq 0$:

$$B^l_{l0}(h/4)\exp[ik_{l0}X] = D^l_{00}\int_{R_3}^{R_4}\psi^c_{00}\exp[-iv_0\pi/2]\cos[(2l\pi/h)(r' - R_3)]\,dr' + \sum_{n=0}^{\infty} D^r_{n0}\int_{R_3}^{R_4}\psi^c_{n0}\exp[iv_n\pi/2]\cos[(2l\pi/h)(r' - R_3)]\,dr'. \quad \text{(A6)}$$

Continuity of tangential velocity at C provides

$l = 0$:

$$B^l_{00}k_{00}(h/2)\exp[ik_{00}X] - B^r_{00}k_{00}(h/2)\exp[-ik_{00}X] = D^l_{00}\int_{R_3}^{R_4}\psi^c_{00}(v_0/r')\exp[-iv_0\pi/2]\,dr' - \sum_{n=0}^{\infty} D^r_{n0}\int_{R_3}^{R_4}\psi^c_{n0}(v_n/r')\exp[iv_n\pi/2]\,dr', \quad \text{(A7)}$$

$l \neq 0$:

$$B^l_{l0}k_{l0}(h/4)\exp[ik_{l0}X] = D^l_{00}\int_{R_3}^{R_4}\psi^c_{00}(v_0/r')\exp[-iv_0\pi/2]\cos[(2l\pi/h)(r' - R_3)]\,dr' - \sum_{n=0}^{\infty} D^r_{n0}\int_{R_3}^{R_4}\psi^c_{n0}(v_n/r')\exp[iv_n\pi/2]\cos[(2l\pi/h)(r' - R_3)]\,dr'. \quad \text{(A8)}$$

At interface D, $x'' = 0$, $\theta = \pi/2$ and $x = 0$, continuity of pressure at D provides

$m = 0$:

$$E^l_{00}h = C^l_{00}\int_{R_1}^{R_2}\psi^c_{00}\exp[-iv_0\pi/2]\,dr + \sum_{n=0}^{\infty} C^r_{n0}\int_{R_1}^{R_2}\psi^c_{n0}\exp[iv_n\pi/2]\,dr + B^l_{00}h/2 + \sum_{l=0}^{\infty} B^r_{l0}\int_0^{h/2}\psi^s_{l0}\,dy'', \quad \text{(A9)}$$

$m \neq 0$:

$$E^l_{m0}h/2 = C^l_{00}\int_{R_1}^{R_2}\psi^c_{00}\exp[-iv_0\pi/2]\cos[(m\pi/h)(r - R_1)]\,dr + \sum_{n=0}^{\infty} C^r_{n0}\int_{R_1}^{R_2}\psi^c_{n0}\exp[iv_n\pi/2]\cos[(m\pi/h)(r - R_1)]\,dr - B^l_{00}(h/2m\pi)[1 - (-1)^m] + \sum_{l=0}^{\infty} B^r_{l0}\int_0^{h/2}\psi^s_{l0}\cos[(m\pi/h)(y'' + h/2)]\,dy''. \quad \text{(A10)}$$

Continuity of tangential velocity at D provides

$m = 0$:

$$E^{l}_{00} k_{00} h = C^{l}_{00} \int_{R_1}^{R_2} \psi^{c}_{00}(\nu_0/r) \exp[-i\nu_0 \pi/2]\, dr - \sum_{n=0}^{\infty} C^{r}_{n0} \int_{R_1}^{R_2} \psi^{c}_{n0}(\nu_n/r) \exp[i\nu_n \pi/2]\, dr$$

$$+ B^{l}_{00} k_{00} h/2 - \sum_{l=0}^{\infty} B^{r}_{l0} k_{l0} \int_{0}^{h/2} \psi^{s}_{l0}\, dy'', \tag{A11}$$

$m \neq 0$:

$$E^{l}_{m0} k_{m0} h/2 = C^{l}_{00} \int_{R_1}^{R_2} \psi^{c}_{00}(\nu_0/r) \exp[-i\nu_0 \pi/2] \cos[(m\pi/h)(r - R_1)]\, dr$$

$$- \sum_{n=0}^{\infty} C^{r}_{n0} \int_{R_1}^{R_2} \psi^{c}_{n0}(\nu_n/r) \exp[i\nu_n \pi/2] \cos[(m\pi/h)(r - R_1)]\, dr$$

$$- B^{l}_{00} k_{00} (h/2m\pi)[1 - (-1)^m] - \sum_{l=0}^{\infty} B^{r}_{l0} k_{l0} \int_{0}^{h/2} \psi^{s}_{l0} \cos[(m\pi/h)(y'' + h/2)]\, dy''. \tag{A12}$$

5.B.

Propagation of sound in a curved bend containing a curved axial partition

Christopher R. Fuller and David A. Bies

Department of Mechanical Engineering, University of Adelaide, South Australia, 5001

Sound transmission in a 180° bend containing a curved partition positioned on the axial center line is investigated theoretically and experimentally using equations for sound propagation in straight and curved ducts. Good agreement is obtained and small discrepancies are discussed. The partition is found to significantly alter the sound propagation through the bend and reasons for the different acoustic behavior are given.

PACS numbers: 43.20.Mv, 43.20.Bi

INTRODUCTION

In recent years attention has been focused on the problem of sound propagation in curved-duct bends. Rostafinski[1–3] has theoretically investigated the acoustic velocity distribution of propagating and nonpropagating modes within curved bends. Cummings[4] has theoretically and experimentally investigated the acoustic discontinuity caused by two 180° bends of different curvature in a straight-duct system of rectangular cross section. He found that even for bends of severe curvature, near the cutoff frequency of the (1, 0) mode in the curved section, the bends provided negligible reflection of sound. Osborne[5] considered the more complex case of higher-mode propagation in short curved bends, but still found no appreciable discontinuity in the acoustic propagation through the duct system.

In this paper the discontinuity caused by a bend divided by a curved partition is considered. As suggested by Rostafinski the introduction of the partition creates essentially new boundary conditions and modifies the original distribution of pressures and velocities.[3] Three parameters, power reflection coefficient, characteristic impedance, and insertion loss are investigated. Experimental values of these parameters are given and compared with theoretical predictions. The presence of the partition is shown to drastically alter the acoustic properties of the bend.

The partition effectively divides the curved bend into two concentric bends. The duct system containing the concentric bends is investigated theoretically by applying equations for sound propagation in straight and curved ducts to the respective sections. Continuity of acoustic pressure and axial particle velocity at adjoining interfaces between straight and curved sections is postulated to determine the Fourier coefficients of each wave. The analysis is limited to frequencies less than the cutoff frequency of the (1, 0) mode in both curved and straight ducts.

I. SOUND PROPAGATION IN RECTANGULAR SECTION DUCTS

Sound propagation in an infinite straight duct of rectangular cross section may be described as follows[6]:

$$p(x,y,z,t)=\sum_{m=0}^{\infty}\sum_{n=0}^{\infty}P_{mn}\psi^{s}_{mn}(y,z)\exp[i(\omega t-k_{mn}x)]. \quad (1)$$

In Eq. 1 the x axis is parallel to the direction of propagation of sound and the characteristic function $\psi^{s}_{mn}(y,z)$, assuming rigid walls is given by Eq. (2).

$$\psi^{s}_{mn}(y,z)=\cos[(m\pi/h_1)y]\cos[(n\pi/h_2)z], \quad (2)$$

where h_1 and h_2 are dimensions of the duct in the y and z directions, respectively.

The wave number k_{mn} is a solution of the characteristic Eq. (3)

$$k_{mn}=[(\omega/c)^2-(m\pi/h_1)^2-(n\pi/h_2)^2]^{1/2}. \quad (3)$$

If k_{mn} is real propagation occurs without attenuation. However, if k_{mn} is imaginary the corresponding (m,n) mode does not propagate; the disturbance decays exponentially away from the generating surface.

Sound propagation in an infinite curved bend of rectangular cross section may be described by a solution of the wave equation in cylindrical coordinates as follows[7]:

$$p(r,\theta,z,t)=\sum_{a=0}^{\infty}\sum_{n=0}^{\infty}C_{an}\psi^{c}_{an}(r,z)\exp[i(\omega t-\nu_a\theta)]. \quad (4)$$

In Eq. (4) ν_a is the angular wave number in the curved duct. The characteristic function $\psi^{c}_{an}(r,z)$ and the characteristic equation are obtained by applying the boundary conditions of rigid duct walls, that is, at $r=R_1$ and $r=R_2$ the radial components of particle velocity are zero.

The characteristic function is

$$\psi^{c}_{an}(r,z)=\{J_{\nu_a}(k_n r)-[J'_{\nu_a}(k_nR_1)/Y'_{\nu_a}(k_nR_1)]\times Y_{\nu_a}(k_n r)\}\cos[(n\pi/h_2)z], \quad (5)$$

where

$$k_n^2=k_0^2-k_z^2 \quad \text{and} \quad k_z=n\pi/h_2.$$

The characteristic equation is

$$J'_{\nu_a}(k_nR_1)Y'_{\nu_a}(k_nR_2)-J'_{\nu_a}(k_nR_2)Y'_{\nu_a}(k_nR_1)=0. \quad (6)$$

Solutions of Eq. (6) using an iterative process and a computer provide values of the angular wave number ν_a. As for straight ducts there will be frequencies below which solutions of Eq. (6) will be imaginary and the corresponding mode will be evanescent. Above these cutoff frequencies, the mode will propagate without attenuation.

 0001-4966/78/6303-0681$00.80

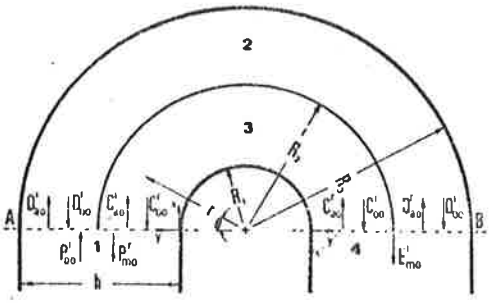

FIG. 1. Arrangement and coordinate system of bend with partition.

II. ANALYSIS

The arrangement of the duct system is shown in Fig. 1. The bend has dimensions $R_1 = 0.127$ m, $R_2 = 0.1905$ m, $R_3 = 0.254$ m, and was analyzed by dividing it into sections with coordinate systems and joining interfaces as shown in the figure. Sound propagation is described by straight-duct equations in sections 1 and 4 and curved-duct equations in sections 2 and 3 of the bend.

The frequencies to be considered are well below the cutoff frequency of the (1, 0) mode in both curved sections, thus any radial particle velocity will be small and negligible so that it will be sufficient to postulate continuity of axial particle velocity. As there is no discontinuity in the z direction it is satisfactory to use a two-dimensional coordinate system, i.e., $k_z = 0$.

The Fourier coefficients of each wave were obtained by applying continuity conditions of acoustic pressure and particle velocity across interfaces A and B. Both sides of each equation are multiplied by $\cos[(m\pi/h)y]$ and integrated with respect to y, y', or r. The orthogonality property of the latter functions allows determination of the coefficients P^r_{m0} and E^i_{m0}, for $m = 0, 1, 2, \ldots$.

The general equations obtained are

Continuity of pressure at A $(x = 0, \theta = 0)$

$m = 0$,

$$P^i_{00} h + P^r_{00} h = \sum_{a=0}^{\infty} C^i_{a0} \int_{R_1}^{R_2} \psi^c_{a0}\, dr + C^r_{00} \int_{R_1}^{R_2} \psi^c_{00}\, dr + \sum_{a=0}^{\infty} D^i_{a0} \int_{R_2}^{R_3} \psi^c_{a0}\, dr + D^r_{00} \int_{R_2}^{R_3} \psi^c_{00}\, dr, \tag{7}$$

where superscript i refers to incident waves and superscript r to reflected waves;

$m \neq 0$,

$$P^r_{m0} \tfrac{1}{2} h = \sum_{a=0}^{\infty} C^i_{a0} \int_{R_1}^{R_2} \psi^c_{a0} \cos\left[\frac{m\pi}{h}(r - R_1)\right] dr + C^r_{00} \int_{R_1}^{R_2} \psi^c_{00} \cos\left[\frac{m\pi}{h}(r - R_1)\right] dr + \sum_{a=0}^{\infty} D^i_{a0} \int_{R_2}^{R_3} \psi^c_{a0} \cos\left[\frac{m\pi}{h}(r - R_1)\right] dr$$
$$+ D^r_{00} \int_{R_2}^{R_3} \psi^c_{00} \cos\left[\frac{m\pi}{h}(r - R_1)\right] dr. \tag{8}$$

Continuity of tangential particle velocity at A

$m = 0$,

$$P^i_{00} k_{00} h - P^r_{00} k_{00} h = \sum_{a=0}^{\infty} C^i_{a0} \int_{R_1}^{R_2} \psi^c_{a0} \frac{\nu_a}{r}\, dr - C^r_{00} \int_{R_1}^{R_2} \psi^c_{00} \frac{\nu_0}{r}\, dr + \sum_{a=0}^{\infty} D^i_{a0} \int_{R_2}^{R_3} \psi^c_{a0} \frac{\nu_a}{r}\, dr - D^r_{00} \int_{R_2}^{R_3} \psi^c_{00} \frac{\nu_0}{r}\, dr; \tag{9}$$

$m \neq 0$,

$$-P^r_{m0} k_{m0} \tfrac{1}{2} h = \sum_{a=0}^{\infty} C^i_{a0} \int_{R_1}^{R_2} \psi^c_{a0} \frac{\nu_a}{r} \cos\left[\frac{m\pi}{h}(r - R_1)\right] dr - C^r_{00} \int_{R_1}^{R_2} \psi^c_{00} \frac{\nu_0}{r} \cos\left[\frac{m\pi}{h}(r - R_1)\right] dr$$
$$+ \sum_{a=0}^{\infty} D^i_{a0} \int_{R_2}^{R_3} \psi^c_{a0} \frac{\nu_a}{r} \cos\left[\frac{m\pi}{h}(r - R_1)\right] dr - D^r_{00} \int_{R_2}^{R_3} \psi^c_{00} \frac{\nu_0}{r} \cos\left[\frac{m\pi}{h}(r - R_1)\right] dr. \tag{10}$$

Continuity of pressure at B $(x' = 0, \theta = \pi)$

$m = 0$,

$$E^i_{00} h = C^i_{00} \int_{R_1}^{R_2} \psi^c_{00} \exp(-i\nu_0 \pi)\, dr + \sum_{a=0}^{\infty} C^r_{a0} \int_{R_1}^{R_2} \psi^c_{a0} \exp(i\nu_a \pi)\, dr + D^i_{00} \int_{R_2}^{R_3} \psi^c_{00} \exp[-i\nu_0 \pi]\, dr$$
$$+ \sum_{a=0}^{\infty} D^r_{a0} \int_{R_2}^{R_3} \psi^c_{a0} \exp(i\nu_a \pi)\, dr; \tag{11}$$

$m \neq 0$,

$$E^i_{00} \tfrac{1}{2} h = C^i_{00} \int_{R_1}^{R_2} \psi^c_{00} \exp(-i\nu_0 \pi) \cos\left[\frac{m\pi}{h}(r - R_1)\right] dr + \sum_{a=0}^{\infty} C^r_{a0} \int_{R_1}^{R_2} \psi^c_{a0} \exp(i\nu_a \pi) \cos\left[\frac{m\pi}{h}(r - R_1)\right] dr$$
$$+ D^i_{00} \int_{R_2}^{R_3} \psi^c_{00} \exp(-i\nu_0 \pi) \cos\left[\frac{m\pi}{h}(r - R_1)\right] dr + \sum_{a=0}^{\infty} D^r_{a0} \int_{R_2}^{R_3} \psi^c_{a0} \exp(i\nu_a \pi) \cos\left[\frac{m\pi}{h}(r - R_1)\right] dr. \tag{12}$$

Continuity of tangential particle velocity at B

$m=0$,

$$E^t_{00}k_{00}h = C^t_{00}\int_{R_1}^{R_2}\psi^c_{00}\frac{\nu_0}{r}\exp(-i\nu_0\pi)dr - \sum_{a=0}^{\infty}C^r_{a0}\int_{R_1}^{R_2}\psi^c_{a0}\frac{\nu_a}{r}\exp(i\nu_a\pi)\,dr + D^t_{00}\int_{R_2}^{R_3}\psi^c_{00}\frac{\nu_c}{r}\exp(-i\nu_0\pi)\,dr - \sum_{a=0}^{\infty}D^r_{a0}\int_{R_2}^{R_3}\psi^c_{a0}\frac{\nu_a}{r}\exp(i\nu_a\pi)\,dr\,; \tag{13}$$

$m\neq 0$,

$$E^t_{m0}k_{m0}\tfrac{1}{2}h = C^t_{00}\int_{R_1}^{R_2}\psi^c_{00}\frac{\nu_0}{r}\exp(-i\nu_0\pi)\cos\left[\frac{m\pi}{h}(r-R_1)\right]dr - \sum_{a=0}^{\infty}C^r_{a0}\int_{R_1}^{R_2}\psi^c_{a0}(\nu_a/r)\exp(i\nu_a\pi)\cos\left[\frac{m\pi}{h}(r-R_1)\right]dr + D^t_{00}\int_{R_2}^{R_3}\psi^c_{00}\frac{\nu_0}{r}\exp(-i\nu_0\pi)\cos\left[\frac{m\pi}{h}(r-R_1)\right]dr - \sum_{a=0}^{\infty}D^r_{a0}\int_{R_2}^{R_3}\psi^c_{a0}\frac{\nu_a}{r}\exp(i\nu_a\pi)\cos\left[\frac{m\pi}{h}(r-R_1)\right]dr\,. \tag{14}$$

At both interfaces an infinite series of modes will be generated. As the frequency over which the bend will be investigated is limited to less than the cutoff frequency of the (1, 0) mode in both straight and curved sections these infinite sets will consist of one propagating and an infinite number of higher-order evanescent modes. In order to determine the coefficients it is necessary to truncate each infinite sum at a value determined by two factors: (1) Since the number of unknown coefficients generated must equal the number of equations, the number of modes considered in straight sections 1 and 4 is truncated at twice the number considered in curved sections 2 and 3. (2) The accuracy of the analysis is determined by the number of modes considered.

Cummings[4] and Osborne[5] have both shown that nonpropagating modes have only a small effect on the sound propagation in a curved bend. Thus in Eqs. (7)–(14) the number of modes considered in the curved sections will be truncated at one while in the straight sections, one propagating and one nonpropagating mode will be considered. This simplification is justified, as will be shown, by the comparison between theoretical and experimental results. The two modes considered in both straight sections are necessary to provide continuity across adjoining interfaces.

III. EXPERIMENTAL APPARATUS AND METHOD

The bend was investigated with the arrangement shown in Fig. 2. The duct system has a 0.0635×0.127-m^2 cross section and was constructed from 0.0254-m-thick wood lined with laminex. The sound source was positioned 1.7 m upstream from the entrance to the bend at which distance any nonpropagating modes are sufficiently attenuated to be negligible. The straight-duct downstream of the bend was terminated by an anechoic termination with a pressure reflection coefficient of less than 0.12.

Three parameters were measured. The power reflection coefficient, an indication of how much sound is reflected back towards the source, and the characteristic impedance, an indication of how severe a discontinuity the bend presents to acoustic propagation, were obtained by measuring the standing wave in the upstream straight duct and applying standing-wave theory.[6] Values of the experimental reflection coefficient plotted against a nondimensional frequency parameter k_0h are shown in Fig. 3. Since the analysis is limited to less than the cut-off frequency of the (1, 0) mode in the straight-duct section, for which $k_0h=\pi$, values of k_0h are terminated at $k_0h=3.02$. Experimental values of the resistive impedance $R/\rho c$ are shown in Fig. 4 while those of the reactive part $X/\rho c$ are shown in Fig. 5.

The insertion loss, a measure of the attenuation in decibels of the incident wave, was measured by traversing a calibrated microphone in the upstream duct until a maximum in sound pressure level P^{max}_{00} was recorded. The sound pressure level of the propagating wave E^t_{00} in the downstream duct was measured with a calibrated microphone inserted through the duct wall. The insertion loss is defined to be the difference in decibels of $P^t_{00}-E^t_{00}$. Thus using standing-wave theory it can be shown that,

$$P^{max}_{00}=(1+\alpha_r^{1/2})P^t_{00}\,,$$

$$\therefore\ P^{max}_{00}(dB)=20\log_{10}(1+\alpha_r^{1/2})+P^t_{00}(dB)\,,$$

$$\therefore\ P^t_{00}=P^{max}_{00}-20\log_{10}(1+\alpha_r^{1/2})\,.$$

Hence the insertion loss of the bend is

$$\text{measured insertion loss (dB)}=P^{max}_{00}(dB)-20\log_{10}(1+\alpha_r^{1/2})-E^t_{00}(dB)\,. \tag{15}$$

In Eq. (15) α_r is the measured power reflection coefficient.

IV. THEORETICAL PREDICTIONS

The radial terms in Eqs. (7)–(14) were expressed as power-series expansion of Bessel and Neumann func-

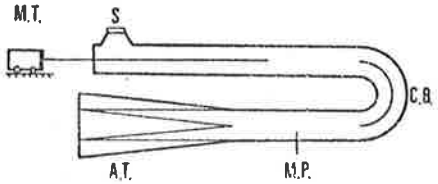

FIG. 2. Arrangement of experimental apparatus. (M. T.) microphone traverse, (S) speaker, (C. B.) compound bend, (A. T.) anechoic termination, and (M. P.) microphone probe.

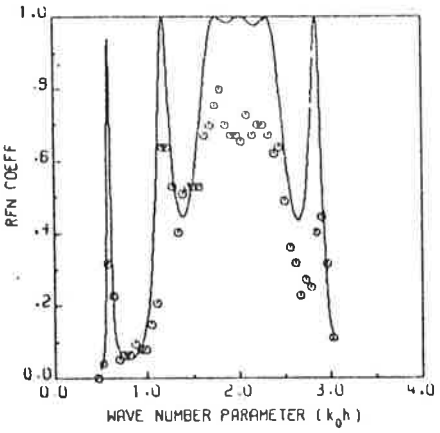

FIG. 3. Sound power reflection coefficient of compound bend, ——theoretical curve, ○ experimental values.

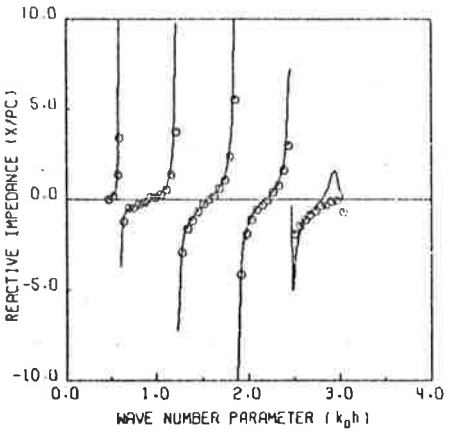

FIG. 5. Reactive part of characteristic impedance of compound bend, ——theoretical curve, ○ experimental values.

tions[9] and integrated using Simpson's rule by a computer. The resulting equations were then solved using a program based on Crout's rule.[10] For convenience a reference amplitude of $P_{00}^{i} = 1 - 0i$ was assumed.

The theoretical power reflection coefficient is given by Eq. (16)

$$\alpha_r = \left| P_{00}^{r} / P_{00}^{i} \right|^2 . \tag{16}$$

The characteristic impedance is

$$Z/\rho c = R/\rho c + (X/\rho c)i = (P_{00}^{i} + P_{00}^{r})/(P_{00}^{i} - P_{00}^{r}) . \tag{17}$$

The theoretical insertion loss is

$$\text{I.L.} = -20 \log_{10}(1 - \alpha_r)^{1/2} . \tag{18}$$

All three parameters are shown with respective experimental values for comparison in Figs. 3–6.

V. DISCUSSION

A. Power reflection coefficient

As can be seen in Fig. 3 there is close agreement between theoretical and experimentally measured values of the frequencies at which maxima occur. The small discrepancies are thought to be due to dimensional inaccuracies and variation in ambient temperature during the course of experimentation.

The magnitude of the experimental reflection coefficient is consistently less than predicted at the maxima. This was thought to be due to the difficulty of determining accurately the standing wave ratio when it is quite large. In the case of large standing wave ratio the minima are quite sharp and very easily obscured by, for example, overtones due to small distortion in the signal. They are thus very difficult to measure and the measured magnitude of sound pressure level is always too high. The standing wave ratio and thus the corresponding power reflection coefficient in this case will always be too small.

As can be seen in Fig. 3, a curved 180° bend with a partition positioned on its centreline provides a large disruption to sound propagation. In fact the theory developed here predicts that at the dimensionless frequencies of k_0h given in Table I the power reflection coefficient is very close to unity. This is in direct contrast to a normal curved bend. Cummings[4] studied two bends, one of radius ratio $R_1/R_2 = 0.097$ representing a very sharp bend, at frequencies below the cut-off frequency of the (1, 0) mode and found that the pressure

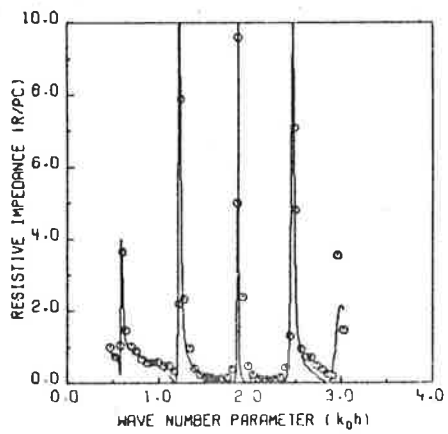

FIG. 4. Resistive part of characteristic impedance of compound bend, ——theoretical curve, ○ experimental values.

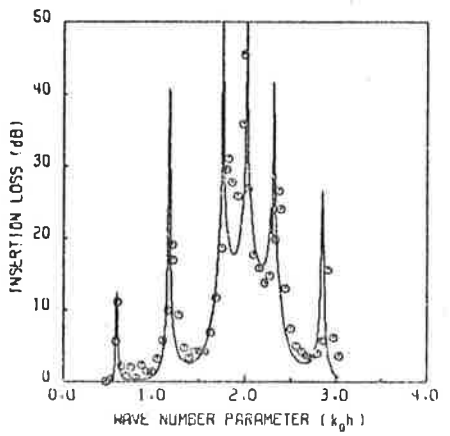

FIG. 6. Insertion loss of compound bend, ——theoretical curve, ○ experimental values.

transmission coefficient of the (0, 0) mode does not fall below 0.975. Thus it can be seen that positioning a splitter or turning vane in a curved bend of a duct system leads to quite different acoustic behavior for frequency below cutoff for the first cross mode.

The reason for the markedly different effect of a partition in a straight and curved duct is due to the resulting variation in path length and phase of the two parts of the acoustic disturbance propagating in the two parts of the compound curved duct. Without the partition the phase of the (0, 0) mode will be maintained radially across the duct and will be determined approximately by the center-line propagation distance. The partition effectively prevents the implied redistribution of the disturbance across the original bend confining it to the two separate concentric ducts formed by the partition.

The effect of curvature on sound propagation in a curved duct in contrast to propagation in a straight duct is reflected in the respective solutions of characteristic Eqs. (3) and (6). For the (0, 0) mode in a straight duct the wave number is independent of duct dimensions, whereas in a curved duct the corresponding angular wave number is dependent on the radii of the curved section as suggested in Ref. 3. Thus the waves travelling in the separate curved sections, shown in Fig. 1, have the same amplitude but different relative phases at each angle θ of propagation, due to different values of angular wave number. Therein lies the explanation for the effect of the partition in a curved duct.

At interface B, shown in Fig. 1, the two incident waves in sections 2 and 3 have a phase difference induced by the different values of respective angular wave number. When these two waves recombine at B, the phase difference leads to generation of nonpropagating cross modes and the resulting impedance mismatch causes reflection of sound. Similarly reflected waves from B have a phase difference at A and an impedance mismatch results here as well. When these phase differences are close to π large reflections of sound occur.

B. Characteristic impedance

Theoretical and experimental values of the resistive and reactive parts of the characteristic impedance are in good agreement as shown in Figs. 4 and 5.

It can be seen that at dimensionless frequencies of k_0h given in Table I a large impedance mismatch relative to the characteristic impedance ρc of the incident wave is generated. Thus one would expect large reflection of sound at these frequencies. This is demonstrated in Fig. 3 which shows high reflection of sound at the characteristic frequencies of Table I.

At intermediate frequencies the characteristic impedance $Z/\rho c$ of the bend is relatively closer to unity than at the characteristic frequencies and incident sound is thus mostly transmitted at these intermediate frequencies.

As the nondimensional frequency k_0h approaches π the reactive part of the characteristic impedance changes its general shape demonstrated at lower frequencies. This was thought to be due to the effect of the evanescent (1, 0) mode in the straight duct becoming predominant near cutoff.

TABLE I. Characteristic frequencies of a compound 180° bend for $R_3/R_1 = 2$.

Characteristic freq. $(k_0h)^a$					
0.6	1.18	1.80	2.08	2.30	2.86

[a]Only frequencies below cutoff ($k_0h = \pi$) for the (1, 0) mode in the straight duct are included.

C. Insertion loss

Much closer agreement is demonstrated by comparison of experimental and theoretical values of insertion loss shown in Fig. 6 than reflection coefficient shown previously in Fig. 3. This observation supports the argument presented previously to explain the discrepancies shown in the latter figure.

At $k_0h = 2.1$ an insertion loss of 45.5 dB was measured. Thus an incident pure tone at this frequency would be virtually completely reflected. Such high levels of attenuation suggest the use of the discontinuity provided by the bend as a reactive attenuator. An attenuator based on the impedance mismatch generated by a center body placed in a 90° bend is discussed in a paper by Fuller and Bies.[11]

VI. CONCLUSIONS

Sound transmission in a duct system containing a curved 180° bend with a central partition has been discussed. Theoretical and experimental values have been given and good agreement obtained.

The partition was found to significantly alter the sound propagation through the bend, resulting in high reflection of sound at a number of discrete frequencies.

The problem discussed illustrates the essential difference between sound propagation in straight and curved ducts. Namely, the angular wave number of the (0, 0) mode in curved ducts is dependent on boundary conditions whereas in a straight duct the wave number is independent of duct geometry.

[1]W. Rostafinski, "On Propagation of Long Waves in Curved Ducts," J. Acoust. Soc. Am. 52, 1411–1420 (1972).
[2]W. Rostafinski, "Analysis of Propagation of Waves of Acoustic Frequencies in Curved Ducts," J. Acoust. Soc. Am. 56, 11–15 (1974).
[3]W. Rostafinski, "Acoustic systems containing curved duct sections," J. Acoust. Soc. Am. 60, 23–28 (1976).
[4]A. Cummings, "Sound Transmission in Curved Duct Bends," J. Sound Vib. 35, 451–477 (1974).
[5]W. Osborne, "Higher Mode Propagation of Sound in Short Curved Bends of Rectangular Cross Section," J. Sound Vib. 45, 39–52 (1976).
[6]S. N. Rschevkin, *The Theory of Sound* (Pergamon, Oxford, 1963), pp. 153–196.
[7]F. E. Grigoryan, "Theory of Sound Wave Propagation in

Curvilinear Waveguides," Sov. Phys. Acoust. 14, 315–321 (1969).
[8]L. L. Beranek, *Acoustic Measurements* (Wiley, New York, 1950), pp. 317–329.
[9]N. W. McLachlan, *Bessel Functions for Engineers* (Oxford U. P., London, 1941), pp. 22–25, pp. 56–61.
[10]C. E. Fröberg, *Introduction to Numerical Analysis* (Addison–Wesley, Reading, MA, 1970), pp. 86–89.
[11]C. R. Fuller and D. A. Bies, "A Reactive Acoustic Attenuator," J. Sound Vib. 56 (in press).

Fuller, C. R. & Bies, D. A. (1978, May). A low pressure drop, compact, reactive acoustic attenuator. *Machinery vibration and noise: Applied Mechanics Conference and workshop, Adelaide University, 29-30 May 1978: preprints of papers*, Institution of Engineers, Australia, Barton, A.C.T.

REFERENCES

ALFREDSON, R.J. & DAVIES, P.O.A.L, (1970). The radiation of sound from an engine exhaust. J. Sound Vib., 13 (4), 389-408.

BAADE, P.K., (1977). Effects of acoustic loading on axial flow fan noise generation. Noise Cont. Eng., 8 (1), 5-15.

BERANEK, L.L., (1950). Acoustic measurements, (John Wiley and Sons, New York,) pp. 317-329.

BUCHOLZ, H., (1939). Der Einfluss der Kreummung von Rechteckigen Hohlleitern auf das Phasemass ultrakurzer Wellen. Elek. Nachr. Tech. 16, 73-85.

CREMER, H., HECKL, M. and UNGAR, E., (1973). Structure-Borne Sound, (Springer-Verlag, Berlin).

CUMMINGS, A., (1974). Sound transmission in curved duct bends. J. Sound Vib., 35 (4), 451-477.

CUMMINGS, A., (1975). Sound transmission in 180° duct bends of rectangular section. J. Sound Vib., 41 (3), 321-334.

DOAK, P.E., (1973). Excitation, transmission and radiation of sound from source distributions in hard walled ducts of finite length (I): The effects of duct cross-section geometry and source distribution space-time pattern. J. Sound Vib., 31 (1), 1-72.

EMBLETON, (1963). Experimental study of noise reduction in centrifugal blowers. J. Acoust. Soc. Amer., 35, 700-705.

FRÖBERG, C.E., (1970). Introduction to numerical analysis, (Addison-Wesley,) pp.86-89.

FULLER, C.R. & ABELL, C.J., (1978). Analysis of sound propagation in curved ducts by conformal mapping techniques. Submitted to J. Sound Vib.

FULLER, C.R. & BIES, D.A., (1978 A). Propagation of sound in a curved bend containing a curved axial partition. J. Acoust Soc. Amer., 63, 681-686.

FULLER, C.R. & BIES, D.A., (1978 B). A reactive acoustic attenuator. J. Sound Vib., 56 (1), 45-59.

FULLER, C.R. & BIES, D.A., (1978C). The effects of flow on the performance of a reactive acoustic attenuator. Provisionally accepted for publication in J. Sound Vib.

FULLER, C.R. & BIES, D.A., (1978 D). A low pressure drop, compact, reactive attenuator. Proc. Applied Mech. conf. and workshop. Adelaide Univ., Australia, p.32.

GRIGOR'YAN, F.E., (1969). Theory of sound wave propagation in curvilinear waveguides. Sov. Phys. Acoust. 14, 315-321.

HARRIS, C.M. (Ed.), (1957). Handbook of noise control. (McGraw-Hill, New York).

INGARD, U., (1969). Influence of fluid motion past a plane boundary on sound reflection, absorption and transmission. J. Acoust. Soc. Amer., 31, 1035-1036.

KHOROSHEV, G.A. & PETROV, Y.I., (1971). Some new methods of fan noise reduction. Procs. 7th Int. Cong. Acoust., Budapest, paper 19N16.

KO, S.H. & HO, L.T., (1977). Sound attenuation in acoustically lined curved ducts in the absence of fluid flow. J. Sound Vib., 53, (2), 189-201.

KORN, G.A. & KORN, T.M., (1968). Mathematical handbook for scientists and engineers. (McGraw-Hill, New York).

KRASNUSHIKIN, P.E., (1945). On waves in curved tubes, Uch. Zap. Mosk. Gos. Univ., No. 75, Bk 2, Pt 2, 9-27.

KURZE, U.J. & ALLEN, C.H., (1971). Influence of flow and high sound level on the attenuation in a lined duct. J. Acoust. Soc. Amer. 49, 1643-1654.

LAMBERT, R.F., (1956). Acoustic filtering in a moving medium. J. Acoust. Soc. Amer., 28, 1054-1058.

LEIDEL, W., (1969). Einfluss von Zugenabstand und Zungenradius auf Kennlinie und Geräusch eines Radialventilators, DLR-FB, 69-16.

LUXTON, R.E., (1968). A low pressure loss attenuating bend for air flow ducts. 6th Int. Cong. Acoust., Tokyo.

LYONS, L.A. & PLATTER, S., (1963). Effect of cutoff configuration on pure tones generated by small centrifugal blowers. J. Acoust. Soc. Amer., 35, 1455-1456.

MASON, V., (1969). Some experiments on the propagation of sound along a cylindrical duct containing flowing air. J. Sound Vib., 10, (2), 208-226.

McLACHLAN, N.W., (1934). Bessell functions for engineers. (Oxford University Press, London).

MECHEL, F., MERTENS, P. & SCHILZ, W.L., (1962). Research on sound propagation in sound-absorbent ducts with superimposed air streams. AMRL Report No. TDR-62-140 (111).

MORFEY, C.L., (1971). Sound transmission and generation in ducts with flow. J. Sound Vib., 14 (1), 37-55.

MORSE, P.M., (1939). The transmission of sound inside pipes. J. Acoust. Soc. Amer., 11, 205-210.

MORSE, P.M. & FESCHACH, H., (1953). Methods of theoretical physics. (McGraw-Hill, New York).

MORSE, P.M. & INGARD, U.K., (1968). Theoretical acoustics. (McGraw-Hill, New York).

NEISE, W., (1976). Noise reduction in centrifugal fans: A literature survey. J. Sound Vib., 45 (3), 375-403.

OSBORNE, W.C., (1974). Calculation of the angular propagation constant for a bend. J. Sound Vib., 37 (1), 65-77.

OSBORNE, W.C., (1976). Higher mode propagation of sound in short curved bends of rectangular cross section. J. Sound Vib., 45, 39-52.

PATRICK, W.P., (1967). Systematic method to determine the acoustical characteristics of series-parallel duct configurations using transmission matrices. Proc. 90th Meeting, A.S.A. Paper D3.

PLONER, B. & HERZ, F., (1969). New design measures to reduce siren tones caused by centrifugal fans in rotating machines. Brown Boveri Revue, 56, 280-287.

POOLE, J.H.B. & LEVENTHALL, H.G., (1976). An experimental study of Swinbank's method of active attenuation of sound in ducts. J. Sound Vib., 49 (2), 257-266.

PRIDMORE-BROWN, D.C., (1958). Sound propagation in a fluid flowing through an attenuating duct. J. Fluid Mech., 4, 393-406.

RAYLEIGH, LORD, (1877). Theory of sound (two vols). (Dover Pubs, New York).

RENNISON, D.C., (1976). The vibrational response of and the acoustic radiation from thin walled pipes, excited by random fluctuating pressure fields. Ph.D. Thesis, University of Adelaide.

ROSTAFINSKI, W., (1972). On propagation of long waves in curved ducts. J. Acoust. Soc. Amer., 52, 1411-1420.

ROSTAFINSKI, W., (1974). Analysis of propagation of waves of acoustic frequencies in curved ducts. J. Acoust. Soc. Amer., 56, 11-15.

ROSTAFINSKI, W., (1976). Acoustic Systems containing curved duct sections. J. Acoust. Soc. Amer., 60, 23-28.

RSCHEVKIN, S.N., (1963). The theory of sound. (Pergamon, New York).

SMITH, W.A., O'MALLEY, J.K. & PHELPS, A.H., (1974). Reducing blade passage noise in centrifugal fans. A.S.H.R.A.E. Trans. II, 80, 45-51.

SWINBANKS, M.A., (1973). The active control of sound propagation in long ducts. J. Sound Vib., 27 (3), 411-436.

WOLLHER, H., (1973). Akustische Untersuchungen an Radialventilatoren unter Verwendung der Vierpoltheorie. Ph.D. Thesis, Technische Universitat, Berlin.